ANL-76-59

ANL-76-59

PLEASE RETURN TO
MFC BRANCH LIBRARY

INL Technical Library
239459

AN AUTOMATED APPROACH TO QUANTITATIVE ERROR ANALYSIS IN NEUTRON TRANSPORT CALCULATIONS

by

Erwin H. Bareiss and Keith L. Derstine

RETURN TO REFERENCE FILE
TECHNICAL PUBLICATIONS
DEPARTMENT

U of C-AUA-USERDA

ARGONNE NATIONAL LABORATORY, ARGONNE, ILLINOIS

Prepared for the U. S. ENERGY RESEARCH
AND DEVELOPMENT ADMINISTRATION
under Contract W-31-109-Eng-38

The facilities of Argonne National Laboratory are owned by the United States Government. Under the terms of a contract (W-31-109-Eng-38) between the U. S. Energy Research and Development Administration, Argonne Universities Association and The University of Chicago, the University employs the staff and operates the Laboratory in accordance with policies and programs formulated, approved and reviewed by the Association.

MEMBERS OF ARGONNE UNIVERSITIES ASSOCIATION

The University of Arizona
Carnegie-Mellon University
Case Western Reserve University
The University of Chicago
University of Cincinnati
Illinois Institute of Technology
University of Illinois
Indiana University
Iowa State University
The University of Iowa
Kansas State University
The University of Kansas
Loyola University
Marquette University
Michigan State University
The University of Michigan
University of Minnesota
University of Missouri
Northwestern University
University of Notre Dame
The Ohio State University
Ohio University
The Pennsylvania State University
Purdue University
Saint Louis University
Southern Illinois University
The University of Texas at Austin
Washington University
Wayne State University
The University of Wisconsin

NOTICE

This report was prepared as an account of work sponsored by the United States Government. Neither the United States nor the United States Energy Research and Development Administration, nor any of their employees, nor any of their contractors, subcontractors, or their employees, makes any warranty, express or implied, or assumes any legal liability or responsibility for the accuracy, completeness or usefulness of any information, apparatus, product or process disclosed, or represents that its use would not infringe privately-owned rights. Mention of commercial products, their manufacturers, or their suppliers in this publication does not imply or connote approval or disapproval of the product by Argonne National Laboratory or the U. S. Energy Research and Development Administration.

Printed in the United States of America
Available from
National Technical Information Service
U. S. Department of Commerce
5285 Port Royal Road
Springfield, Virginia 22161
Price: Printed Copy $6.75; Microfiche $3.00

Distribution Category:
Mathematics and Computers
(UC-32)

ANL-76-59

ARGONNE NATIONAL LABORATORY
9700 South Cass Avenue
Argonne, Illinois 60439

AN AUTOMATED APPROACH TO QUANTITATIVE ERROR ANALYSIS IN NEUTRON TRANSPORT CALCULATIONS

by

Erwin H. Bareiss
Northwestern University and Applied Mathematics Division

and

Keith L. Derstine
Applied Physics Division

September 1976

TABLE OF CONTENTS

Page

LIST OF TABLES 6

LIST OF FIGURES 7

ABSTRACT 11

INTRODUCTION 11

CHAPTER

I. THE BENCHMARK ERROR ANALYSIS PROCEDURE 15

1.1 Creation of Benchmark Problems for the One Speed Transport Equation 17

1.1.1 The transport equation in computational cells . . . 17

1.1.2 Elementary solutions to the transport equation . . . 18

1.1.3 Construction of benchmark problems from elementary solutions 19

1.1.4 Automatic superposition of elementary solutions . . 24

1.1.5 Residual checking of the benchmark solution 30

1.1.6 Two cell problem considerations 31

1.2 Solution of Benchmark Problems by Approximate Numerical Methods 33

1.3 Error Analysis of Approximate Methods 34

II. THE STOCHASTIC TRANSPORT EQUATION 36

2.1 Numerical Methods 36

2.1.1 The discrete ordinates method with Hermite Birkhoff interpolation in space 36

2.1.2 The discrete ordinates method with Galerkin Finite Element method in space 40

2.2 Examples of the Benchmark Problem Error Analysis Procedures 45

2.2.1 Benchmark Problem #1, an asymptotic eigenmode . . . 45

2.2.2 Benchmark Problem #2, a transient eigenmode 57

2.2.3 Benchmark Problem #3, a one cell least squares modes analysis. 62

2.2.4 Benchmark Problem #4, a two cell least squares modes analysis. 86

2.2.5 Discussion. 100

III. THE SYMMETRIZED TRANSPORT EQUATION. 102

3.1 The Equation and Elementary Solutions. 102

3.2 Numerical Methods. 106

3.2.1 Discrete ordinates with 1st order finite differences in space. 106

3.2.2 Piecewise bilinear finite element method in phase space 110

3.3 An Example of the Benchmark Problem Error Analysis Procedure 115

3.3.1 Benchmark #5, a one cell least squares modes analysis. 115

IV. SUMMARY AND CONCLUSION. 128

APPENDICES

A. CHAPEAU FUNCTION EXPANSION OF A(ν). 131

A.1 The Expansion for the Angular Flux 131

A.1.1 The standard basis. 131

A.1.2 A special basis 133

A.2 The Expansion for Angular Flux Derivative. 144

A.2.1 The standard basis. 144

A.2.2 A special basis 145

A.3 The Expansion for the Scalar Flux. 146

A.3.1 The standard basis. 146

A.3.2 A special basis 147

B. EXPONENTIAL INTEGRALS AND RELATED FUNCTIONS 151

B.1 The Exponential Integral $E_n(x)$ 151

B.1.1 The general expression. 151

B.1.2 Limit cases 151

B.1.3 The generalized exponential integral $E_n^{(a,b)}(x)$.152

B.1.4 Limit cases for the generalized form. 153

B.2 The Exponential Integral $I_n(x,\mu)$ 154

B.2.1 The general expression. 154

B.2.2 Limit cases 155

B.2.3 The generalized exponential integral $I_n^{(a,b)}(x,\mu)$ 156

B.2.4 Limit cases for the generalized form. 157

REFERENCES. 159

ACKNOWLEDGEMENTS. 161

NOMENCLATURE. 162

LIST OF TABLES

Page

2.1. Maximum absolute signed scalar flux error $\pm\|\phi_E\|_\infty$ tabulated for twenty space/angle discretization sets of Benchmark #1 for the DB1, DB3 and DGF methods. 47

2.2. Maximum absolute signed angular flux error $\pm\|\psi_E\|_\infty$ tabulated for twenty space/angle discretization sets of Benchmark #1 for the DB1, DB3 and DGF methods. 51

2.3. Average absolute scalar flux error for DB1, DB3, and DGF methods for twenty discretization sets of Benchmark #1. 55

2.4. Relative sum error of pointwise scalar flux for DB1, DB3 and DGF methods for twenty discreitzation sets of Benchmark #1. . 56

2.5. Maximum absolute signed scalar flux error $\pm\|\phi_E\|_\infty$ tabulated for twenty space/angle mesh discretization sets of Benchmark #2 for the DB1, DB3 and DGF methods. 59

2.6. Maximum absolute signed angular flux error $\pm\|\psi_E\|_\infty$ tabulated for twenty space/angle discretization sets of Benchmark #2 for DB1, DB3 and DGF methods 61

2.7. Maximum absolute signed scalar flux error $\pm\|\phi_E\|_\infty$ tabulated for twenty space/angle discretization sets of Benchmark #3 for DB1, DB3 and DGF methods. 77

2.8. Maximum absolute signed angular flux error $\pm\|\psi_E\|_\infty$ for twenty space/angle discretization sets of Benchmark #3 for DB1, DB3 and DGF methods 79

2.9. Average absolute scalar flux error for DB1, DB3 and DGF methods for twenty discretization sets of Benchmark #3. 84

2.10. Relative sum error of pointwise scalar flux for DB1, DB3 and DGF methods for twenty discretization sets of Benchmark #3. . 85

2.11. Maximum absolute signed scalar flux error $\pm\|\phi_E\|_\infty$ tabulated for sixteen space/angle discretization sets of Benchmark #4 for DB1, DB3 and DGF methods. 92

2.12. Maximum absolute signed angular flux error $\pm\|\psi_E\|_\infty$ for twenty space/angle discretization sets of Benchmark #4 for DB1, DB3 and DGF methods 94

2.13. Average absolute scalar flux error for DB1, DB3 and DGF methods for sixteen discretization sets of Benchmark #4 98

2.14. Relative sum error of pointwise scalar flux for DB1, DB3 and DGF methods for sixteen discretization sets of Benchmark #4. 99

LIST OF TABLES (cont'd)

3.1. Maximum absolute signed scalar flux error $\pm\|\phi_E\|_\infty$ tabulated for twenty space/angle discretization sets of Benchmark #5 for DFD and FEM methods 121

3.2. Maximum absolute signed angular flux error $\pm\|\psi_E\|_\infty$ for twenty space/angle discretization sets of Benchmark #5 for DFD and FEM methods 123

3.3. Average absolute scalar flux error and relative sum error of pointwise scalar flux for DFD and FEM methods for twenty discretization sets of Benchmark #5 127

A.1. Computational equations for $q_n(x,\mu)$ 134

A.2. Partitioning of the integration domains D_p for $I(\nu,\mu)$ 136

A.3. Subdomain integration formulas. 138

A.4. Numerical integration of $G_{3p}(x,\mu)$ 140

LIST OF FIGURES

Page

1.1. Simplified logical flow diagram for BEAPAC-1T 16

1.2. Approximation of $A(\nu)$ by Chapeau functions. 22

2.1. Flux distributions for Benchmark #1 46

2.2. Scalar flux error ϕ_E for DB1, DB3 and DGF methods for eight selected discretizations of Benchmark #1. 49

2.3. Angular flux error traverses $\psi_E(0,\mu)$ for DB1, DB3, and DGF methods for eight selected discretizations of Benchmark #1 52

2.4. Angular flux error traverses $\psi_E(.5,\mu)$ for DB1, DB3, and DGF methods for eight selected discretization sets of Benchmark #1. . 53

2.5. Angular flux error traverse $\psi_E(1,\mu)$ for DB1, DB3 and DGF methods for eight selected discretization sets of Benchmark #1. 54

2.6. Flux distributions for Benchmark #2 58

2.7. Scalar flux error $\phi_E(x)$ for (a) DB1, (b) DB3, (c) DGF methods for eight selected discretizations of Benchmark #2. 60

2.8. The function $g(\nu,c)$ 62

2.9. Angular flux traverses for DB3 reference solution ($h = .125$, DP_8) 64

LIST OF FIGURES (cont'd)

2.10. Angular flux for Benchmark #3 66

2.11. Comparison of reference and benchmark solutions for Benchmark #3. 67

2.12. Combining coefficients $A(\nu)$ and $a_0^{\pm}$ from least squares modes analysis. 69

2.13. Contributions of elementary solutions $a_n q_n(x,\mu)$ to $\psi_B(x,\mu)$ in Benchmark #3 70

2.14. Detailed enlargement of elementary solution contributions to Benchmark #3 71

2.15. Angular flux for Benchmark #3A. 72

2.16. Comparison of reference and benchmark solutions for Benchmark #3A 73

2.17. Contributions of elementary solutions $q_n(x,\mu)$ to $\psi_B(x,\mu)$ Benchmark #3A 74

2.18. Detailed enlargement of elementary solution contributions to Benchmark #3A. 75

2.19. Scalar flux error $\phi_E(x)$ for DB1, DB3 and DGF methods for eight selected discretizations of Benchmark #3. 78

2.20. Angular flux error traverses $\psi_E(.5,\mu)$ for DB1, DB3 and DGF methods for eight selected discretizations of Benchmark #3. . . . 81

2.21. Angular flux error traverses $\psi_E(1,\mu)$ for DB1, DB3 and DGF methods for eight selected discretizations of Benchmark #3. . . . 82

2.22. Angular flux error traverses $\psi_E(1.5,\mu)$ for DB1, DB3 and DGF methods for eight selected discretizations of Benchmark #3. . . . 83

2.23. Angular flux traverses for Benchmark #4 87

2.24. Comparison of DB3 reference and benchmark solutions for Benchmark #4. 88

2.25. (a) Combining coefficients $A(\nu)$ and $a_0^{\pm}$ from least squares modes analysis, (b) Regionwise constant sources in Cell I and Cell II for Benchmark #4. 89

2.26. Contributions of elementary solutions $a_n q_n(x,\mu)$ to $\psi_B(x,\mu)$ in Benchmark #4 for μ traverse at (a) $x = 0$, (b) $x = .5$, (c) $x = 1.5$ 90

LIST OF FIGURES (cont'd)

2.27. Scalar flux error $\phi_E(x)$ for DB1, DB3 and DGF methods for seven selected discretizations of Benchmark #4. 93

2.28. Angular flux error traverses $\psi_E(0,\mu)$ for DB1, DB3 and DGF methods for seven selected discretizations of Benchmark #4. . . . 95

2.29. Angular flux error traverses $\psi_E(.5,\mu)$ for DB1, DB3 and DGF methods for seven selected discretizations of Benchmark #4. . . . 96

2.30. Angular flux error traverses $\psi_E(1.5,\mu)$ for DB1, DB3 and DGF methods for seven selected discretizations of Benchmark #4. . . . 97

3.1. Comparison of DB3 reference solution and benchmark solutions for Benchmark #5. 116

3.2. (a) Combining coefficients $A(\nu)$ and $a_0^{\pm}$ from least squares modes analysis, (b) Regionwise constant angular source in cell I for Benchmark #5. 117

3.3. Even parity angular flux traverses for Benchmark #5 118

3.4. Even and odd parity sources for Benchmark #5. 119

3.5. Scalar flux error $\phi_E(x)$ for DFD and FEM methods for eight selected discretizations of Benchmark #5. 122

3.6. Even parity angular flux error traverses $\psi_E^+(0,\mu)$ for DFD and FEM for eight selected discretizations of Benchmark #5. 124

3.7. Even parity angular flux error traverses $\psi_E^+(.25,\mu)$ for DFD and FEM methods for seven selected discretizations of Benchmark #5. .125

AN AUTOMATED APPROACH TO QUANTITATIVE ERROR ANALYSIS IN NEUTRON TRANSPORT CALCULATIONS

by

Erwin H. Bareiss and Keith L. Derstine

ABSTRACT

A method is described how a quantitative measure for the robustness of a given transport theory code for coarse network calculations can be obtained. A code, that performs this task automatically and at only nominal cost, is described and has been implemented for slab geometry. This code generates also user oriented benchmark problems which exhibit the analytic behavior at interfaces.

INTRODUCTION

The problem which we address here is concerned with ascertaining the reliability of neutron transport calculations by high-speed computers. Today's general approach is to check one computer code against another, often for mathematically not identical problem settings. The best way of checking approximate numerical calculations is to compare the results against mathematically exact solutions. Unfortunately, in transport theory such solutions are, in general, not available, or if available, they are very expensive to obtain. There is however the possibility to create benchmark problems with given meaningful exact solutions.

What we have started is a new discipline in Numerical Analysis, namely Quantitative and Computerized Error Analysis. Clearly, this discipline can be (and is) applied to other operator equations than the transport equation. Traditionally, a new numerical technique was conceived, analyzed for qualitative error bounds, implemented in a computer code, tested against other codes, and then distributed. An alternative approach is to make a systematic analysis of the mathematical properties of the solution and the new technique, and then test the theoretical predictions on inexpensive well designed small numerical benchmark problems. The basic difference between classical or qualitative error analysis and the quantitative error analysis is that in quantitative

error analysis we aim at obtaining realistic error bounds for coarse mesh calculations and performance predictions before a code is implemented. What we do can be described by mathematical expressions, but the formulas are very lengthy, complicated and difficult to evaluate. For all practical purposes analytic coarse mesh error analysis would be much too expensive and too time consuming. Our automated approach yields not only new insight, but simultaneously provides numerical results that give a quantitative assessment of the approximation method under investigation. It is a new type of analysis that combines modern and classical analysis with computer technology and computer graphics. A very high efficiency is possible because we exploit the use of dimensional analysis and invariant theory. This is important, since the operators we deal with are linear. We have now available a systematic and complete tabulation of all scaling, translation, rotation and other group properties of the transport equation. [Inonu 1975]

To give a perspective of an application of the procedures described in this report, we shall briefly outline the major parts of our research project. This report is concerned with part A only.

The entire code system, when the project is finished, will consist of three parts with the following functions:

A. Cell Calculations (including 2-Cell Calculations)
B. Global Analysis
C. Computational Complexity

A. The code for part A is again subdivided into three major parts.

a) Creation of Benchmark Problems

b) Numerical Solution of the Benchmark Problems by Approximate Methods

c) Calculation of the Error. The user will specify the appropriate error norm.

Part A can also be characterized by calling its purpose Basic Quantitative Error Analysis. It is designed to evaluate the desired error norms

for calculations over a coarse network or with large finite elements. To our knowledge there exists no other systematic approach to deal with the coarse mesh error analysis. As will become evident, such an analysis is practical only by automation and use of the computer.

B. The codes for part B will conduct a global analysis for multi-region, multigroup calculation. The algorithms will be subject to:

a) Global Error Analysis

b) Stability Analysis

c) Convergence Analysis

We note that the classical concept of consistency analysis does not appear explicitly. The codes will supply various error bounds. However, the main goal is to provide Probabilistic Error Estimates. Research in all areas is underway. The tools employed are borrowed from functional analysis, perturbation-, matrix-, operator-, and probability theory and statistics.

C. The codes for part C are concerned with computational complexity. By this we understand:

a) Performance Prediction

b) Code Evaluation

c) Data Management Analysis

Basically, part C is cost accounting. It will be based on the total operations count (inclusive iterations count), error estimates, and memory requirements. It will also provide a ratio of the actual operations count of the implemented transport code to the theoretical minimum operations count as determined from the mathematically defined algorithm. If this ratio is much greater than one, the entire program (computer code as well as theoretical background) should be investigated for potential significant reductions in computer time.

This report describes the development of the one-dimensional phase of Part A outlined in the previous paragraphs. It also describes the

implementation of the procedures in BEAPAC-1T, a FORTRAN program operational at Argonne National Laboratory on the IBM 370/195. (A simple preprocessor described in the User's manual [Bareiss and Derstine 1977] is provided to facilitate conversion to CDC 6000 or 7000 series installations.) The present code is designed for the one-dimensional transport equation and supplements the theoretical results presented at the Fourth National Conference on Transport Theory [Zweifel, Greenberg 1976], which was concerned mainly with one-dimensional problems.

Section I details the major steps of the benchmark error analysis procedure applied to one-dimensional transport problems. To maintain presentation clarity, special derivations are included in the Appendices. Sections II and III are each devoted to a different form of the transport equation. Each section summarizes in matrix form selected numerical approximation methods applied to its form of the transport equation. Results from the application of the theory in Section I applied to the approximation methods in II and III by BEAPAC-1T are presented and discussed. The conclusion assesses the experience gained with BEAPAC-1T and proposes future directions to be considered.

The guiding principle of the project is to store on tape for easy access and in computable form the theoretical knowledge of numerical analysis which is pertinent to the quantitative (numerical) solution of neutron transport problems, algorithms for approximate solutions and special functions from instructions for their proper use. The output is in tabular form and in visual displays, meaningful to the engineers and scientists who are not specialists in numerical analysis. A systematic analysis of a code requires detailed attention, knowledge, and time. As we will demonstrate, BEAPAC-1T can do this tedious work fast and economically. We want to point out that for an extensive error analysis using Part A, the computer costs are only a fraction of a dollar. This performance cannot be matched even by a very experienced numerical analyst or engineer.

I. THE BENCHMARK ERROR ANALYSIS PROCEDURE

BEAPAC-1T stands for Benchmark Error Analysis Package for one-dimensional Transport theory calculations. Figure 1.1 shows the master-flow chart. We shall discuss the function of the different boxes, but for a more detailed description we refer to the text and to the User's manual [Bareiss, Derstine 1977].

In general a benchmark solution ψ_B is given as a linear combination of known exact eigenmodes with combining coefficients $a_{\pm n}$. ψ_C is a computed (i.e. approximate) solution to the given benchmark problem uniquely defined by ψ_B. With ψ_B and ψ_C available, an error analysis can be performed.

Often, one wishes ψ_B to have a certain shape, ψ_R. ψ_R is called the reference solution and may have been obtained from an approximate calculation. It will not satisfy the transport equation. BEAPAC-1T employs an algorithm to find an exact solution ψ_B to the transport equation, which satisfies ψ_R on a selected subset of fluxes ψ_A in a least squares sense.

The first tenets for the implementation of BEAPAC-1T are to give the user Freedom to set his own Standards and Flexibility in Applications. BEAPAC-1T is therefore an open-ended (expandable) collection of subroutines. The user chooses his own performance criteria for his particular problem by calling available options.

Although the linear neutron transport equation is mathematically uniquely defined, there are several forms of the transport equation which are mathematically equivalent. At this time, the user has the option to base his tests on the following stationary operator equations:

Stochastic Transport Equation (Standard form) [Davison 1957]

Symmetrized Transport Equation (Canonical form, Vladimirov equation) [Vladimirov 1963]

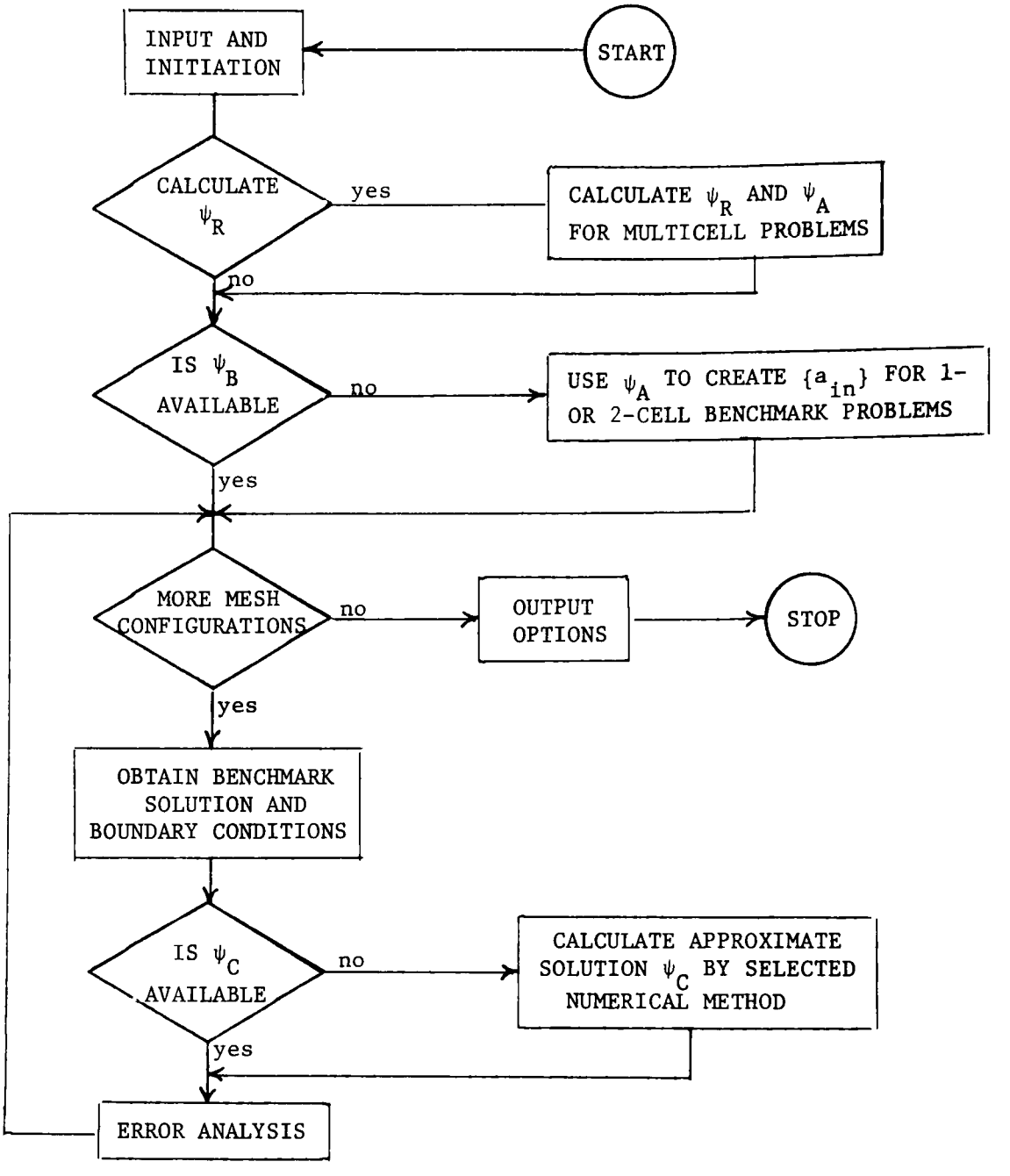

Figure 1.1. Simplified logical flow diagram for BEAPAC-1T

1.1 Creation of Benchmark Problems for the One Speed Transport Equation

To specify benchmark problems is in general not a too difficult job for an engineer [ANL-7416, 1968]. However, to design meaningful benchmark problems for which the exact answer is known, proved rather difficult. It is necessary to have knowledge of the analytic behavior of the solution at interfaces, boundaries, and corners (for multi-dimensional calculations).

Historically, the solution of differential equations was based on "Hard Analysis." The more recent approach to numerical methods is based on "Soft Analysis." The solution is imbedded in a given Sobolev space. This approach is good for asymptotic error analysis, for proving existence-, convergence- and consistency-theorems. However, it is not sufficient for analyzing "coarse network" calculations. We have shown early in our research by pilot calculations that some "low" order algorithms gave better results than "high" order methods. An illustration of this fact is given in [Bareiss 1971].

1.1.1 The transport equation in computational cells

The one speed neutron transport equation in a homogeneous computational cell D(0,a) is given by

$$\mu \frac{\partial \psi}{\partial x}(x,\mu) + \sigma\, \psi(x,\mu) - \frac{\sigma c}{2} \int_{-1}^{1} \psi(x,\mu')d\mu' = S \tag{1.1}$$

where

$\psi(x,\mu)$ is the neutron angular flux

σ is the macroscopic total cross section (cm^{-1})

c is the macroscopic average number of secondaries per collision

σc is the macroscopic scattering cross section

S is a constant distributed source of neutrons

μ is the cosine of the angular direction ($\mu = \cos \Theta$)

x is the spatial distance perpendicular to the plane of the infinite slab

$D(0,a)$ denotes the domain $0 \leq x \leq a$ and $|\mu| \leq 1$

A particular solution of (1.1) is

$$\psi_p = S/\sigma(1-c)$$

which is a constant.

The associated homogeneous equation to (1.1) is

$$\mu \frac{\partial\psi}{\partial x}(x,\mu) + \sigma\,\psi(x,\mu) - \frac{\sigma c}{2}\int_{-1}^{1}\psi(x,\mu')d\mu' = 0 \,. \tag{1.2}$$

The general solution of (1.1) is the superposition of the particular solution and the general solution of (1.2).

The neutron mean free path length (the average distance traveled between collisions) is given by σ^{-1}. The transformation

$$z = \int_0^x \sigma(x')dx' = \sigma x$$

applied to (1.2) expresses distances in terms of mean free paths and (1.2) becomes the dimensionless form of the transport equation

$$\mu \frac{\partial\psi}{\partial z}(z,\mu) + \psi(z,\mu) - \frac{c}{2}\int_{-1}^{1}\psi(z,\mu')d\mu' = 0 \,. \tag{1.3}$$

Obviously, it is sufficient to investigate the analytical behavior of the homogeneous equation (1.3).

1.1.2 Elementary solutions to the transport equation

Case [1967] showed and Bareiss [1966] gave a mathematically rigorous proof that the general solution $\psi(x,\mu)$ to (1.3) in an infinite slab is composed of linear combinations of elementary solutions. The solution is given by

$$\psi(x,\mu) = a_0^+\,\phi_{\nu_0}(\mu)\,e^{-x/\nu_0} + a_0^-\,\phi_{-\nu_0}(\mu)\,e^{+x/\nu_0} + \int_{-1}^{1} A(\nu)\,\phi_\nu(\mu)e^{-x/\nu}d\nu \tag{1.4a}$$

where the $\phi_{\pm\nu_0}(\mu)$ are called asymptotic solutions, and $a_0^{\pm}$ are constant expansion coefficients.

$$\phi_{\pm\nu_0}(\mu) = \frac{c}{2}\frac{\nu_0}{\nu_0 \mp \mu} \tag{1.5}$$

where $\pm\nu_0$ are the roots of the characteristic equation

$$1 - \frac{c\nu}{2}\ln\left(\frac{\nu + 1}{\nu - 1}\right) = 0 \ . \tag{1.6}$$

For $c \leq 1$, $1 \leq \nu_0 < \infty$, for $c > 1$, $\nu_0 = ik_0$, $0 < k_0 < \infty$.

The transient solutions with Hölder continuous expansion function $A(\nu)$ are defined symbolically by

$$\phi_\nu(\mu) = \frac{c}{2} P \frac{\nu}{\nu - \mu} + \lambda(\nu)\ \delta(\nu - \mu) \qquad |\nu| \leq 1 \tag{1.7}$$

where

$$\lambda(\nu) = 1 - \frac{c}{2}\nu\ \ln\left(\frac{1 + \nu}{1 - \nu}\right) \tag{1.8}$$

is the dispersion function.

The definition (1.7) is valid only under integration where P indicates Cauchy principal value integration and $\delta(\nu - \mu)$ is the Dirac delta distribution function (Stakgold 1969) defined by

$$\int_{-\infty}^{\infty} \delta(x - x_0) f(x)dx = f(x_0) \ .$$

Bareiss [1966], Abu-Shumays and Bareiss [1969], Hängelbroek [1973] and Larsen [1975] showed completeness of (1.4a) and conditions for the space of the coefficient functions $A(\nu)$ in different function spaces for the solutions $\psi(x,\mu)$.

1.1.3 Construction of benchmark problems from elementary solutions

Our objective is to create benchmark problems to a known exact benchmark solution $\psi_B(x,\mu)$. This solution will have the form

$$\psi_B(x,\mu) = \sum_{n=0}^{N} a_{\pm n}\, q_{\pm n}(x,\mu) \ . \tag{1.9}$$

The $q_n(x,\mu)$ are a set of appropriately chosen analytic functions which satisfy (1.3); the a_n are appropriately chosen combining coefficients. The construction of the $q_n(x,\mu)$ as used in the present code BEAPAC-1T [Bareiss, Derstine 1976] is described below. We emphasize that this represents only one realization of many possibilities. It demonstrates a general method to construct "Eigenmodes" $q_n(x,\mu)$ based on an established theory.

We generate arbitrary problem (1.9) based on the solution (1.4a) as follows:

Rewrite (1.4a) as

$$\psi(x,\mu) = a_0^+ \phi_{\nu_0}(\mu)\, e^{-x/\nu_0} + \tilde{a}_0^- \phi_{-\nu_0}\, e^{-(a-x)/\nu_0} + \int_0^1 A(\nu)\, \phi_\nu(\mu)\, e^{-x/\nu} d\nu + \int_0^1 \tilde{A}(-\nu)\, \phi_\nu(-\mu) e^{-(a-x)/\nu} d\nu \tag{1.4b}$$

where

$$\tilde{a}_0^- = a_0^-\, e^{-a/\nu_0}$$

$$\tilde{A}(\nu) = A(\nu) e^{-a/\nu}$$

A simple physical motivation can be given for (1.4b). The terms with the e^{-x} factor represent decay of neutrons from a source at $x = 0$, while the terms with the $e^{-(a-x)}$ factor represent decay from $x = a$.

We denote the asymptotic coefficients a_0^+, $\tilde{a}_0^-$ by a_N and a_{-N} respectively; likewise q_N and q_{-N} are defined by

$$q_N(x,\mu) = \phi_{\nu_0}(\mu) e^{-x/\nu_0} \tag{1.10a}$$

$$q_{-N}(x,\mu) = \phi_{\nu_0}(-\mu) e^{-(a-x)/\nu_0} \tag{1.10b}$$

The transient coefficients are obtained by requiring the $A(\nu)$ to have the form

$$A(\nu) = \sum_{n=0}^{N-1} a_n \Theta_n(\nu) \qquad 0 < \nu \leq 1 \tag{1.11a}$$

$$\tilde{A}(\nu) = \sum_{n=0}^{N-1} \tilde{a}_{-n} \Theta_n(-\nu) \qquad -1 \leq \nu < 0 \tag{1.11b}$$

where the $\Theta_n(\nu)$ must be Hölder continuous functions. Except in the neighborhood of $\nu = \pm 1$, we represent $A(\nu)$ by a superposition of Chapeau functions (linear splines) -- see Fig. 1.2 -- defined by

$$\Theta_n(\nu) = \begin{cases} \dfrac{\nu - \nu_{n-1}}{\Delta\nu_{n-1}} & \nu_{n-1} \leq \nu \leq \nu_n \qquad n = 1,2,\ldots,N-2 \\[2ex] \dfrac{\nu_{n+1} - \nu}{\Delta\nu_n} & \nu_n \leq \nu \leq \nu_{n+1} \qquad n = 0,1,\ldots,N-2 \\[2ex] 0 & \text{otherwise} \end{cases} \tag{1.12a}$$

where $\Delta\nu_n = \nu_{n+1} - \nu_n$

for the discretization of ν given by the N+1 nodes $0 = \nu_0, \nu_1, \ldots, \nu_N = 1$.

When $n = N-1$ a special basis element $\Theta_{N-1}(\nu)$ defined by

$$\Theta_{N-1}(\nu) = \begin{cases} \dfrac{\nu - \nu_{N-2}}{\Delta\nu_{N-2}} & \nu_{N-2} \leq \nu \leq \nu_{N-1} \\[2ex] \left(\dfrac{1 - \nu}{\Delta\nu_{N-1}}\right)^{\alpha} & \nu_{N-1} \leq \nu \leq 1 \qquad 0 < \alpha \leq 1 \\[2ex] 0 & \text{otherwise} \end{cases} \tag{1.12b}$$

is introduced so that we obtain an appropriate approximation basis in the neighborhood of $\nu = \pm 1$. In Section 2.2 we will show the effects of this element on the approximation.

It is also obvious that the Chapeau functions can be replaced by other functions such as cubic splines.

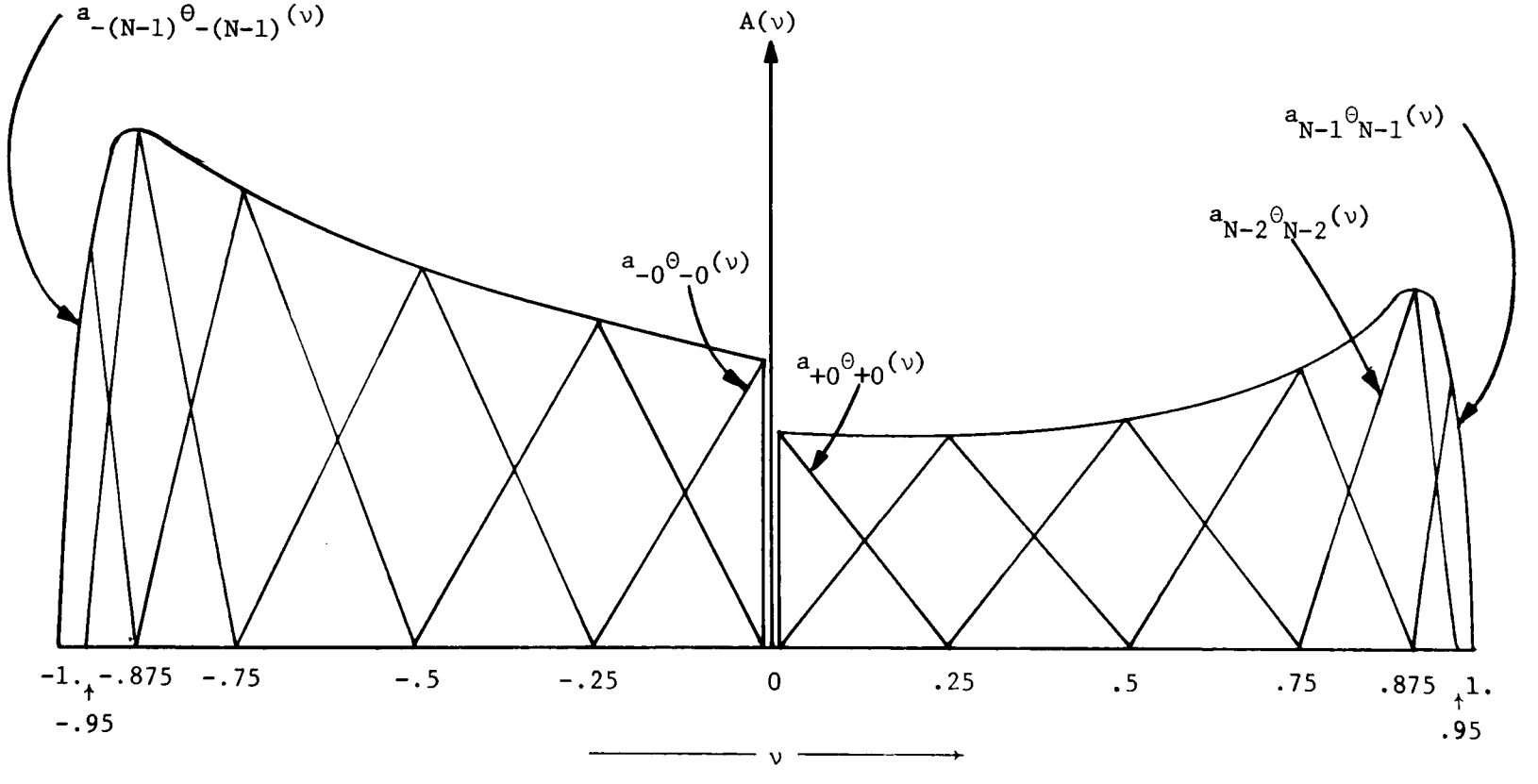

Figure 1.2 Approximation of $A(\nu)$ by Chapeau Functions

Upon substitution of (1.11a) into the first integral of (1.4b) we define

$$q_n(x,\mu) = \int_{\nu_{n-1}}^{\nu_{n+1}} \Theta_n(\nu)\phi_\nu(\mu)e^{-x/\nu}d\nu \qquad (n = 0,1,\ldots,N-1). \tag{1.13a}$$

By symmetry arguments we find

$$q_{-n}(x,\mu) = q_n(a-x,-\mu) \qquad (n = 0,1,\ldots,N-1). \tag{1.13b}$$

As shown in the Appendix A.1, the integrals in (1.13) are manipulated analytically to obtain exponential integrals. Appendix B shows how the $q_n(x,\mu)$ i.e. the $E_n^{(a,b)}(x)$ and $I_n^{(a,b)}(x,\mu)$ can be evaluated very accurately using the exponential integral routine DEI in the ANL Applied Mathematics Division program library [Cody 1971]. Substitution of the elementary modes $q_n(x,\mu)$, so obtained, into the transport equation yields a residual on the order of 10^{-15} for $q_{\pm n}(x,\mu)$, $n=0,1,\ldots,N-2$ and 10^{-12} for $q_{\pm(N-1)}(x,\mu)$.

Using a set of coefficient values $[a_{\pm 0},a_{\pm 1},\ldots,a_{\pm N}]$ we can evaluate (1.9) numerically at any point (x,μ) in $D(0,a)$ with as much accuracy as needed, hence these solution values are considered exact for all practical purposes. Hence the benchmark solution $\psi_B(x,\mu)$ of (1.9) is well defined, and $\psi_B(x,\mu)$ for $x=0, x=a$ can be used to specify the inhomogeneous boundary conditions

$$B_1\psi_B(0,\mu) = f_1(0,\mu) \qquad \mu > 0 \tag{1.14a}$$

$$B_2\psi_B(a,\mu) = f_2(a,\mu) \qquad \mu < 0 \tag{1.14b}$$

for a finite inhomogeneous boundary value slab problem. B_1 and B_2 are boundary condition operators chosen by the user to create specific benchmark problems with the known exact solution $\psi_B(x,\mu)$. For example, if an incident flux boundary condition is specified at $x=0$, then $f_1(0,\mu)$ is defined by

$$f_1(0,\mu) = \psi_B(0,\mu) \qquad \mu > 0.$$

Discussion of available boundary conditions for each form of the transport equation are found in the corresponding Sections II and III.

1.1.4 Automatic superposition of elementary solutions

In this section we develop two algorithms for generating the combining coefficients a_n for a one-cell benchmark solution

$$\psi_B(x,\mu) = \sum_{n=0}^{N} a_{\pm n}\, q_{\pm n}(x,\mu). \tag{1.9}$$

From a purely mathematical standpoint any choice of coefficients a_n defines an exact solution to (1.2). Practical considerations suggest that benchmark solutions with physically meaningful solutions are desirable. Such solutions will enable us to analyze the error behavior of an approximate numerical method at cell boundaries and interfaces.

The two algorithms considered require an initial angular flux distribution $\underline{\psi}_A(x,\mu)$ specified for discrete directions $1 \geq \mu_1 > \mu_2 > \ldots, \mu_M > -1$ at the boundaries of the cell of interest. $\underline{\psi}_A(x,\mu)$ is usually obtained by solving a multicell problem via some standard approximate transport theory method such as the discrete ordinates method. $\underline{\psi}_A(x,\mu)$ is the angular flux solution values calculated in the cell of interest. The distribution $\underline{\psi}_A(x,\mu)$ serves only as a device to drive the coefficient generation algorithms. The resulting benchmark solution $\psi_B(x,\mu)$ will be a perturbation of $\underline{\psi}_A(x,\mu)$

$$\underline{\psi}_A(x,\mu) \approx \sum_{n=0}^{N} a_n \underline{q}_n(x,\mu) + \tilde{a}_{-n}\underline{q}_{-n}(x,\mu) \tag{1.15}$$

but once we have calculated the a_n we forget about the original $\underline{\psi}_A(x,\mu)$ and proceed to generate benchmark problems based on $\psi_B(x,\mu)$.

In the first algorithm the coefficients a_n are chosen to minimize the approximation error in (1.15) in the discrete least squares sense. The problem is mathematically defined by

$$\|Q\underline{a} - \underline{\psi}_A\|_2 = \min \tag{1.16a}$$

where Q is the $M \times (2N+2)$ rectangular matrix ($(2N+2) \leq M$). The columns $\underline{q}_p$ of Q are defined by

$$\underline{q}_p = (q_n(x_i,\mu_m)) \qquad \begin{array}{l} (m = 1,2,\ldots,\frac{M}{2},\ i = 1) \\ (m = \frac{M}{2}+1,\ \frac{M}{2}+2,\ldots,M,\ i = 2) \end{array}$$

where $(p = 1,2,\ldots,N)$ corresponds to $(n = 0^+,1,2,\ldots,N-1)$,

$(p = N+1,\ldots,2N)$ corresponds to $(n = 0^-,-1,-2,\ldots,-N+1)$

$(p = 2N+1,2N+2)$ corresponds to $(n = N,-N)$

$$\underline{a} = [a_0,a_1,\ldots,a_{N-1},\tilde{a}_{-0},\tilde{a}_{-1},\ldots,\tilde{a}_{-N+1},a_N,\tilde{a}_{-N}]$$

on the discrete set of space points and angular directions for the numerically given flux values $\{\psi_A(x_i,\mu_m)\}$. To approximate the continuous least squares problem corresponding to (1.16a), Q and $\underline{\psi}_A$ are modified by the angular and spatial weights ω_{mi} of the corresponding numerical integration. Hence, the actual problem solved is

$$\|\tilde{Q}\underline{a} - \tilde{\underline{\psi}}_A\|_2 = \min \tag{1.16b}$$

where $\tilde{Q} = (\omega_{mi}q_p(x_i,\mu_m))$

and $\tilde{\psi}_A = (\omega_{mi}\underline{\psi}_A(x_i,\mu_m))$.

A simple modification to the problem of (1.16) permits the inclusion of $K \leq M$ linear constraints on the approximation at particular points (i,m) in the equations (1.15) and their corresponding rows in (1.16). If we permute the rows of (1.16) such that the K equations which must satisfy linear constraints are first, the least squares problem with linear constraints becomes

$$\left[\begin{array}{c|c} Q^{GG} & Q^{GH} \\ \hline Q^{HG} & Q^{HH} \end{array}\right]\left[\begin{array}{c} \underline{a}^G \\ \underline{a}^H \end{array}\right] - \left[\begin{array}{c} \underline{\psi}_A^G \\ \hline \underline{\psi}_A^H \end{array}\right] = \left[\begin{array}{c} 0 \\ \hline \min \end{array}\right] \tag{1.17}$$

where the linear constraints are represented by

$$\left[\begin{array}{c|c} Q^{GG} & Q^{GH} \end{array}\right]\left[\begin{array}{c} \underline{a}^G \\ \underline{a}^H \end{array}\right] = \left[\underline{\psi}_A^G\right] \tag{1.18}$$

and where the partitioned submatrices of Q and vectors $\underline{a}$ and $\underline{\psi}_A$ have dimensions

$$Q^{GG}: \quad K \times K, \quad Q^{GH}: \quad K \times (2N+2-K) \qquad K \leq M$$

$$Q^{HG}: \quad (M-K) \times K, \quad Q^{HH}: \quad (M-K) \times (2N+2-K)$$

$$\underline{a}^{G}: \quad K \quad , \quad \underline{a}^{H}: \quad 2N+2-K$$

$$\underline{\psi}_A^{G}: \quad K \quad , \quad \underline{\psi}_A^{H}: \quad 2M-K$$

The procedure for solving (1.17) has three major steps which are

(a) Perform the first K steps of the forward sweep of the Gaussian elimination algorithm on (1.17).

(b) Perform the Householder least squares minimization on the remaining (M-K) equations modified by step (a)

(1.19) $$\|\hat{Q}^{HH}\,\underline{a}^{H} - \hat{\underline{\psi}}_A^{H}\|_2 = \min$$

(where $\hat{Q}^{HH}$, $\hat{\underline{\psi}}_a^{H}$ are the modified matrix and vector from step (a)) to obtain the coefficients $\underline{a}^{H}$.

(c) Perform the backward substitution of the Gaussian elimination algorithm on the first K equations using $\underline{a}^{H}$ from step (b) to obtain $\underline{a}^{G}$.

The second algorithm obtains the coefficients a_n by evaluating analytic formulas based on related formulas [Case 1967] for the infinite medium problem. The asymptotic coefficients are defined by

(1.20a) $$a_0^{\pm} = \frac{1}{N_0^{\pm}} \int_{-1}^{1} \mu\phi_0^{\pm}(\mu)\psi(\mu)\,d\mu$$

where

$\psi(\mu)$ is the angular flux distribution

(1.21) $$N_0^{\pm} = \int_{-1}^{1} \mu[\phi_0^{\pm}(\mu)]^2 d\mu$$

The transient coefficients function $A(\nu)$ is defined by

(1.22a) $$A(\nu) = \frac{1}{N(\nu)} \int_{-1}^{1} \mu\phi_\nu(\mu)\psi(\mu)\,d\mu$$

where

(1.23a) $$N(\nu) = \frac{\nu}{g(\nu,c)}$$

and

(1.23b) $$g(\nu,c) = \frac{1}{[\lambda^2(\nu) + (\frac{\pi c \nu}{2})^2]} .$$

In order to use equations (1.20) and (1.22) we need a flux distribution $\psi(\mu)$. The initial angular flux distribution vector $\underline{\psi}_A(x,\mu)$ can be used for this purpose in the following way. (Note that we are again using $\underline{\psi}_A(x,\mu)$ merely as a device for obtaining coefficients a_n to a benchmark solution $\psi_B(x,\mu)$ which is some perturbation of $\underline{\psi}_A(x,\mu)$.)

Recall that the elementary modes $q_n(x,\mu)$ $(n = 0^+,1,\ldots,N)$ decay exponentially from the left boundary of the slab, whereas $q_n(x,\mu)$ $(n = 0^-,-1,\ldots,-N)$ decay exponentially from the right boundary of the slab. Using this knowledge we determine the coefficients a_n for $(n = 0^+,1,\ldots,N)$ and $(n = 0^-,-1,\ldots,-N)$ by replacing $\psi(\mu)$ in (1.20) and (1.22) by $\underline{\psi}_A(0,\mu)$ for $n \geq 0$ and $\underline{\psi}_A(a,\mu)$ for $n \leq 0$. To simplify the integration in (1.20) and (1.22) we replace the vector $\underline{\psi}_A(x,\mu)$ by $\tilde{\psi}_A(x,\mu)$, the piecewise linear function defined as follows:

(1.24) $$\tilde{\psi}_A(x,\mu) = \sum_{\ell=0}^{L} \psi_A(x,\mu_{\pm\ell})\Theta_\ell(\pm\mu)$$

where

(1.25) $$\Theta_\ell(\mu) = \begin{cases} \dfrac{\mu_{\ell+1} - \mu}{\Delta\mu_\ell} & \mu_\ell \leq \mu \leq \mu_{\ell+1} \qquad \ell = 0,1,\ldots,L-1 \\[2ex] \dfrac{\mu - \mu_{\ell-1}}{\Delta\mu_{\ell-1}} & \mu_{\ell+1} \leq \mu \leq \mu_\ell \qquad \ell = 1,2,\ldots,L \\[2ex] 0 & \mu \text{ otherwise} \end{cases}$$

$$\Delta\mu_\ell = \mu_{\ell+1} - \mu_\ell$$

for $0 = \mu_0 < \mu_1 < \ldots < \mu_L = 1$. Note that this representation permits discontinuities in the flux at $\mu=0$ since $\Theta_{\pm 0}(\mu)$ has coefficients $\psi_A(x,\mu_{\pm 0})$. The representation (1.24) enables us to perform analytically the integrations in equation (1.20) and (1.22) involving the singular eigenmodes and the piecewise linear angular flux $\tilde{\psi}_A(x,\mu)$. The computational formulas for (1.20a) and (1.22a), are

(1.20b)
$$a_0^+ = \frac{1}{N_0^+}\int_{-1}^{1} \mu\phi_0^+(\mu)\tilde{\psi}_A(0,\mu)d\mu$$
$$= \frac{1}{N_0^+}\sum_{\ell=0}^{L} \psi_A(0,\mu_{\pm\ell})p_{\pm\ell}(\nu)$$

(1.20c)
$$\tilde{a}_0^- = a_0^- e^{a/\nu_0}$$
$$= \frac{1}{N_0^-}\int_{-1}^{1} \mu\phi_0^-(\mu)\tilde{\psi}_A(a,\mu)d\mu$$
$$= \frac{1}{N_0^-}\sum_{\ell=0}^{L} \psi_A(a,\mu_{\pm\ell})p_{\pm\ell}(\nu)$$

(1.22b)
$$A(\nu) = \frac{1}{N(\nu)}\int_{-1}^{1} \mu\phi_\nu(\mu)\tilde{\psi}_A(0,\mu)d\mu \qquad (0 \le \nu \le 1)$$
$$= g(\nu,c)\sum_{\ell=0}^{L} \psi_A(0,\mu_{\pm\ell})p_{\pm\ell}(\nu)$$

and

(1.22c)
$$\tilde{A}(\nu) = \frac{1}{N(\nu)}\int_{-1}^{1} \mu\phi_\nu(\mu)\tilde{\psi}_A(a,\mu)d\mu \qquad (-1 \le \nu \le 0)$$
$$= g(\nu,c)\sum_{\ell=0}^{L} \psi_A(a,\mu_{\pm\ell})p_{\pm\ell}(\nu)$$

where

$$p_\ell(\nu) = \frac{1}{\nu}\int_{\mu_{\ell-1}}^{\mu_{\ell+1}} \mu\phi_\nu(\mu)\Theta_\ell(\mu)d\mu, \tag{1.26}$$

When $\nu \neq \mu_\ell$, $p_\ell(\nu)$ is defined as follows:

$$p_{\pm\ell}(\nu) = \frac{c}{2}\left\{\begin{array}{ll} p(\nu,\mu_\ell,\mu_{\ell+1}) & \\ p(\nu,\mu_\ell,\mu_{\ell+1}) - p(\nu,\mu_\ell,\mu_{\ell-1}) & \\ \qquad\qquad - p(\nu,\mu_\ell,\mu_{\ell-1}) & \end{array}\right\} + \Theta_\ell(\nu)\lambda(\nu) \quad \begin{array}{l} \ell=+0, \ell=-L \\ \ell=\pm1,\pm2,\ldots, \\ \qquad \pm(L-1) \\ \ell=L,\ \ell=-0 \end{array} \tag{1.27}$$

and when $\nu=\mu_\ell$

$$p_\ell(\mu_\ell) = \frac{c}{2}\left\{\begin{array}{l} -\dfrac{\Delta\mu_\ell}{2} \\ pp(\mu_\ell,\mu_{\ell-1},\mu_{\ell+1}) \\ \qquad -\dfrac{\Delta\mu_{\ell-1}}{2} \end{array}\right\} + \lambda(\mu_\ell) \quad \begin{array}{l} \ell=0 \\ \ell=1,2,\ldots,L-1 \\ \ell=-0 \end{array}$$

where

$$p(\nu,a,b) = \nu - \frac{b-a}{2} + \nu\,\frac{(b-\nu)}{b-a}\log\left|\frac{\nu-a}{b-\nu}\right| \tag{1.29}$$

$$\begin{aligned} pp(\nu,a,b) &= p(\nu,\nu,b) - p(\nu,\nu,a) \\ &= -\frac{(b-a)}{2} + \nu\log\left|\frac{\nu-a}{b-\nu}\right|. \end{aligned} \tag{1.30}$$

Note that $p_L(1)$ and $p_{-L}(-1)$ are undefined since $\lambda(\pm1)$ is undefined. However, we know from analytic considerations that $A(\pm1) = 0$, hence we may omit the calculation of $A(\pm1)$. Note also that both asymptotic and transient modes are treated by formulas (1.26) to (1.29).

1.1.5 Residual checking of the benchmark solution

Two related quantities to the $q_n(x,\mu)$ are available in BEAPAC-1T. They are the elementary angular flux derivative $q_n^{(1)}(x,\mu)$ and the elementary scalar flux $q_n^{(-1)}(x)$.

These quantities have several useful roles. The elementary scalar flux $q_n^{(-1)}(x)$ is defined by

$$q_n^{(-1)}(x) \equiv \int_{-1}^{1} q_n(x,\mu)d\mu \tag{1.31}$$

and computational expressions are derived in Appendix A.3. It may be used to investigate the discretization error and truncation error in the numerical integration of the angular flux. The elementary angular flux derivative is defined as

$$q_n^{(1)}(x,\mu) \equiv \frac{\partial q_n(x,\mu)}{\partial x} \tag{1.32}$$

and computational expressions are derived in Appendix A.2. Given a_n, $q_n^{(-1)}$, and $q_n^{(1)}$ we can calculate the scalar flux

$$\phi_B(x) = \sum_{n=0}^{N} a_{\pm n} q_{\pm n}^{(-1)}(x) \tag{1.33}$$

and the angular flux derivative

$$\frac{\partial \psi_B(x,\mu)}{\partial x} = \sum_{n=0}^{N} a_{\pm n} q_{\pm n}^{(1)}(x,\mu) \tag{1.34}$$

exactly.

Given $\psi_B(x,\mu)$, $\phi_B(x)$, and $\frac{\partial \psi_B(x,\mu)}{\partial x}$ we can compute a residual vector $\underline{r}$ where $\underline{r}$ is defined on a given reference net by

$$L\underline{\psi}_B = \mu \frac{\partial \underline{\psi}_B(x,\mu)}{\partial x} + \underline{\psi}_B(x,\mu) - \frac{c}{2}\underline{\phi}_B(x) = \underline{r} \ . \tag{1.35}$$

The underlined symbols represent computed quantities.

Evaluation of (1.35) provides a method for checking the pointwise accuracy of the elementary solutions $q_n(x,\mu)$. Numerical experiments have consistently shown bounds of the order

$$\|\underline{r}\|_\infty \leq \begin{cases} 10^{-15} & \text{standard basis elements} \\ 10^{-12} & \text{special basis element} \end{cases}$$

1.1.6 Two cell problem considerations

The preceding discussion was directed toward one cell problems. We would like to point out that a variety of interesting problems can be treated in the one cell case. We may solve a large one-dimensional complex reactor configuration by some production code, then successively select cells of interest and analyze the reliability of the solution in each cell with the technique just discussed. In this case, we can observe local boundary and interface effects on the numerical method.

We solve two cell problems to observe the solution behavior at the cell interface where now the flux values are not specified at the interface.

The two cell problem is represented by the operators

$$L^{(i)} = \mu \frac{\partial}{\partial x} + \sigma_i - \frac{\sigma_i c_i}{2} \int_{-1}^{+1} d\mu \qquad (i = I,II) \tag{1.36}$$

and

$$L^{(I)} \psi_B^{(I)}(x,\mu) = S^I \qquad 0 \leq x \leq a \tag{1.37}$$

$$L^{(II)} \psi_B^{(II)}(x,\mu) = S^{II} \qquad a \leq x \leq b \tag{1.38}$$

with interface condition

$$\psi_B^{(I)}(a,\mu) = \psi_B^{(II)}(a,\mu). \tag{1.39}$$

The particular solutions due to the constant sources S^I and S^{II} in each cell are given by

$$\psi_p^{(i)} = \frac{S^i}{\sigma_i(1-c_i)} \qquad (i = I,II). \tag{1.40}$$

The homogeneous solutions $\psi_H^{(I)}(x,\mu)$ and $\psi_H^{(II)}(x,\mu)$ are obtained in turn by the procedures of sections 1.1.3 and 1.1.4, using an initial flux distribution $\psi_A^{(I)}(x,\mu)$ and $\psi_A^{(II)}(x,\mu)$ for the two cells. The benchmark solutions in cells I and II are now

$$\psi_B^{(i)}(x,\mu) = \psi_H^{(i)}(x,\mu) + \psi_p^{(i)} \qquad (i = I,II). \tag{1.41}$$

To satisfy the continuity condition (1.39) an angular dependent source term $Q(\mu)$ is added to cell II.

Let

$$\tilde{\psi}_B^{(II)}(x,\mu) = \psi_B^{(II)}(x,\mu) + (\psi_B^{(I)}(a,\mu) - \psi_B^{(II)}(a,\mu)) \tag{1.42}$$

so that (1.39) is satisfied. Equation (1.38) is now replaced by

$$L^{(II)}\tilde{\psi}_B^{(II)}(x,\mu) = S_{II} + Q(\mu) \tag{1.43}$$

where

$$Q(\mu) = L^{(II)}(\psi_B^{(I)}(a,\mu) - \psi_B^{(II)}(a,\mu)) \ ,$$

i.e.,

$$Q(\mu) = \sigma_{II}(\psi_B^{(I)}(a,\mu) - \psi_B^{(II)}(a,\mu)) - \frac{\sigma_{II}c_{II}}{2}(\phi_B^{(I)}(a)-\phi_B^{(II)}(a)) \tag{1.44}$$

since the derivative term of the operator is zero in this case. The interface condition is now exactly satisfied for $\psi_B^{I}(a,\mu) = \tilde{\psi}_B^{II}(a,\mu)$ by (1.42).

1.2 Solution of Benchmark Problems by Approximate Numerical Methods

We are now ready to test a numerical method to solve the transport equation with the solution ψ_B. BEAPAC-1T contains a set of subroutines for the numerical solution of the transport equation by methods which are widely used. They are all in a standard form. The numerical methods are reduced to the problem of solving a linear matrix equation of the form

$$A\underline{v} = \underline{b}. \tag{1.45}$$

Hence, a particular subroutine contains instructions to calculate the elements of the matrix A and the vector $\underline{b}$. The process is as follows. First, the desired network $D_{IM}(0,a)$ is set up. Then the necessary boundary values $f_1(0,\mu)$ and $f_2(a,\mu)$ are calculated. With this information the elements of A and b are calculated, and the linear equation is solved accurately by a direct method, usually by Gaussian elimination utilizing the band matrix structure. Calculations are performed in single precision on the CDC 6400 and in double precision on the IBM 370/195. A special feature for analyzing the rounding error in the matrix solution is included in the IBM version of BEAPAC-1T. The matrix equation is truncated to single precision values and calculations are performed in single precision arithmetic.

In most cases, the elements of $\underline{v}$ represent the discrete directional fluxes, and are denoted by $\underline{\psi}_C = \psi_C(x_i,\mu_m)$ $i=1,2,\ldots,I$, $m=1,2,\ldots,M$.

The available numerical methods for the various forms of the transport operator are described in Sections II and III.

The user can also interface with BEAPAC-1T, the angular flux results $\underline{\psi}_C$ from existing codes for the numerical solution of the transport equation by preparing the necessary interface files discussed in the users manual (Bareiss and Derstine 1977).

1.3 Error Analysis of Approximate Methods

In Section 1.1 we developed the tools necessary for generating exact benchmark problems with solutions $\psi_B(x,\mu)$. In Section 1.2 it is outlined how we obtain approximate solutions $\underline{\psi}_C$ to these benchmark problems. In this section, the error $\underline{\psi}_E$ of the approximate solution $\underline{\psi}_C$ is calculated using the exact solution $\psi_B(x,\mu)$. Two pointwise error options are available:

(1.46)

a. algebraic flux error $\underline{\psi}_E = \underline{\psi}_B - \underline{\psi}_C$

b. relative flux error $\underline{\psi}_E = \dfrac{\underline{\psi}_B - \underline{\psi}_C}{\underline{\psi}_B}$

Norms available in BEAPAC-1T based on $\underline{\psi}_E$ are:

a. $\|\underline{\psi}_E\|_\infty$: maximum absolute $\underline{\psi}_E$ with associated mesh location, algebraic sign and flux value.

b. $\dfrac{\|\underline{\psi}_E\|_1}{N}$: average absolute $\underline{\psi}_E$
N = number of calculated fluxes

The norms may be computed for a variety of domains.

1. Global : all calculated flux nodes
2. Boundary : boundary and interface flux nodes
3. Interior : interior flux nodes (non-boundary)

(GLOBAL = BOUNDARY ∪ INTERIOR)

The corresponding scalar flux $\underline{\phi}_B$, $\underline{\phi}_C$, or $\underline{\phi}_E$ may be optionally tabulated for any desired set of spatial points.

The objective of coarse mesh error analysis is to obtain quantitative error bounds on the performance of numerical approximation methods. Specific items of interest are boundary condition effects, spatial and angular mesh refinement effects and effects of materials with extreme properties such as strong absorption, strong scattering, or regions with a strong source.

BEAPAC-1T has built into it a special procedure for obtaining a set of K successive mesh refinements of D(0,a), designated $D^k_{IM}(0,a)$, (k = 1,2,...,K). Summaries of the error norms are tabulated for the benchmark problem in a manner that readily shows space angle mesh refinement effects. Detailed flux edits and two-dimensional plots are available for further analysis of the results. Particular examples are given in the sample problems in Sections 2.2 and 3.3.

II. THE STOCHASTIC TRANSPORT EQUATION

2.1 Numerical Methods

2.1.1 The discrete ordinates method with Hermite Birkhoff interpolation

This method uses discrete ordinate approximations in angle and Hermite-Birkhoff Interpolation in the space variable [Bareiss 1956]. It will be denoted by the DB-Method. In one-dimensional slab geometry problems, the discrete ordinates SN-Method widely used [Carlson and Lathrop 1968] is a special case of the DB-Method, limited to linear approximation in space.

The approximation is illustrated by rewriting (1.1) for the multi-cell problem as follows:

$$\frac{\partial\psi(x,\mu)}{\partial x} = \frac{1}{\mu}\left[-\sigma(x)\psi(x,\mu) + \frac{\sigma(x)c(x)}{2}\int_{-1}^{1}\psi(x,\mu')d\mu' + S(x,\mu)\right]. \tag{2.1}$$

We observe that the two point Euler Maclaurin Sum formula [Isaacson and Keller, 1966] yields, by letting $x_{i+1}-x_i = h_i$ $(i=1,2,\ldots,I)$ and $D = \frac{d}{dx}$

$$\begin{aligned}\psi(x_{i+1},\mu) - \psi(x_i,\mu) &= \int_{x_i}^{x_{i+1}} \frac{\partial\psi(x,\mu)}{\partial x}\,dx \\ &= \frac{h_i D}{2}\left[\psi(x_{i+1},\mu) + \psi(x_i,\mu)\right] \\ &\quad - \left[\frac{h_i^2D^2}{12} - \frac{h_i^4D^4}{720} + \frac{h_i^6D^6}{30240} - \cdots\right]\left[\psi(x_{i+1},\mu) - \psi(x_i,\mu)\right].\end{aligned} \tag{2.2}$$

Equation (2.2) is equivalent to a two-point Hermite Birkhoff interpolation with subsequent integration.

We solve (2.1) by the discrete ordinates method, hence we approximate the integral by numerical integration methods including single or double Gauss quadrature. Therefore, (2.1) becomes a system of discrete first order differential equations.

(2.3a) $$D\underline{\psi} = M^{-1}[-\sigma I + \frac{\sigma c}{2} W]\underline{\psi} + M^{-1}\underline{S}$$

where

$$M = \begin{bmatrix} \mu_1 & & & & \\ & \mu_2 & & & \\ & & \ddots & & \\ & & & \ddots & \\ & & & & \mu_M \end{bmatrix}, \quad \underline{\psi} = \begin{bmatrix} \psi_1(x) \\ \psi_2(x) \\ \vdots \\ \psi_M(x) \end{bmatrix}$$

and

$$W = \begin{bmatrix} w_1 w_2 \cdots w_M \\ w_1 w_2 \cdots w_M \\ \vdots \quad \vdots \quad \vdots \\ w_1 w_2 \cdots w_M \end{bmatrix}, \quad \underline{S} = \begin{bmatrix} S_1(x) \\ S_2(x) \\ \vdots \\ S_M(x) \end{bmatrix}$$

σ and c are assumed constant within a cell. Therefore the kth power of (2.3a) evaluated at the endpoints of cell i (i.e., $x_{i+} \leq x \leq x_{i+1}-$), and cell i-1 (i.e., $x_{i-1}+ \leq x \leq x_i-$) is given at $x = x_i$ by

(2.3b) $$D^k \underline{\psi}_{i+} = A_i^k \underline{\psi}_i + \underline{b}_{i+}^{(k)}$$

$$D^k \underline{\psi}_{i-} = A_{i-1}^k \underline{\psi}_i + \underline{b}_{i-}^{(k)}$$

where

(2.5a) $$A_i = M^{-1}[-\sigma_i I + \frac{\sigma_i c_i}{2} W]$$

(2.5b) $$\underline{b}_{i\pm}^{(k)} = M^{-1} \sum_{j=0}^{k-1} \frac{\partial^j}{\partial x^j} \underline{S}(x) \Big|_{x = x_{i\pm}}$$

$$\sigma_i = \sigma(x_i), \quad c_i = c(x_i).$$

The assumption that $S_m(x)$ is constant within a mesh cell implies that $\partial^j S/\partial x^j = 0$ for $j > 0$. Thus

$$\text{(2.5c)} \qquad \underline{b}_{i^\pm}^{(k)} = M^{-1}\underline{S}_{i^\pm} \qquad \text{where } \underline{S}_{i^\pm} = \underline{S}(x_{i^\pm}) \ .$$

Substituting (2.3b) into (2.2) yields a system of linear equations for $\psi_m(x_i) = \psi(x_i,\mu_m)$ $(i=1,2,\ldots,I)$, $(m=1,2,\ldots,M)$. We write this system for cell i as follows, letting $x_i \equiv x_{i^+}$ and $x_{i+1} \equiv x_{i+1^-}$.

$$\text{(2.6)} \qquad E_i\underline{\psi}_i + H_i\underline{\psi}_{i+1} = \underline{g}_i \qquad (i=1,2,\ldots,I-1)$$

where

$$\text{(2.7a)} \qquad H_i = \left[I - \frac{h_iA_i}{2} + \frac{h_i^2}{12}A_i^2 - \frac{h_i^4}{720}A_i^4 + \ldots\right]$$

$$\text{(2.7b)} \qquad E_i = -H_i - h_iA_i$$

$$\text{(2.7c)} \qquad \underline{g}_i = \frac{h_i}{2}\left(\underline{b}_{i+1}^{(1)} + \underline{b}_i^{(1)}\right) - \frac{h_i^2}{12}\left(\underline{b}_{i+1}^{(2)} - \underline{b}_i^{(2)}\right) + \frac{h_i^4}{720}\left(\underline{b}_{i+1}^{(4)} - \underline{b}_i^{(4)}\right)$$

$$= h_iM^{-1}\underline{S}_i \ .$$

The last two terms of (2.7c) are zero, since we assume a piecewise constant source $S_m(x)$ for $x_i \le x \le x_{i+1}$. Combining the equations (2.6) and (2.7) with the boundary conditions into matrix form we obtain

$$\text{(2.8)} \qquad \begin{bmatrix} B_1 & & & & & 0 \\ E_1 & H_1 & & & & \\ & E_2 & H_2 & & & \\ & & \cdot & \cdot & & \\ & & & \cdot & \cdot & \\ & & & & E_{I-1} & H_{I-1} \\ 0 & & & & & B_2 \end{bmatrix} \begin{bmatrix} \underline{\psi}_1 \\ \underline{\psi}_2 \\ \cdot \\ \cdot \\ \cdot \\ \cdot \\ \underline{\psi}_I \end{bmatrix} = \begin{bmatrix} \underline{f}_1 \\ \underline{g}_1 \\ \underline{g}_2 \\ \cdot \\ \cdot \\ \cdot \\ \cdot \\ \underline{g}_{I-1} \\ \underline{f}_2 \end{bmatrix}$$

The matrices E_i and H_i have exactly the same configuration independent of the order of approximation (i.e. power in A^k). B_1 and B_2 are the $\frac{M}{2}$ x M boundary condition matrices defined by

$$(2.9) \qquad B_1 = \begin{bmatrix} \alpha & & & & & \beta \\ & \alpha & & & \beta & \\ & & \ddots & \ddots & & \\ & & \ddots & \ddots & & \\ & & & \alpha & \beta & \end{bmatrix}, \quad B_2 = \begin{bmatrix} & & & \beta & \alpha & \\ & & \beta & & \alpha & \\ & \ddots & & & & \ddots \\ \ddots & & & & & \ddots \\ \beta & & & & & \alpha \end{bmatrix}$$

where

$$(2.10) \qquad (\alpha,\beta) = \begin{cases} (1,0) \text{ for incident flux boundary condition} \\ (1,-1) \text{ for reflecting flux boundary condition.} \end{cases}$$

$\underline{f}_1$ and $\underline{f}_2$ are inhomogeneous boundary source vectors of dimension $\frac{M}{2}$ defined by

$$(2.11a) \qquad f_1(\mu_m) = \begin{cases} \psi_B(0,\mu_m) & \mu_m > 0 \quad \text{incident} \\ \psi_B(0,\mu_m) - \psi_B(0,-\mu_m) & \mu_m > 0 \quad \text{reflected} \end{cases}$$

$$(2.11b) \qquad f_2(\mu_m) = \begin{cases} \psi_B(a,\mu_m) & \mu_m < 0 \quad \text{incident} \\ \psi_B(a,\mu_m) - \psi_B(a,-\mu_m) & \mu_m < 0 \quad \text{reflected} \end{cases}$$

First, third or fifth order approximations are obtained by truncating (2.7a) after the second, third or fourth terms, respectively. Then (2.6) becomes

$$(2.12) \qquad E_i^{(k)} \underline{\psi}_i + H_i^{(k)} \underline{\psi}_{i+1} = \underline{g}_i \qquad (i=1,2,\ldots,I), \ (k=1,3,5)$$

where the superscript k denotes the order of approximation.

Block tridiagonal Gaussian elimination is employed by partitioning the subblocks in (2.8) such that the following structure is obtained.

$$(2.13)\qquad \begin{bmatrix} D_1 & C_1 & & & 0 \\ A_2 & B_2 & C_2 & & \\ & A_3 & B_3 & C_3 & \\ & & \cdot & \cdot & \\ & & & \cdot & \cdot \\ 0 & & & A_I & D_I \end{bmatrix}$$

A_i and C_i have dimension $M \times \frac{M}{2}$ and B_i has dimension $M \times M$. Boundary condition submatrices D_1, C_1, A_I and D_I have dimension $\frac{M}{2} \times \frac{M}{2}$. The matrices are stored in a rectangular array with dimension $IM \times 2M$.

2.1.2 The discrete ordinates method with Galerkin Finite Element method in space

The approximation method discussed is a discrete ordinates method in the directional variable μ with a Galerkin Finite Element approximation in the spatial variable x. We denote this method by the DGF method.

Let

$$(2.14)\qquad L\psi(x,\mu) = S(x,\mu) \qquad \begin{array}{l} 0 \le x \le a \\ -1 \le \mu \le 1 \end{array}$$

represent Eq. (1.1). $\psi(x,\mu)$ is expanded in a set of piecewise linear Chapeau functions $\{\Theta_i(x)\}$ as follows:

$$(2.15)\qquad \psi(x,\mu) = \sum_{i=1}^{I} b_i(\mu)\Theta_i(x) \qquad 0 \le x \le a$$

where $\{\Theta_i(x)\}$ is defined as in (1.25). The DGF method finds solutions $\psi(x,\mu)$ which satisfy the weak (Galerkin) form of (2.14) [Strang and Fix, 1973] given by

$$(2.16)\qquad \langle\Theta_i(x),\ L\psi(x,\mu)\rangle = \langle\Theta_i(x),\ S(x,\mu)\rangle \quad (i = 1,2,\ldots,I)$$

where

$$<\cdot> = \int_{x_{i-1}}^{x_{i+1}} dx \ .$$

Application of the discrete ordinates approximation to (2.16) leads to a set of IM equations

$$(2.17) \qquad <\Theta_i(x),\ L\psi(x,\mu_m)> = <\Theta_i(x),\ S(x,\mu_m)> \qquad \begin{pmatrix} i = 1,2,\ldots,I \\ m = 1,2,\ldots,M \end{pmatrix}$$

which upon substitution of (2.15) becomes

$$(2.18) \quad <\Theta_i(x),\ \left(\mu_m \frac{d}{dx} + \sigma(x)\right) \sum_{k=1}^{I} b_{km}\Theta_k(x) - \frac{\sigma(x)c(x)}{2} \sum_{m'=1}^{M} w_{m'} \sum_{k=1}^{I} b_{km'}\Theta_k(x)>$$

$$= <\Theta_i(x),\ S(x,\mu_m)> \ .$$

The discrete ordinates approximation is derived by evaluating the angular flux distribution in a number of discrete directions; hence the scattering integral in the ith equation is approximated by

$$\int_{-1}^{1} d\mu b_i(\mu) \approx \sum_{m=1}^{M} w_m b_{im} \ .$$

The numerical integration is usually double Gauss quadrature.

It is easily shown that

$$b_{im} \equiv b_i(\mu_m) = \psi(x_i,\mu_m)$$

since $\qquad \Theta_i(x_i) = 1, \quad \Theta_j(x_i) = 0 \quad \text{for} \quad i \neq j.$

The matrix representation of (2.18) becomes

$$(2.19) \qquad K\underline{\psi} = \underline{g} \ .$$

Here

$$(2.20a)\qquad K = \begin{bmatrix} K_{11} & K_{12} & & & \\ K_{21} & K_{22} & K_{23} & & \\ \cdot & \cdot & \cdot & & \\ & \cdot & \cdot & \cdot & \\ & & \cdot & \cdot & \cdot \\ K_{I-1,I-2} & K_{I-1,I-1} & K_{I-1,I} & & \\ & K_{I,I-1} & K_{II} & & \end{bmatrix}, \quad \underline{\psi} = \begin{bmatrix} \underline{\psi}(x_1) \\ \underline{\psi}(x_2) \\ \cdot \\ \cdot \\ \cdot \\ \cdot \\ \underline{\psi}(x_I) \end{bmatrix}, \quad \underline{g} = \begin{bmatrix} \underline{g}_1(x) \\ \underline{g}_2(x) \\ \cdot \\ \cdot \\ \cdot \\ \cdot \\ \underline{g}_I(x) \end{bmatrix}$$

and

$$(2.20b)\qquad K_{ik} = k_{ik}^{(1)}M + k_{ik}^{(0)-}\cdot\sigma_{i-1}\left(I - \frac{c_{i-1}}{2}W\right) + k_{ik}^{(0)+}\cdot\sigma_i\left(I - \frac{c_i}{2}W\right)$$

where I is the identity matrix, $M = \mathrm{diag}(\mu_m)$ $(m = 1,2,\ldots,M)$ and

$$W = \begin{bmatrix} w_1 & w_2 & \cdots & w_M \\ w_1 & w_2 & \cdots & w_M \\ \cdot & \cdot & & \cdot \\ \cdot & \cdot & & \cdot \\ \cdot & \cdot & & \cdot \\ w_1 & w_2 & \cdots & w_M \end{bmatrix}$$

except for i=1, where the first M/2 rows in K_{11} and K_{12} are the (M/2 xM) matrices B_{11} and B_{12} respectively, and for i=I, where the last M/2 rows in $K_{I,I-1}$ and $K_{I,I}$ are the (M/2 xM) matrices B_{21} and B_{22} as defined below. The $k_{ik}^{(0)\pm}$ are defined so that

$$\langle\Theta_i(x),\ \Theta_k(x)\rangle = k_{ik}^{(0)-} + k_{ik}^{(0)+}$$

where

$$(2.21a)\qquad k_{ik}^{(0)-} = \int_{x_{i-1}}^{x_i} \Theta_i(x)\Theta_k(x)\,dx = \frac{\Delta x_{i-1}}{3}\begin{cases} 1 & 1<i=k\leq I \\ \frac{1}{2} & i=k-1 \\ 0 & \text{otherwise} \end{cases}$$

and

$$(2.21b)\qquad k_{ik}^{(0)+} = \int_{x_i}^{x_{i+1}} \Theta_i(x)\Theta_k(x)\,dx = \frac{\Delta x_i}{3}\begin{cases} 1 & 1\leq i=k<I \\ \frac{1}{2} & i=k+1 \\ 0 & \text{otherwise} \end{cases}$$

The $k_{ik}^{(1)}$ are defined so that

$$(2.21c)\qquad k_{ik}^{(1)} = \langle\Theta_i(x),\ \Theta_k'(x)\rangle = \tfrac{1}{2}\cdot\begin{cases} 0 & 1<i=k<I \\ 1 & i=k-1 \text{ or } i=k=I \\ -1 & i=k+1 \text{ or } i=k=1 \\ 0 & \text{otherwise} \end{cases}$$

Boundary conditions $B\psi(x,\mu) = f(x,\mu)$ at $x=0$, $\mu>0$ and $x=1$, $\mu<0$ are incorporated into the matrix K in (2.20a) by defining the first M/2 rows of K_{11} and K_{12} by B_{11} and B_{12} and the last M/2 rows of K_{II-1} and K_{II} by B_{21} and B_{22}.

B_{11} and B_{12} are the left side (x=0) boundary condition matrices and B_{21} and B_{22} are the right side (x=a) boundary condition matrices defined for incident or reflected flux boundary conditions so that

$$(2.22a)\qquad B_{11} = \begin{bmatrix} 1 & & & & & & & \beta \\ & 1 & & & & & \beta & \\ & & \cdot & & & \cdot & & \\ & & & \cdot & \cdot & & & \\ & & & \cdot & \cdot & & & \\ & & & 1 & \beta & & & \end{bmatrix},\quad B_{12} = 0$$

$$\beta = \begin{cases} 0 & \text{incident flux} \\ 1 & \text{reflected flux} \end{cases}$$

$$(2.22b)\qquad B_{22} = \begin{bmatrix} & & & \beta & 1 & & \\ & & \beta & & & 1 & \\ & \cdot & & & & & \cdot \\ \cdot & & & & & \cdot & \\ \beta & & & & & & 1 \end{bmatrix},\quad B_{21} = 0$$

$\underline{\psi}^T(x_i)$ is defined so that

$$(2.23a)\qquad \underline{\psi}^T(x_i) = [\psi(x_i,\mu_1),\ \psi(x_i,\mu_2),\ldots,\psi(x_i,\mu_M)]$$

and $\underline{g}_i(x) = (g_{im})$ is defined so that

$$(2.23b)\qquad g_{im} = \langle\Theta_i(x),\ S(x,\mu_m)\rangle = \tfrac{1}{2}\cdot\begin{cases} \Delta x_1 S_1(\mu_m) \\ \Delta x_{i-1} S_{i-1}(\mu_m) + \Delta x_i S_i(\mu_m) \\ \Delta x_I S_I(\mu_m) \end{cases}$$

except that the corresponding inhomogeneous boundary condition terms

$f_1(\mu_m)$ and $f_2(\mu_m)$ replace g_{1m}, $m = 1,\ldots,M/2$ and g_{Im}, $m = M/2 + 1,\ldots,M$ respectively. $f_1(\mu_m)$ and $f_2(\mu_m)$ are defined so that for $\mu > 0$

$$f_1(\mu) = \begin{cases} \psi_B(0,\mu) & \text{incident flux} \\ \psi_B(0,\mu) - \psi_B(0,-\mu) & \text{reflected flux} \end{cases} \qquad (\mu > 0) \tag{2.24a}$$

and for $\mu < 0$,

$$f_2(\mu) = \begin{cases} \psi_B(a,\mu) & \text{incident flux} \\ \psi_B(a,\mu) - \psi_B(a,-\mu) & \text{reflected flux} \end{cases} \qquad (\mu < 0) \tag{2.24b}$$

K is a block tridiagonal matrix which is stored in a rectangular array of dimensions IM x 3M. The system of equations (2.19) is solved by block Gauss elimination.

2.2 Examples of the Benchmark Problem Error Analysis Procedures

Four monoenergetic slab benchmark problems with isotropic scattering (denoted by BP1, BP2, BP3 and BP4) are presented which illustrate several types of investigations which may be performed using BEAPAC-1T. BP1 and BP2 are one-cell benchmark problems with angular flux solutions $\psi_B(x,\mu)$ given by an asymptotic and transient Case eigenmode respectively. BP3 and BP4 are benchmark problems whose solutions are linear combinations of asymptotic and transient Case eigenmodes. The latter two problems illustrate the automatic procedure (section 1.1.4) for obtaining the eigenmode combining coefficients. This procedure employs the Householder least squares solution of an overdetermined system of equations and is shown to be a prototype of a new numerical solution method.

2.2.1 Benchmark Problem #1, an asymptotic eigenmode

BP1 is defined in the unit cell $0 \leq x \leq 1$ with angular direction cosines $|\mu| \leq 1$. The cell composition is defined by the total cross section $\sigma = 1$, the asymptotic eigenvalue $\nu_0 = 1.05$ (i.e. $c \doteq .5129$ by Eq. (1.6)) and isotropic source $S = 0$. The benchmark solution $\psi_B(x,\mu)$ is defined from Eq. (1.4b) with $a_0^+ = 1$ and all other combining coefficients zero. Incident flux boundary conditions are defined by $\psi_B(x,\mu)$ evaluated at the boundaries. Figures 2.1a,b,c illustrate respectively the scalar flux $\phi_B(x)$ and the angular flux traverses of $\psi_B(x,\mu)$ along x for μ fixed and along μ for x fixed.

The numerical methods denoted by DB1, DB3 and DGF corresponding to the first (SN-Method) and third order discrete ordinate Hermite Birkhoff method and the discrete ordinate Galerkin finite element method respectively are applied to BP1 for successive sets of space/angle mesh discretization. Five spatial refinements $h = 1/I$ (I=1,2,4,8,16) and four double Gauss ($DP_{N/2}$, N=2,4,8,16) quadrature sets define twenty problems.

The numerical results for the twenty discretized problems are tabulated in Tables 2.1, 2.2, 2.3 and 2.4. Each table contains three

(a)

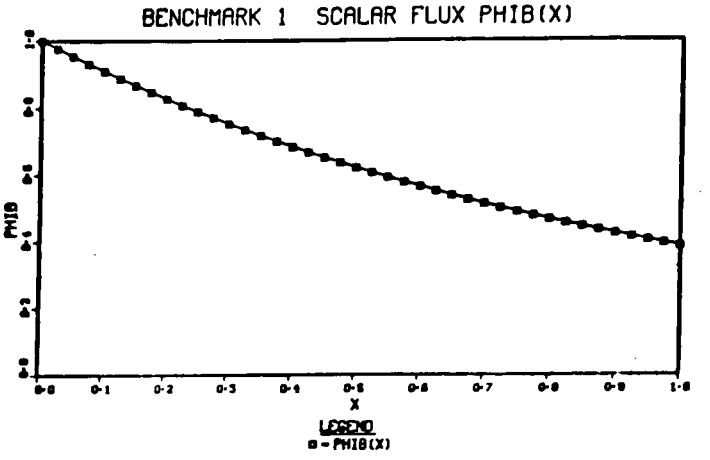

(b)

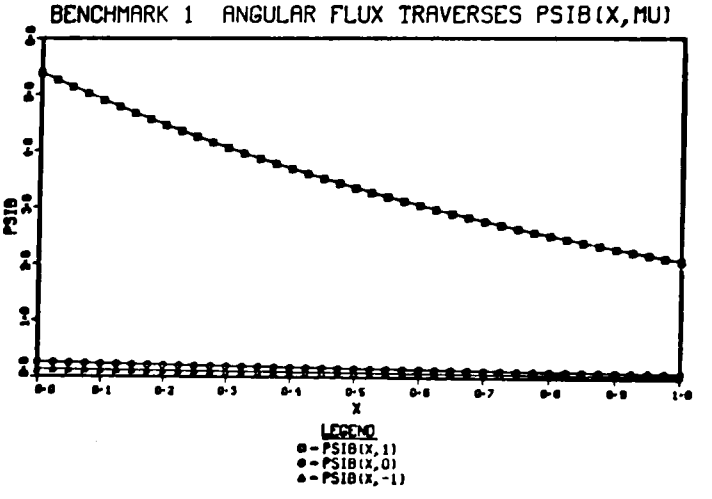

(c)

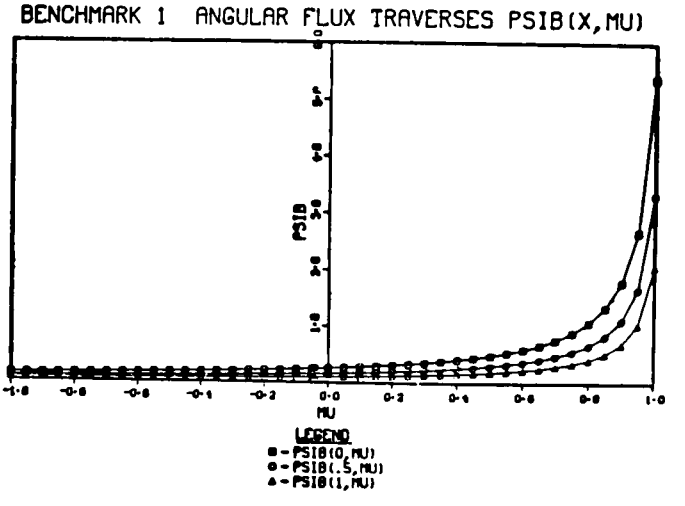

Figure 2.1. Flux Distributions for Benchmark #1
(a) Scalar flux $\phi_B(x)$
(b) Angular flux traverse $\psi_B(x,\mu)$ along x for fixed μ
(c) Angular flux traverse $\psi_B(x,\mu)$ along μ for fixed x

Table 2.1. Maximum absolute signed scalar flux error $\pm\|\underline{\phi}_E\|_\infty$ tabulated for twenty space/angle discretization sets of Benchmark #1 for the DB1, DB3 and DGF methods

BEAPAC 05/76 BP#1.1 ASYMPTOTIC SOLUTION A0+=1,NU0=1.05,X:(0,1),BC(I,I),S=0

MAX. ABS. SCALAR FLUX ERROR AND LOCATION (GLOBAL)

I: NO. OF XMESH INTERVALS J: NO. OF MU POINTS

(a) DB1

I	J: 2	4	8	16
ERROR 1	4.14D-01	1.82D-01	4.12D-02	2.50D-02
EXACT	1.000	1.000	0.386	0.386
X LOC	0.0	0.0	1.000	1.000
ERROR 2	4.13D-01	1.79D-01	3.28D-02	6.17D-03
EXACT	1.000	1.000	1.000	0.621
X LOC	0.0	0.0	0.0	0.500
ERROR 4	4.12D-01	1.79D-01	3.32D-02	2.12D-03
EXACT	1.000	1.000	1.000	0.490
X LOC	0.0	0.0	0.0	0.750
ERROR 8	4.12D-01	1.79D-01	3.33D-02	1.14D-03
EXACT	1.000	1.000	1.000	0.700
X LOC	0.0	0.0	0.0	0.375
ERROR 16	4.12D-01	1.79D-01	3.33D-02	1.05D-03
EXACT	1.000	1.000	1.000	0.942
X LOC	0.0	0.0	0.0	0.063

BEAPAC 05/76 BP#1.2 ASYMPTOTIC SOLUTION A0+=1,NU0=1.05,X:(0,1),BC(I,I),S=0

MAX. ABS. SCALAR FLUX ERROR AND LOCATION (GLOBAL)

I: NO. OF XMESH INTERVALS J: NO. OF MU POINTS

(b) DB3

I	J: 2	4	8	16
ERROR 1	4.12D-01	1.78D-01	3.30D-02	1.05D-03
EXACT	1.000	1.000	1.000	1.000
X LOC	0.0	0.0	0.0	0.0
ERROR 2	4.12D-01	1.79D-01	3.33D-02	1.03D-03
EXACT	1.000	1.000	1.000	1.000
X LOC	0.0	0.0	0.0	0.0
ERROR 4	4.12D-01	1.79D-01	3.33D-02	1.03D-03
EXACT	1.000	1.000	1.000	1.000
X LOC	0.0	0.0	0.0	0.0
ERROR 8	4.12D-01	1.79D-01	3.33D-02	1.03D-03
EXACT	1.000	1.000	1.000	1.000
X LOC	0.0	0.0	0.0	0.0
ERROR 16	4.12D-01	1.79D-01	3.33D-02	1.03D-03
EXACT	1.000	1.000	1.000	1.000
X LOC	0.0	0.0	0.0	0.0

BEAPAC 05/76 BP#1.4 ASYMPTOTIC SOLUTION A0+=1,NU0=1.05,X:(0,1),BC(I,I),S=0

MAX. ABS. SCALAR FLUX ERROR AND LOCATION (GLOBAL)

I: NO. OF XMESH INTERVALS J: NO. OF MU POINTS

(c) DGF

I	J: 2	4	8	16
ERROR 1	3.97D-01	1.66D-01	2.01D-02	-2.56D-02
EXACT	1.000	1.000	1.000	0.386
X LOC	0.0	0.0	0.0	1.000
ERROR 2	4.10D-01	1.77D-01	3.77D-02	1.28D-02
EXACT	1.000	1.000	0.621	0.621
X LOC	0.0	0.0	0.500	0.500
ERROR 4	4.12D-01	1.78D-01	3.37D-02	4.16D-03
EXACT	1.000	1.000	0.788	0.788
X LOC	0.0	0.0	0.250	0.250
ERROR 8	4.12D-01	1.78D-01	3.33D-02	1.85D-03
EXACT	1.000	1.000	0.888	0.888
X LOC	0.0	0.0	0.125	0.125
ERROR 16	4.12D-01	1.79D-01	3.34D-02	1.25D-03
EXACT	1.000	1.000	0.942	0.942
X LOC	0.0	0.0	0.063	0.063

subtables (a,b,c) corresponding to the three methods listed above. The entries to Tables 2.1a,b,c have the three following items for each of the twenty problems:

(1) ERROR: the maximum absolute pointwise scalar flux error $\|\underline{\phi}_E\|_\infty$ with associated algebraic sign

(2) EXACT: the exact scalar flux solution $\phi_B(x)$ at the ERROR location

(3) X LOC: the mesh point coordinate of the ERROR

Reading the rows of the table from left to right corresponds to an increasing number of angular mesh refinements (J=2,4,8,16) for a fixed spatial mesh I. Reading the columns of the table from top to bottom corresponds to an increasing number of spatial mesh refinements (I=1,2,4,8,16) for a fixed angular discretization J. For example, the entry in Table 2.1a for 8 angles and 4 spatial mesh intervals has the maximum absolute scalar flux ERROR 3.32D-02 associated with the EXACT scalar flux of 1.000 at X LOC x=0 in the cell.

Within a given row or column of 2.1a the error for DB1 converges, but not to zero, as the corresponding refinement increases. On each table of 2.1, the spatial mesh convergence is indicated by connected line segments. Mesh refinements chosen below this line are clearly not warranted.

The results in Table 2.1a and 2.1b clearly illustrate the faster spatial convergence of the DB3 method compared to the DB1 method. The spatial error convergence for the DGF method, Table 2.1c, is slower than the DB1 method. In this problem where the scattering and absorption are nearly equal we see that the asymptotic solution in Fig. 2.1c has an extremely high gradient with respect to μ near $\mu = 1$. This means a large number of angular points will be required to obtain an accurate scalar flux. Notice that with eight double Gauss angles the error in the scalar flux is about 3% for a mesh discretization of .5 mean free paths; for 4 angles the error is at least 18%. Figures 2.2a,b,c display the pointwise scalar flux error $\underline{\phi}_E$ for the three solution methods under consideration for eight of the twenty problems. The problems displayed

(a) DB1

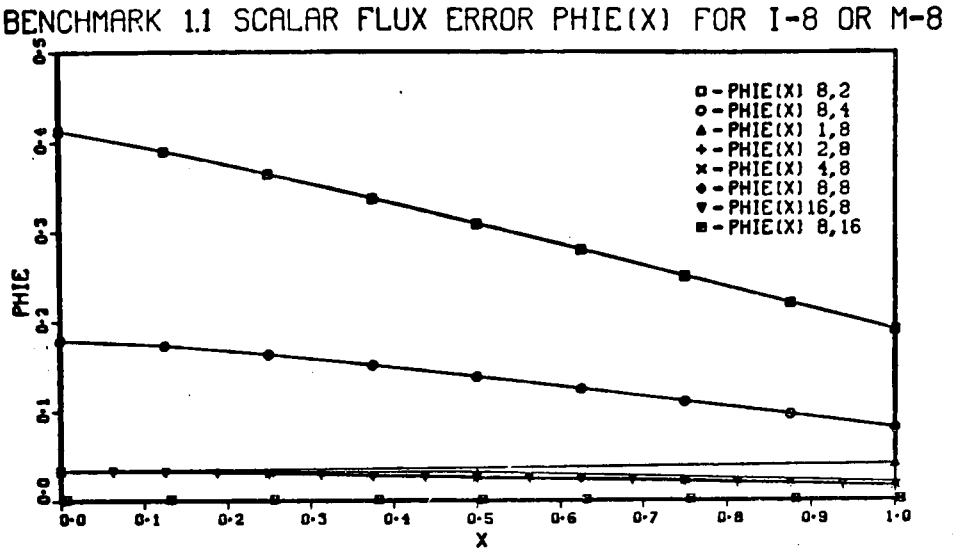

(b) DB3

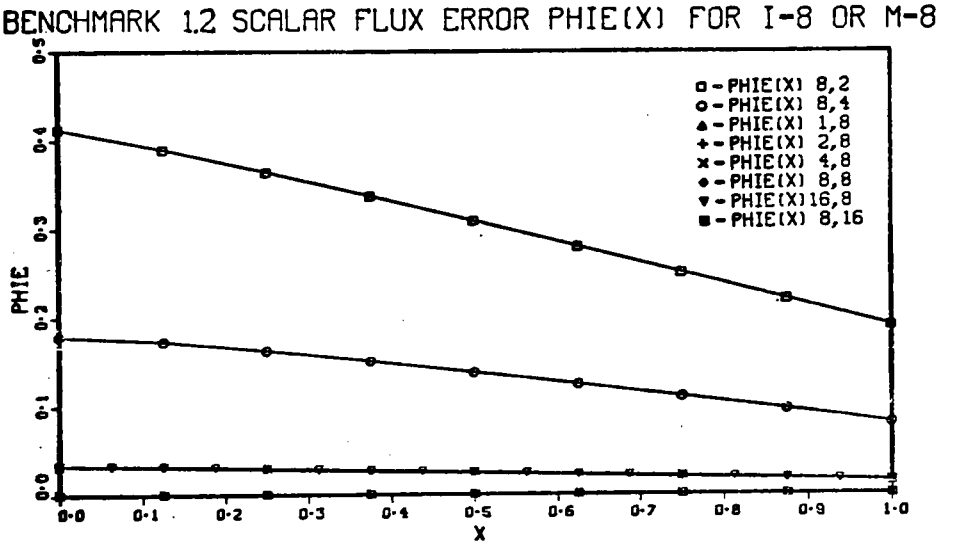

(c) DGF

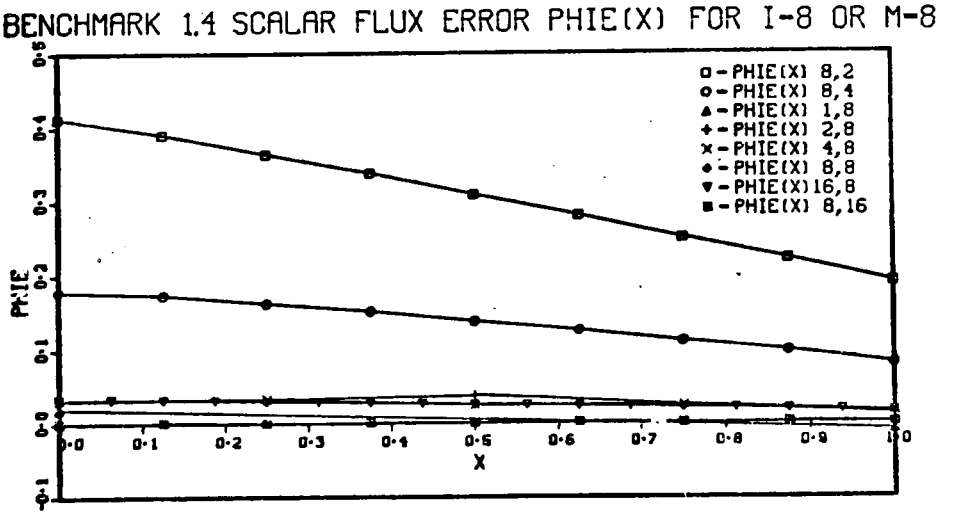

Figure 2.2. Scalar flux error $\underline{\phi}_E$ for DB1, DB3 and DGF methods for eight selected discretizations of Benchmark #1

correspond to the four problems with spatial mesh I = 8 and the five problems with angular mesh M = 8 (i.e. column 3 and row 4 in Tables 2.1a,b,c). The most significant error reductions occur as the number of angles are increased. For the fixed quadrature set of eight angles the scalar flux error shows negligible improvement with increased number of mesh cells.

It is evident from these results that the angular approximation is the major factor in the error performance and that high order spatial methods are of secondary interest.

The angular flux error performance is also available and Tables 2.2a,b,c tabulate the maximum absolute pointwise angular flux error $\|\underline{\psi}_E\|_\infty$ with algebraic sign.

Tables 2.2a,b,c are organized similar to Tables 2.1a,b,c with one additional entry:

MULOC: the angular coordinate of the maximum flux error

The angular flux error tables illustrate the same general error convergence patterns as in the scalar flux case. The error is not weighted in this case, therefore the angular location must be considered when applying the error contribution to the scalar flux. Figures 2.3a,b,c, 2.4a,b,c and 2.5a,b,c illustrate the angular flux error traverse along the μ axis for three fixed x values (0.,.5,1.). Each figure has three subplots corresponding to the three methods under consideration. The same subset of eight problems is chosen for illustration as in Fig. 2.2. The qualitative error behaviour is similar to that observed when studying the scalar flux error; the angular approximation is critical. Note that at the cell boundaries the error for the incident flux is zero since incident flux boundary conditions are employed.

Tables 2.3a,b,c and 2.4a,b,c are two additional tables available to study the average pointwise scalar flux error and the relative sum error of the pointwise flux errors for the (global and boundary) domain for the twenty discretization sets. For the three methods the average flux error converges to equivalent limits, but the convergence is more rapid for DB3.

The relative sum error illustrates the superior accuracy of DB3 to DB1 or DB4.

Table 2.2. Maximum absolute signed angular flux error $\pm\|\psi_E\|_\infty$ tabulated for twenty space/angle discretization sets of Benchmark #1 for the DB1, DB3 and DGF methods

(a) DB1

BEAPAC 05/76 BP#1.1 ASYMPTOTIC SOLUTION A0+=1,BU0=1.05,X:(0,1),BC(I,I),S=0

MAX. ABS. VECTOR FLUX ERROR AND LOCATION (GLOBAL)

I: NO. OF MESH INTERVALS J: NO. OF SU POINTS

I	J: 2	4	8	16
ERROR 1	9.29D-02	5.83D-02	7.38D-02	1.19D-01
EXACT	0.189	0.398	0.870	1.487
X LOC	1.000	1.000	1.000	1.000
BULOC	0.500	0.789	0.931	0.980
ERROR 2	7.61D-02	4.66D-02	2.01D-02	2.75D-02
EXACT	0.174	0.199	0.870	1.487
X LOC	0.0	0.500	1.000	1.000
BULOC	-0.500	0.211	0.931	0.980
ERROR 4	7.58D-02	4.20D-02	1.08D-02	6.83D-03
EXACT	0.174	0.213	0.216	1.487
X LOC	0.0	0.0	0.250	1.000
BULOC	-0.500	-0.211	0.069	0.980
ERROR 8	7.57D-02	4.19D-02	8.43D-03	1.79D-03
EXACT	0.174	0.213	0.241	1.487
X LOC	0.0	0.0	0.0	1.000
BULOC	-0.500	-0.211	-0.069	0.980
ERROR 16	7.57D-02	4.19D-02	8.43D-03	5.37D-04
EXACT	0.174	0.213	0.241	1.487
X LOC	0.0	0.0	0.0	1.000
BULOC	-0.500	-0.211	-0.069	0.980

(b) DB3

BEAPAC 05/76 BP#1.2 ASYMPTOTIC SOLUTION A0+=1,BU0=1.05,X:(0,1),BC(I,I),S=0

MAX. ABS. VECTOR FLUX ERROR AND LOCATION (GLOBAL)

I: NO. OF MESH INTERVALS J: NO. OF SU POINTS

I	J: 2	4	8	16
ERROR 1	7.57D-02	4.08D-02	7.15D-03	-1.59D-03
EXACT	0.174	0.213	0.195	1.487
X LOC	0.0	0.0	0.0	1.000
BULOC	-0.500	-0.211	-0.330	0.980
ERROR 2	7.57D-02	4.18D-02	8.31D-03	2.58D-04
EXACT	0.174	0.213	0.241	0.234
X LOC	0.0	0.0	0.0	0.0
BULOC	-0.500	-0.211	-0.069	-0.102
ERROR 4	7.57D-02	4.19D-02	8.43D-03	2.63D-04
EXACT	0.174	0.213	0.241	0.252
X LOC	0.0	0.0	0.0	0.0
BULOC	-0.500	-0.211	-0.069	-0.020
ERROR 8	7.57D-02	4.19D-02	8.43D-03	2.65D-04
EXACT	0.174	0.213	0.241	0.252
X LOC	0.0	0.0	0.0	0.0
BULOC	-0.500	-0.211	-0.069	-0.020
ERROR 16	7.57D-02	4.19D-02	8.43D-03	2.65D-04
EXACT	0.174	0.213	0.241	0.252
X LOC	0.0	0.0	0.0	0.0
BULOC	-0.500	-0.211	-0.069	-0.020

(c) DGF

BEAPAC 05/76 BP#1.4 ASYMPTOTIC SOLUTION A0+=1,BU0=1.05,X:(0,1),BC(I,I),S=0

MAX. ABS. VECTOR FLUX ERROR AND LOCATION (GLOBAL)

I: NO. OF MESH INTERVALS J: NO. OF SU POINTS

I	J: 2	4	8	16
ERROR 1	6.02D-02	3.09D-02	-6.79D-02	-1.22D-01
EXACT	0.174	0.213	0.870	1.487
X LOC	0.0	0.0	1.000	1.000
BULOC	-0.500	-0.211	0.931	0.980
ERROR 2	7.33D-02	4.03D-02	2.43D-02	3.58D-02
EXACT	0.174	0.199	1.400	2.398
X LOC	0.0	0.500	0.500	0.500
BULOC	-0.500	0.211	0.931	0.980
ERROR 4	7.51D-02	4.10D-02	9.26D-03	9.61D-03
EXACT	0.174	0.213	0.216	3.038
X LOC	0.0	0.0	0.250	0.250
BULOC	-0.500	-0.211	0.069	0.980
ERROR 8	7.55D-02	4.16D-02	8.34D-03	2.51D-03
EXACT	0.174	0.213	0.214	3.422
X LOC	0.0	0.0	0.125	0.125
BULOC	-0.500	-0.211	-0.069	0.980
ERROR 16	7.57D-02	4.18D-02	8.37D-03	6.86D-04
EXACT	0.174	0.213	0.241	1.579
X LOC	0.0	0.0	0.0	0.938
BULOC	-0.500	-0.211	-0.069	0.980

(a) DB1

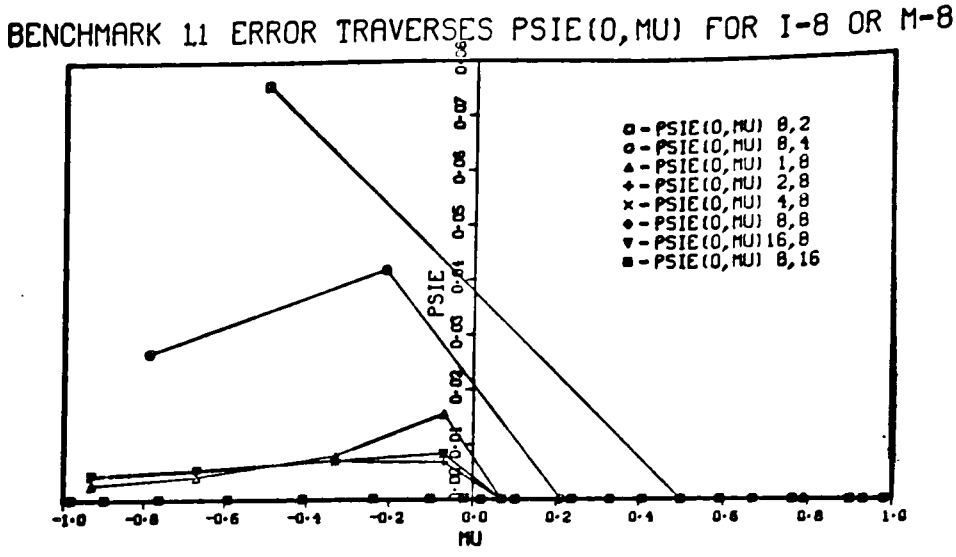

(b) DB3

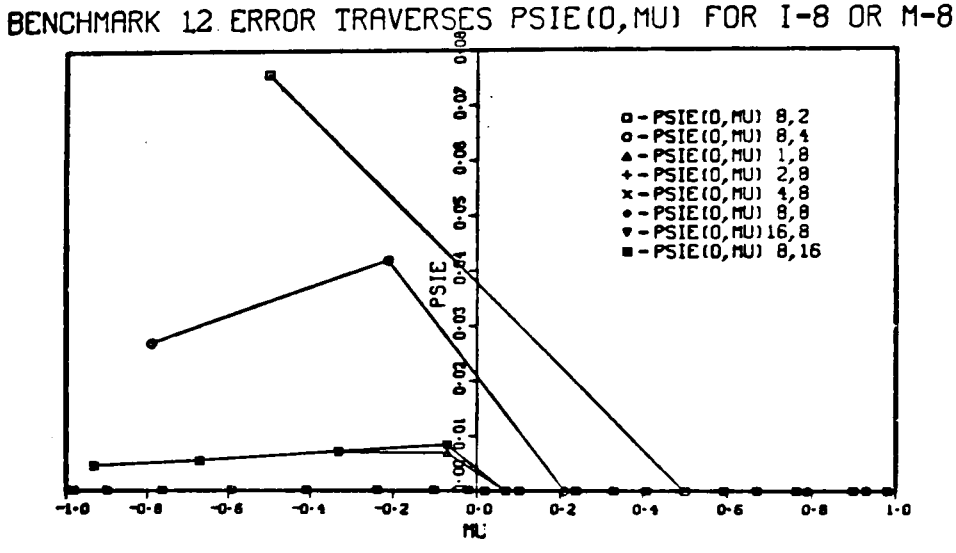

(c) DGF

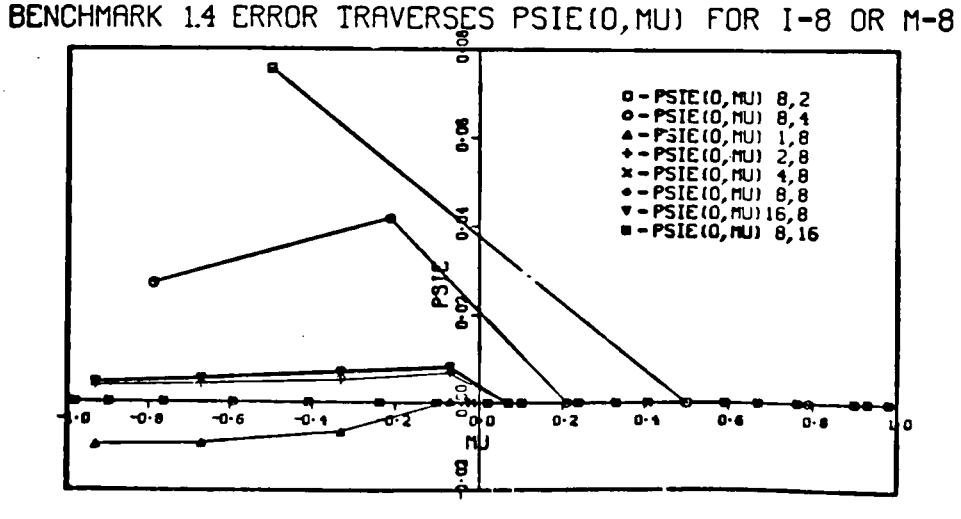

Figure 2.3. Angular flux error traverses $\psi_E(0,\mu)$ for DB1, DB3, and DGF methods for eight selected discretizations of Benchmark #1

(a) DB1

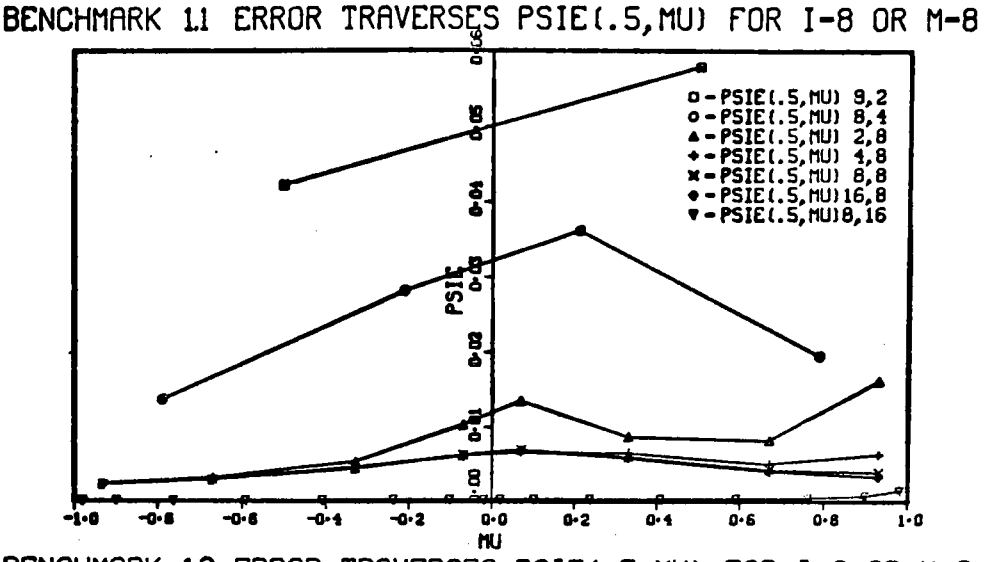

(b) DB3

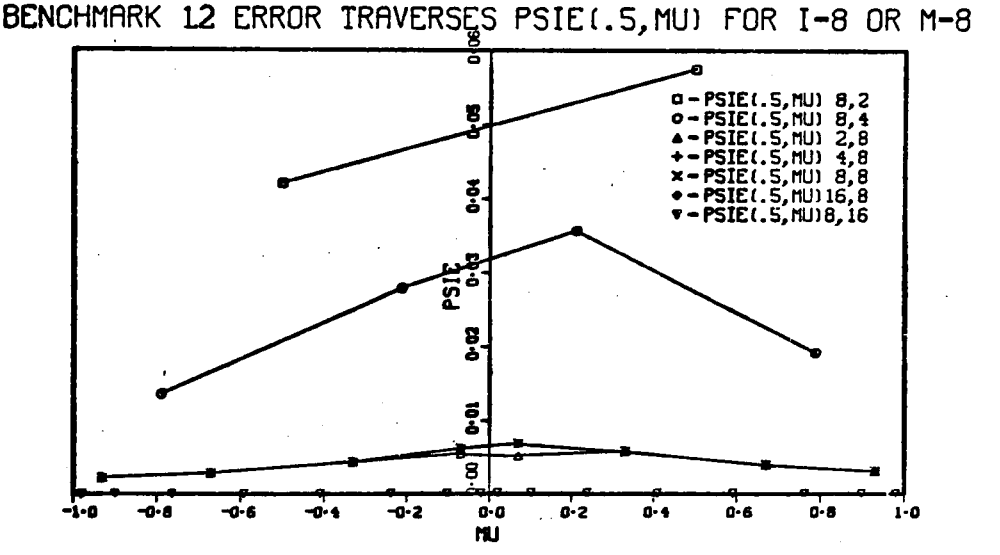

(c) DGF

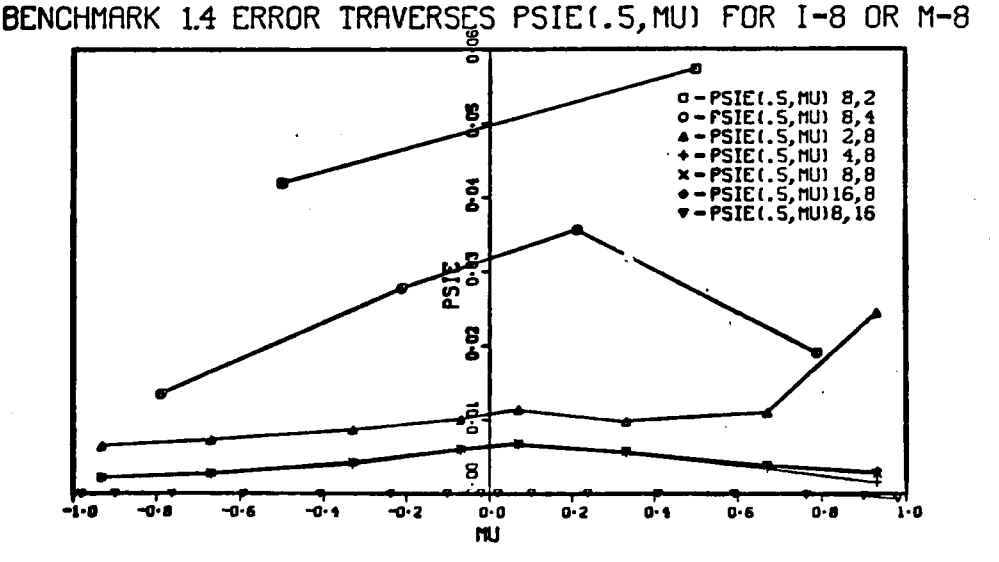

Figure 2.4. Angular flux error traverses $\psi_E(.5,\mu)$ for DB1, DB3, and DGF methods for eight selected discretization sets of Benchmark #1

(a) DB1

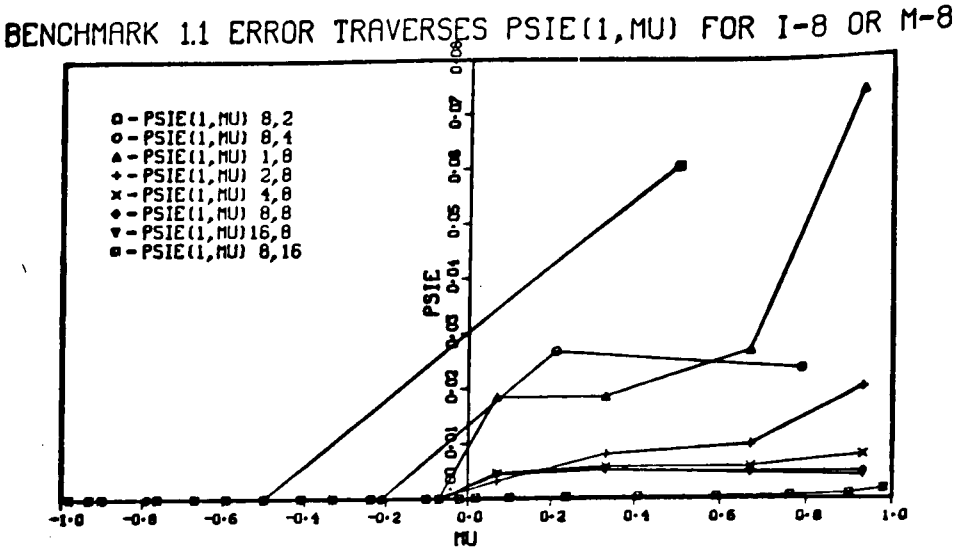

(b) DB3

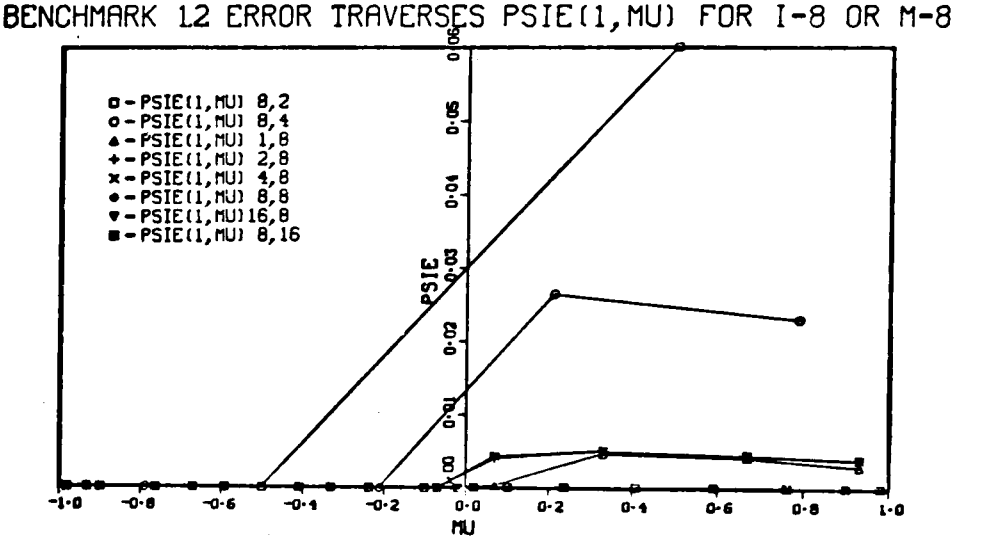

(c) DGF

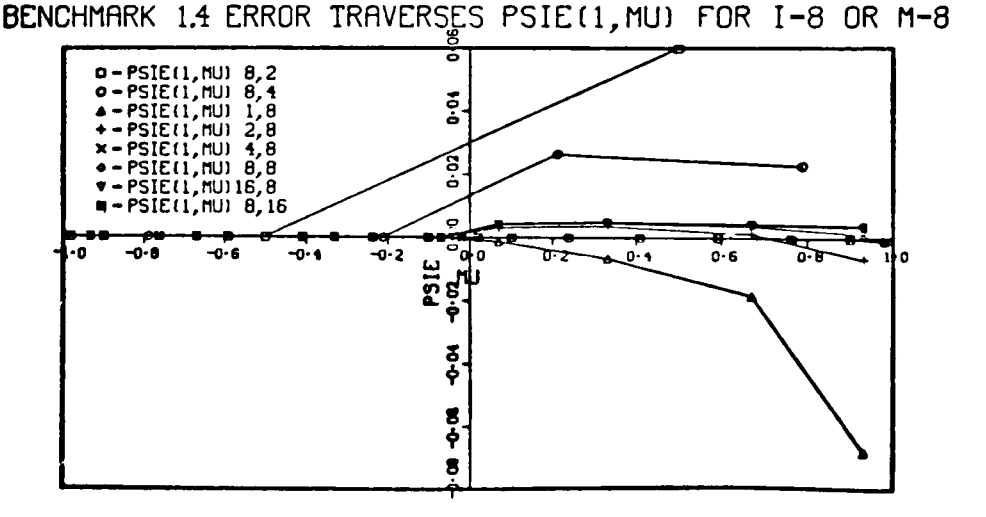

Figure 2.5. Angular flux error traverse $\psi_E(1,\mu)$ for DB1, DB3 and DGF methods for eight selected discretization sets of Benchmark #1

Table 2.3. Average absolute scalar flux error for DB1, DB3, and DGF methods for twenty discretization sets of Benchmark #1

(a) DB1

BRAPAC 05/76 BP#1.1 ASYMPTOTIC SOLUTION A0=-1,W00=1.05,X:(0,1),BC(X,X),S=0

AVG. ABS. SCALAR FLUX ERROR (GLOBAL)

I: NO. OF MESH INTERVALS J: NO. OF SU POINTS

I \ J	2	4	8	16
ERROR 1	3.19D-01	1.48D-01	3.76D-02	1.30D-02
ERROR 2	3.09D-01	1.38D-01	2.85D-02	4.32D-03
ERROR 4	3.07D-01	1.36D-01	2.60D-02	1.75D-03
ERROR 8	3.06D-01	1.35D-01	2.54D-02	1.03D-03
ERROR 16	3.06D-01	1.35D-01	2.53D-02	8.46D-04

AVG. ABS. SCALAR FLUX ERROR (BOUNDARY)

I: NO. OF MESH INTERVALS J: NO. OF SU POINTS

I \ J	2	4	8	16
ERROR 1	3.19D-01	1.48D-01	3.76D-02	1.30D-02
ERROR 2	3.05D-01	1.32D-01	2.65D-02	3.40D-03
ERROR 4	3.02D-01	1.30D-01	2.48D-02	1.40D-03
ERROR 8	3.01D-01	1.30D-01	2.43D-02	9.13D-04
ERROR 16	3.01D-01	1.30D-01	2.42D-02	7.89D-04

(b) DB3

BRAPAC 05/76 BP#1.2 ASYMPTOTIC SOLUTION A0=-1,W00=1.05,X:(0,1),BC(X,X),S=0

AVG. ABS. SCALAR FLUX ERROR (GLOBAL)

I: NO. OF MESH INTERVALS J: NO. OF SU POINTS

I \ J	2	4	8	16
ERROR 1	3.01D-01	1.29D-01	2.35D-02	5.69D-04
ERROR 2	3.04D-01	1.32D-01	2.44D-02	7.41D-04
ERROR 4	3.05D-01	1.34D-01	2.49D-02	7.69D-04
ERROR 8	3.06D-01	1.35D-01	2.51D-02	7.78D-04
ERROR 16	3.06D-01	1.35D-01	2.52D-02	7.81D-04

AVG. ABS. SCALAR FLUX ERROR (BOUNDARY)

I: NO. OF MESH INTERVALS J: NO. OF SU POINTS

I \ J	2	4	8	16
ERROR 1	3.01D-01	1.28D-01	2.35D-02	5.69D-04
ERROR 2	3.01D-01	1.29D-01	2.41D-02	7.35D-04
ERROR 4	3.01D-01	1.30D-01	2.41D-02	7.48D-04
ERROR 8	3.01D-01	1.30D-01	2.41D-02	7.46D-04
ERROR 16	3.01D-01	1.30D-01	2.41D-02	7.48D-04

(c) DGF

BRAPAC 05/76 BP#1.4 ASYMPTOTIC SOLUTION A0=-1,W00=1.05,X:(0,1),BC(X,X),S=0

AVG. ABS. SCALAR FLUX ERROR (GLOBAL)

I: NO. OF MESH INTERVALS J: NO. OF SU POINTS

I \ J	2	4	8	16
ERROR 1	2.85D-01	1.14D-01	1.49D-02	1.90D-02
ERROR 2	3.05D-01	1.35D-01	2.69D-02	5.47D-03
ERROR 4	3.06D-01	1.35D-01	2.57D-02	1.81D-03
ERROR 8	3.06D-01	1.35D-01	2.53D-02	1.03D-03
ERROR 16	3.06D-01	1.35D-01	2.52D-02	8.49D-04

AVG. ABS. SCALAR FLUX ERROR (BOUNDARY)

I: NO. OF MESH INTERVALS J: NO. OF SU POINTS

I \ J	2	4	8	16
ERROR 1	2.85D-01	1.14D-01	1.49D-02	1.90D-02
ERROR 2	2.98D-01	1.27D-01	2.15D-02	1.81D-03
ERROR 4	3.00D-01	1.29D-01	2.34D-02	5.55D-04
ERROR 8	3.01D-01	1.29D-01	2.39D-02	5.72D-04
ERROR 16	3.01D-01	1.29D-01	2.41D-02	7.04D-04

Table 2.4. Relative sum error of pointwise scalar flux for DB1, DB3 and DGF methods for twenty discretization sets of Benchmark #1

(a) DB1

BEAPAC 05/76 BP#L3 ASYMPTOTIC SOLUTION A0=-1,BU0=1.05,X:(0,1),BC(X,X),S=0

REL. ABS. SCALAR FLUX ERROR (GLOBAL)

I: NO. OF MESH INTERVALS J: NO. OF SU POINTS

I \ J	2	4	8	16
ERROR 1	4.60D-01	2.13D-01	5.43D-02	1.88D-02
ERROR 2	4.62D-01	2.06D-01	4.26D-02	6.46D-03
ERROR 4	4.67D-01	2.06D-01	3.96D-02	2.66D-03
ERROR 8	4.70D-01	2.08D-01	3.90D-02	1.59D-03
ERROR 16	4.73D-01	2.09D-01	3.90D-02	1.31D-03

REL. ABS. SCALAR FLUX ERROR (BOUNDARY)

I: NO. OF MESH INTERVALS J: NO. OF SU POINTS

I \ J	2	4	8	16
ERROR 1	4.60D-01	2.13D-01	5.43D-02	1.88D-02
ERROR 2	4.40D-01	1.91D-01	3.83D-02	4.91D-03
ERROR 4	4.36D-01	1.88D-01	3.58D-02	2.03D-03
ERROR 8	4.35D-01	1.87D-01	3.51D-02	1.32D-03
ERROR 16	4.35D-01	1.87D-01	3.49D-02	1.14D-03

(b) DB3

BEAPAC 05/76 BP#L2 ASYMPTOTIC SOLUTION A0=-1,BU0=1.05,X:(0,1),BC(X,X),S=0

REL. ABS. SCALAR FLUX ERROR (GLOBAL)

I: NO. OF MESH INTERVALS J: NO. OF SU POINTS

I \ J	2	4	8	16
ERROR 1	4.34D-01	1.85D-01	3.39D-02	8.21D-04
ERROR 2	4.54D-01	1.96D-01	3.65D-02	1.11D-03
ERROR 4	4.64D-01	2.04D-01	3.79D-02	1.17D-03
ERROR 8	4.70D-01	2.07D-01	3.85D-02	1.19D-03
ERROR 16	4.72D-01	2.09D-01	3.89D-02	1.21D-03

REL. ABS. SCALAR FLUX ERROR (BOUNDARY)

I: NO. OF MESH INTERVALS J: NO. OF SU POINTS

I \ J	2	4	8	16
ERROR 1	4.34D-01	1.85D-01	3.39D-02	8.21D-04
ERROR 2	4.35D-01	1.87D-01	3.48D-02	1.06D-03
ERROR 4	4.35D-01	1.87D-01	3.48D-02	1.08D-03
ERROR 8	4.35D-01	1.87D-01	3.48D-02	1.08D-03
ERROR 16	4.35D-01	1.87D-01	3.48D-02	1.08D-03

(c) DGF

BEAPAC 05/76 BP#L4 ASYMPTOTIC SOLUTION A0=-1,BU0=1.05,X:(0,1),BC(X,X),S=0

REL. ABS. SCALAR FLUX ERROR (GLOBAL)

I: NO. OF MESH INTERVALS J: NO. OF SU POINTS

I \ J	2	4	8	16
ERROR 1	4.12D-01	1.64D-01	2.15D-02	2.74D-02
ERROR 2	4.56D-01	2.01D-01	4.02D-02	8.18D-03
ERROR 4	4.65D-01	2.05D-01	3.92D-02	2.75D-03
ERROR 8	4.70D-01	2.08D-01	3.89D-02	1.58D-03
ERROR 16	4.72D-01	2.09D-01	3.90D-02	1.21D-03

REL. ABS. SCALAR FLUX ERROR (BOUNDARY)

I: NO. OF MESH INTERVALS J: NO. OF SU POINTS

I \ J	2	4	8	16
ERROR 1	4.12D-01	1.64D-01	2.15D-02	2.74D-02
ERROR 2	4.31D-01	1.83D-01	3.10D-02	2.61D-03
ERROR 4	4.33D-01	1.86D-01	3.38D-02	8.01D-04
ERROR 8	4.34D-01	1.87D-01	3.46D-02	8.25D-04
ERROR 16	4.35D-01	1.87D-01	3.48D-02	1.03D-03

2.2.2 Benchmark Problem #2, a transient eigenmode

The cross sections and dimensions of BP1 apply to the cell in BP2. Here the transient eigenvalue spectrum $|\nu| \leq 1$ is discretized into 2N+2 nodes $\{\nu_{\pm n} | n=0,1,\ldots,N\} = \{\pm 0, \pm .94919, \pm .99, \pm 1.\}$ for N = 3. The choice of the ν_n is arbitrary. In this case we choose to generate the benchmark problem defined by

$$\psi_B(x,\mu) = q_{+0}(x,\mu)$$

which corresponds to Eqn. (1.9) with all $a_{\pm n} = 0$ except for $a_{+0} = 1$, where $q_{+0}(x,\mu)$ is the mode corresponding to the interval $0 \leq \nu \leq .94919$.

Figure 2.6a,b,c illustrates the angular and scalar flux traverses for BP2. Note in particular that the $q_{+0}(x,\mu)$ mode contains a flux discontinuity along μ at $\mu = 0$ for the cell boundary at $x = 0$.

The same twenty sets of space/angle mesh discretization are applied in BP2 as in BP1 and incident flux boundary conditions are given by $\psi_B(x,\mu)$ at the cell boundaries. The maximum absolute scalar flux error $\|\underline{\phi}_E\|_\infty$ with algebraic sign is tabulated in Table 2.5a,b,c for each of the twenty problems. Comparison of the results for DB1, DB3 and DGF shows that the DB3 method is more accurate than DB1 and DGF, a result expected and observed in BP1. Counter to BP1, however, error convergence in BP2 is not achieved in Table 2.5a,b,c for J > 2. The DGF method has a better error performance than the DB1 method for BP2; the magnitude of the tabulated errors are two to three times smaller for DGF than for DB1.

Figures 2.7a,b,c display the scalar flux maximum absolute error traverse for eight selected space/angle mesh refinements (same as BP1). It is obvious from the figure that the errors are largest for space/angle mesh discretization outside of an optimal band. The error traverses for successively finer mesh refinements oscillate about zero with the maximum error shifting successively closer to x = 0 where the angular flux discontinuity occurs.

The maximum angular flux error $\|\psi_E\|_\infty$ with algebraic sign is tabulated in Tables 2.6a,b,c. The tabulation indicates that the angular flux error is much larger for BP2 than for BP1. The largest error is always located along the μ coordinate with minimum absolute value for a given μ discretization J.

(a)

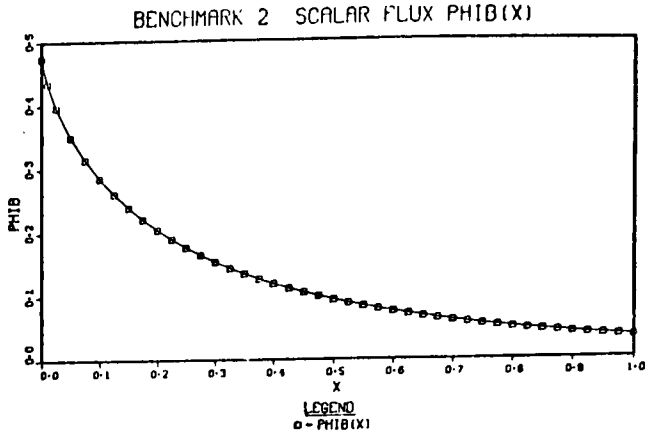

(b)

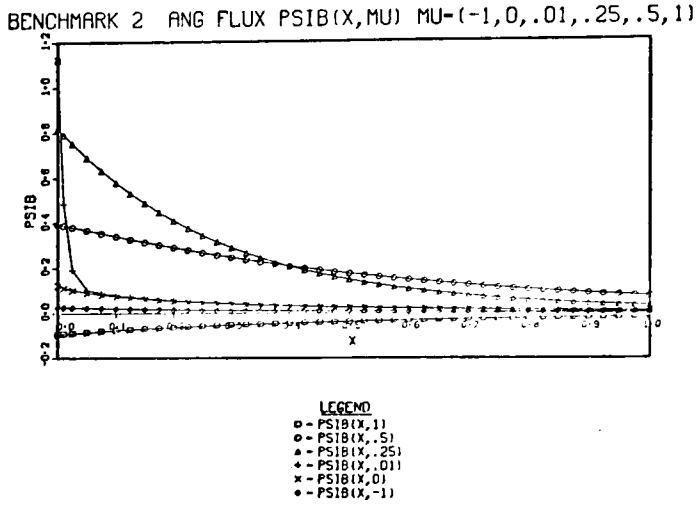

(c)

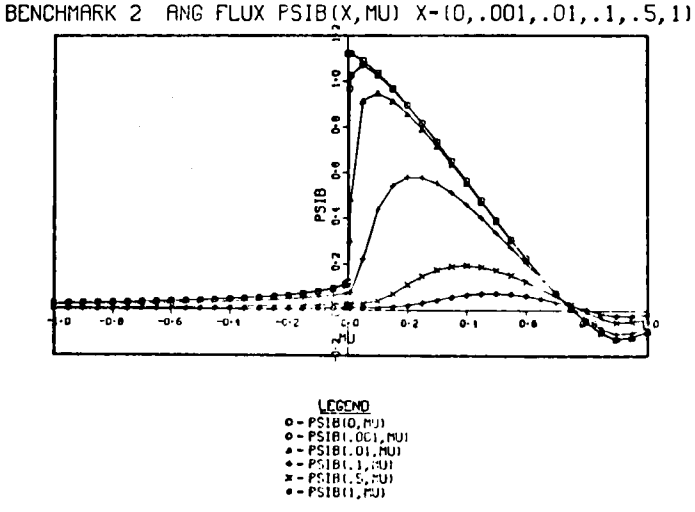

Figure 2.6. Flux Distributions for Benchmark #2
(a) scalar flux $\phi_B(x)$
(b) angular flux traverse $\psi_B(x,\mu)$ along x for fixed μ
(c) angular flux traverse $\psi_B(x,\mu)$ along μ for fixed x

Table 2.5. Maximum absolute scalar flux error $\|\phi_E\|_\infty$ tabulated for twenty space/angle mesh discretization sets of Benchmark #2 for the DB1, DB3 and DGF methods

BEAPAC 05/76 BP#2.1 TRANSIENT SOLUTION A+0=1,NU0=1.05,X: (0,1),BC(I,I),S=0

MAX. ABS. SCALAR FLUX ERROR AND LOCATION (GLOBAL)

I: NO. OF XMESH INTERVALS J: NO. OF MU POINTS

(a) DB1

I \ J		2	4	8	16
ERROR	1	-3.97D-02	1.64D-01	1.69D-01	1.68D-01
EXACT		0.033	0.033	0.033	0.033
X LOC		1.000	1.000	1.000	1.000
ERROR	2	-1.23D-01	9.21D-02	1.10D-01	1.10D-01
EXACT		0.094	0.094	0.094	0.094
X LOC		0.500	0.500	0.500	0.500
ERROR	4	-1.44D-01	3.88D-02	5.87D-02	6.07D-02
EXACT		0.177	0.094	0.177	0.177
X LOC		0.250	0.500	0.250	0.250
ERROR	8	-1.45D-01	3.06D-02	2.44D-02	3.19D-02
EXACT		0.177	0.071	0.261	0.261
X LOC		0.250	0.625	0.125	0.125
ERROR	16	-1.45D-01	-3.26D-02	9.56D-03	1.56D-02
EXACT		0.177	0.331	0.261	0.331
X LOC		0.250	0.063	0.125	0.063

BEAPAC 05/76 BP#2.2 TRANSIENT SOLUTION A+0=1,NU0=1.05,X: (0,1),BC(I,I),S=0

MAX. ABS. SCALAR FLUX ERROR AND LOCATION (GLOBAL)

I: NO. OF XMESH INTERVALS J: NO. OF MU POINTS

(b) DB3

I \ J		2	4	8	16
ERROR	1	-6.72D-02	-7.07D-03	-7.21D-02	-7.41D-02
EXACT		0.033	0.033	0.033	0.033
X LOC		1.000	1.000	1.000	1.000
ERROR	2	-1.30D-01	2.38D-02	-3.19D-02	-4.11D-02
EXACT		0.094	0.094	0.094	0.094
X LOC		0.500	0.500	0.500	0.500
ERROR	4	-1.45D-01	2.73D-02	-2.58D-03	-2.08D-02
EXACT		0.177	0.094	0.177	0.177
X LOC		0.250	0.500	0.250	0.250
ERROR	8	-1.45D-01	2.86D-02	5.18D-03	-8.07D-03
EXACT		0.177	0.071	0.261	0.261
X LOC		0.250	0.625	0.125	0.125
ERROR	16	-1.45D-01	-3.31D-02	6.25D-03	-5.76D-04
EXACT		0.177	0.331	0.212	0.261
X LOC		0.250	0.063	0.188	0.125

BEAPAC 05/76 BP#2.4 TRANSIENT SOLUTION A+0=1,NU0=1.05,X: (0,1),BC(I,I),S=0

MAX. ABS. SCALAR FLUX ERROR AND LOCATION (GLOBAL)

I: NO. OF XMESH INTERVALS J: NO. OF MU POINTS

(c) DGF

I \ J		2	4	8	16
ERROR	1	-7.82D-02	6.14D-02	5.96D-02	5.92D-02
EXACT		0.033	0.033	0.033	0.033
X LOC		1.000	1.000	1.000	1.000
ERROR	2	-1.22D-01	4.88D-02	4.24D-02	4.16D-02
EXACT		0.094	0.094	0.094	0.094
X LOC		0.500	0.500	0.500	0.500
ERROR	4	-1.43D-01	3.07D-02	2.17D-02	1.98D-02
EXACT		0.177	0.055	0.177	0.177
X LOC		0.250	0.750	0.250	0.250
ERROR	8	-1.46D-01	2.97D-02	1.03D-02	9.39D-03
EXACT		0.177	0.071	0.261	0.261
X LOC		0.250	0.625	0.125	0.125
ERROR	16	-1.45D-01	-3.27D-02	6.96D-03	4.73D-03
EXACT		0.177	0.331	0.212	0.331
X LOC		0.250	0.063	0.188	0.063

(a) DB1

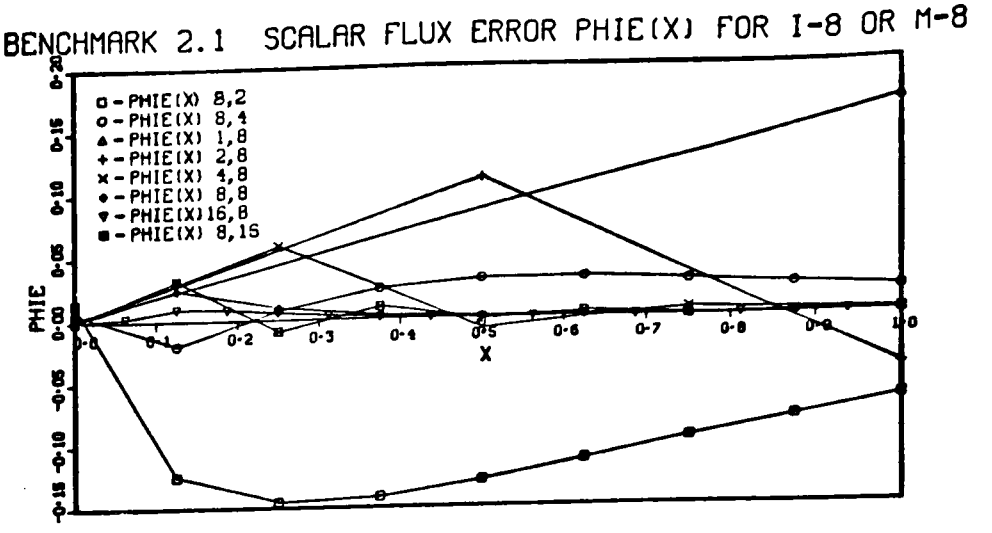

(b) DB3

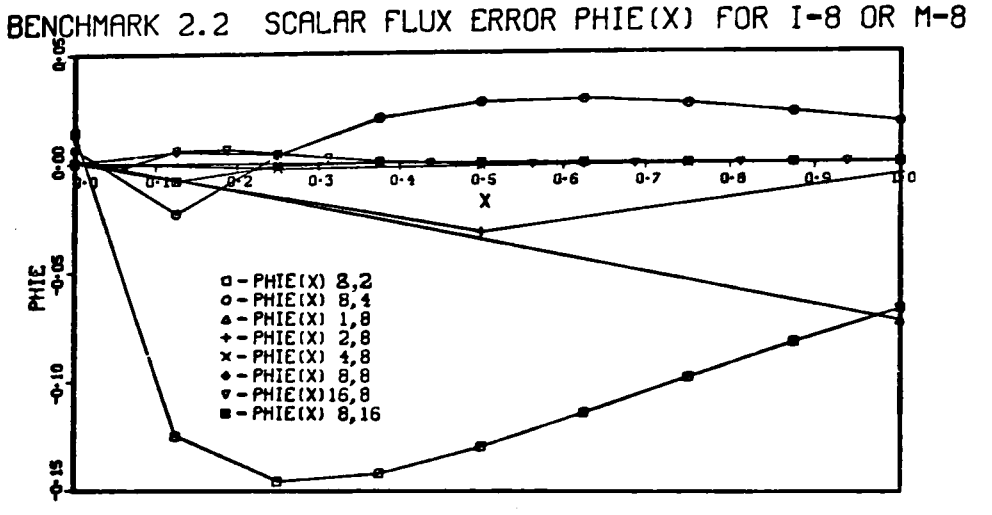

(c) DGF

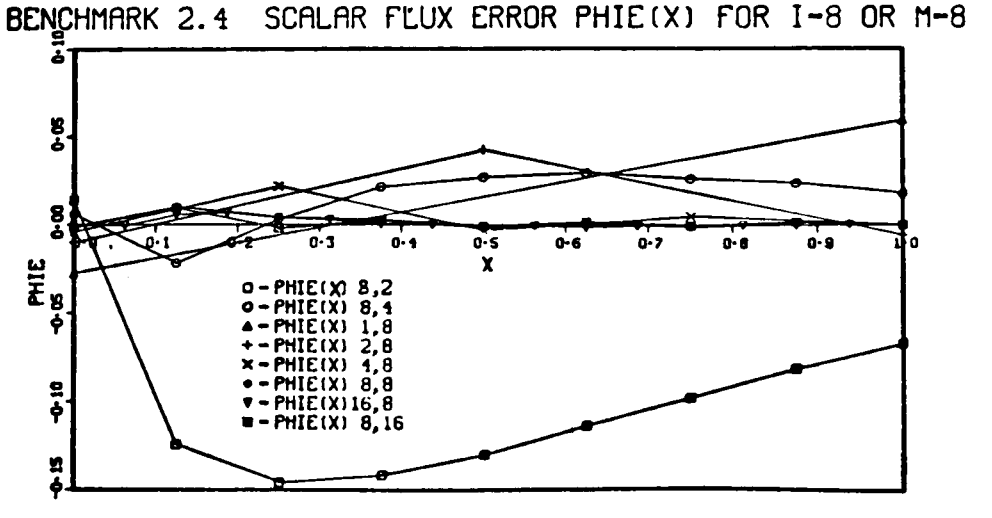

Figure 2.7. Scalar flux error $\phi_E(x)$ for (a) DB1, (b) DB3, (c) DGF methods for eight selected discretizations of Benchmark #2

Table 2.6. Maximum absolute signed angular flux error $\pm\|\psi_E\|_\infty$ tabulated for twenty space/angle discretization sets of Benchmark #2 for DB1, DB3 and DGF methods

BEAPAC 05/76 BP#2.1 TRANSIENT SOLUTION A+0=1,NU0=1.05,X: (0,1),BC(X,X),S=0

MAX. ABS. VECTOR FLUX ERROR AND LOCATION (GLOBAL)

X: NO. OF XMESH INTERVALS J: NO. OF MU POINTS

(a) DB1

	I \ J	2	4	8	16
ERROR	1	-2.70D-02	3.19D-01	7.44D-01	9.55D-01
EXACT		0.042	0.022	0.010	0.009
X LOC		0.0	1.000	1.000	1.000
MULOC		-0.500	0.211	0.069	0.020
ERROR	2	-2.57D-02	1.26D-01	5.43D-01	8.67D-01
EXACT		0.042	0.118	0.030	0.025
X LOC		0.0	0.500	0.500	0.500
MULOC		-0.500	0.211	0.069	0.020
ERROR	4	-2.54D-02	2.93D-02	2.92D-01	7.27D-01
EXACT		0.042	0.315	0.084	0.048
X LOC		0.0	0.250	0.250	0.250
MULOC		-0.500	0.211	0.069	0.020
ERROR	8	-2.68D-02	8.71D-03	1.02D-01	5.14D-01
EXACT		0.028	0.075	0.244	0.074
X LOC		0.125	0.625	0.125	0.125
MULOC		-0.500	0.211	0.069	0.020
ERROR	16	-2.70D-02	6.62D-03	2.30D-02	2.61D-01
EXACT		0.034	0.039	0.493	0.136
X LOC		0.063	0.813	0.063	0.063
MULOC		-0.500	0.211	0.069	0.020

BEAPAC 05/76 BP#2.2 TRANSIENT SOLUTION A+0=1,NU0=1.05,X: (0,1),BC(X,X),S=0

MAX. ABS. VECTOR FLUX ERROR AND LOCATION (GLOBAL)

X: NO. OF XMESH INTERVALS J: NO. OF MU POINTS

(b) DB3

	I \ J	2	4	8	16
ERROR	1	-2.53D-02	-4.83D-02	-4.69D-01	-7.93D-01
EXACT		0.042	0.022	0.010	0.009
X LOC		0.0	1.000	1.000	1.000
MULOC		-0.500	0.211	0.069	0.020
ERROR	2	-2.53D-02	5.77D-03	-1.74D-01	-6.17D-01
EXACT		0.042	0.017	0.030	0.025
X LOC		0.0	0.500	0.500	0.500
MULOC		-0.500	-0.211	0.069	0.020
ERROR	4	-2.53D-02	6.26D-03	-3.76D-02	-3.80D-01
EXACT		0.042	0.017	0.084	0.048
X LOC		0.0	0.500	0.250	0.250
MULOC		-0.500	-0.211	0.069	0.020
ERROR	8	-2.68D-02	6.29D-03	-4.19D-03	-1.49D-01
EXACT		0.028	0.017	0.244	0.074
X LOC		0.125	0.500	0.125	0.125
MULOC		-0.500	-0.211	0.069	0.020
ERROR	16	-2.70D-02	6.41D-03	1.41D-03	-2.96D-02
EXACT		0.034	0.019	0.055	0.136
X LOC		0.063	0.438	0.125	0.063
MULOC		-0.500	-0.211	-0.069	0.020

BEAPAC 05/76 BP#2.4 TRANSIENT SOLUTION A+0=1,NU0=1.05,X: (0,1),BC(X,X),S=0

MAX. ABS. VECTOR FLUX ERROR AND LOCATION (GLOBAL)

X: NO. OF XMESH INTERVALS J: NO. OF MU POINTS

(c) DGF

	I \ J	2	4	8	16
ERROR	1	-3.63D-02	1.02D-01	3.41D-01	4.62D-01
EXACT		0.042	0.022	0.010	0.009
X LOC		0.0	1.000	1.000	1.000
MULOC		-0.500	0.211	0.069	0.020
ERROR	2	-2.69D-02	2.37D-02	1.55D-01	2.55D-01
EXACT		0.042	0.118	0.030	0.025
X LOC		0.0	0.500	0.500	0.500
MULOC		-0.500	0.211	0.069	0.020
ERROR	4	-2.59D-02	8.87D-03	6.56D-02	2.08D-01
EXACT		0.042	0.030	0.084	0.048
X LOC		0.0	0.250	0.250	0.250
MULOC		-0.500	-0.211	0.069	0.020
ERROR	8	-2.66D-02	7.21D-03	1.25D-02	1.39D-01
EXACT		0.028	0.022	0.244	0.074
X LOC		0.125	0.375	0.125	0.125
MULOC		-0.500	-0.211	0.069	0.020
ERROR	16	-2.69D-02	6.64D-03	-2.12D-03	5.36D-02
EXACT		0.034	0.019	0.088	0.136
X LOC		0.063	0.438	0.0	0.063
MULOC		-0.500	-0.211	-0.069	0.020

2.2.3 Benchmark Problem #3, a one cell least squares modes analysis

BP3 (and BP4) is based on a two cell reference problem with dimensions $0 \leq x \leq .5$ in cell I and $.5 \leq x \leq 1.5$ in cell II. An isotropic source $S_I = .5$ is in cell I. Compositions of the two cells are identical and have the same cross sections defined for BP1. Boundary conditions are reflecting at $x = 0$ and vacuum at $x = 1.5$.

The transient eigenvalue spectrum $-1 \leq \nu \leq 1$ is discretized into the following six intervals $\{\nu_{\pm n}\} = \{0, \pm.94919, \pm.999, \pm1.\}$. The discretization is based on knowledge and experience with the behaviour of the function $A(\nu)$ for various values of c, the number of secondaries per collision. Case and Zweifel (1967) illustrate (Figure 2.8) the behaviour of $g(\nu,c)$ (Eqn. 1.23b) for various values of c.

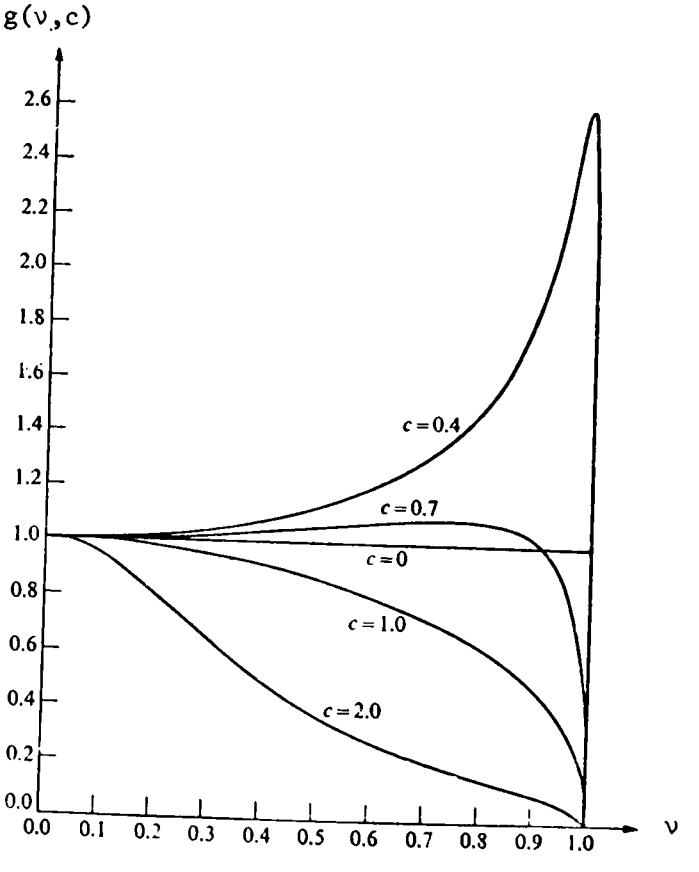

Figure 2.8. The function $g(\nu,c)$

For simple choices of $\psi(\mu)$ in Eqn. (1.22a) such as $\psi(\mu) \equiv \mu^k$ for $k=0,1,\ldots$ it is easily shown that $g(\nu,c)$ plays a dominant role in the behaviour of $A(\nu)$ in the neighborhood of $\nu = 1$, e.g. when $\psi(\mu) \equiv 1$ then $A(\nu) = (1-c)g(\nu,c)$ and when $\psi(\mu) = \mu$ then $A(\nu) = \nu(1-c)g(\nu,c)$. For $c \doteq .5129$ in BP3 we can estimate that $g(\nu,c)$ in Fig. 2.8 has a maximum in the neighborhood of $\nu = .95$. Therefore we chose a value in that neighborhood as one of the ν discretization points. The choice $\nu_{\pm 0} = 0$ and $\nu_{\pm 3} = \pm 1$ are obvious; the choice of $\nu_{\pm 2} = \pm .999$ is necessary to include the special basis element Eqn. (1.12b) which is designed to approximate the logarithmic singularity in $A(\nu)$ for $\nu = \pm 1$.

There are six transient eigenmodes $q_{\pm n}(x,\mu)$ $(n=0,1,2)$ Eqn. (1.13a,b) corresponding to the ν discretization and two asymptotic eigenmodes $q_{\pm 3}(x,\mu)$ Eqn. (1.10a,b). Note that we may alternately refer to the asymptotic eigenmodes with the notation $q_{0^{\pm}}(x,\mu)$ where the subscript $0^{\pm}$ is a carryover from the Case notation. In cell II of the reference problem we want to generate a benchmark problem with solution $\psi_B(x,\mu)$ which is a superposition of the eight homogeneous eigenmodes $q_{\pm n}(x,\mu)$ $(n=0,1,2,3)$. The procedure for obtaining the combining coefficients is denoted by modes analysis. Section 1.1.4 gives two modes analysis methods. For BP3 the least squares method is chosen with the option of performing the least squares analysis at discrete directions μ_m $(m=1,2,\ldots,M)$ along the incident flux boundaries of the cell; the emergent boundaries are omitted. An initial reference solution $\psi_R(x,\mu)$ for the two cell problem is obtained using the DB3 method with thirteen equally spaced spatial coordinates $x_i = .125i$ $(i=0,1,\ldots,12)$ and a DP_8 quadrature set for an S_{16} angular approximation. Figure 2.9 illustrates $\psi_R(x,\mu)$ for traverses along x for fixed $\pm\mu = .98,.76,.41,.02$ and for traverses along μ for fixed $x = .25i$ $(i=0,1,\ldots,6)$. At the cell interface $x = .5$ we notice the angular flux discontinuity due to the source in cell I (Fig. 2.9b).

At the incident flux cell boundaries of cell II, $\psi_R(x,\mu)$ is linearly interpolated to obtain a solution $\psi_A(x,\mu)$ defined at the μ discretization coordinates assigned to the least squares problem. Experimentation has indicated that for a fixed set $\{\nu_{\pm n}\}$ of the transient spectrum discretization the $\{\mu_n\}$ should be chosen by the formulas:

(a)

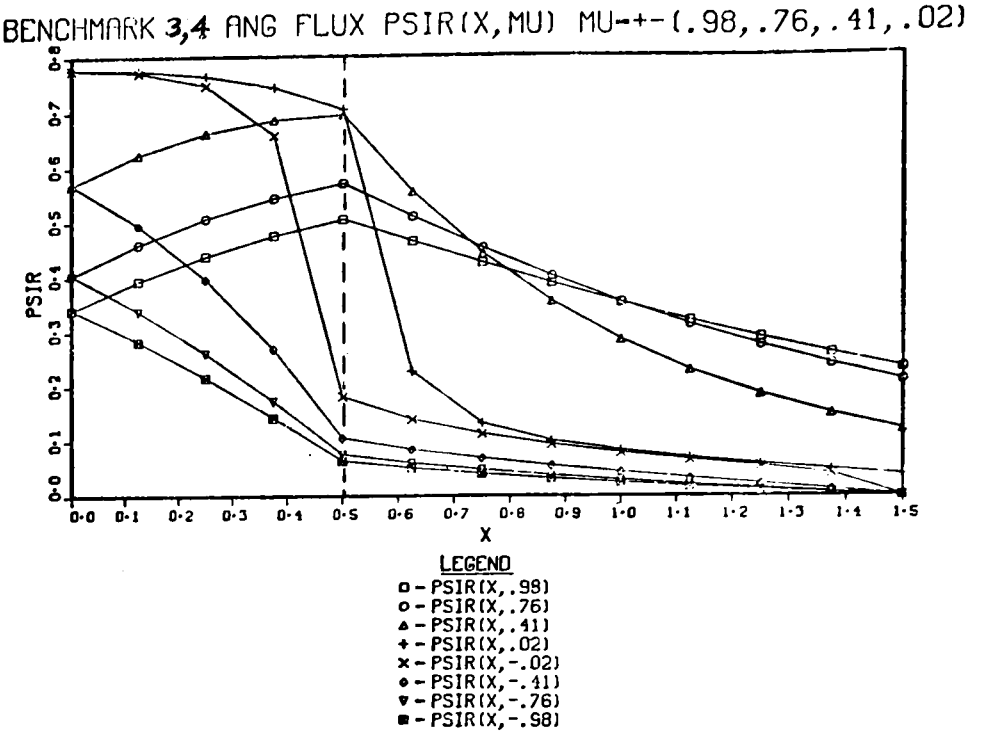

(b)

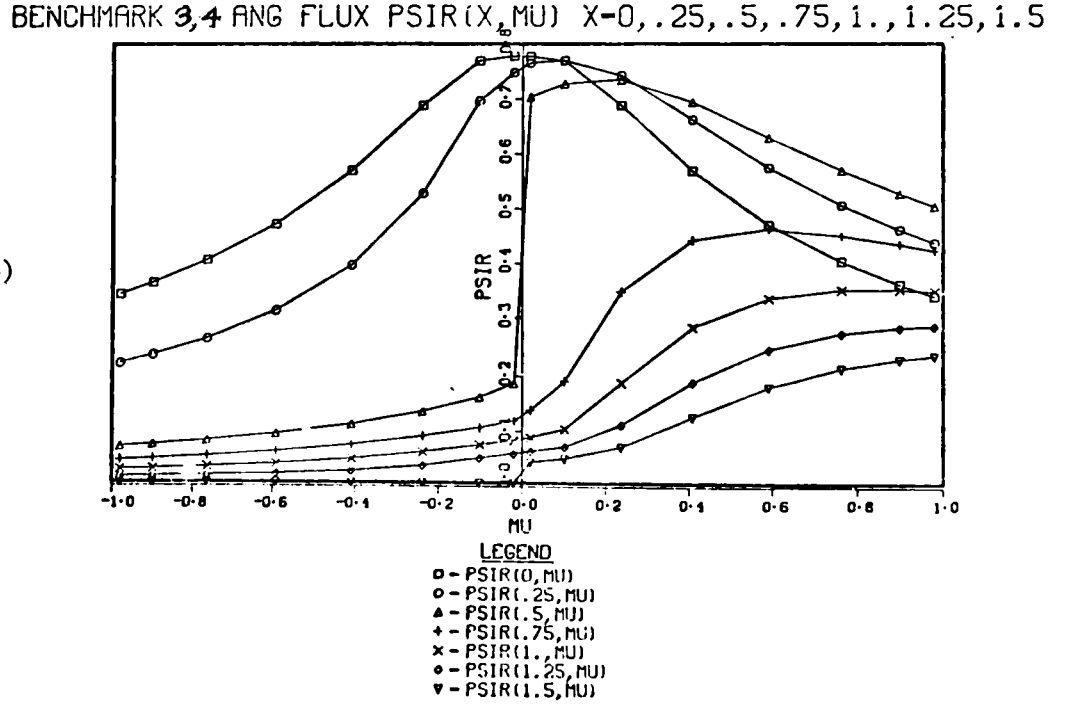

Figure 2.9. Angular flux traverses for DB3 reference solution ($h = .125$, DP_8) - (a) traverse along x for fixed μ, (b) traverse along μ for fixed x

(2.25a) $\mu_0 = \nu_0 \qquad n = 0$

(2.25b) $\mu_n = \dfrac{\nu_{n-1} + \nu_{n+1}}{2} \qquad n = 1,N-1$

(2.25c) $\mu_N = \nu_N \qquad n = N$

This choice places the μ_n in the neighborhood of the maximum amplitude of each eigenmode $q_n(x,\mu)$. Note that two zero values of μ denoted symbolically by ± 0 are used to permit treatment of discontinuities at boundaries and interfaces when they are present.

Figure 2.10 illustrates the resulting benchmark solution $\psi_B(x,\mu)$ in cell II generated by the least squares modes analysis using only eight flux values (four at each incident boundary). The $\{\mu_n\}$ for the least squares are calculated by Eqn. (2.25) using the $\{\nu_n\}$ given above. The display is in the format of Fig. 2.9.

A comparison of $\psi_R(x,\mu)$ and $\psi_B(x,\mu)$ along μ at the cell boundaries $x = .5$ and $x = 1.5$ and the scalar fluxes $\phi_R(x)$ and $\phi_B(x)$ is given in Fig. 2.11. The large rectangular symbols indicate the least squares μ discretization. The maximum relative scalar flux difference is about 4% near the interface at $x = .5$. The maximum angular flux difference occurs at the interface $x = .5$ in the μ interval (.9,1.) and is approximately 9%. Several factors which can contribute to the difference are:

(1) coarseness of the ν_n discretization

(2) placement of the ν_n coordinates

(3) placement of the μ_n coordinates for the least squares

(4) value of the parameter α in the q_{N-1} modes

The above four items must be thoroughly understood for implementation of this modes analysis technique as a new numerical transport theory method. Our present objectives are to generate exact benchmark problems which are related to physically meaningful problems. $\psi_B(x,\mu)$ satisfies the objectives and is used for the benchmark error performance analysis at the end of this section.

(a)

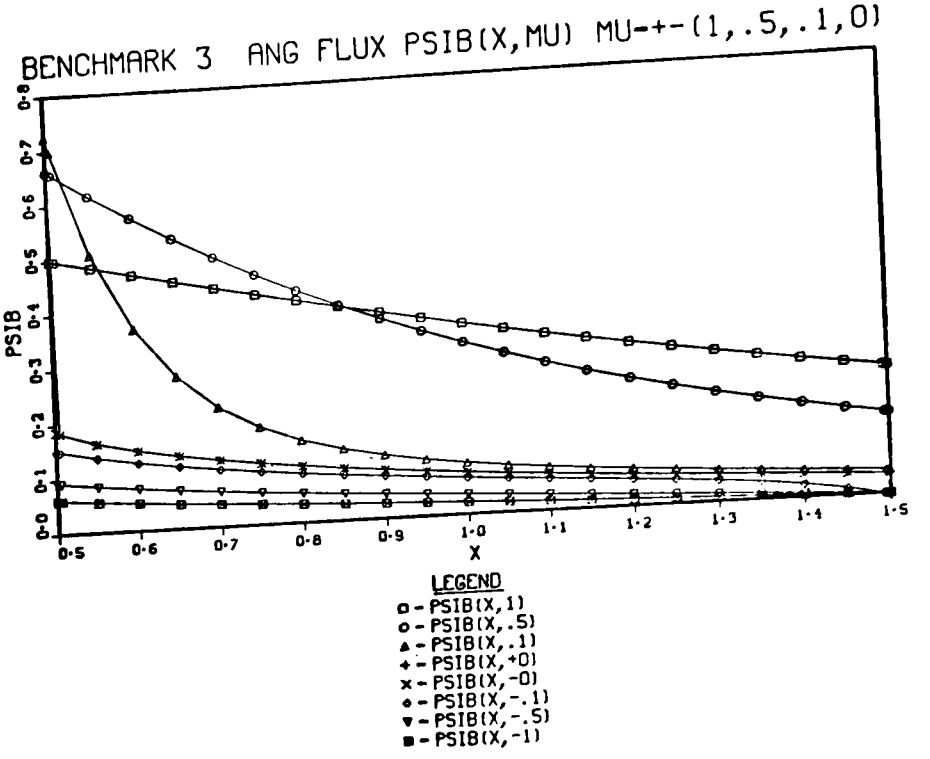

(b)

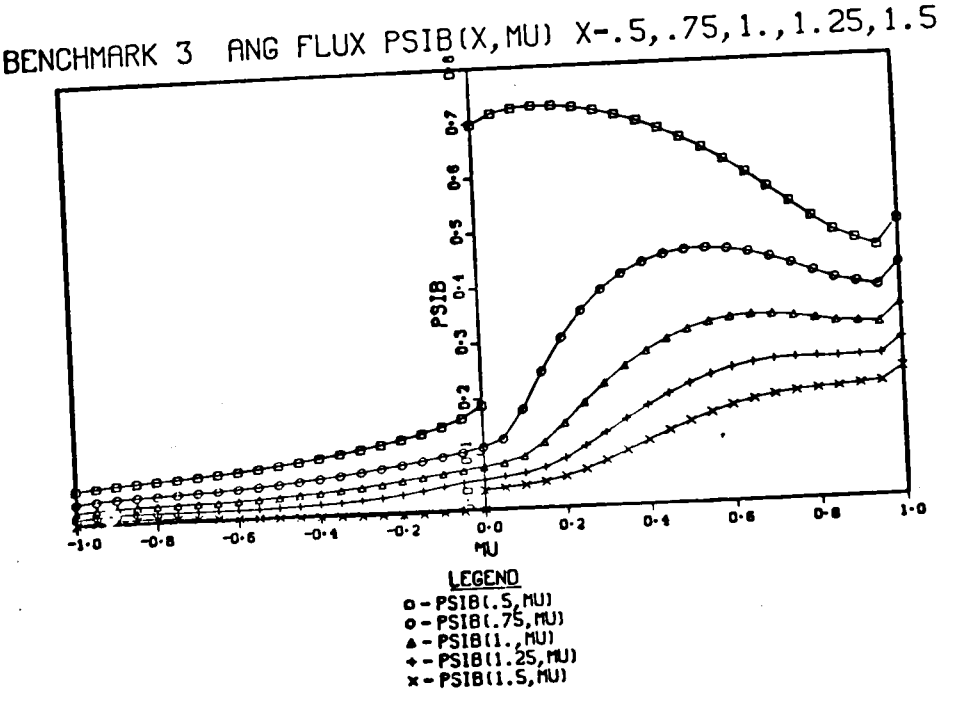

Figure 2.10. Angular flux for Benchmark #3
(a) Angular flux traverse $\psi_B(x,\mu)$ along x for fixed μ
(b) Angular flux traverse $\psi_B(x,\mu)$ along μ for fixed x

(a)

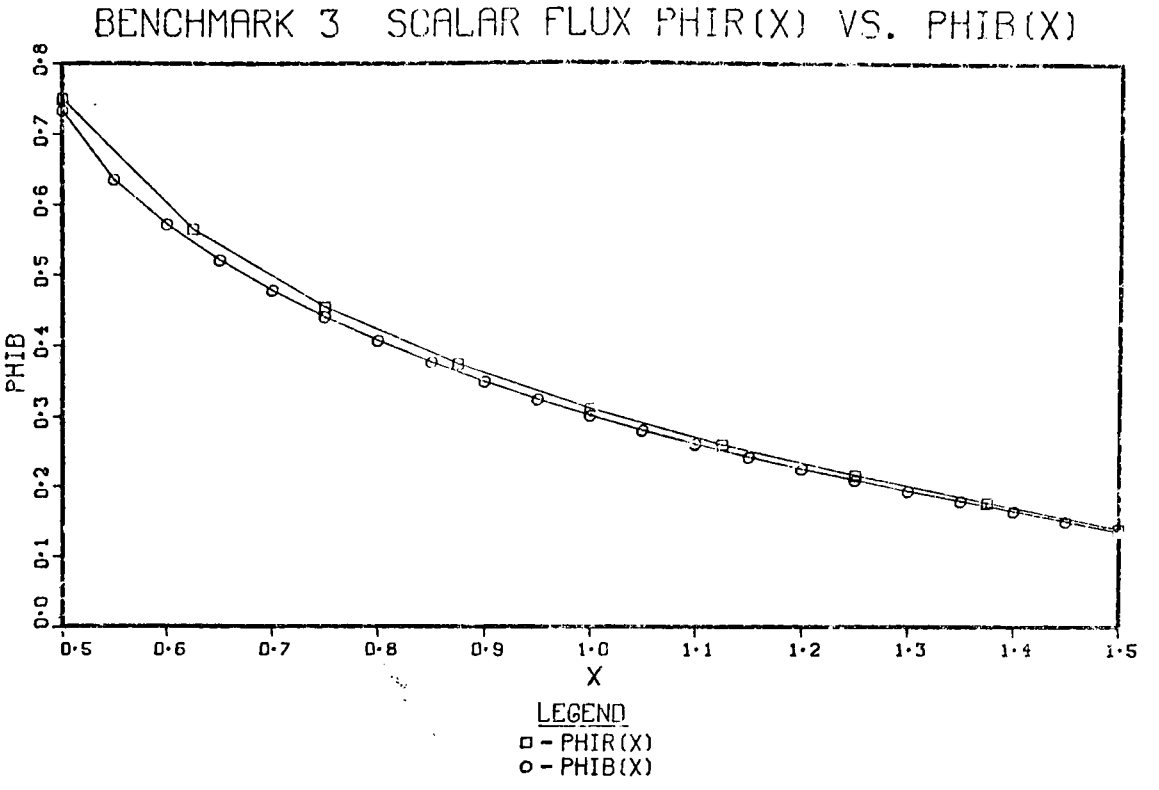

(b)

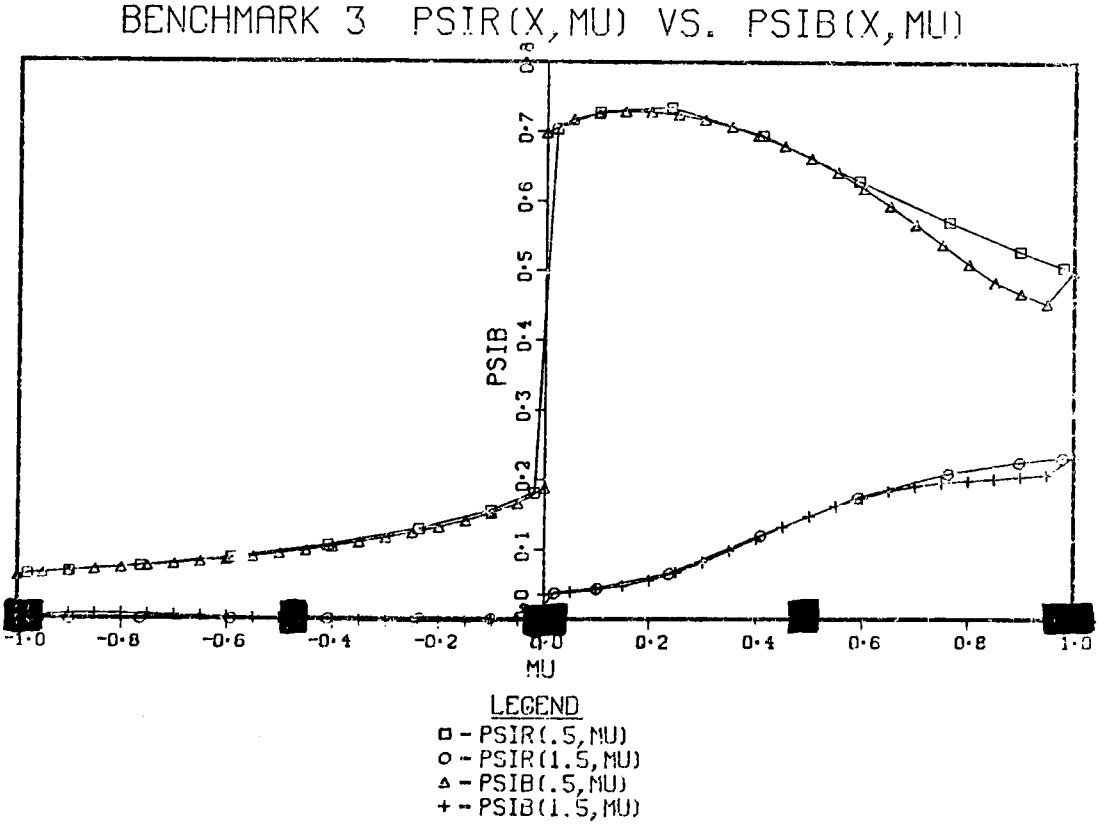

Figure 2.11. Comparison of reference and benchmark solutions for Benchmark #3
(a) Scalar flux $\phi_R(x)$ vs. $\phi_B(x)$
(b) Angular flux $\psi_R(x,\mu)$ vs. $\psi_B(x,\mu)$ at x = .5 and x = 1.5

We now examine some details of benchmark solution $\psi_B(x,\mu)$. Figure 2.12(a) illustrates the transient combining coefficients $A(\pm\nu_n) = a_{\pm n}$ (n=0,1,2) obtained by the least squares. Also included is $A(\pm 1) \equiv 0$. The asymptotic coefficients $a_0^{\pm}$ are tabulated at the lower right of the figure. Notice that $a_0^- \approx 0$ and $A(\nu) \approx 0$ $(\nu \leq 0)$. This is attributed to the vacuum condition at the boundary x = 1.5 since the coefficients a_{-n} correspond to modes $q_{-n}(x,\mu)$ which represent contributions of a source at the right boundary of the cell. The behavior of a_0^+ and $A(\nu)$ $(\nu \geq 0)$ are likewise controlled by the incident flux distribution at x = .5.

The scaled modes $a_{\pm n}q_{\pm n}(x,\mu)$ are illustrated in Fig. 2.13 and 2.14. $\psi_B(x,\mu)$ is included to illustrate the superposition of the modes. Modes a_0q_0 and a_1q_1 corresponding to $\nu_0 = 0$ and $\nu_1 = .94919$ and the asymptotic mode $a_0^+q_0^+$ are easily observed for $\nu \geq 0$. Notice that in Fig. (2.13a) the flux discontinuity at $\mu = 0$ is largely contributed to by a_0q_0. The rapid decay of q_0 as illustrated in BP2 forces $\psi_B(x,\mu)$ to behave similarly, so that at x = 1.5 the discontinuity is relatively very small.

The eigenmode $q_2(x,\mu)$ is barely visible in Fig. 2.13, but in Fig. 2.14a,b two scale magnifications illustrate the mode behaviour for $.90 \leq \mu \leq 1.$ and $.99 \leq \mu \leq 1.$ respectively. In Fig. 2.14a we note that the steepness in the gradient of q_2 for $.99 \leq \mu \leq 1.$ cannot be matched by any of the other modes including the asymptotic q_0^+ so that $\psi_B(x,\mu)$ has a 10% drop at $\mu = 1$. This deficiency is reflected in the results of the least squares which includes a data point at $\mu = 1$. Figure 2.11 shows that the least squares matches the boundary point $\mu = 1$ excellently, but away from the boundary the 10% difference reappears. Additional least squares points and varied placement are under investigation.

Figures 2.12a, 2.15, 2.16, 2.17 and 2.18 illustrate BP3A a problem similar to BP3 in all respects except that the parameter $\alpha = 1$ instead of $\alpha = .18$, where α is the exponent of the Chapeau function in $q_{N-1}(x,\mu)$. The main difference we note is the error in $\psi_B(x,\mu)$ is reduced in the interval $.95 \leq \mu \leq 1$. In the expanded scale plots, the change in q_2 is quite evident. The mode has a well defined minimum near $\mu = .999$ in contrast to BP3 where the mode continues decreasing until $\mu = .99975$. The

(a)

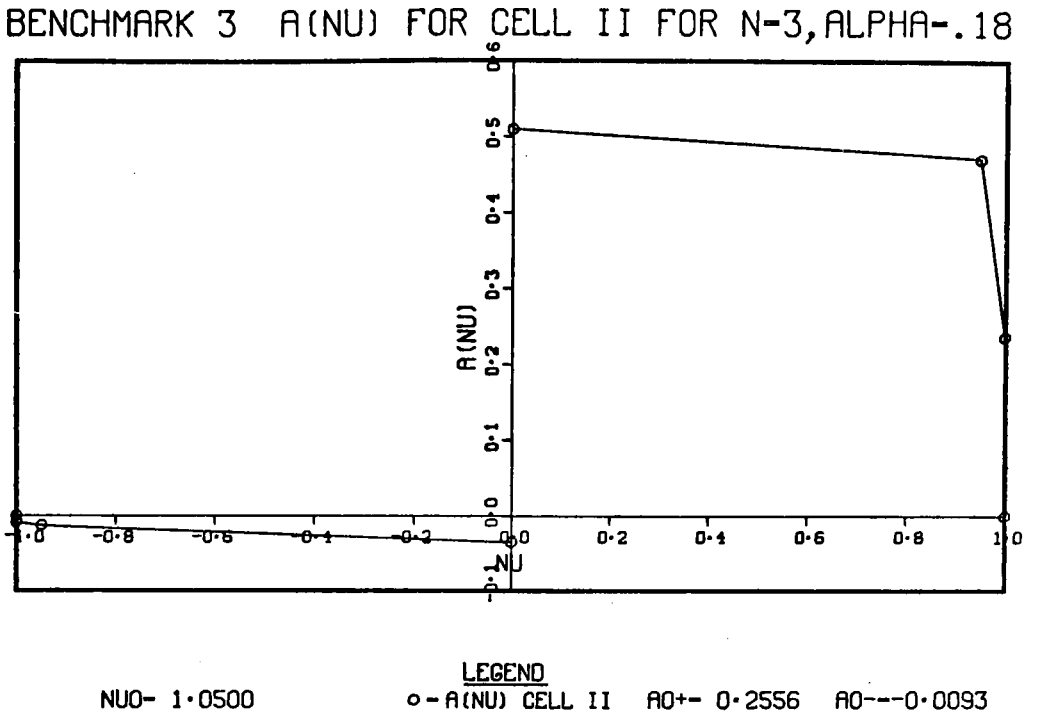

(b)

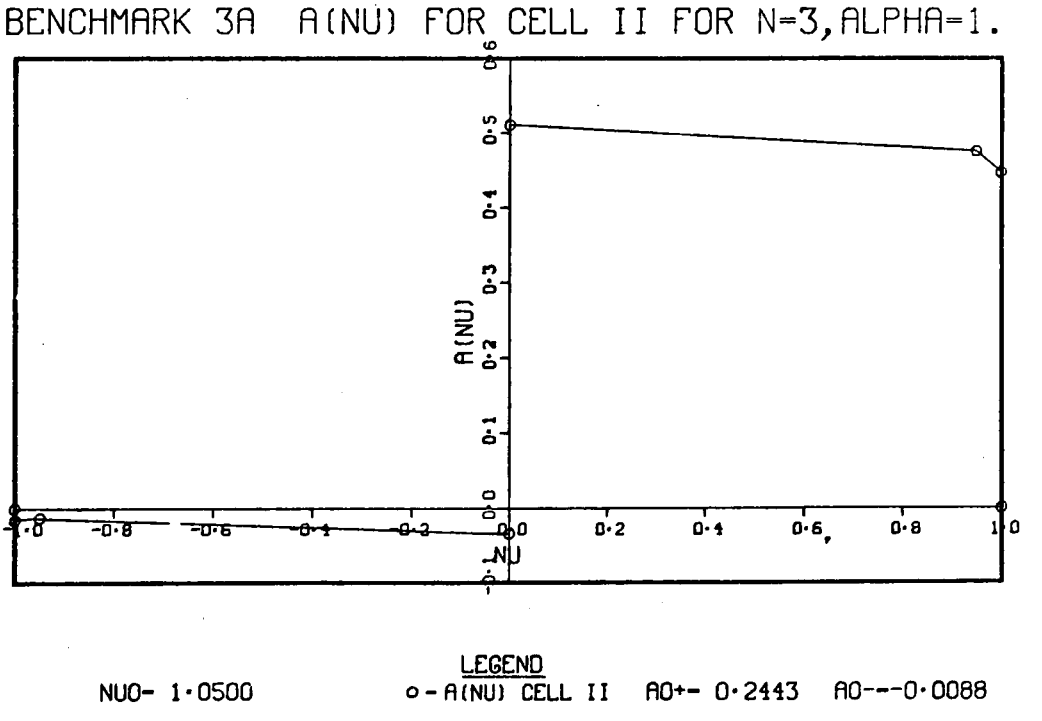

Figure 2.12. Combining coefficients $A(\nu)$ and $a_0\pm$ from least squares modes analysis
(a) Benchmark #3 with α = .18
(b) Benchmark #3A with α = 1.

(a)

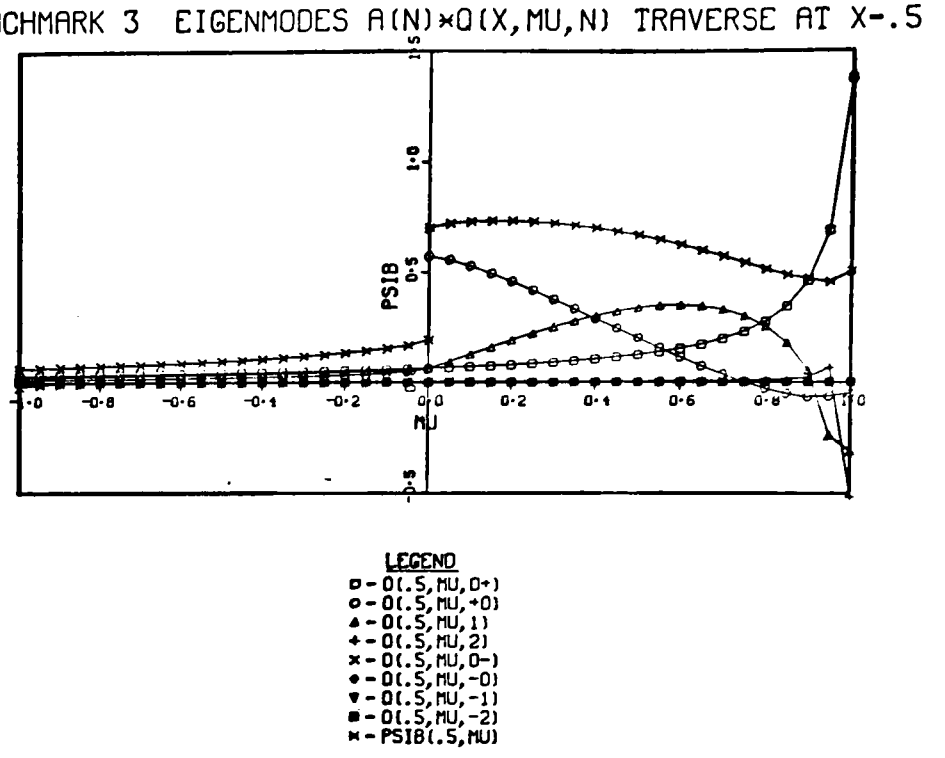

(b)

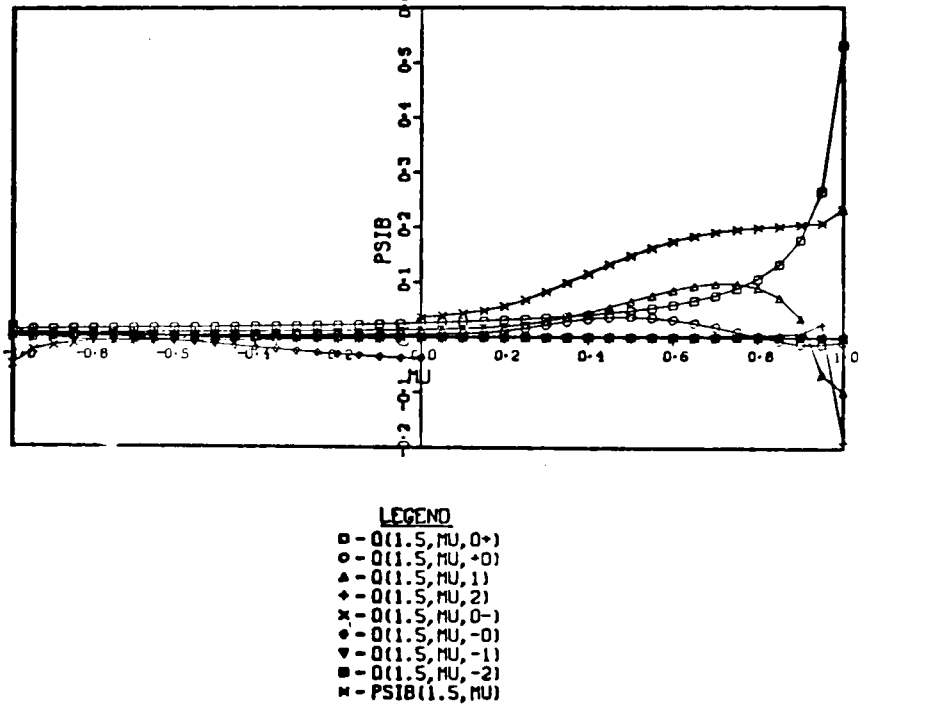

Figure 2.13. Contributions of elementary solutions $a_n q_n(x,\mu)$ to $\psi_B(x,\mu)$ in Benchmark #3
(a) μ traverse at $x = .5$, (b) μ traverse at $x = 1.5$

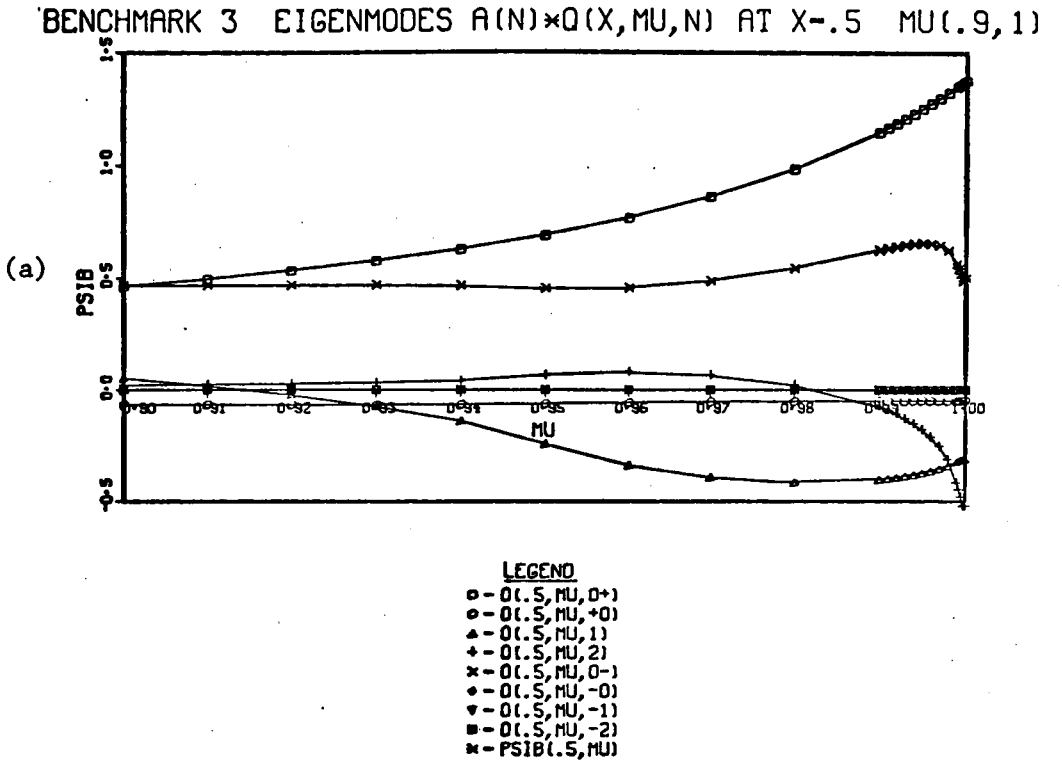

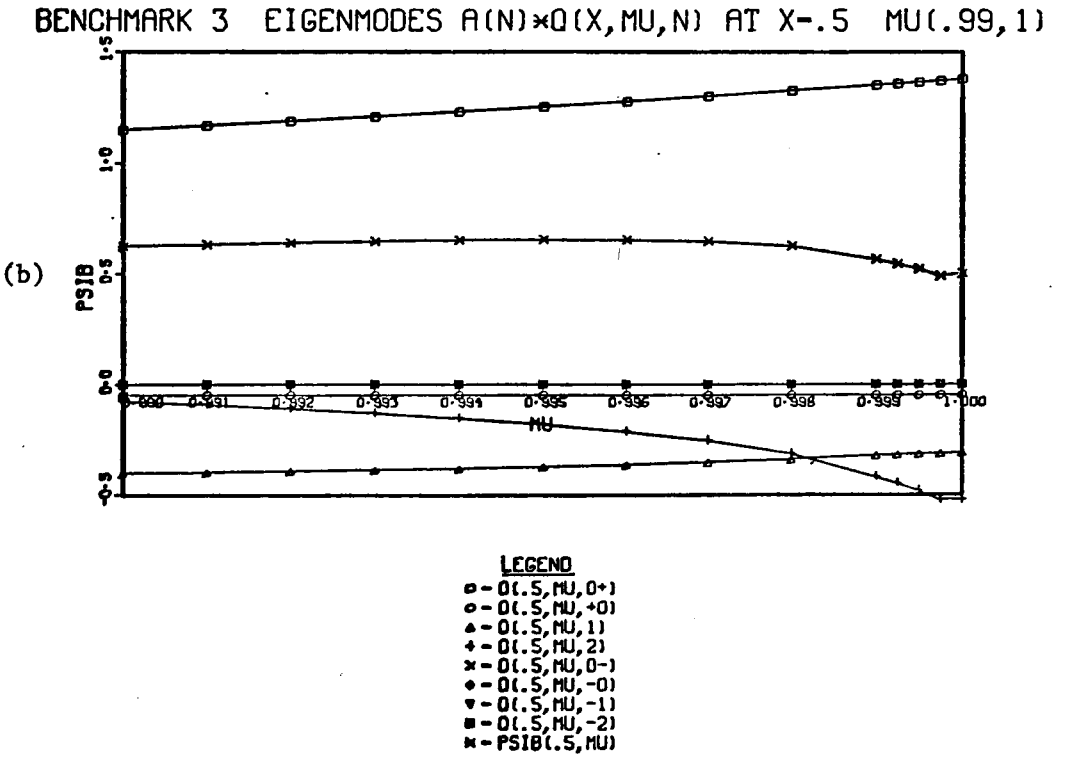

Figure 2.14. Detailed enlargement of elementary solution contributions to Benchmark #3
(a) $.9 \leq \mu \leq 1$, (b) $.99 \leq \mu \leq 1$

(a)

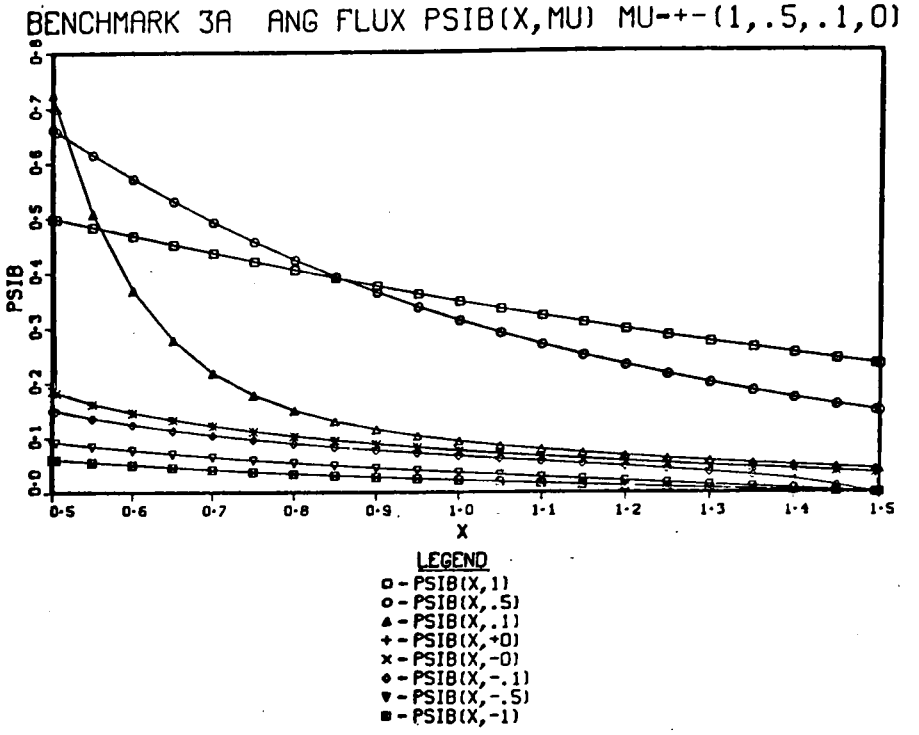

(b)

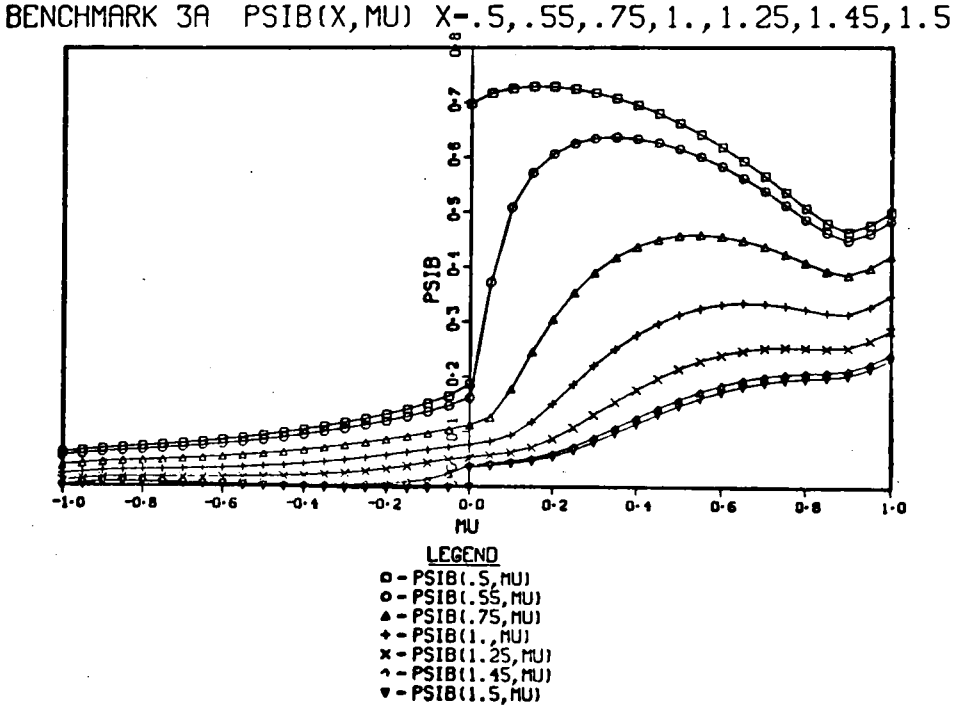

Figure 2.15. Angular flux for Benchmark #3A
(a) Angular flux traverse $\psi_B(x,\mu)$ along x for fixed μ
(b) Angular flux traverse $\psi_B(x,\mu)$ along μ for fixed x

(a)

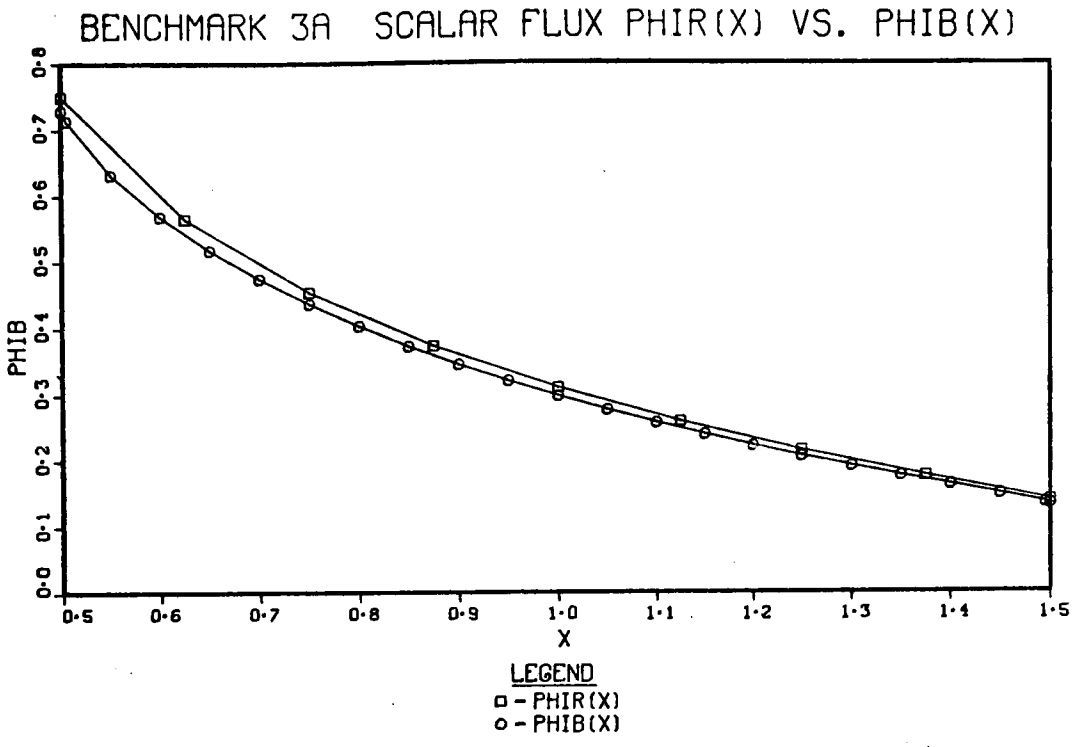

(b)

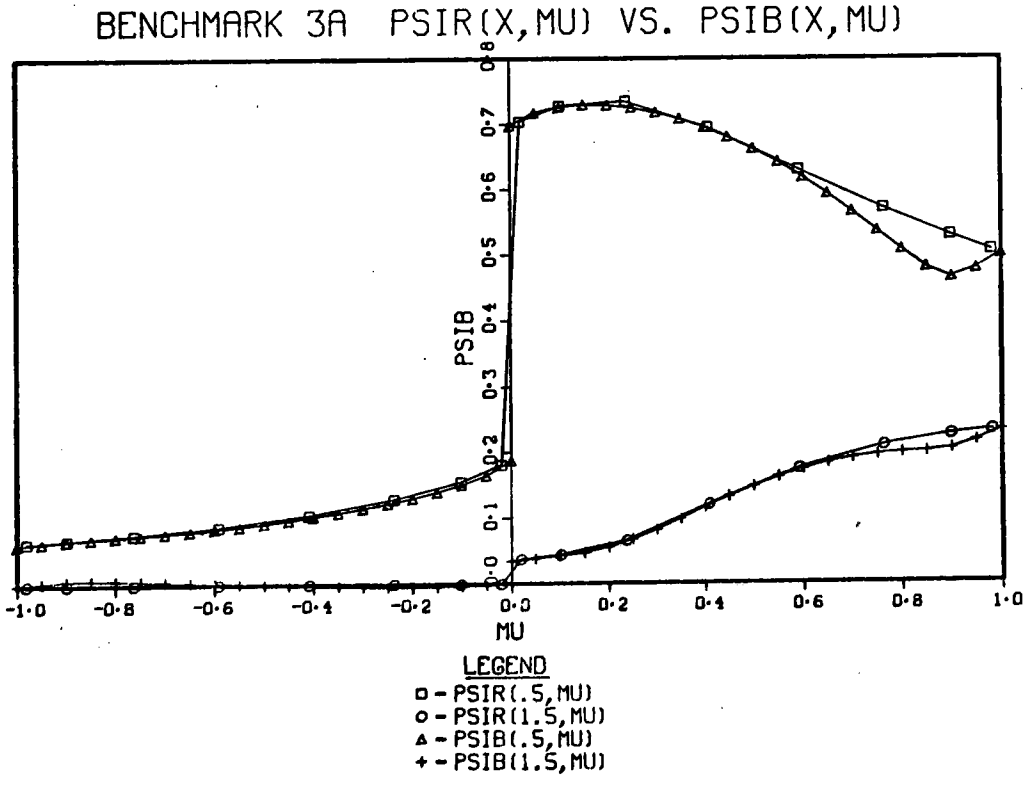

Figure 2.16. Comparison of reference and benchmark solutions for Benchmark #3A
(a) Scalar flux $\phi_R(x)$ vs. $\phi_B(x)$
(b) Angular flux $\psi_R(x,\mu)$ vs. $\psi_B(x,\mu)$ at x = .5 and x = 1.5

(a)

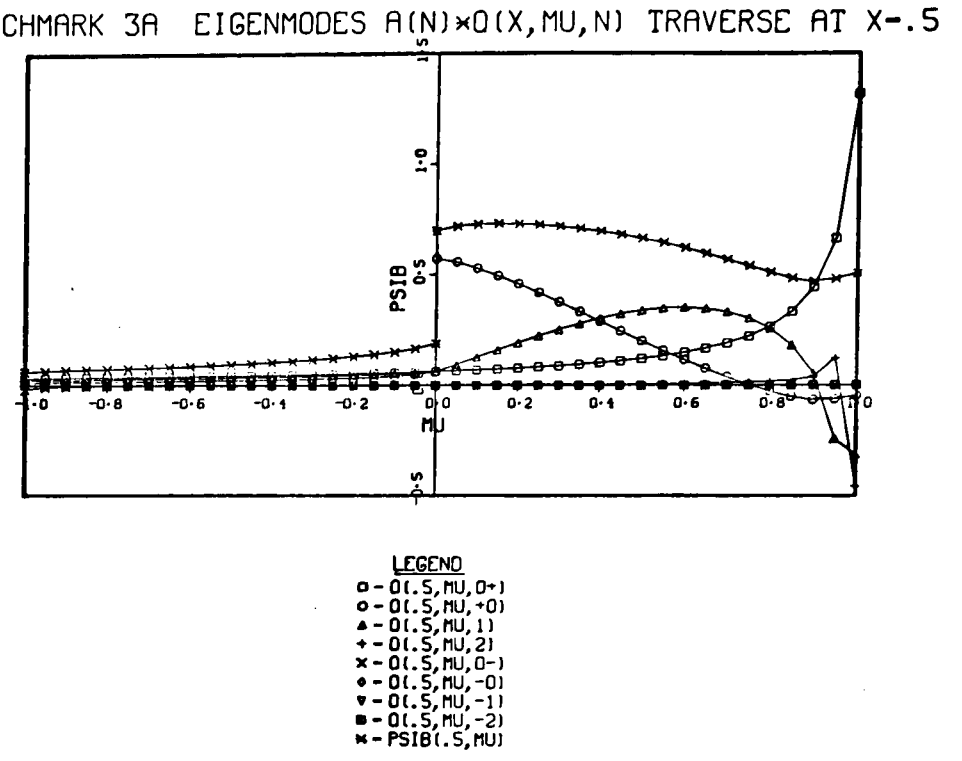

(b)

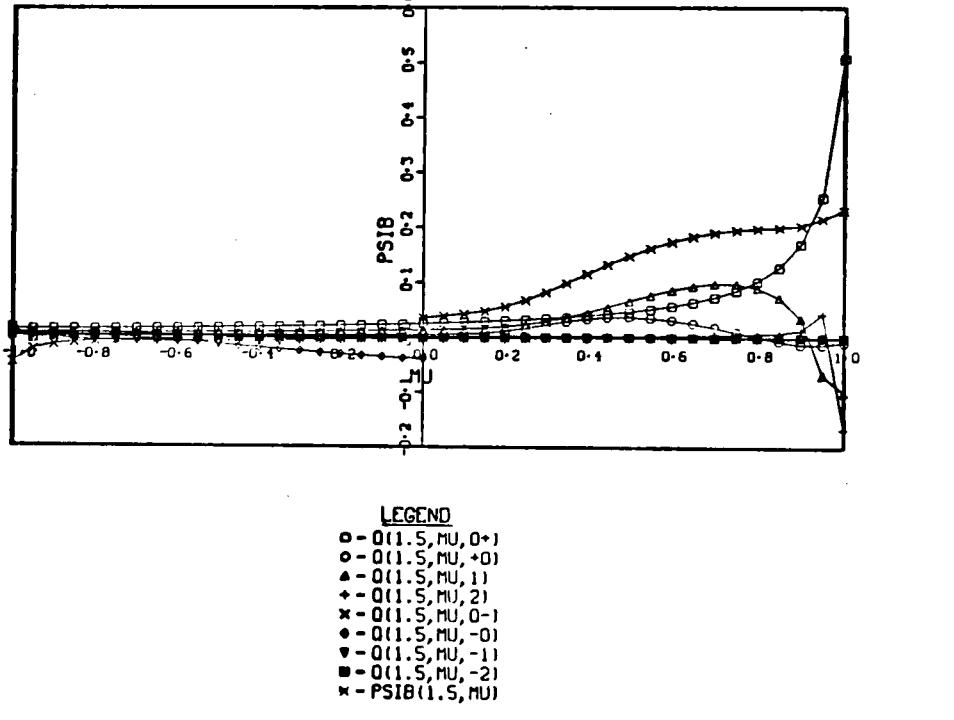

Figure 2.17. Contributions of elementary solutions $q_n(x,\mu)$ to $\psi_B(x,\mu)$ Benchmark #3A
(a) μ traverse at $x = .5$, (b) μ traverse at $x = 1.5$

(a)

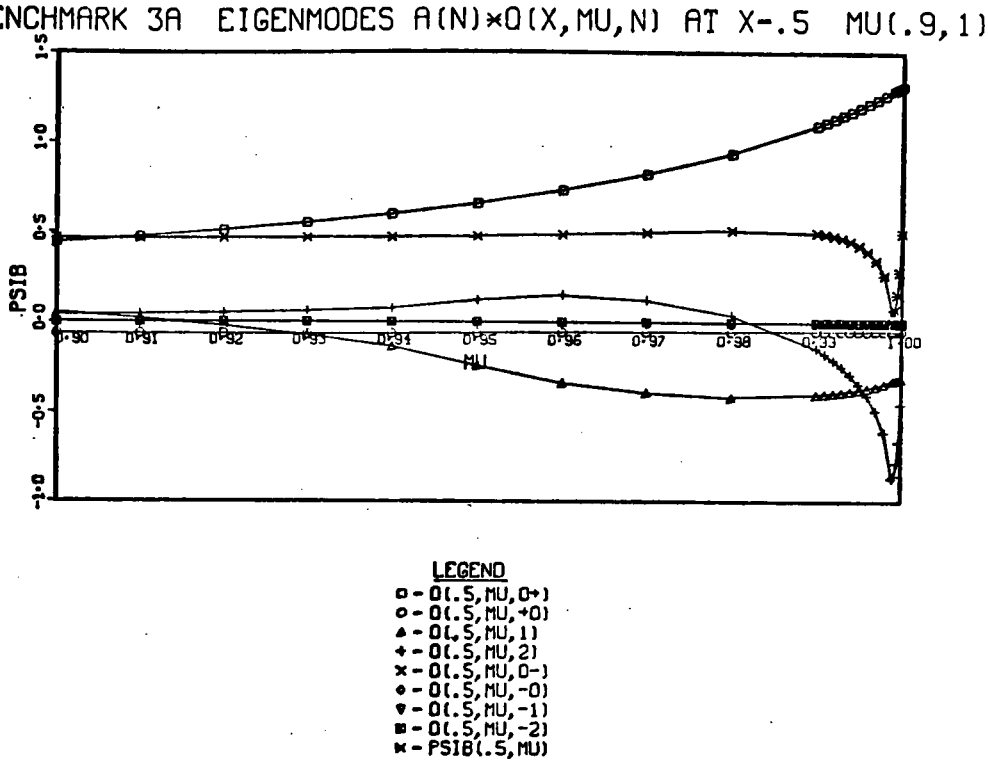

(b)

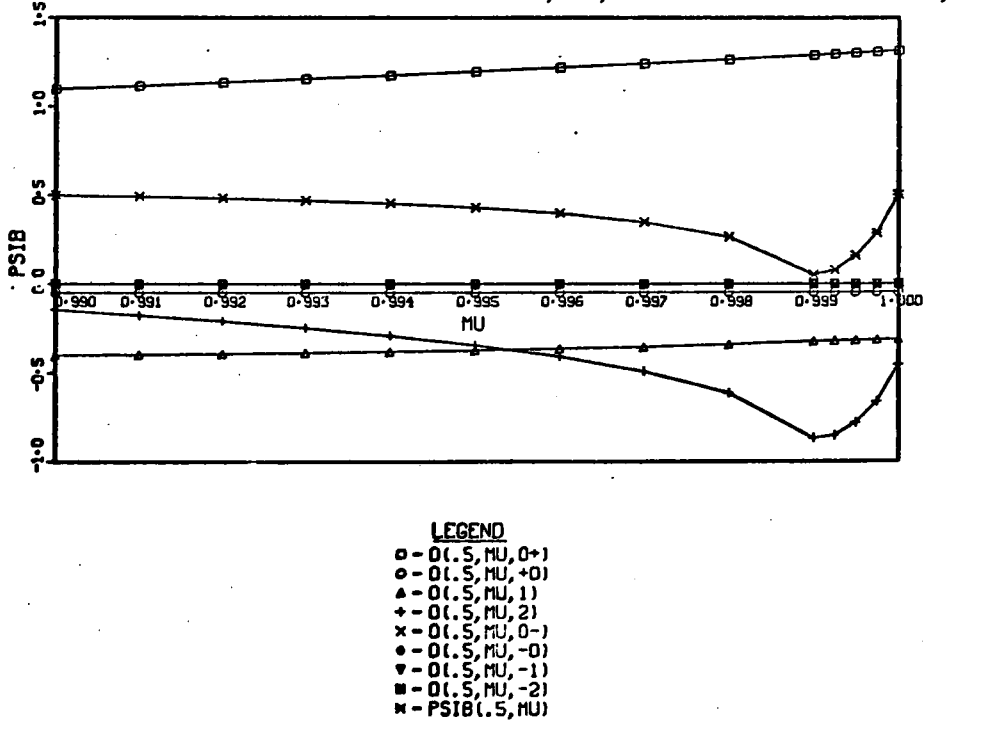

Figure 2.18. Detailed enlargement of elementary solution contributions to Benchmark #3A (a) $.9 \leq \mu \leq 1$, (b) $.99 \leq \mu \leq 1$

difference in behaviour of $a_2 q_2(x,\mu)$ in BP3 and BP3A, taking into account the different scaling factors a_2, indicates that as α is decreased the minimum point of $q_2(x,\mu)$ is continuously decreased and moves closer to $\mu = 1$. The difference in scaling factor a_2 is expected because of the difference in $q_2(x,\mu)$ at the least squares node $\mu = 1$.

Overall the effects of the α parameter do not appear to have major significance. However, should an improved discretization scheme manifest itself, then α must be reconsidered.

A set of twenty problems where the space/angle mesh refinements are varied as in BP1 are solved via the DB1, DB3 and DGF methods. The maximum absolute scalar flux error $\|\phi_E\|_\infty$ with associated sign is tabulated in Table 2.7 for each of the twenty problems. The overall error performance for the three methods shows that the DB3 and DGF methods have errors about two to three times smaller than the DB1 method. The location of the maximum error is usually the same for all methods and varies depending upon the mesh discretization. As the number of spatial mesh points are increased the maximum absolute error shifts towards the boundary at $x = .5$. This is partly due to the fact that the angular flux is a maximum at $x = .5$ and partly due to the discontinuity at $\mu = 0$ and $x = .5$.

Figure 2.19 illustrates the scalar flux error for eight of the twenty problems. The problems are chosen to illustrate the dependence of the error on spatial and angular refinements. Four problems have $I = 16$ mesh intervals with the number of angles varied from 2,4,8 to 16 and five problems have $M = 16$ with the number of spatial intervals varied from 1,2,4,8 to 16. For $M = 2$ and $M = 4$ or $I = 1$, 2 and 4 (i.e. discretizations with very large or very small space angle mesh ratios) we observe large errors.

Table 2.8 tabulates the maximum absolute angular flux error $\|\psi_E\|_\infty$ with associated algebraic sign for the three methods. The same relative behaviour of the methods is observed as described in the scalar flux analysis. Error convergence is obtained for $J = 2$ and $J = 4$ for the DB3 method. The angular location of the error consistently is located at the μ coordinates of minimum absolute value (i.e. closest to $\mu = 0$) where the

Table 2.7. Maximum absolute signed scalar flux error $\pm\|\phi_E\|_\infty$ tabulated for twenty space/angle discretization sets of Benchmark #3 for DB1, DB3 and DGF Methods

BEAPAC 05/76 BP#3.1 DB1 1 CELL M.A. X(0,.5) S=1, X(.5,1.5) S=0, NU0=1.05

MAX. ABS. SCALAR FLUX ERROR AND LOCATION (GLOBAL)

I: NO. OF XMESH INTERVALS J: NO. OF MU POINTS

(a) DB1

I		J = 2	4	8	16
ERROR	1	-4.32D-02	1.20D-01	1.19D-01	1.17D-01
EXACT		0.733	0.135	0.135	0.135
X LOC		0.500	1.500	1.500	1.500
ERROR	2	-6.06D-02	6.32D-02	6.52D-02	6.23D-02
EXACT		0.301	0.301	0.301	0.301
X LOC		1.000	1.000	1.000	1.000
ERROR	4	-9.83D-02	2.74D-02	3.51D-02	3.24D-02
EXACT		0.439	0.301	0.439	0.439
X LOC		0.750	1.000	0.750	0.750
ERROR	8	-1.01D-01	2.15D-02	1.57D-02	1.61D-02
EXACT		0.545	0.301	0.545	0.545
X LOC		0.625	1.000	0.625	0.625
ERROR	16	-1.03D-01	2.01D-02	7.47D-03	7.15D-03
EXACT		0.487	0.301	0.545	0.618
X LOC		0.688	1.000	0.625	0.563

BEAPAC 05/76 BP#3.2 DB3 1 CELL M.A. X(0,.5) S=1, X(.5,1.5) S=0, NU0=1.05

MAX. ABS. SCALAR FLUX ERROR AND LOCATION (GLOBAL)

I: NO. OF XMESH INTERVALS J: NO. OF MU POINTS

(b) DB3

I		J = 2	4	8	16
ERROR	1	-3.97D-02	1.20D-02	-4.00D-02	-4.21D-02
EXACT		0.733	0.733	0.135	0.135
X LOC		0.500	0.500	1.500	1.500
ERROR	2	-7.10D-02	1.73D-02	-1.49D-02	-2.13D-02
EXACT		0.301	0.301	0.301	0.301
X LOC		1.000	1.000	1.000	1.000
ERROR	4	-1.00D-01	1.95D-02	2.59D-03	-1.17D-02
EXACT		0.439	0.301	0.733	0.439
X LOC		0.750	1.000	0.500	0.750
ERROR	8	-1.01D-01	1.96D-02	5.02D-03	-5.18D-03
EXACT		0.545	0.301	0.545	0.545
X LOC		0.625	1.000	0.625	0.625
ERROR	16	-1.03D-01	1.96D-02	5.42D-03	-1.28D-03
EXACT		0.487	0.301	0.545	0.545
X LOC		0.688	1.000	0.625	0.625

BEAPAC 05/76 BP#3.4 DGF 2 CELL M.A. X(0,.5) S=1, X(.5,1.5) S=0, NU0=1.05

MAX. ABS. SCALAR FLUX ERROR AND LOCATION (GLOBAL)

I: NO. OF XMESH INTERVALS J: NO. OF MU POINTS

(c) DGF

I		J = 2	4	8	16
ERROR	1	-5.91D-02	2.87D-02	2.55D-02	-2.74D-02
EXACT		0.733	0.135	0.135	0.733
X LOC		0.500	1.500	1.500	0.500
ERROR	2	-5.80D-02	3.83D-02	3.03D-02	2.75D-02
EXACT		0.301	0.301	0.301	0.301
X LOC		1.000	1.000	1.000	1.000
ERROR	4	-9.65D-02	2.00D-02	1.53D-02	1.14D-02
EXACT		0.439	0.209	0.439	0.439
X LOC		0.750	1.250	0.750	0.750
ERROR	8	-1.00D-01	1.94D-02	8.24D-03	4.39D-03
EXACT		0.545	0.251	0.545	0.545
X LOC		0.625	1.125	0.625	0.625
ERROR	16	-1.03D-01	1.95D-02	5.84D-03	1.56D-03
EXACT		0.487	0.330	0.487	0.618
X LOC		0.688	0.938	0.688	0.563

(a) DB1

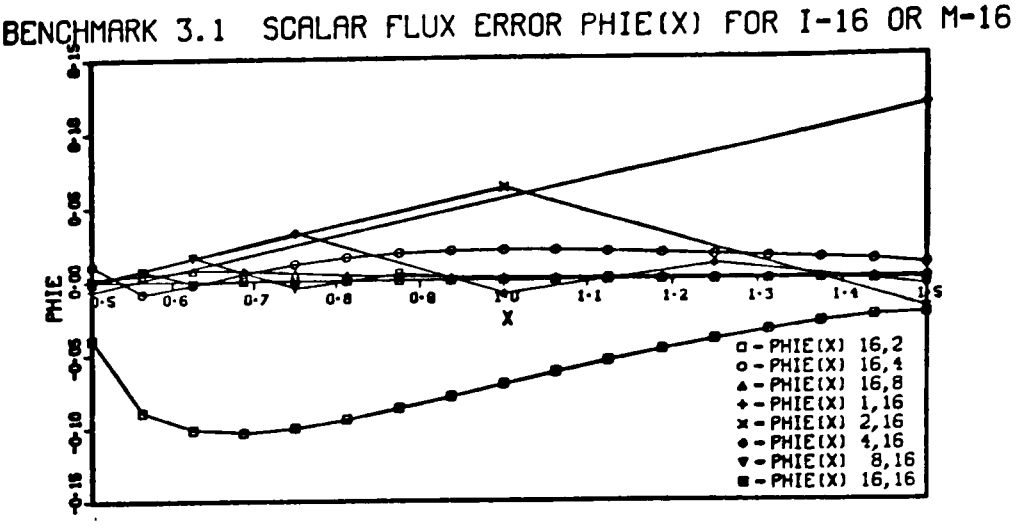

(b) DB3

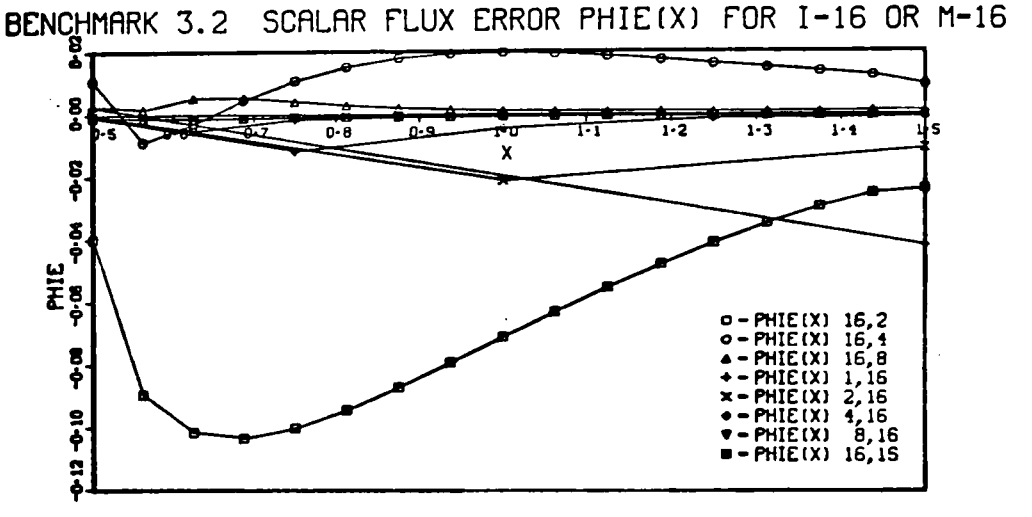

(c) DGF

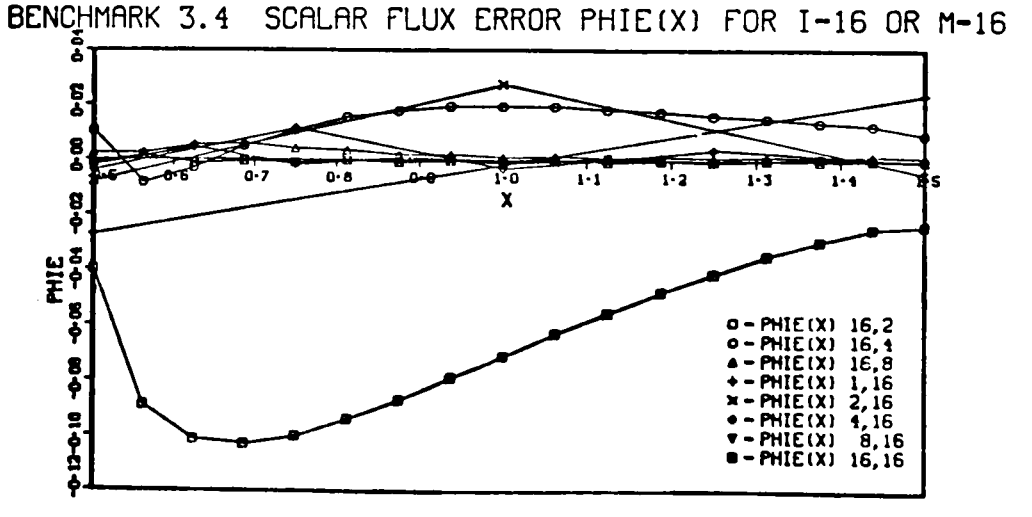

Figure 2.19. Scalar flux error $\phi_E(x)$ for DB1, DB3 and DGF methods for eight selected discretizations of Benchmark #3

Table 2.8. Maximum absolute signed angular flux error $\pm\|\psi_E\|_\infty$ for twenty space/angle discretization sets of Benchmark #3 for DB1, DB3 and DGF methods

(a) DB1

BEAPAC 05/76 BP#3.1 DB1 1 CELL M.A. X(0,.5) S=1, X(.5,1.5) S=0, MUO=1.05

MAX. ABS. VECTOR FLUX ERROR AND LOCATION (GLOBAL)

I: NO. OF XMESH INTERVALS J: NO. OF MU POINTS

	I \ J	2	4	8	16
ERROR	1	3.33D-02	2.19D-01	4.16D-01	5.03D-01
EXACT		0.147	0.058	0.040	0.036
X LOC		1.500	1.500	1.500	1.500
MULOC		0.500	0.211	0.069	0.020
ERROR	2	-1.02D-02	8.72D-02	3.00D-01	4.53D-01
EXACT		0.093	0.160	0.086	0.079
X LOC		0.500	1.000	1.000	1.000
MULOC		-0.500	0.211	0.069	0.020
ERROR	4	-1.76D-02	2.19D-02	1.61D-01	3.78D-01
EXACT		0.093	0.317	0.142	0.116
X LOC		0.500	0.750	0.750	0.750
MULOC		-0.500	0.211	0.069	0.020
ERROR	8	-1.75D-02	6.74D-03	5.64D-02	2.67D-01
EXACT		0.093	0.160	0.247	0.146
X LOC		0.500	1.000	0.625	0.625
MULOC		-0.500	0.211	0.069	0.020
ERROR	16	-1.74D-02	4.69D-03	1.31D-02	1.35D-01
EXACT		0.093	0.105	0.393	0.188
X LOC		0.500	1.188	0.563	0.563
MULOC		-0.500	0.211	0.069	0.020

(b) DB3

BEAPAC 05/76 BP#3.2 DB3 1 CELL M.A. X(0,.5) S=1, X(.5,1.5) S=0, MUO=1.05

MAX. ABS. VECTOR FLUX ERROR AND LOCATION (GLOBAL)

I: NO. OF XMESH INTERVALS J: NO. OF MU POINTS

	I \ J	2	4	8	16
ERROR	1	-1.73D-02	-3.30D-02	-2.25D-01	-4.13D-01
EXACT		0.093	0.058	0.040	0.036
X LOC		0.500	1.500	1.500	1.500
MULOC		-0.500	0.211	0.069	0.020
ERROR	2	-1.74D-02	4.01D-03	-9.52D-02	-3.21D-01
EXACT		0.093	0.056	0.086	0.079
X LOC		0.500	1.000	1.000	1.000
MULOC		-0.500	-0.211	0.069	0.020
ERROR	4	-1.74D-02	4.10D-03	-2.02D-02	-1.98D-01
EXACT		0.093	0.084	0.142	0.116
X LOC		0.500	0.750	0.750	0.750
MULOC		-0.500	-0.211	0.069	0.020
ERROR	8	-1.74D-02	4.43D-03	-1.77D-03	-7.76D-02
EXACT		0.093	0.069	0.247	0.146
X LOC		0.500	0.875	0.625	0.625
MULOC		-0.500	-0.211	0.069	0.020
ERROR	16	-1.74D-02	4.43D-03	1.27D-03	-1.56D-02
EXACT		0.093	0.069	0.125	0.188
X LOC		0.500	0.875	0.625	0.563
MULOC		-0.500	-0.211	-0.069	0.020

(c) DGF

BEAPAC 05/76 BP#3.4 DGF 2 CELL M.A. X(0,.5) S=1, X(.5,1.5) S=0, MUO=1.05

MAX. ABS. VECTOR FLUX ERROR AND LOCATION (GLOBAL)

I: NO. OF XMESH INTERVALS J: NO. OF MU POINTS

	I \ J	2	4	8	16
ERROR	1	-3.57D-02	6.51D-02	1.85D-01	2.37D-01
EXACT		0.093	0.058	0.040	0.036
X LOC		0.500	1.500	1.500	1.500
MULOC		-0.500	0.211	0.069	0.020
ERROR	2	-2.01D-02	1.82D-02	8.67D-02	1.34D-01
EXACT		0.093	0.160	0.086	0.079
X LOC		0.500	1.000	1.000	1.000
MULOC		-0.500	0.211	0.069	0.020
ERROR	4	-1.81D-02	7.25D-03	3.69D-02	1.06D-01
EXACT		0.093	0.084	0.142	0.116
X LOC		0.500	0.750	0.750	0.750
MULOC		-0.500	-0.211	0.069	0.020
ERROR	8	-1.76D-02	5.10D-03	7.50D-03	7.16D-02
EXACT		0.093	0.069	0.247	0.146
X LOC		0.500	0.875	0.625	0.625
MULOC		-0.500	-0.211	0.069	0.020
ERROR	16	-1.75D-02	4.59D-03	1.77D-03	2.76D-02
EXACT		0.093	0.076	0.140	0.188
X LOC		0.500	0.813	0.563	0.563
MULOC		-0.500	-0.211	-0.069	0.020

effects of the flux discontinuity are greatest. The spatial location of the error is usually the interior mesh point closest to the left boundary. Figures 2.20, 2.21 and 2.22 illustrate the angular flux errors along μ at $x = .5$, 1. and 1.5 respectively for the three methods. The same eight problems are considered as in the scalar flux analysis. The error significantly improves as the spatial mesh size decreases for $M = 16$. Considering this result and the results of problems BP1 and BP2, we note that for space/angle mesh discretization ratios outside of an optimal band, the errors increase.

Tables 2.9 and 2.10 tabulate the average absolute scalar flux error and the relative sum errors of the pointwise scalar flux error $\underline{\varepsilon}_E$ respectively. The average error decreases monotonically for all methods for $J = 8$ and 16, but for $J = 2$ and $J = 4$ the error decreases, reaches a minimum and then increases. A similar error behaviour is observed in Table 2.10. For equivalent discretizations the DB3 method is more accurate than the DGF method by about a factor of two.

BENCHMARK 3.1 ERROR TRAVERSES PSIE(.5,MU) FOR I-16 OR M-16

(a) DB1

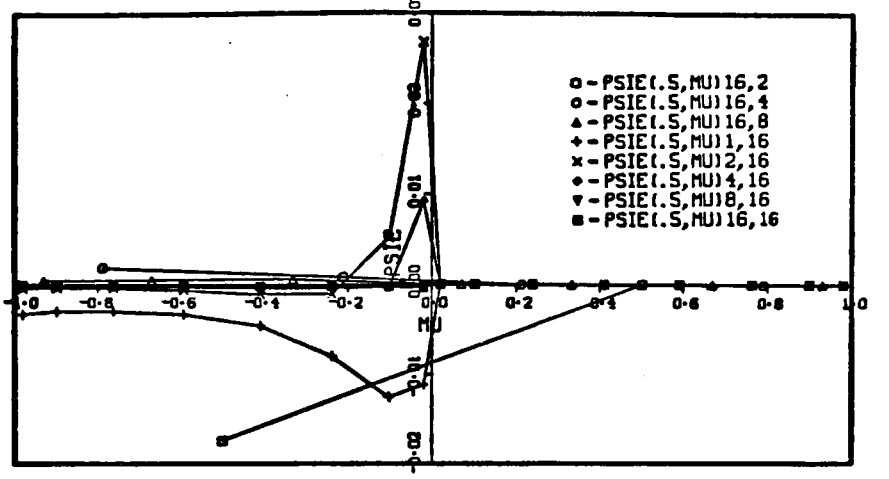

BENCHMARK 3.2 ERROR TRAVERSES PSIE(.5,MU) FOR I-16 OR M-16

(b) DB3

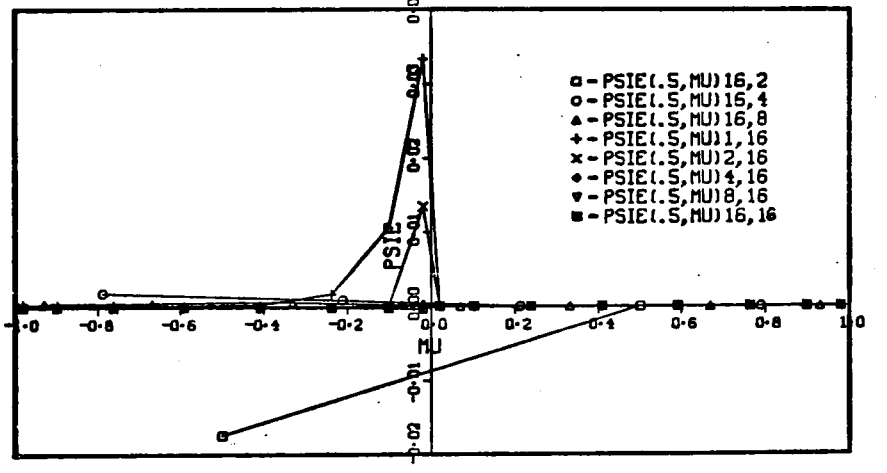

BENCHMARK 3.4 ERROR TRAVERSES PSIE(.5,MU) FOR I-16 OR M-16

(c) DGF

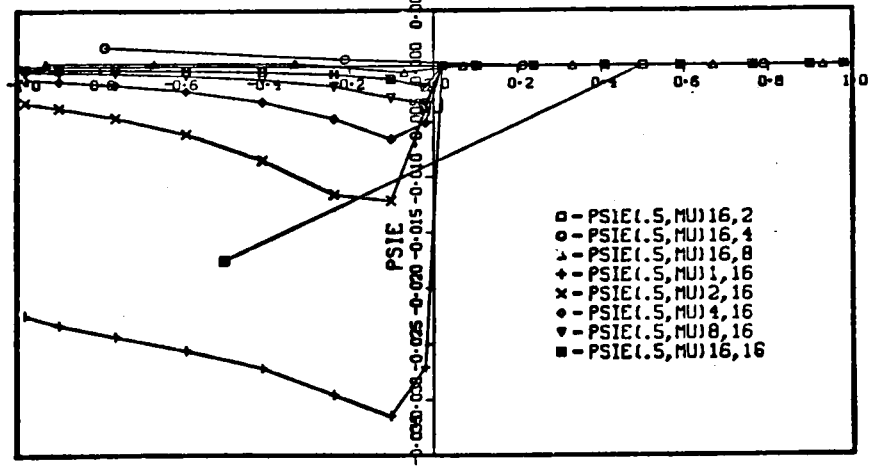

Figure 2.20. Angular flux error traverses $\psi_E(.5,\mu)$ for DB1, DB3 and DGF methods for eight selected discretizations of Benchmark #3

BENCHMARK 3.1 ERROR TRAVERSE PSIE(1,MU) FOR I-16 OR M-16

(a) DB1

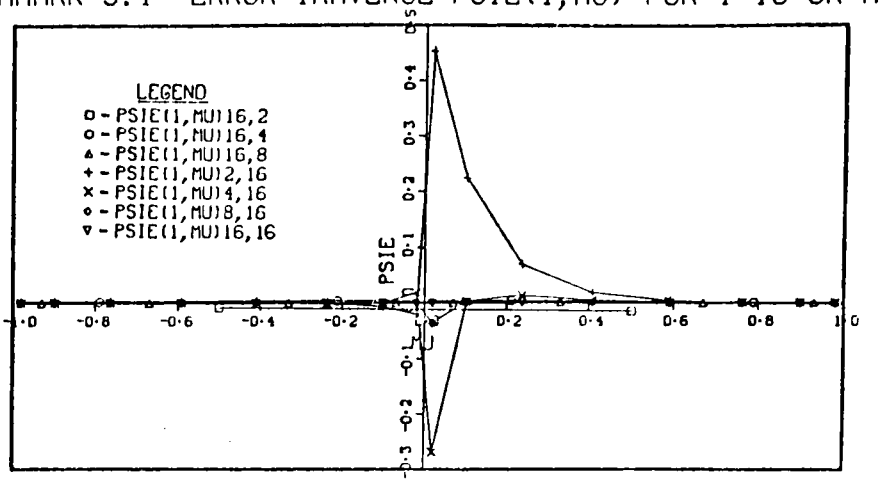

BENCHMARK 3.2 ERROR TRAVERSE PSIE(1,MU) FOR I-16 OR M-16

(b) DB3

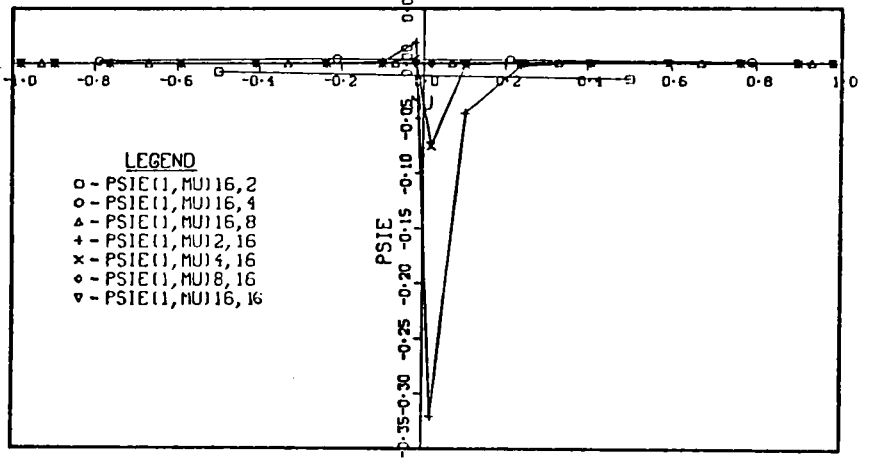

BENCHMARK 3.4 ERROR TRAVERSE PSIE(1,MU) FOR I-16 OR M-16

(c) DGF

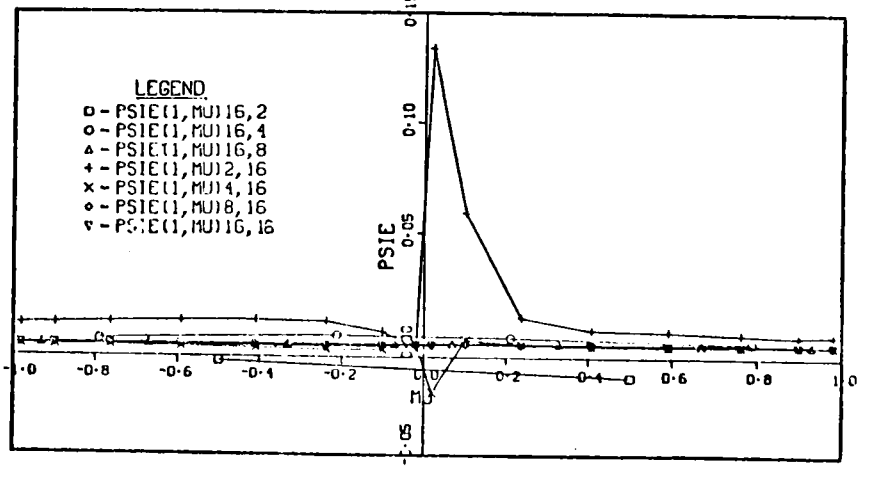

Figure 2.21. Angular flux error traverses $\psi_E(1,\mu)$ for DB1, DB3 and DGF methods for eight selected discretizations of Benchmark #3

BENCHMARK 3.1 ERROR TRAVERSE PSIE(1.5,MU) FOR I-16 OR M-16

(a) DB1

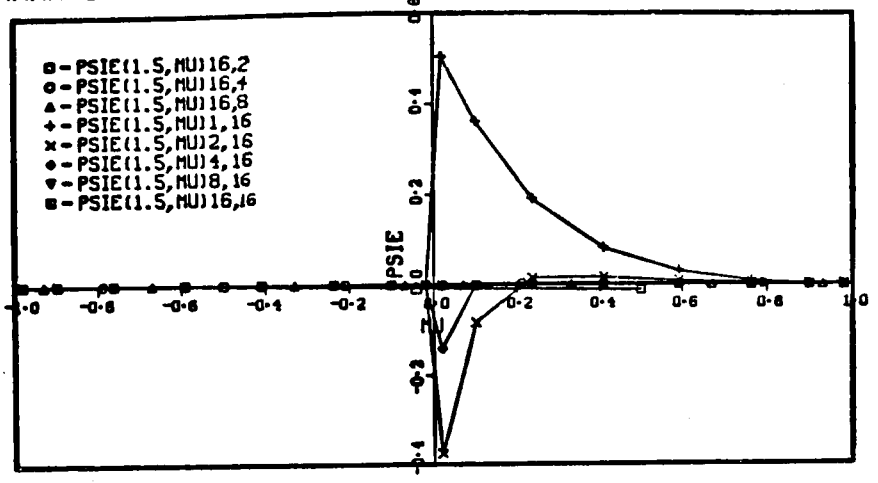

BENCHMARK 3.2 ERROR TRAVERSE PSIE(1.5,MU) FOR I-16 OR M-16

(b) DB3

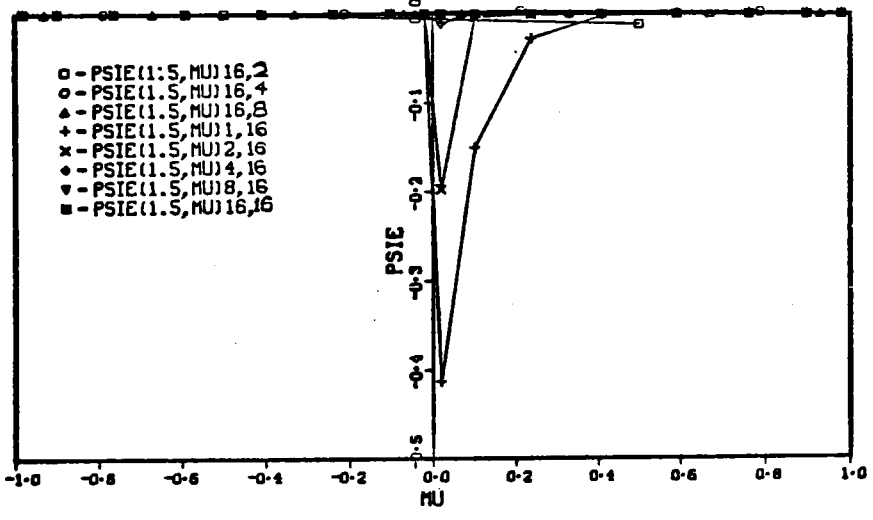

BENCHMARK 3.4 ERROR TRAVERSE PSIE(1.5,MU) FOR I-16 OR M-16

(c) DGF

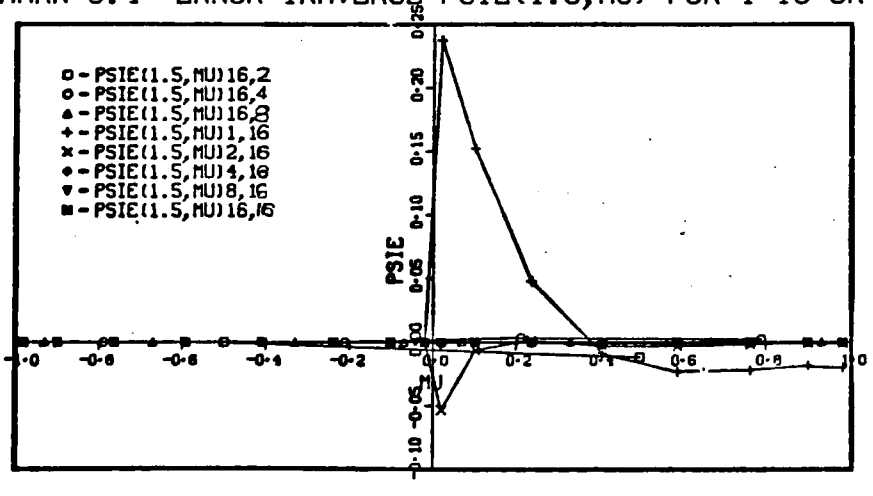

Figure 2.22. Angular flux error traverses $\psi_E(1.5,\mu)$ for DB1, DB3 and DGF methods for eight selected discretizations of Benchmark #3

Table 2.9. Average absolute scalar flux error for DB1, DB3 and DGF methods for twenty discretization sets of Benchmark #3

BEAPAC 05/76 BP#3.1 DB1 1 CELL M.A. X(0,.5) S=1, X(.5,1.5) S=0, NU0=1.05

AVG. ABS. SCALAR FLUX ERROR (GLOBAL)

I: NO. OF XMESH INTERVALS J: NO. OF MU POINTS

I \ J	2	4	8	16
ERROR 1	3.22D-02	6.26D-02	6.08D-02	6.18D-02
ERROR 2	3.85D-02	2.99D-02	2.89D-02	2.78D-02
ERROR 4	5.33D-02	1.83D-02	9.08D-03	1.17D-02
ERROR 8	6.05D-02	1.42D-02	4.06D-03	3.28D-03
ERROR 16	6.37D-02	1.38D-02	2.56D-03	8.74D-04

BEAPAC 05/76 BP#3.2 DB3 1 CELL M.A. X(0,.5) S=1, X(.5,1.5) S=0, NU0=1.05

AVG. ABS. SCALAR FLUX ERROR (GLOBAL)

I: NO. OF XMESH INTERVALS J: NO. OF MU POINTS

I \ J	2	4	8	16
ERROR 1	3.24D-02	1.00D-02	2.30D-02	2.22D-02
ERROR 2	4.49D-02	1.22D-02	6.57D-03	1.08D-02
ERROR 4	5.51D-02	1.32D-02	1.17D-03	3.86D-03
ERROR 8	6.09D-02	1.32D-02	2.06D-03	1.22D-03
ERROR 16	6.38D-02	1.36D-02	2.03D-03	7.45D-04

BEAPAC 05/76 BP#3.4 DGF 2 CELL M.A. X(0,.5) S=1, X(.5,1.5) S=0, NU0=1.05

AVG. ABS. SCALAR FLUX ERROR (GLOBAL)

I: NO. OF XMESH INTERVALS J: NO. OF MU POINTS

I \ J	2	4	8	16
ERROR 1	5.08D-02	2.21D-02	2.47D-02	2.56D-02
ERROR 2	4.28D-02	1.70D-02	1.28D-02	1.35D-02
ERROR 4	5.43D-02	1.43D-02	4.41D-03	4.63D-03
ERROR 8	6.07D-02	1.32D-02	2.64D-03	1.48D-03
ERROR 16	6.37D-02	1.36D-02	2.15D-03	6.80D-04

Table 2.10. Relative sum error of pointwise scalar flux for DB1, DB3 and DGF methods for twenty discretization sets of Benchmark #3

BEAPAC 05/76 BP#3.1 DB1 1 CELL M.A. X(0,.5) S=1, X(.5,1.5) S=0, NU0=1.05

REL. ABS. SCALAR FLUX ERROR (GLOBAL)

I: NO. OF XMESH INTERVALS J: NO. OF MU POINTS

I \ J	2	4	8	16
ERROR 1	7.41D-02	1.44D-01	1.40D-01	1.42D-01
ERROR 2	9.89D-02	7.68D-02	7.43D-02	7.14D-02
ERROR 4	1.47D-01	5.04D-02	2.50D-02	3.21D-02
ERROR 8	1.73D-01	4.05D-02	1.16D-02	9.39D-03
ERROR 16	1.86D-01	4.04D-02	7.46D-03	2.55D-03

BEAPAC 05/76 BP#3.2 DB3 1 CELL M.A. X(0,.5) S=1, X(.5,1.5) S=0, NU0=1.05

REL. ABS. SCALAR FLUX ERROR (GLOBAL)

I: NO. OF XMESH INTERVALS J: NO. OF MU POINTS

I \ J	2	4	8	16
ERROR 1	7.46D-02	2.31D-02	5.29D-02	5.12D-02
ERROR 2	1.15D-01	3.12D-02	1.69D-02	2.77D-02
ERROR 4	1.52D-01	3.63D-02	3.23D-03	1.06D-02
ERROR 8	1.74D-01	3.79D-02	5.90D-03	3.50D-03
ERROR 16	1.86D-01	3.96D-02	5.93D-03	2.17D-03

BEAPAC 05/76 BP#3.4 DGF 2 CELL M.A. X(0,.5) S=1, X(.5,1.5) S=0, NU0=1.05

REL. ABS. SCALAR FLUX ERROR (GLOBAL)

I: NO. OF XMESH INTERVALS J: NO. OF MU POINTS

I \ J	2	4	8	16
ERROR 1	1.17D-01	5.09D-02	5.68D-02	5.90D-02
ERROR 2	1.10D-01	4.37D-02	3.28D-02	3.48D-02
ERROR 4	1.50D-01	3.92D-02	1.21D-02	1.27D-02
ERROR 8	1.74D-01	3.79D-02	7.54D-03	4.24D-03
ERROR 16	1.86D-01	3.98D-02	6.29D-03	1.98D-03

2.2.4 Benchmark Problem #4, a two cell least squares modes analysis

The reference problem configuration for BP4 is given in section 2.2.3 and the reference solution $\psi_R(x,\mu)$ is displayed in Fig. 2.9. In this problem we generate a benchmark solution $\psi_B(x,\mu)$ in two cells as described in section 1.1.6. Figure 2.23 illustrates $\psi_B(x,\mu)$ for x traverses and μ traverses in the usual fashion. At the interface x = .5 there is a flux discontinuity for $\mu = 0$ due to the source in cell I.

Comparisons of scalar flux $\phi_R(x)$ and $\phi_B(x)$, and angular flux $\psi_R(x,\mu)$ and $\psi_B(x,\mu)$ are illustrated in Fig. 2.24a,b respectively. The maximum relative scalar flux differences are about 4% in cell I. The angular flux differences in cell I are about .15 (arbitrary units) at the interface x = .5 for $\mu \leq 0$ (in particular near $\mu = -.9$). The difficulty in approximating the angular flux in cell I is not evident, but may be related to the reflecting boundary condition at x = 0.

The benchmark solution $\psi_B(x,\mu)$ in cell II is obtained exactly as in BP3 but is then modified by a regionwise constant angular source $Q(\mu)$ which is required to satisfy the interface condition of flux continuity. Figure (2.25b) illustrates the constant source $S_I = .5$ in cell I and the interface condition source $Q(\mu)$ in cell II. The angular flux difference of $\psi_B(.5,\mu)$ and $\psi_R(.5,\mu)$ in cell I is the dominant factor in the shape of $Q(\mu)$ in cell II.

Again we recall our original purpose in this work is to create exact benchmark problems which can be related to physical problems. We claim BP4 is such a problem and as such can be used to analyze the error performance of numerical methods with particular interest in observing the error at the interface x = .5.

First we examine $\psi_B(x,\mu)$ in more detail. Figure 2.25a illustrates the transient combining coefficients $A(\nu_n)$ and asymptotic coefficients $a_0\pm$ for cells I and II. In cell II the $A(\nu)$ are precisely the same as in BP3. The coefficients a_n in cell I can be better understood by analyzing Fig. 2.26a which displays the contribution of the $a_n q_n$ to $\psi_B(x,\mu)$ at the cell boundary x = 0. The negative contributions of the $a_n q_n$ are added to the particular solution corresponding to the source in each cell.

Sixteen different space/angle mesh discretizations for BP4 were

(a)

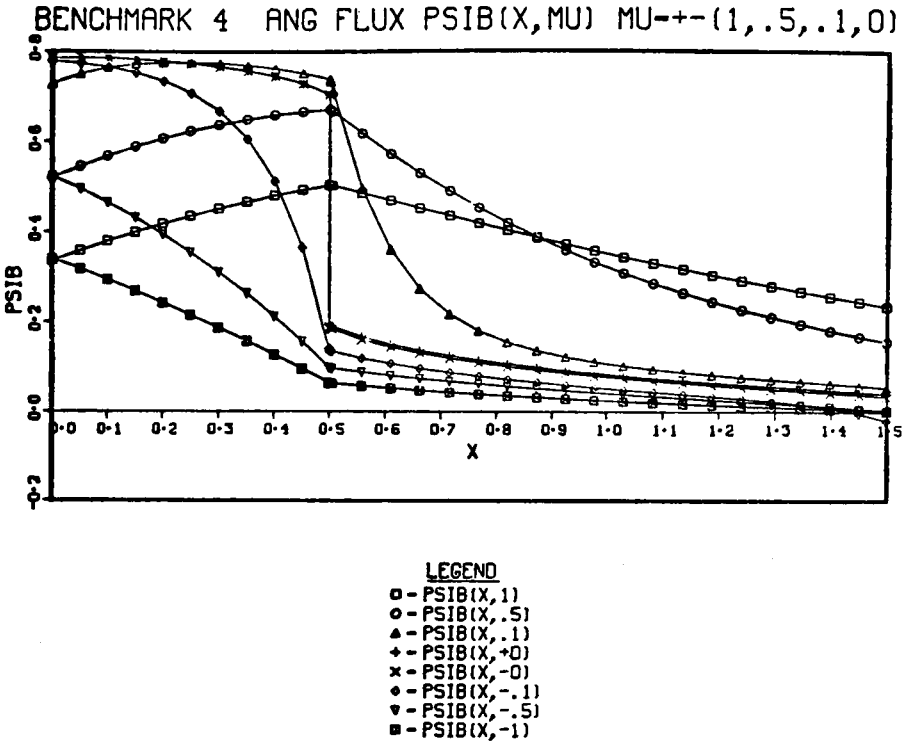

(b)

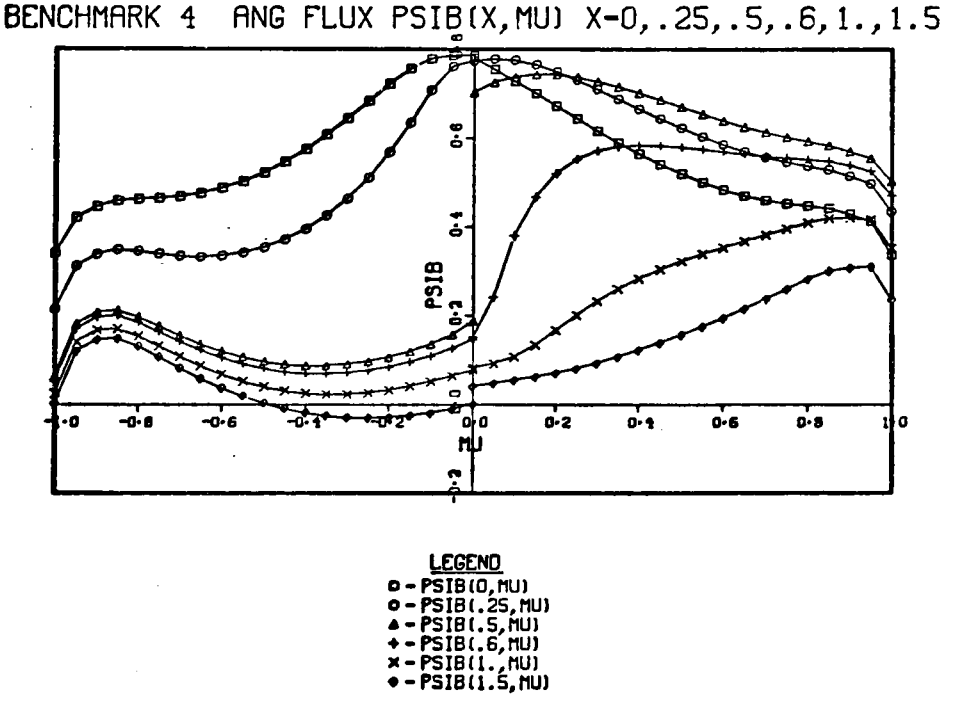

Figure 2.23. Angular flux traverses for Benchmark #4
(a) Traverse along x for fixed μ
(b) Traverse along μ for fixed x

(a)

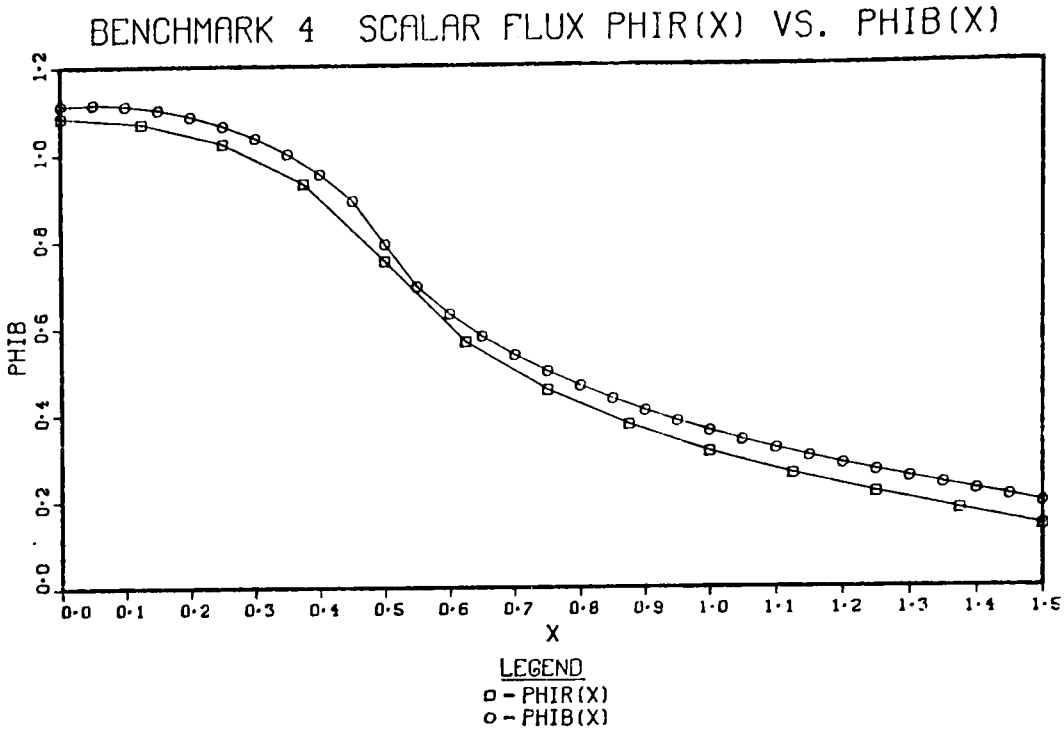

(b)

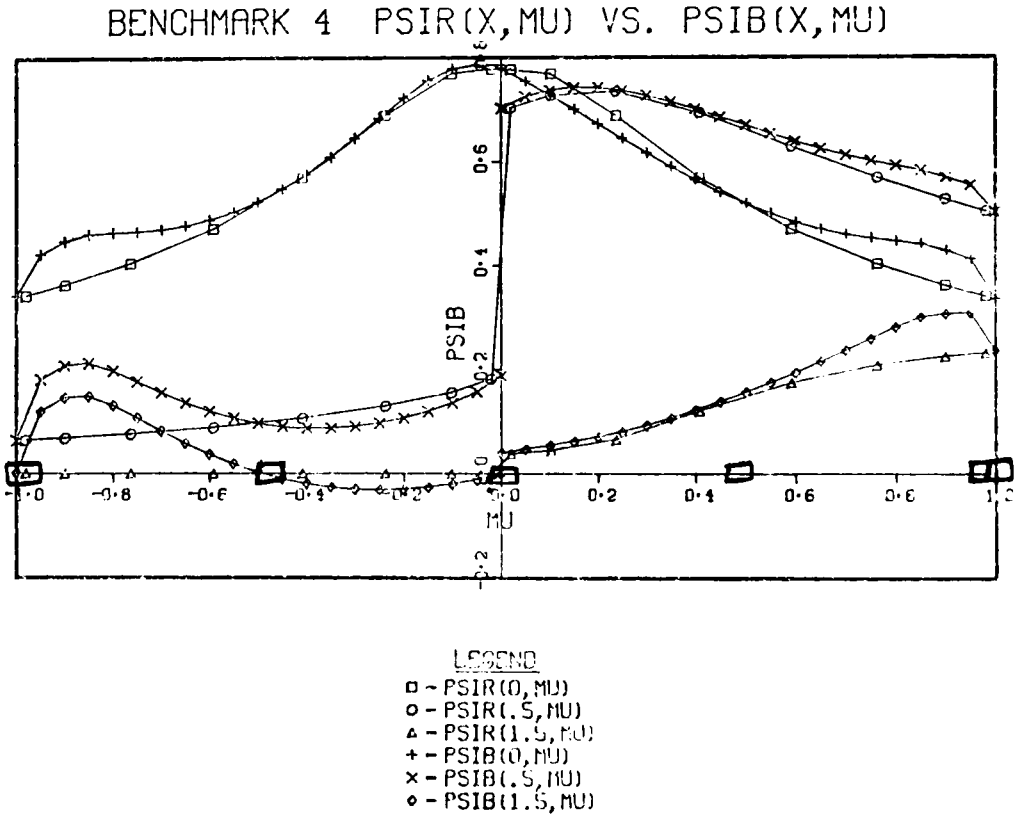

Figure 2.24. Comparison of DB3 reference and benchmark solutions for Benchmark #4

a. Scalar flux $\phi_R(x)$ vs. $\phi_B(x)$

b. Angular flux $\psi_R(x,\mu)$ vs. $\psi_B(x,\mu)$ at x=0, x=.5 and x=1.

(a)

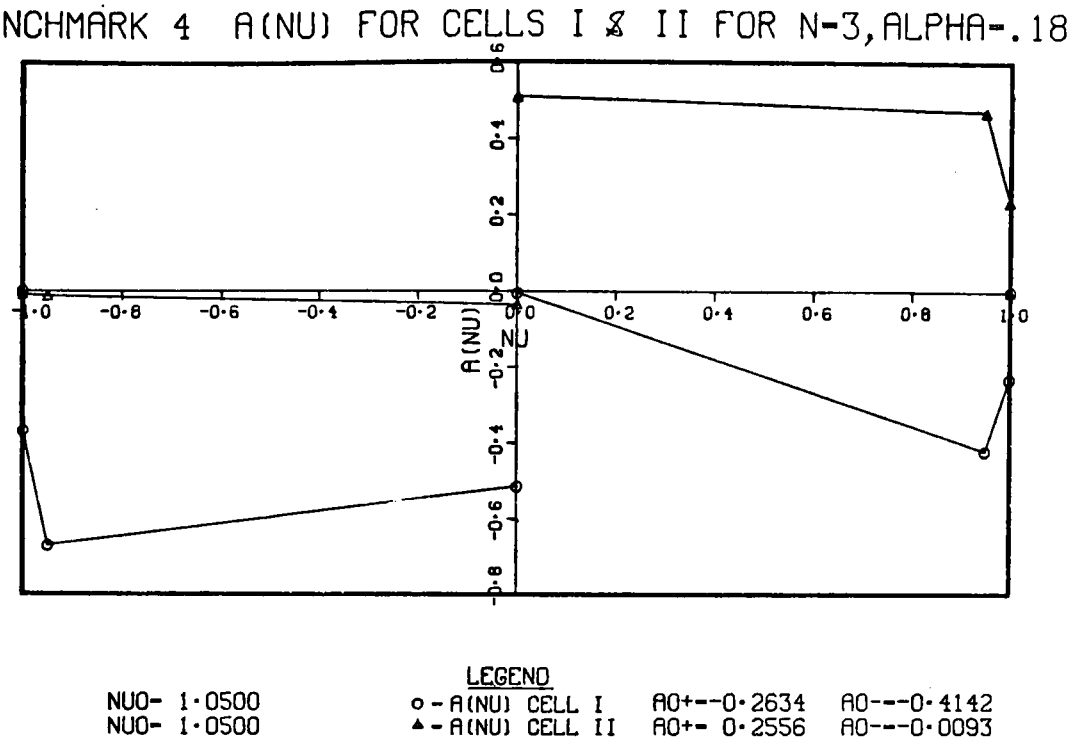

(b)

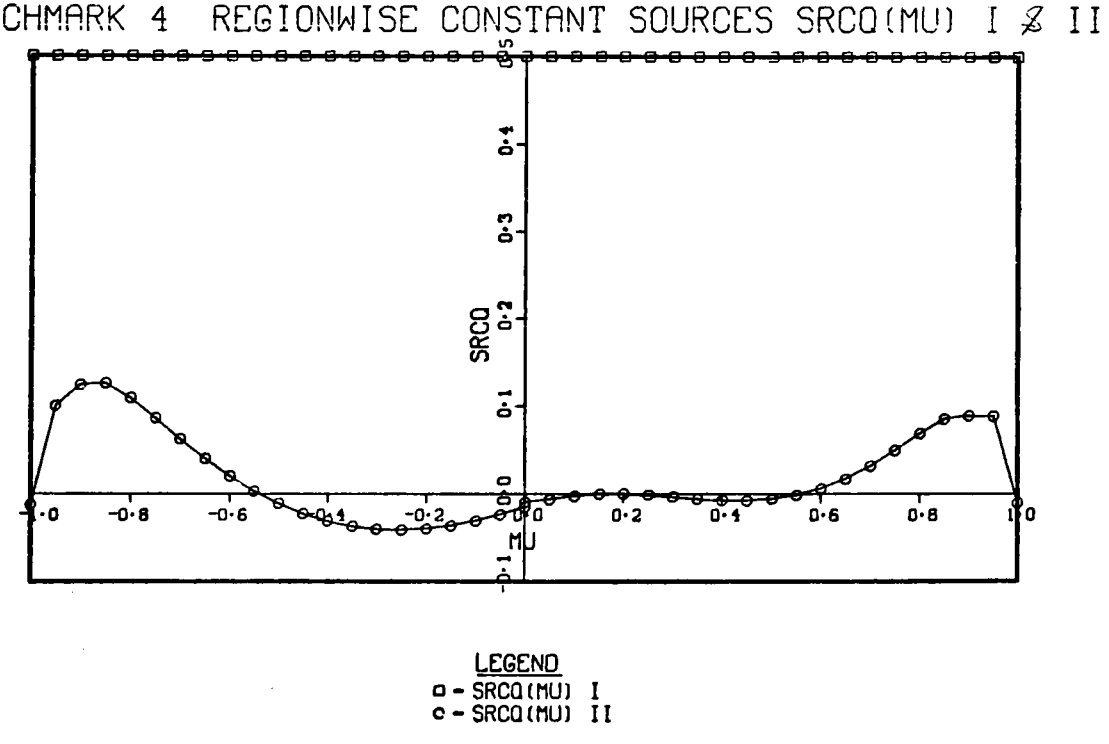

Figure 2.25. (a) Combining coefficients $A(\nu)$ and $a_0^{\pm}$ from least squares modes analysis
(b) Regionwise constant sources in Cell I and Cell II for Benchmark #4

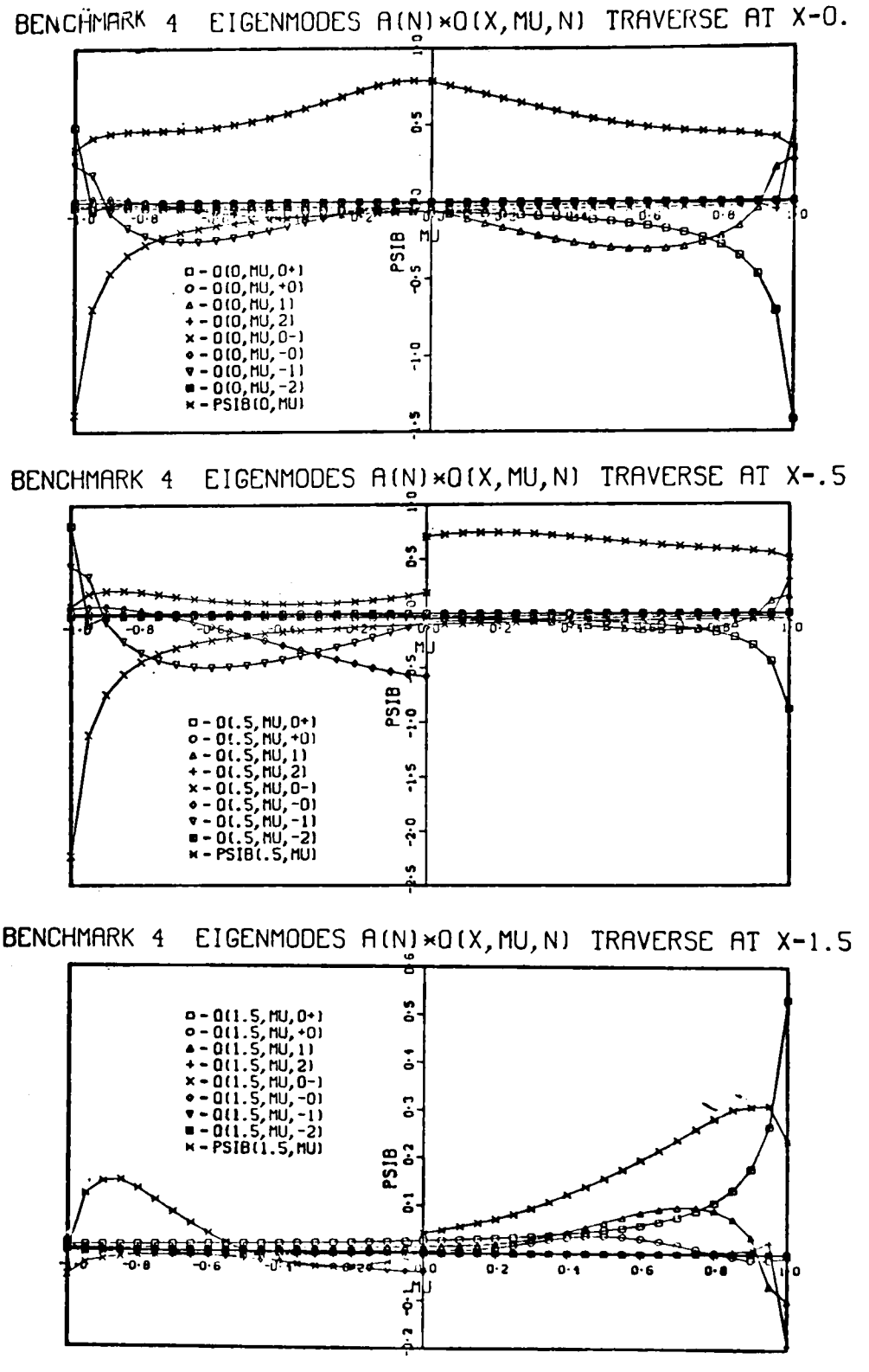

Figure 2.26. Contributions of elementary solutions $a_n q_n(x,\mu)$ to $\psi_B(x,\mu)$ in Benchmark #4 for μ traverse at (a) x=0, (b) x=.5, (c) x=1.5

solved. The spatial mesh discretization is equally spaced in the two cells. The angular discretization is the same as in the previous problems. The absolute maximum scalar flux error $\|\underline{\phi}_E\|_\infty$ with associated sign is tabulated in Table 2.11 for the three methods of the previous sections. For equivalent mesh discretizations, omitting the cases when I = 3, the DB1 and DGF methods have comparable accuracy. For I = 3 or 6 and J = 8 or 16 the maximum error in DB1 and DGF is about three or four times the error of DB3. Figure 2.27 illustrates this clearly for seven selected discretizations. Also apparent is a significant error fluctuation about the interface at x = .5 for low angular approximations.

The optimum space/angle mesh ratio phenomenon is particularly noticeable for DB1 and DGF where the combination (I,M) = (3,16) has an error comparable to (I,M) = (24,4). As the mesh is refined for M = 16 the error magnitude oscillates about zero with the location of the maximum error approaching the interface x = .5.

The maximum absolute angular flux error $\|\psi_E\|_\infty$ with associated algebraic sign is tabulated in Table 2.12. The maximum error is located at the μ coordinates with smallest absolute value for all methods. For DB1 it is always located in cell I. For DGF it is located at the cell interface x = .5 for all but two problems (J = 4). For DB3 it is usually in cell I with two exceptions when J = 8.

Figures 2.28, 2.29 and 2.30 illustrate the angular flux error for traverses along x = 0, .5, 1.5. For low order spatial discretizations the error magnitude is largest in the neighborhood of $\mu = 0$. At x = 0 the error (Fig. 2.28) is symmetric for all three methods due to the reflecting boundary condition. At the interface x = .5, the error is largest near $\mu = 0$ for $\mu > 0$. In the DGF method the error is antisymmetric about $\mu = 0$. At x = 1.5 the error shape is similar to the shape at x = .5, except the antisymmetric behavior is absent from DGF.

The average absolute scalar flux error and the relative sum error of the scalar flux is tabulated in Tables 2.13 and 2.14. A comparison of the errors for the three methods for low order spatial discretizations (Table 2.13) reveals that the methods (DB1, DB3 and DGF) are ranked in order of decreasing error magnitude. As the number of space mesh intervals increases, the average error magnitudes for the three methods for equivalent mesh discretizations become less distinct.

Table 2.11. Maximum absolute signed scalar flux error $\pm\|\phi_E\|_\infty$ tabulated for sixteen space/angle discretization sets of Benchmark #4 for DB1, DB3 and DGF methods

(a) DB1

BEAPAC 05/76 BP#4.1 DB1 2 CELL M.A. X(0,.5) S=1, X(.5,1.5) S=0, MU0=1.05

MAX. ABS. SCALAR FLUX ERROR AND LOCATION (GLOBAL)

I: NO. OF XMESH INTERVALS J: NO. OF MU POINTS

I \ J		2	4	8	16
ERROR	3	7.60D-02	-1.63D-01	-1.60D-01	-1.47D-01
EXACT		1.113	1.113	1.113	1.113
X LOC		0.0	0.0	0.0	0.0
ERROR	6	1.15D-01	-7.67D-02	-5.24D-02	-4.93D-02
EXACT		1.064	1.113	1.064	1.064
X LOC		0.250	0.0	0.250	0.250
ERROR	12	1.20D-01	-6.37D-02	-2.45D-02	1.97D-02
EXACT		1.064	0.602	0.976	0.602
X LOC		0.250	0.625	0.375	0.625
ERROR	24	1.21D-01	-7.05D-02	-1.51D-02	1.13D-02
EXACT		1.064	0.674	0.976	0.674
X LOC		0.250	0.563	0.375	0.563

(b) DB3

BEAPAC 05/76 BP#4.2 DB3 2 CELL M.A. X(0,.5) S=1, X(.5,1.5) S=0, MU0=1.05

MAX. ABS. SCALAR FLUX ERROR AND LOCATION (GLOBAL)

I: NO. OF XMESH INTERVALS J: NO. OF MU POINTS

I \ J		2	4	8	16
ERROR	3	1.08D-01	-5.19D-02	2.72D-02	4.96D-02
EXACT		1.113	1.113	1.113	1.113
X LOC		0.0	0.0	0.0	0.0
ERROR	6	1.22D-01	-5.73D-02	-1.25D-02	1.61D-02
EXACT		1.064	1.113	0.496	1.064
X LOC		0.250	0.0	0.750	0.250
ERROR	12	1.22D-01	-6.51D-02	-1.23D-02	7.50D-03
EXACT		1.064	0.602	0.976	0.976
X LOC		0.250	0.625	0.375	0.375
ERROR	24	1.22D-01	-7.06D-02	-1.27D-02	3.59D-03
EXACT		1.064	0.674	0.976	0.386
X LOC		0.250	0.563	0.375	0.938

(c) DGF

BEAPAC 05/76 BP#4.4 DGF 2 CELL M.A. X(0,.5) S=1, X(.5,1.5) S=0, MU0=1.05

MAX. ABS. SCALAR FLUX ERROR AND LOCATION (GLOBAL)

I: NO. OF XMESH INTERVALS J: NO. OF MU POINTS

I \ J		2	4	8	16
ERROR	3	1.35D-01	5.39D-02	8.83D-02	1.03D-01
EXACT		1.113	0.358	0.358	0.358
X LOC		0.0	1.000	1.000	1.000
ERROR	6	1.08D-01	-9.22D-02	-5.33D-02	-3.96D-02
EXACT		1.113	1.064	1.064	1.064
X LOC		0.0	0.250	0.250	0.250
ERROR	12	1.22D-01	-6.82D-02	-3.14D-02	1.94D-02
EXACT		1.064	1.107	0.976	0.602
X LOC		0.250	0.125	0.375	0.625
ERROR	24	1.22D-01	-6.76D-02	-1.69D-02	1.23D-02
EXACT		1.064	0.674	0.907	0.674
X LOC		0.250	0.563	0.438	0.563

(a) DB1

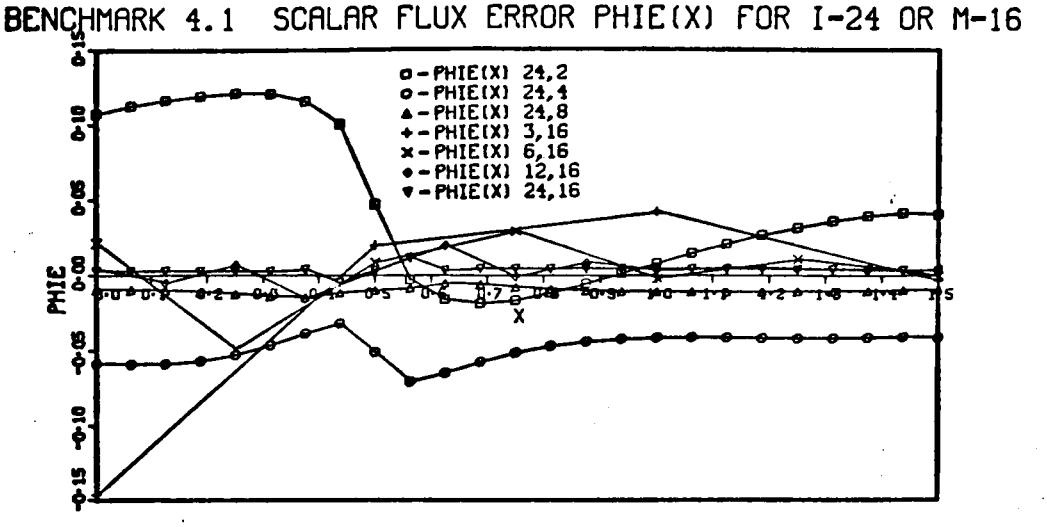

(b) DB3

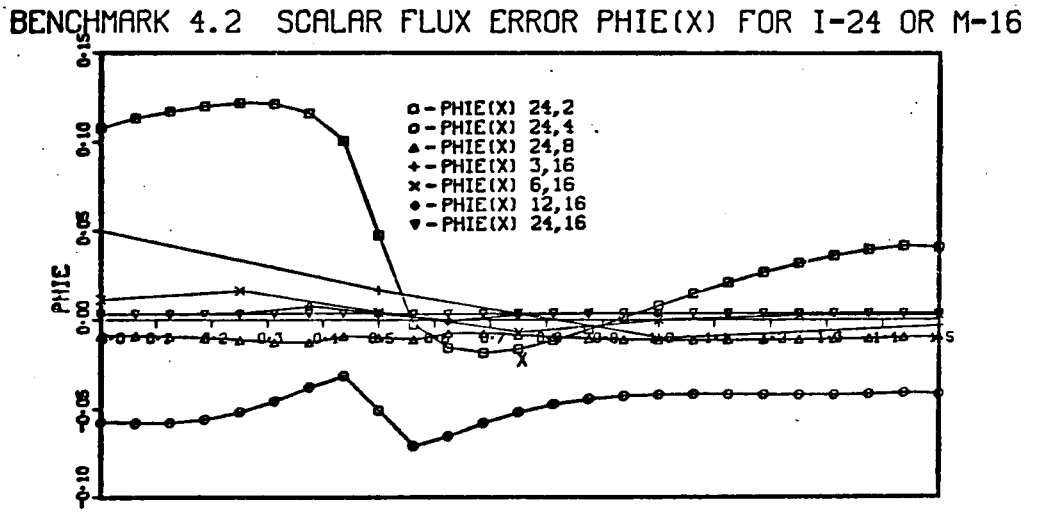

(c) DGF

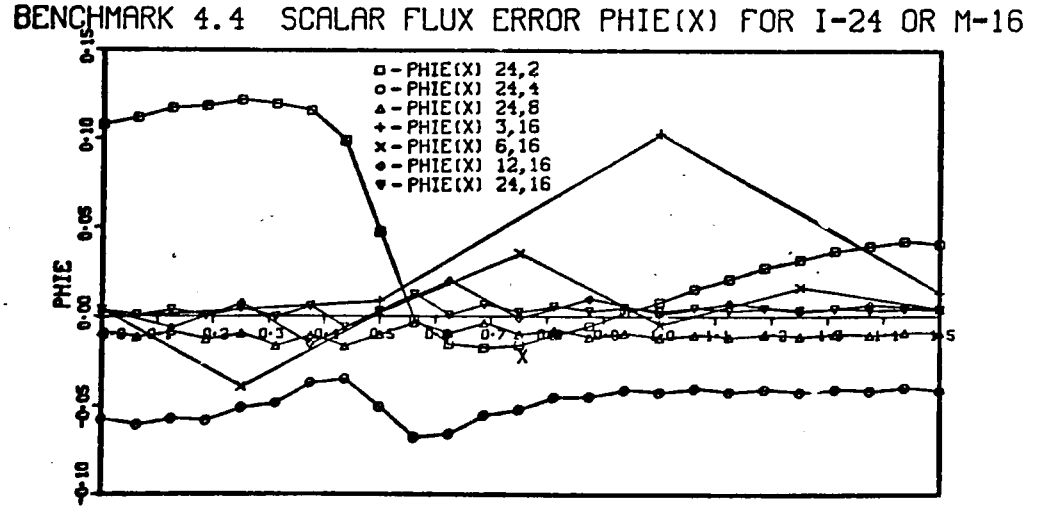

Figure 2.27. Scalar flux error $\phi_E(x)$ for DB1, DB3 and DGF methods for seven selected discretizations of Benchmark #4

Table 2.12. Maximum absolute signed angular flux error $\pm\|\psi_E\|_\infty$ for twenty space/angle discretization sets of Benchmark #4 for DB1, DB3 and DGF methods

BEAPAC 05/76 BP#4.1 DB1 2 CELL B.A. X(0,.5) S=1, X(.5,1.5) S=0, SUO=1.05

MAX. ABS. VECTOR FLUX ERROR AND LOCATION (GLOBAL)

I: NO. OF MESH INTERVALS J: NO. OF SU POINTS

I \ J	2	4	8	16
ERROR 3	1.47D-02	-1.15D-01	-3.33D-01	-4.99D-01
EXACT	0.156	0.666	0.784	0.786
X LOC	1.500	0.0	0.0	0.0
SULOC	0.500	0.211	-0.069	-0.020
ERROR 6	2.15D-02	-3.71D-02	-1.71D-01	-3.94D-01
EXACT	0.671	0.554	0.745	0.770
X LOC	0.500	0.250	0.250	0.250
SULOC	0.500	-0.211	-0.069	-0.020
ERROR 12	2.40D-02	-1.82D-02	-6.09D-02	-2.72D-01
EXACT	0.654	0.655	0.640	0.744
X LOC	0.375	0.125	0.375	0.375
SULOC	0.500	-0.211	-0.069	-0.020
ERROR 24	2.50D-02	-1.52D-02	-1.60D-02	-1.37D-01
EXACT	0.664	0.719	0.488	0.702
X LOC	0.438	0.125	0.438	0.438
SULOC	0.500	0.211	-0.069	-0.020

BEAPAC 05/76 BP#4.2 DB3 2 CELL B.A. X(0,.5) S=1, X(.5,1.5) S=0, SUO=1.05

MAX. ABS. VECTOR FLUX ERROR AND LOCATION (GLOBAL)

I: NO. OF MESH INTERVALS J: NO. OF SU POINTS

I \ J	2	4	8	16
ERROR 3	2.48D-02	-1.68D-02	9.97D-02	3.46D-01
EXACT	0.671	0.174	0.745	0.770
X LOC	0.500	1.000	0.0	0.0
SULOC	0.500	0.211	0.069	0.020
ERROR 6	2.47D-02	-1.48D-02	-2.34D-02	2.02D-01
EXACT	0.671	0.104	0.152	0.770
X LOC	0.500	0.500	0.750	0.250
SULOC	0.500	-0.211	0.069	-0.020
ERROR 12	2.49D-02	-1.49D-02	-4.86D-03	7.97D-02
EXACT	0.654	0.104	0.257	0.744
X LOC	0.375	0.500	0.625	0.375
SULOC	0.500	-0.211	0.069	-0.020
ERROR 24	2.52D-02	-1.49D-02	-3.13D-03	1.65D-02
EXACT	0.664	0.104	0.763	0.702
X LOC	0.438	0.500	0.375	0.438
SULOC	0.500	-0.211	0.069	-0.020

BEAPAC 05/76 BP#4.4 DGF 2 CELL B.A. X(0,.5) S=1, X(.5,1.5) S=0, SUO=1.05

MAX. ABS. VECTOR FLUX ERROR AND LOCATION (GLOBAL)

I: NO. OF MESH INTERVALS J: NO. OF SU POINTS

I \ J	2	4	8	16
ERROR 3	6.74D-02	-1.35D-01	-2.00D-01	2.52D-01
EXACT	0.671	0.104	0.148	0.714
X LOC	0.500	0.500	0.500	0.500
SULOC	0.500	-0.211	-0.069	0.020
ERROR 6	2.88D-02	-5.79D-02	-1.54D-01	-2.26D-01
EXACT	0.671	0.746	0.148	0.173
X LOC	0.500	0.250	0.500	0.500
SULOC	0.500	0.211	-0.069	-0.020
ERROR 12	2.58D-02	-2.67D-02	-8.24D-02	-1.91D-01
EXACT	0.671	0.719	0.148	0.173
X LOC	0.500	0.125	0.500	0.500
SULOC	0.500	0.211	-0.069	-0.020
ERROR 24	2.51D-02	-1.79D-02	-3.15D-02	-1.34D-01
EXACT	0.654	0.104	0.148	0.173
X LOC	0.375	0.500	0.500	0.500
SULOC	0.500	-0.211	-0.069	-0.020

BENCHMARK 4.1 ERROR TRAVERSES PSIE(0,MU) FOR I-24 OR M-16

(a) DB1

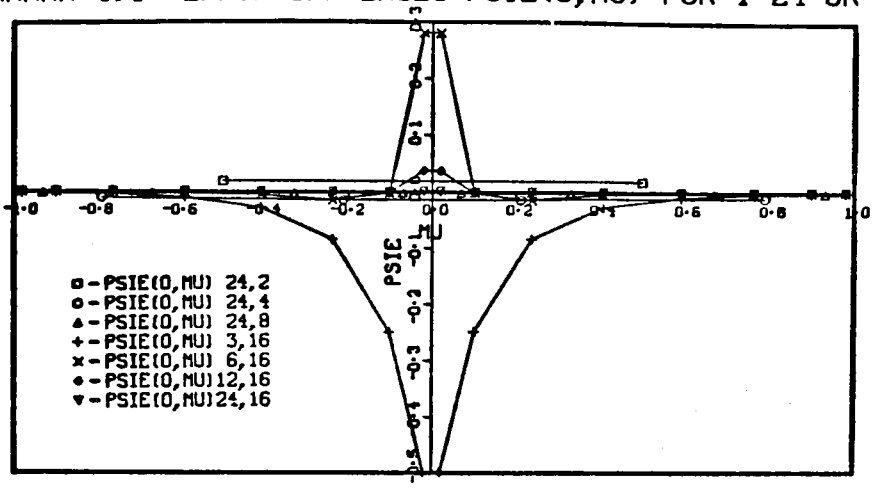

BENCHMARK 4.2 ERROR TRAVERSES PSIE(0,MU) FOR I-24 OR M-16

(b) DB3

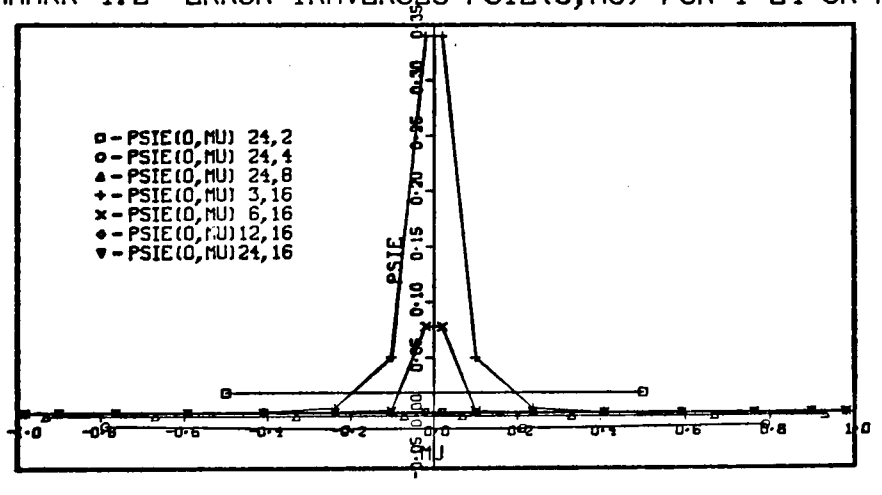

BENCHMARK 4.4 ERROR TRAVERSES PSIE(0,MU) FOR I-24 OR M-16

(c) DGF

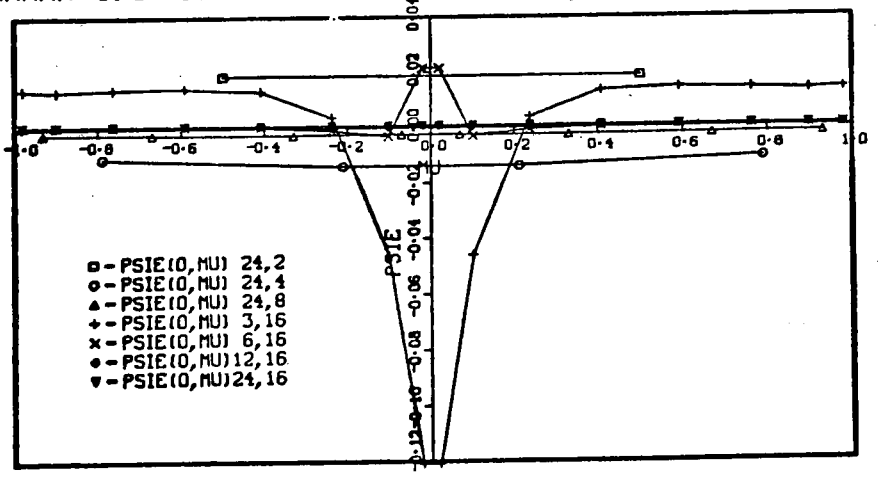

Figure 2.28. Angular flux error traverses $\psi_E(0,\mu)$ for DB1, DB3 and DGF methods for seven selected discretizations of Benchmark #4

BENCHMARK 4.1 ERROR TRAVERSES PSIE(.5,MU) FOR I-24 OR M-16

(a) DB1

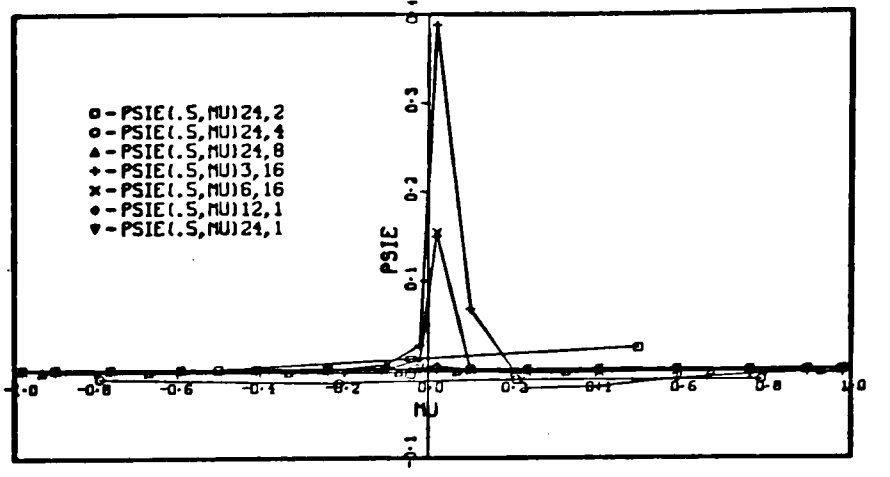

BENCHMARK 4.2 ERROR TRAVERSES PSIE(.5,MU) FOR I-24 OR M-16

(b) DB3

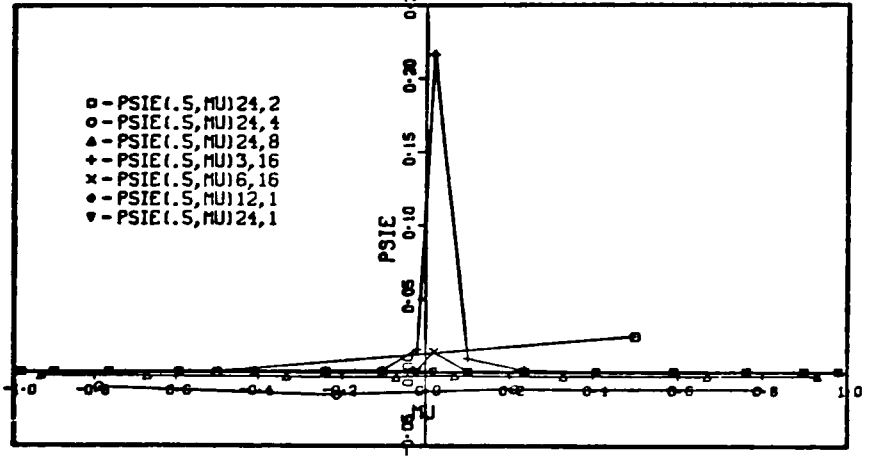

BENCHMARK 4.4 ERROR TRAVERSES PSIE(.5,MU) FOR I-24 OR M-16

(c) DGF

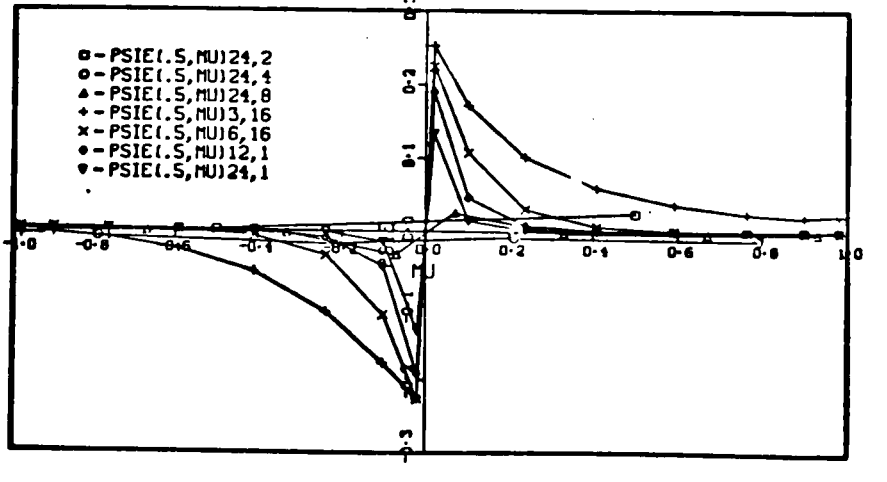

Figure 2.29. Angular flux error traverses $\psi_E(.5,\mu)$ for DB1, DB3 and DGF methods for seven selected discretizations of Benchmark #4

BENCHMARK 4.1 ERROR TRAVERSE PSIE(1.5,MU) FOR I-24 OR M-16

(a) DB1

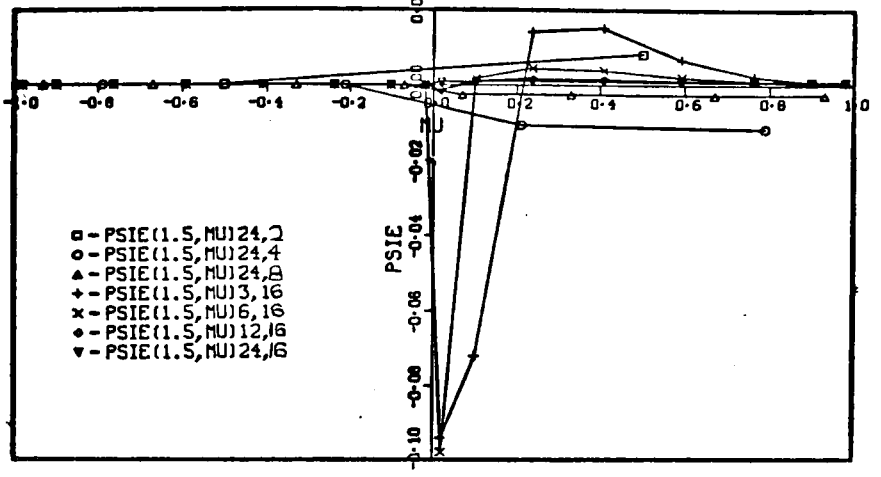

BENCHMARK 4.2 ERROR TRAVERSE PSIE(1.5,MU) FOR I-24 OR M-16

(b) DB3

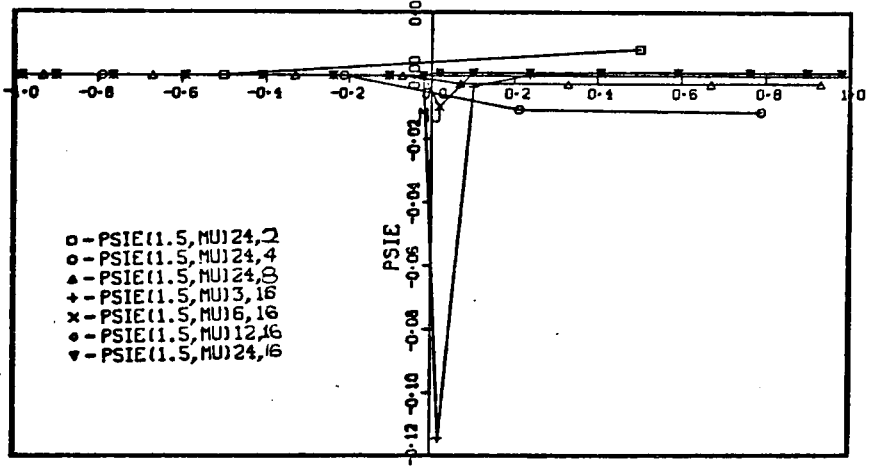

BENCHMARK 4.4 ERROR TRAVERSE PSIE(1.5,MU) FOR I-24 OR M-16

(c) DGF

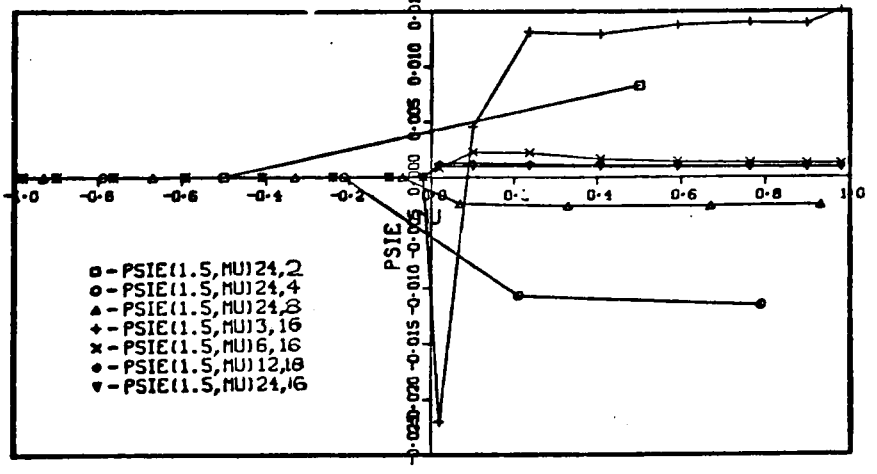

Figure 2.30. Angular flux error traverses $\psi_E(1.5,\mu)$ for DB1, DB3 and DGF methods for seven selected discretizations of Benchmark #4

Table 2.13. Average absolute scalar flux error for DB1, DB3 and DGF methods for sixteen discretization sets of Benchmark #4

BEAPAC 05/76 BP#4.1 DB1 2 CELL M.A. X(0,.5) S=1, X(.5,1.5) S=0, NU0=1.05

AVG. ABS. SCALAR FLUX ERROR (GLOBAL)

I: NO. OF XMESH INTERVALS J: NO. OF MU POINTS

(a) DB1

I \ J	2	4	8	16
ERROR 3	4.15D-02	6.68D-02	5.49D-02	5.30D-02
ERROR 6	5.15D-02	5.14D-02	1.75D-02	1.73D-02
ERROR 12	5.26D-02	4.88D-02	1.12D-02	6.26D-03
ERROR 24	5.18D-02	4.82D-02	1.04D-02	3.60D-03

BEAPAC 05/76 BP#4.2 DB3 2 CELL M.A. X(0,.5) S=1, X(.5,1.5) S=0, NU0=1.05

AVG. ABS. SCALAR FLUX ERROR (GLOBAL)

I: NO. OF XMESH INTERVALS J: NO. OF MU POINTS

(b) DB3

I \ J	2	4	8	16
ERROR 3	5.11D-02	4.69D-02	1.78D-02	1.99D-02
ERROR 6	5.24D-02	4.81D-02	9.92D-03	6.28D-03
ERROR 12	5.30D-02	4.81D-02	1.02D-02	3.51D-03
ERROR 24	5.19D-02	4.80D-02	1.03D-02	3.35D-03

BEAPAC 05/76 BP#4.4 DGF 2 CELL M.A. X(0,.5) S=1, X(.5,1.5) S=0, NU0=1.05

AVG. ABS. SCALAR FLUX ERROR (GLOBAL)

I: NO. OF XMESH INTERVALS J: NO. OF MU POINTS

(c) DGF

I \ J	2	4	8	16
ERROR 3	8.67D-02	4.39D-02	2.71D-02	3.14D-02
ERROR 6	4.96D-02	4.94D-02	1.82D-02	1.50D-02
ERROR 12	5.20D-02	4.84D-02	1.19D-02	6.69D-03
ERROR 24	5.17D-02	4.81D-02	1.03D-02	3.83D-03

Table 2.14. Relative sum error of pointwise scalar flux errors for DB1, DB3 and DGF methods for sixteen discretization sets of Benchmark #4

BEAPAC 05/76 BP#4.1 DB1 2 CELL M.A. X(0,.5) S=1, X(.5,1.5) S=0, NU0=1.05

REL. ABS. SCALAR FLUX ERROR (GLOBAL)

I: NO. OF XMESH INTERVALS J: NO. OF MU POINTS

(a) DB1

I \ J	2	4	8	16
ERROR 3	6.77D-02	1.09D-01	8.95D-02	8.65D-02
ERROR 6	8.42D-02	8.40D-02	2.86D-02	2.83D-02
ERROR 12	8.63D-02	8.01D-02	1.84D-02	1.03D-02
ERROR 24	8.53D-02	7.93D-02	1.72D-02	5.93D-03

BEAPAC 05/76 BP#4.2 DB3 2 CELL M.A. X(0,.5) S=1, X(.5,1.5) S=0, NU0=1.05

REL. ABS. SCALAR FLUX ERROR (GLOBAL)

I: NO. OF XMESH INTERVALS J: NO. OF MU POINTS

(b) DB3

I \ J	2	4	8	16
ERROR 3	8.33D-02	7.65D-02	2.90D-02	3.24D-02
ERROR 6	8.74D-02	7.87D-02	1.62D-02	1.03D-02
ERROR 12	8.70D-02	7.89D-02	1.68D-02	5.76D-03
ERROR 24	8.54D-02	7.90D-02	1.69D-02	5.51D-03

BEAPAC 05/76 BP#4.4 DGF 2 CELL M.A. X(0,.5) S=1, X(.5,1.5) S=0, NU0=1.05

REL. ABS. SCALAR FLUX ERROR (GLOBAL)

I: NO. OF XMESH INTERVALS J: NO. OF MU POINTS

(c) DGF

I \ J	2	4	8	16
ERROR 3	1.41D-01	7.16D-02	4.42D-02	5.12D-02
ERROR 6	8.12D-02	8.07D-02	2.98D-02	2.45D-02
ERROR 12	8.53D-02	7.94D-02	1.95D-02	1.10D-02
ERROR 24	8.51D-02	7.91D-02	1.70D-02	6.30D-03

2.2.5 Discussion

The examples above illustrate types of benchmark problems that can be created for studying the error performance of various numerical methods. More detailed error studies are necessary to completely characterize the error behaviour for various classes of problems, i.e. boundary conditions, cross sections and relative cell sizes in multicell problems. An advantage of the automated approach taken here is that such studies are performed with minimal effort by the analyst.

An interesting byproduct of this research is the least squares modes analysis technique. For creation of one or two cell benchmark problems we treat each cell independently and in two cell problems generate the source necessary to satisfy the interface condition exactly.

A simple variant of this procedure treats all cells simultaneously, performing the least squares modes analysis for the entire system. The boundary and interface conditions are satisfied in the least squares sense. Several attractive features of this new numerical transport method are:

(1) least squares nodes are required only on the problem boundaries and cell interfaces.

(2) relatively few expansion functions and least squares nodes should be required for obtaining accurate solutions.

(3) given the combining coefficients the corresponding angular or scalar flux solution can be calculated at any point in the problem domain.

(4) flux discontinuities at interfaces are easily represented.

As mentioned earlier, questions related to the choice of eigenmodes and the placement of the least squares coefficients must be answered before the procedure is generally applicable.

A matrix representation of the proposed method applied to the two cell reference problem for BP4 is given by

$$(2.26)\qquad \begin{bmatrix} Q_I^+(0)-Q_I^-(0) & 0 \\ -Q_I^+(.5) & Q_{II}^+(.5) \\ -Q_I^-(.5) & Q_{II}^-(.5) \\ 0 & Q_{II}^-(1.5) \end{bmatrix} \begin{bmatrix} \underline{a}_I \\ \underline{a}_{II} \end{bmatrix} = \begin{bmatrix} 0 \\ S_I \\ S_I \\ 0 \end{bmatrix}$$

where

$$(2.27)\qquad Q_i^{\pm}(x) = [q_1(x), q_2(x), \ldots, q_{2N}(x)]^{\pm}$$

$$[q_n(x)]^{\pm} = \begin{bmatrix} q_n(x,\pm\mu_1) \\ q_n(x,\pm\mu_2) \\ \vdots \\ q_n(x,\pm\mu_{M/2}) \end{bmatrix} \qquad 1 \geq \mu_1 \geq \cdots \mu_{M/2} \geq 0 \ .$$

$\underline{a}_I$, $\underline{a}_{II}$ are the combining coefficients vectors of length 2N+2 for the eigenmodes $q_n(x,\mu)$ in cells I and II, respectively. S_I is the constant source in cell I.

The solution is obtained by solving Eqn. (2.26) via the Householder least squares method for overdetermined systems. The first row $(Q_T^+ - Q_T^-)a_I = 0$ in Eqn. (2.26) represents the reflecting boundary condition at x = 0. The second and third row represents the interface condition at x = .5 and the last row corresponds to the vacuum condition x = 1.5.

III. THE SYMMETRIZED TRANSPORT EQUATION

3.1 The Equation and Elementary Solutions

An alternative approach to solving neutron transport problems is realized by the symmetrized (canonical) transport equation [Vladirimov 1963]. The symmetrized operator is self-adjoint and positive definite in the case $c < 1$, where c is the number of secondaries per collision.

The derivation of the symmetrized equation begins by writing the standard equation (1.1) for positive and negative μ:

$$\mu \frac{\partial\psi(x,\mu)}{\partial x} + \sigma(x)\psi(x,\mu) - \frac{\sigma(x)c(x)}{2}\int_{-1}^{1}\psi(x,\mu')d\mu' = S(x,\mu) \tag{3.1}$$

and

$$-\mu \frac{\partial\psi(x,-\mu)}{\partial x} + \sigma(x)\psi(x,-\mu) - \frac{\sigma(x)c(x)}{2}\int_{-1}^{1}\psi(x,-\mu')d\mu' = S(x,-\mu) \ . \tag{3.2}$$

Adding and subtracting (3.1) and (3.2) gives respectively

$$\mu \frac{\partial}{\partial x}\psi^{-}(x,\mu) + \sigma(x)\psi^{+}(x,\mu) - \sigma(x)c(x)\int_{0}^{1}\psi^{+}(x,\mu')d\mu' = S^{+}(x,\mu) \tag{3.3}$$

and

$$\mu \frac{\partial\psi^{+}(x,\mu)}{\partial x} + \sigma(x)\psi^{-}(x,\mu) = S^{-}(x,\mu) \tag{3.4}$$

where

$$2\psi^{+}(x,\mu) = \psi(x,\mu) + \psi(x,-\mu), \quad 2S^{+}(x,\mu) = S(x,\mu) + S(x,-\mu) \tag{3.5}$$

$$2\psi^{-}(x,\mu) = \psi(x,\mu) - \psi(x,-\mu), \quad 2S^{-}(x,\mu) = S(x,\mu) - S(x,-\mu) \ . \tag{3.6}$$

Solving (3.4) for $\psi^{-}(x,\mu)$ we find

$$\psi^{-}(x,\mu) = -\frac{\mu}{\sigma(x)}\frac{\partial\psi^{+}}{\partial x}(x,\mu) + \frac{1}{\sigma(x)}S^{-}(x,\mu) \ . \tag{3.7}$$

Note, when $S(x,\mu)$ is isotropic, $S^-(x,\mu) = 0$. Substituting (3.7) into (3.3) for regionwise (cellwise) constant cross sections and isotropic source yields the equation

$$(3.8) \qquad -\frac{\mu^2}{\sigma(x)}\frac{\partial^2\psi^+(x,\mu)}{\partial x^2} + \sigma(x)\psi^+(x,\mu) - \sigma(x)c(x)\int_0^1 \psi^+(x,\mu')d\mu' = S^+(x,\mu).$$

Boundary conditions usually considered for this operator are the reflecting condition and the vacuum condition. The standard form of the reflecting condition at the boundary x=b is

$$(3.9) \qquad \psi(b,\mu) = \psi(b,-\mu) \qquad (0 \leq \mu \leq 1)$$

which is equivalent to

$$(3.10) \qquad \psi^-(b,\mu) = 0 .$$

By (3.7) in (3.10) we find for $\mu \geq 0$

$$(3.11a) \qquad \mu \left.\frac{\partial\psi^+(x,\mu)}{\partial x}\right|_{x=b} = S^-(x,\mu) . \quad \text{(reflecting)}$$

The standard form of the vacuum condition is

$$(3.12) \qquad \psi(b,\mu) = 0 \qquad \begin{array}{ll} \mu > 0 & \text{at } b=0 \\ \mu < 0 & \text{at } b=a \end{array}$$

which is equivalent to

$$(3.13) \qquad \psi^+(b,\mu) + \psi^-(b,\mu) = 0 .$$

Substituting (3.7) into (3.13) for $\mu \geq 0$ yields

$$(3.14a) \qquad \psi^+(b,\mu) = \pm\left[\frac{\mu}{\sigma(b)}\left.\frac{\partial\psi^+(x,\mu)}{\partial x}\right|_{x=b} - \frac{1}{\sigma(b)}S^-(b,\mu)\right] \quad \text{(vacuum)}$$

where the + sign is used if b=0, the - sign if b=a.

We apply the benchmark error analysis procedure to study methods which solve equation (3.8) and its boundary conditions (3.11a) and (3.14a), hence we need to obtain exact solutions to these equations. Given a solution $\psi_B(x,\mu)$ to the standard equation (1.1), we can obtain the corresponding solution $\psi_B^+(x,\mu)$ by using formulas (3.5) and (3.6).

The inhomogeneous boundary source terms required to make the boundary conditions exact are generated from $\psi_B(x,\mu)$. Note that the source terms arise when the exact solution does not exactly satisfy the homogeneous boundary conditions. For example, when a vacuum boundary condition is specified in the standard equation, a non-zero inhomogeneous source term effectively makes it an incident flux boundary condition. In the reflecting boundary condition case, the inhomogeneous source term gives the difference between the incident and emergent flux at the appropriate boundary.

The canonical transport equation boundary conditions are more complicated. The inhomogeneous source for the reflecting condition is derived from eq. (3.6) and (3.10) and is defined by

$$\psi^-(b,\mu) = \tfrac{1}{2}[\psi_B(b,\mu) - \psi_B(b,-\mu)] = \tfrac{1}{2}f_r(b,\mu) \ . \tag{3.15}$$

The general inhomogeneous reflecting boundary corresponding to eq. (3.11a) is

$$\mu \left.\frac{\partial\psi^+(x,\mu)}{\partial x}\right|_{x=b} = S^-(b,\mu) - \frac{\sigma(b)}{2} f_r(b,\mu) \qquad \mu \geq 0 \ . \tag{3.11b}$$

The inhomogeneous source for the vacuum (i.e. incident flux) boundary condition is derived from eq. (3.5) and (3.6) and is defined by

$$\psi^+(b,\mu) + \psi^-(b,\mu) = \psi_B(b,\mu) \begin{cases} b = 0 & \mu \geq 0 \\ b = a & \mu \leq 0 \end{cases} = f_v(b,\mu) \ . \tag{3.16}$$

The general inhomogeneous vacuum boundary condition corresponding to eq. (3.14a) becomes

$$(3.14b)\qquad \psi^{+}(b,\mu) \mp \frac{\mu}{\sigma(b)} \frac{\partial\psi^{+}(x,\mu)}{\partial x}\bigg|_{x=b} = \mp\frac{1}{\sigma(x)} S^{-}(b,\mu) + f_v(b,\mu) \ .$$

For expedient application of the benchmark analysis we replace the vacuum condition with the following simpler condition. We define

$$(3.17)\qquad \begin{aligned} \psi^{+}(b,\mu) &= \tfrac{1}{2}(\psi_B(b,\mu) + \psi_B(b,-\mu)) \\ &= f_e(b,\mu) \ . \end{aligned}$$

In Section 3.2.2 (below) we describe the application of a variational method to the canonical equation. Miller (1973) noted that the reflecting boundary condition is a natural (or essential) boundary condition of the functional minimization. Therefore to properly apply the FEM method, we need to generate benchmark problems $\psi_B(x,\mu)$ (hence $\psi_B^{+}(x,\mu)$) which satisfy the reflecting boundary conditions (3.9) exactly.

The simplest approach is to generate a typical benchmark solution $\psi_B(x,\mu)$ for a reflecting problem as previously outlined. Then to force a homogeneous boundary condition we define the benchmark solution

$$(3.18)\qquad \psi_B^{R}(x,\mu) = \psi_B(x,\mu) - \tfrac{1}{2}[\psi_B(0,\mu) - \psi_B(0,-\mu)]$$

which satisfies a reflecting boundary condition at $x = 0$. $\psi_B^{R}(x,\mu)$ is the solution to the new benchmark problem

$$(3.19)\qquad L\psi_B^{R}(x,\mu) = S(x,\mu) + \frac{\sigma(0)}{2}\,[\psi_B(0,-\mu)-\psi_B(0,\mu)] = S(x,\mu) + Q(\mu)$$

where the right side is in general not symmetric in μ, and

$$(3.20)\qquad L\psi_B(x,\mu) = S(x,\mu)$$

is the symbolic description of the original benchmark problem. We can generate the corresponding solution $\psi_B^+(x,\mu)$ and boundary conditions using the solution $\psi_B^R(x,\mu)$.

Two cell problems are treated by the procedure described in Section 1.1.6. Here $\psi_B^{(I)}(x,\mu)$ is replaced by $\psi_B^{R^{(I)}}(x,\mu)$. The source term $Q_{II}(\mu)$ in cell II is defined by

$$(3.21) \qquad Q_{II}(\mu) = \sigma_{II}(\psi_B^{R^{(I)}}(a,\mu)-\psi_B^{(II)}(a,\mu)) - \sigma_{II}c_{II}(\phi_B^{R^{(I)}}(a)-\phi_B^{(II)}(a))$$

similar to Eq. (1.44).

The present implementation of the canonical transport equation includes homogeneous reflecting condition at the left boundary and condition (3.17) at the right boundary for the FEM method.

3.2 Numerical Methods

3.2.1 The discrete ordinates method with first order finite differences in space

This method uses discrete ordinates approximation in angle and first order finite differences to approximate spatial derivatives in eq. (3.8). It will be referred to as the DFD method.

We solve (3.8) by the discrete ordinates method, hence we approximate the integral by numerical integration methods including single Gauss quadrature. Then (3.8) becomes a system of discrete second order differential equations with D = d/dx:

$$(3.22) \qquad [-\frac{1}{\sigma} M^2 D^2 + \sigma I - \sigma c W]\, \underline{\psi}^+(x) = \underline{S}^+(x) \qquad (0 \le x \le a)$$

where

$$M = \begin{bmatrix} \mu_1 & & & \\ & \mu_2 & & \\ & & \ddots & \\ & & & \mu_M \end{bmatrix}, \quad W = \begin{bmatrix} w_1 w_2 \cdots w_M \\ w_1 w_2 \cdots w_M \\ \vdots \\ w_1 w_2 \cdots w_M \end{bmatrix}, \quad \underline{\psi}^+(x) = \begin{bmatrix} \psi^+(x,\mu_1) \\ \psi^+(x,\mu_2) \\ \vdots \\ \psi^+(x,\mu_M) \end{bmatrix}, \quad \underline{S}^+(x) = \begin{bmatrix} S^+(x,\mu_1) \\ S^+(x,\mu_2) \\ \vdots \\ S^+(x,\mu_M) \end{bmatrix}.$$

To approximate the solution $\underline{\psi}^+(x)$ by means of finite differences, we generate an equal spaced mesh structure

$$x_i = (i-1)h \qquad (i = 1,2,\ldots,I)$$

$$h = \frac{a}{I-1}$$

where the cell boundaries are x_1 and x_I. The center of each mesh interval $(x_{i-\frac{1}{2}} \leq x \leq x_{i+\frac{1}{2}})$ is at x_i, except for the two boundary cells $(x_1 \leq x \leq x_{3/2})$ and $(x_{I-\frac{1}{2}} \leq x \leq x_I)$.

Consider the differential equations (3.22) in the ith cell; the integral of eq. (3.22) becomes

$$\int_{x_{i-\frac{1}{2}}}^{x_{i+\frac{1}{2}}} [-\frac{1}{\sigma} M^2 D^2 + \sigma(I-cW)]\underline{\psi}^+(x)\,dx = \int_{x_{i-\frac{1}{2}}}^{x_{i+\frac{1}{2}}} \underline{S}^+(x)\,dx \ . \tag{3.23}$$

Here, let $\underline{\psi}_i^+ = \underline{\psi}^+(x_i)$ and $\underline{S}_i^+ = \underline{S}^+(x_i)$; then we make the approximation

$$\int_{x_{i-\frac{1}{2}}}^{x_{i+\frac{1}{2}}} \underline{\psi}^+(x)\,dx \cong h\underline{\psi}_i^+ \ ; \quad \int_{x_{i-\frac{1}{2}}}^{x_{i+\frac{1}{2}}} \underline{S}^+(x)\,dx \cong h\underline{S}_i^+ \ . \tag{3.24}$$

In the term involving the second derivative there are three cases to consider.

$$-\int_{\Delta x_i} \frac{1}{\sigma} MD^2\underline{\psi}^+(x)\,dx = -\frac{1}{\sigma} M^2 \begin{cases} D\underline{\psi}_{3/2}^+ - D\underline{\psi}_1^+ & \Delta x_1 \quad (3.25a) \\ D\underline{\psi}_{i+\frac{1}{2}}^+ - D\underline{\psi}_{i-\frac{1}{2}}^+ & \Delta x_i,\ i=2,3,\ldots,I-1 \quad (3.25b) \\ D\underline{\psi}_I^+ - D\underline{\psi}_{I-\frac{1}{2}}^+ & \Delta x_I \quad (3.25c) \end{cases}$$

A first order finite difference approximation yields

$$D\underline{\psi}_{i+\frac{1}{2}}^+ \cong \frac{\underline{\psi}_{i+1}^+ - \underline{\psi}_i^+}{h} \qquad i = 1,2,\ldots,I-1. \tag{3.26}$$

The boundary conditions (3.11b) and (3.14b) are applied to specify $D\underline{\psi}_1^+$ and $D\underline{\psi}_I^+$.

Substituting eqs. (3.24), (3.25) and (3.26) into (3.23) and dividing by h (h/2 when i=1 or i=I) yields the linear system of equations for $\underline{\psi}_i^+$

$$B_i\underline{\psi}_{i-1}^+ + D_i\underline{\psi}_i^+ + E_i\underline{\psi}_{i+1}^+ = \hat{\underline{S}}_i^+ \qquad (i = 1,2,\ldots,I) \tag{3.27}$$

where

$$B_i = \begin{cases} 0 & i = 1 \\ B & (i = 2,3,\ldots,I-1), \\ \hat{B} & i = I \end{cases} \tag{3.28a}$$

$$D_i = \begin{cases} \hat{D}_1 & i = 1 \\ D & (i = 2,3,\ldots,I-1), \\ \hat{D}_I & i = I \end{cases} \tag{3.28b}$$

$$E_i = \begin{cases} \hat{E} & i = 1 \\ B & (i = 2,3,\ldots,I-1), \\ 0 & i = I \end{cases} \tag{3.28c}$$

$$\hat{\underline{S}}_i^+ = \underline{S}_i^+ \qquad (i = 2,3,\ldots,I-1), \tag{3.28d}$$

$$D = \frac{2}{\sigma h^2} M^2 + \sigma(I-cW), \tag{3.28e}$$

$$B = -\frac{1}{\sigma h^2} M^2. \tag{3.28f}$$

$\hat{B}$, $\hat{D}_1$, $\hat{D}_I$, $\hat{E}$, $\hat{\underline{S}}_1$ and $\hat{\underline{S}}_I$ are dependent on the boundary conditions and are defined below.

The reflecting boundary condition (3.11b) at $x = x_1$ yields

(3.29a) $$\hat{D}_1 = D$$

(3.29b) $$\hat{E} = 2B$$

and

(3.29c) $$\underline{S}_1^+ = \underline{S}_1^+ + \frac{2}{h} M[\tfrac{1}{2}\underline{f}_r(x_1) - \frac{1}{\sigma}\underline{S}^-(x_1)] \quad .$$

The vacuum boundary (3.14b) at $x = x_I$ yields

(3.30a) $$\hat{B} = 2B$$

(3.30b) $$\hat{D}_I = D + \frac{2}{h} M$$

and

(3.30c) $$\hat{\underline{S}}_I^+ = \underline{S}_I^+ + \frac{2}{h} M[\underline{f}_v(x_I) + \frac{1}{\sigma}\underline{S}^-(x_I)] \quad .$$

The special boundary condition (3.17) at $x = x_I$ yields

(3.31a) $$E_I = 0$$

(3.31b) $$D_I = I$$

and

(3.31c) $$\hat{\underline{S}}_I = \underline{f}_e(x_I)$$

The matrix representation for the case of a reflecting boundary condition at the origin and vacuum boundary condition at $x = a$ is

(3.32) $$\begin{bmatrix} D & 2B & & & & \\ B & D & B & & & \\ & B & D & B & & \\ & & \ddots & \ddots & \ddots & \\ & & B & D & B & \\ & & & 2B & \hat{D}_I \end{bmatrix} \begin{bmatrix} \underline{\psi}_1^+ \\ \underline{\psi}_2^+ \\ \underline{\psi}_3^+ \\ \vdots \\ \underline{\psi}_I^+ \end{bmatrix} = \begin{bmatrix} \hat{\underline{S}}_1 \\ \hat{\underline{S}}_2 \\ \hat{\underline{S}}_3 \\ \vdots \\ \hat{\underline{S}}_I \end{bmatrix} \quad .$$

Eq. (3.32) is a block tridiagonal system of order IM×IM with block matrices of order M×M. The solution technique is block tridiagonal Gauss elimination.

3.2.2 Piecewise bilinear finite element method in phase space

This method uses piecewise bilinear polynomial functions in phase space. It will be denoted as the FEM method. We outline the basic method here; the reader is referred to [Miller, 1973] for a detailed derivation.

Equations (3.8) and (3.14a) minimize the functional

$$(3.33)\quad F[\psi^+(x,\mu)] = \left\langle \frac{1}{\sigma}\left(\mu \frac{\partial\psi^+(x,\mu)}{\partial x}\right)^2 + \sigma\psi^+(x,\mu)^2 - \sigma c\psi^+(x,\mu)\int_0^1 \psi^+(x,\mu')d\mu' \right.$$

$$\left. - 2\psi^+(x,\mu)\, S^+(x,\mu) - 2\mu \frac{\partial\psi^+}{x} S^-(x,\mu)\right\rangle$$

$$+ \langle\langle \psi^+(x,\mu),\ \psi^+(x,\mu)-2f_v(x,\mu)\rangle\rangle_{\partial x_{vac}} \pm \langle\langle \psi^+(x,\mu),\ f_r(x,\mu)\rangle\rangle_{\partial x_{refl}}$$

where

$$(3.34a)\quad \langle f(x,\mu)\rangle = \int_0^a dx \int_0^1 d\mu\ f(x,\mu)$$

and

$$(3.34b)\quad \langle\langle f(x,\mu)\rangle\rangle_{\partial x_{\substack{refl\\vac}}} = \int_0^1 d\mu\mu f(x,\mu)\Big|_{x\in\partial x_{\substack{refl\\vac}}}$$

That is, finding the minimum point of equation (3.33) is equivalent to solving its Euler equations, (3.8) and (3.14a). Reflecting boundary conditions are natural (essential) boundary conditions [Strang and Fix, 1973] of the minimization and are applied wherever the vacuum boundary does not apply.

In order to solve for $\psi^+(x,\mu)$ in Eq. (3.33), the phase space domain is divided into $(I-1)\cdot(M-1)$ connecting, but non-overlapping rectangular subdomains or finite elements defined by $(x_i \le x \le x_{i+1})$ and $(\mu_m \le \mu \le \mu_{m+1})$ for $i=1,2,\ldots,I-1$ and $m=1,2,\ldots,M-1$. The cross sections are assumed piecewise constant in space with discontinuities permitted at interelement boundaries. The solution $\psi^+(x,\mu)$ is approximated by piecewise bilinear polynomial trial functions $\phi_{im}(x,\mu)$ such that

$$(3.35)\qquad \psi^+(x,\mu) \approx \tilde{\psi}^+(x,\mu) = \sum_{i=1}^{I}\sum_{m=1}^{M} q_{im}\phi_{im}(x,\mu)\ .$$

The $\phi_{im}(x,\mu)$ are defined by

$$\phi_{im}(x,\mu) = \begin{cases} \Theta_i^+(x)\Theta_m^+(\mu) \\ \Theta_i^+(x)\Theta_m^-(\mu) \\ \Theta_i^-(x)\Theta_m^+(\mu) \\ \Theta_i^-(x)\Theta_m^-(\mu) \end{cases} \qquad (i=1,2,\ldots,I),\ (m=1,2,\ldots,M) \tag{3.36}$$

where

$$\Theta_i^+(t) = \begin{cases} \dfrac{t_{i+1}-t}{\Delta t_i} & t_i \leq t \leq t_{i-1} \\ 0 & \text{otherwise} \end{cases} \tag{3.37a}$$

$$\Theta_i^-(t) = \begin{cases} \dfrac{t-t_{i-1}}{\Delta t_{i-1}} & t_{i-1} \leq t \leq t_i \\ 0 & \text{otherwise} \end{cases} \tag{3.37b}$$

$$\Delta t_i = t_{i+1}-t_i \ .$$

The ϕ_{im} are defined so that

$$\phi_{im}(x_j,\mu_n) = \delta_{ij}\delta_{mn}$$

where δ_{rs} is the Kronecker delta. If $I(\tilde{\psi}^+)$ = minimum then

$$q_{im} = \tilde{\psi}^+(x_i,\mu_m) \ . \tag{3.38}$$

Substituting (3.35) into (3.33) and minimizing $F[\tilde{\psi}(x,\mu)]$ with respect to variations in the q_{im} yields the matrix equations

$$[-K^{(1)} + K^{(0)} - K^{(-1)} + K^{(vac)}]\underline{q} = \underline{S} \tag{3.39}$$

where

$$\underline{q} = \begin{bmatrix} \vdots \\ q_{im} \\ q_{im+1} \\ \vdots \end{bmatrix} \qquad (m=1,2,\ldots,M),\ (i=1,2,\ldots,I) \tag{3.40}$$

The symmetric block tridiagonal streaming matrix is defined by

$$K^{(1)} = \begin{bmatrix} K_{11}^{(1)} & K_{12}^{(1)} & & & 0 \\ K_{21}^{(1)} & K_{22}^{(1)} & K_{23}^{(1)} & & \\ \vdots & \vdots & \vdots & & \\ & \ddots & \ddots & \ddots & \\ & K_{I-1,I-2}^{(1)} & K_{I-1,I-1}^{(1)} & K_{I-1,I}^{(1)} & \\ 0 & & K_{I,I-1}^{(1)} & K_{II}^{(1)} & \end{bmatrix} \tag{3.41a}$$

where

$$\left(K_{ij}^{(1)}\right)_{mk} = \left\langle \frac{\mu^2}{\sigma_n} \phi_{im}^{(x)},\ \phi_{jk}^{(x)} \right\rangle \quad \begin{matrix} (i=1,2,\ldots,I),\ (m=1,2,\ldots,M), \\ (j=i-1,i,i+1),\ (k=m-1,m,m+1) \end{matrix} \tag{3.41b}$$

and

$$\phi_{im}^{(x)}(x,\mu) = \frac{\partial \phi_{im}}{\partial x}(x,\mu) \ .$$

$K_{ij}^{(1)}$ is a tridiagonal matrix.

The symmetric block tridiagonal collision matrix is defined by

$$K^{(0)} = \begin{bmatrix} K_{11}^{(0)} & K_{12}^{(0)} & & & 0 \\ K_{21}^{(0)} & K_{22}^{(0)} & K_{23}^{(0)} & & \\ \vdots & \vdots & \vdots & & \\ & \ddots & \ddots & \ddots & \\ & K_{I-1,I-2}^{(0)} & K_{I-1,I-1}^{(0)} & K_{I-1,I}^{(0)} & \\ 0 & & K_{I,I-1}^{(0)} & K_{II}^{(0)} & \end{bmatrix} \tag{3.42a}$$

where

$$(3.42b)\qquad \left(K_{ij}^{(0)}\right)_{mk} = \langle \sigma_n \phi_{im}, \phi_{jk} \rangle \qquad \begin{array}{l} (i=1,2,\ldots,I),\ (m=1,2,\ldots,M) \\ (j=i-1,i,i+1),\ (k=m-1,m,m+1) \\ n=\min(i,j)\ . \end{array}$$

$K_{ij}^{(0)}$ is a tridiagonal matrix.

The symmetric block tridiagonal scattering matrix is defined by

$$(3.43a)\qquad K^{(-1)} = \begin{bmatrix} K_{11}^{(-1)} & K_{12}^{(-1)} & & & 0 \\ K_{21}^{(-1)} & K_{22}^{(-1)} & K_{23}^{(-1)} & & \\ \cdot & \cdot & \cdot & & \\ & \cdot & K_{I-2,I-1}^{(-1)} & K_{I-1,I-1}^{(-1)} & K_{I-1,I}^{(-1)} \\ 0 & & & K_{I,I-1}^{(-1)} & K_{II}^{(-1)} \end{bmatrix}$$

where

$$(3.43b)\qquad \left(K_{ij}^{(-1)}\right)_{mk} = \langle \sigma_n c_n \phi_{jk}, \int_0^1 d\mu'\ \phi_{im} \rangle \qquad \begin{array}{l} (i=1,2,\ldots,I),\ (m=1,2,\ldots,M) \\ (j=i-1,i,i+1),\ (k=1,2,\ldots,M) \\ n=\min(i,j). \end{array}$$

$K_{ij}^{(-1)}$ is a dense matrix.

The symmetric block diagonal vacuum boundary condition matrix is defined so that

$$(3.44a)\qquad K^{(vac)} = \begin{bmatrix} K_{11}^{(vac)} & & & & 0 \\ & 0 & & & \\ & & \cdot & & \\ & & & \cdot & \\ & & & 0 & \\ 0 & & & & K_{II}^{(vac)} \end{bmatrix}$$

where

$$(3.44b)\qquad \left(K_{ij}^{(vac)}\right)_{mk} = \langle\langle \phi_{im}, \phi_{jk} \rangle\rangle_{\partial x_{vac}} \qquad \begin{array}{l} i=j=1 \text{ or } i=j=I \\ (m=1,2,\ldots,M),\ (k=m-1,m,m+1). \end{array}$$

$K_{ij}^{(vac)}$ is a tridiagonal block matrix.

The source vector has the form

$$\underline{S} = \begin{bmatrix} \underline{S}_1(x) \\ \underline{S}_2(x) \\ \cdot \\ \cdot \\ \cdot \\ \underline{S}_I(x) \end{bmatrix} \tag{3.45a}$$

$$\underline{S}_i(x) = \begin{bmatrix} S^+_{i1} + S^-_{i1} \\ S^+_{i2} + S^-_{i2} \\ \cdot \quad \cdot \\ \cdot \quad \cdot \\ \cdot \quad \cdot \\ S^+_{iM} \quad S^-_{iM} \end{bmatrix} \tag{3.45b}$$

$$S^+_{im} = \langle \phi_{im}, S^+(x,\mu) \rangle \tag{3.45c}$$

$$S^-_{im} = \langle \frac{\mu \partial \phi_{im}}{\partial x}, S^-(x,\mu) \rangle \tag{3.45d}$$

where $S^+(x,\mu)$ and $S^-(x,\mu)$ are assumed piecewise constant in space and piecewise linear in angle.

As noted in section 3.1, special benchmark solutions $\psi^R_B(x,\mu)$ (eq. 3.18) are created which satisfy the reflecting boundary condition at the origin $x = x_1 = 0$. The vacuum condition at $x = x_I$ may be replaced by eq. (3.17) which specifies the even parity flux $\psi^+(x_I,\mu)$. The last block of equations in (3.40), block I, is eliminated and the given flux values $\psi^+(x_I,\mu)$ are substituted into the equations for block I-1 with the resulting terms added to the source term.

The system of equations (3.40) are solved by Choleski decomposition using a storage scheme which utilizes the symmetric band matrix property, i.e., only the upper triangular half of the matrix is stored in a rectangular array of dimension 2M×IM.

3.3 An Example of the Benchmark Problem Error Analysis Procedure

A one cell benchmark problem is presented which illustrates a typical application of the benchmark error analysis procedure to the DFD and FEM methods of this chapter. The error performance for twenty space/angle discretization sets is discussed.

3.3.1 Benchmark #5, a one cell least squares modes analysis

The reference problem configuration for BP5 is identical to the one used in BP4 in section 2.2.3. The corresponding reference solution $\psi_R(x,\mu)$ is displayed in Fig. 2.9. We generate a one cell benchmark solution $\psi_B(x,\mu)$ in the first cell of the reference problem subject to the requirement that $\psi_B(0,\mu)$ satisfies exactly the homogeneous reflecting boundary condition at $x = 0$ (i.e. $\psi_B(0,\mu) = \psi_B(0,-\mu)$) as in Eqn. (3.19).

The reference and benchmark problem scalar flux $\phi_R(x)$ and $\phi_B(x)$, and the angular flux $\psi_R(x,\mu)$ and $\psi_B(x,\mu)$ are illustrated in Fig. 3.1. A comparison with the corresponding solutions in cell I of Benchmark 4 in Fig. 2.24 reveals that the most noticeable change in $\psi_B(x,\mu)$ occurs in the neighborhood of $\mu = .1$ where the enforcement of the homogeneous boundary condition in BP5 causes $\psi_B(0,\mu)$ to be symmetric about $\mu = 0$.

The least squares modes analysis in cell I results in combining coefficients $A(\nu)$ and $a_0\pm$ (Fig. 3.2a) which are identical to the coefficients for cell I in BP4 (Fig. 2.25). The sum of the fixed source (S=.5) and $Q(\mu)$, the source term required to satisfy the homogeneous reflecting boundary condition at $x = 0$, are displayed for cell I in Fig. 3.2b.

Traverses of the even parity angular flux $\psi_B^+(x,\mu)$ corresponding to $\psi_B(x,\mu)$ are displayed in Fig. 3.3 for $0 \leq \mu \leq 1$ in cell I (note that $\psi_B^+(x,\mu)$ is symmetric about $\mu = 0$). The flux discontinuity observed in Fig. 3.1b at $\mu = 0$ at the interface $x = .5$ causes the even parity flux to decay rapidly near the interface $x = .5$ as μ approaches zero.

The even and odd parity source terms corresponding to the source in Fig. 3.2b are displayed in Fig. 3.4. The odd parity source $S_B^-(\mu)$ is due to the source $Q(\mu)$ introduced to satisfy the homogeneous reflecting boundary condition at $x = 0$.

(a)

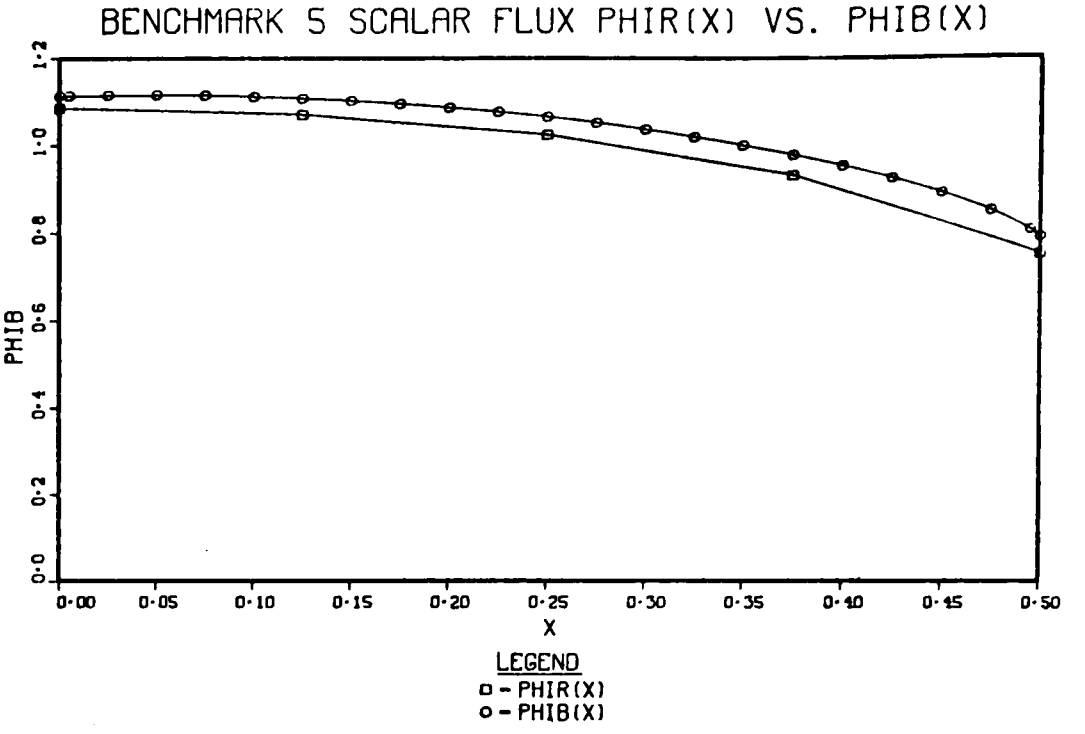

(b)

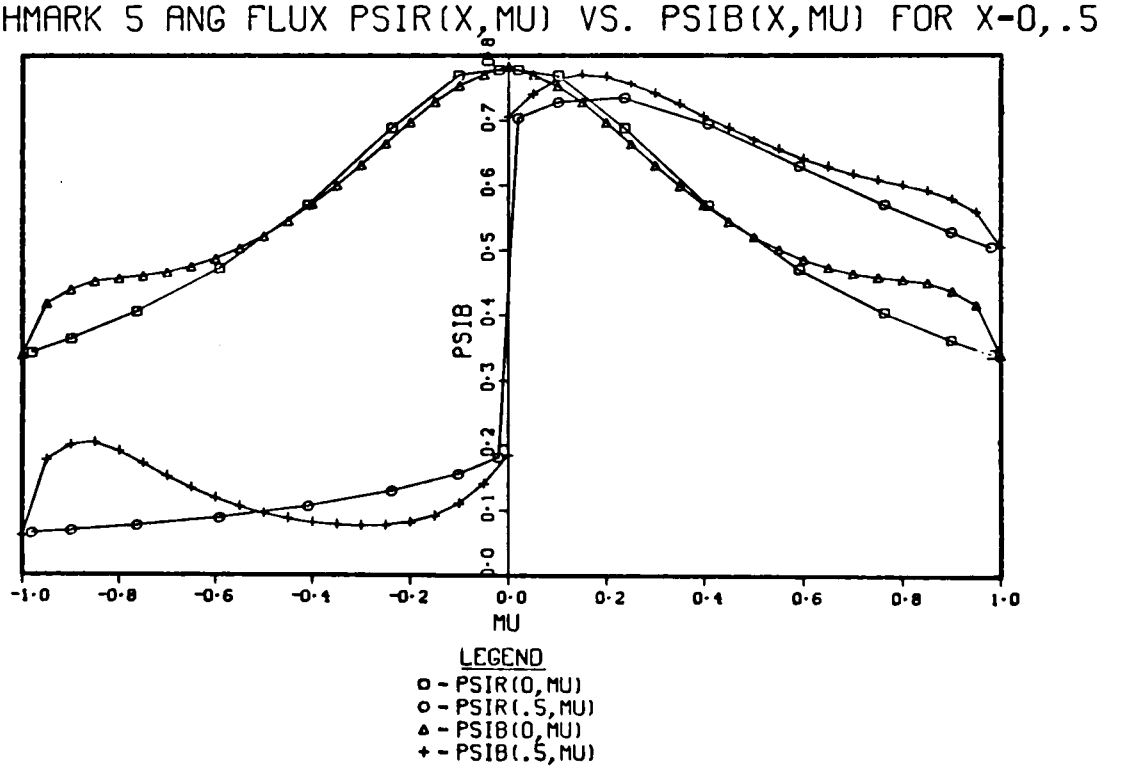

Figure 3.1. Comparison of DB3 reference solution and benchmark solutions for Benchmark #5

a. Scalar flux $\phi_R(x)$ vs. $\phi_B(x)$.

b. Angular flux $\psi_R(x,\mu)$ vs. $\psi_B(x,\mu)$ at x = 0 and x = .5.

(a)

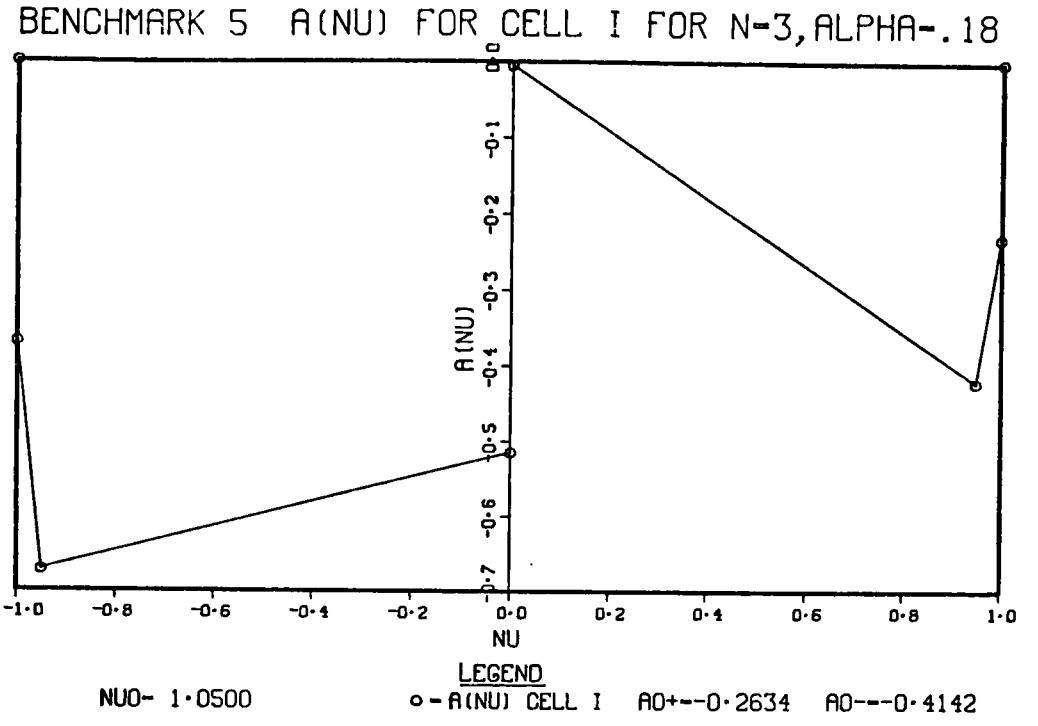

(b)

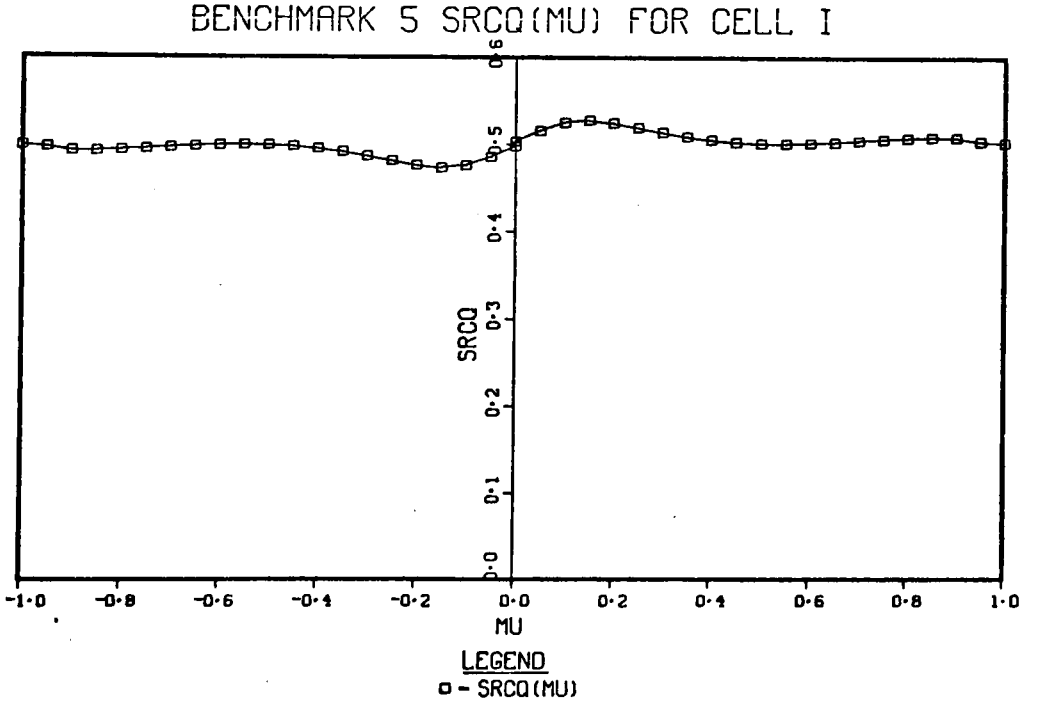

Figure 3.2. (a) Combining coefficients $A(\nu)$ and $a_0\pm$ from least squares modes analysis.
(b) Regionwise constant angular source in cell I for Benchmark #5.

(a)

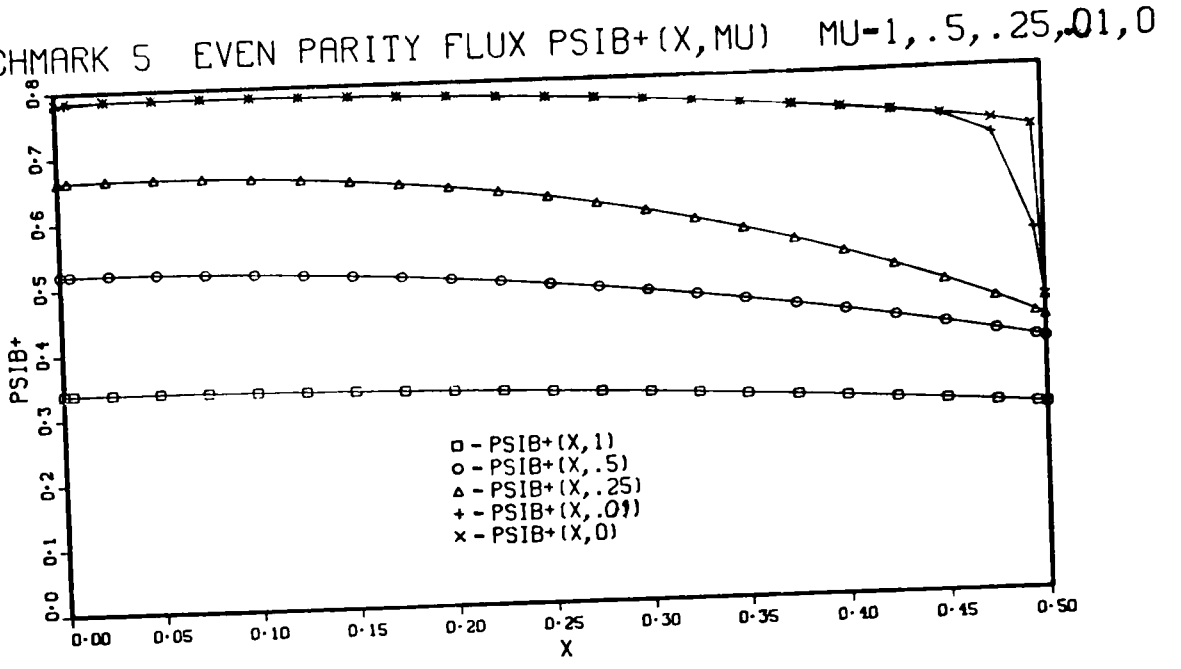

(b)

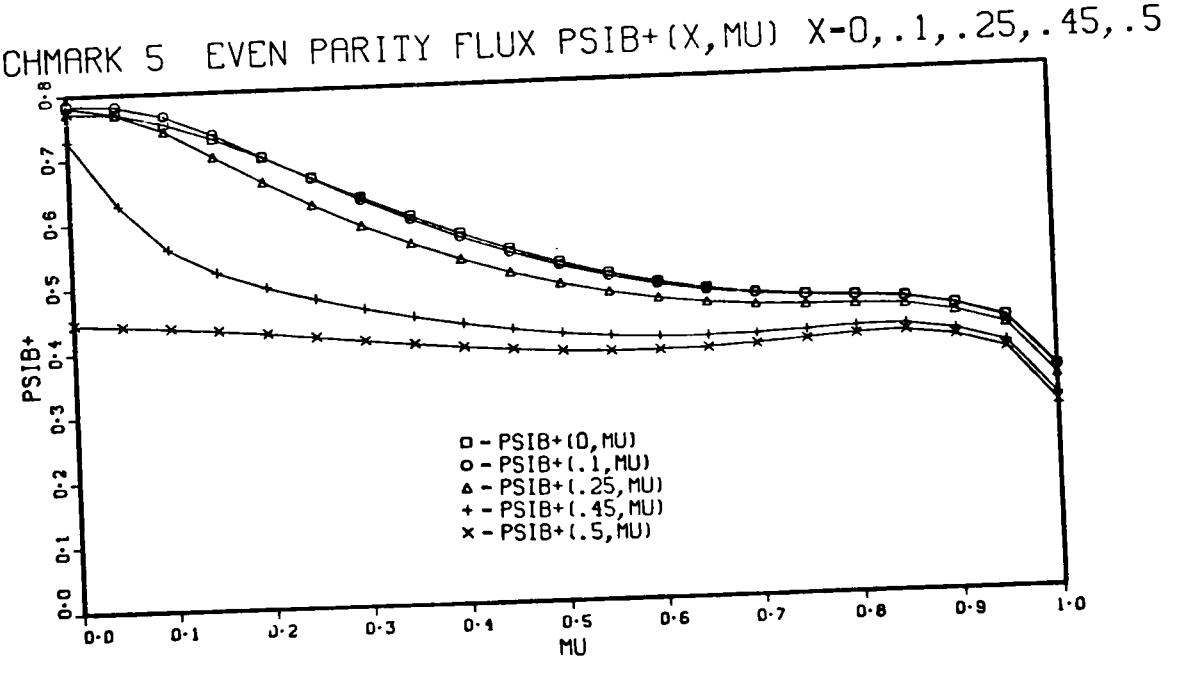

Figure 3.3. Even parity angular flux traverses for Benchmark #5
(a) Traverse along x for fixed μ
(b) Traverse along μ for fixed x

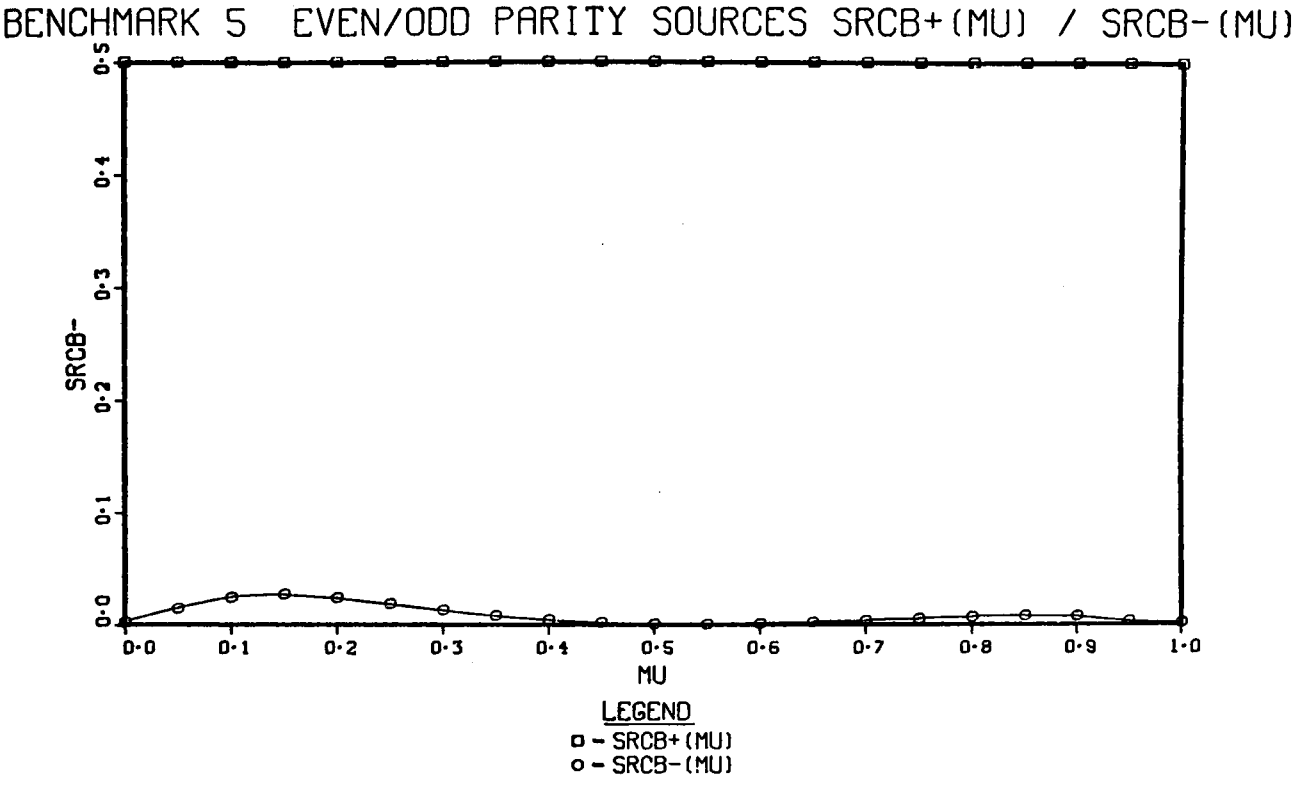

Figure 3.4. Even and odd parity sources for Benchmark #5

Similar to BP1, BP2 and BP3 we generate twenty space/angle mesh discretization sets and solve the resulting one cell benchmark problems by the DFD and FEM methods of this chapter. The equally spaced mesh intervals are successively halved in length so that $h = .5/i$ ($i=1,2,4,8,16$). The angular quadrature for the DFD method is the P_N quadrature set ($N=1,2,4,8$) for the interval ($0 \leq \mu \leq 1$). This corresponds to the same quadrature sets used in the previous examples for each half range of μ (i.e. $0 \leq \mu \leq 1$, $-1 \leq \mu \leq 0$). The FEM quadrature sets have equal spaced mesh points with $\Delta\mu = 1/j$ ($j=1,2,4,8$). At the interface $x = .5$ we apply the inhomogeneous source boundary condition Eqn. (3.17) which supplies the even parity flux values $\psi_B^+(.5,\mu)$. This means we need not solve for $\psi_C^+(.5,\mu)$. The values of $\psi_B^+(.5,\mu)$ are substituted into the matrix equations for the unknown fluxes and the resulting terms are transferred to the right hand side of the equations and treated as a source term.

The maximum absolute scalar flux error $\|\underline{\phi}_E\|_\infty$ with associated sign is tabulated in Table 3.1. For all but the highest order quadrature set, the error $\underline{\phi}_E$ reaches a minimum and subsequently begins increasing as the number of mesh intervals increases. Figure 3.5 illustrates the scalar flux error behaviour for the DFD and FEM methods. For a majority of the discretizations the maximum error successively shifts towards the mesh interval adjacent to the interface at $x = .5$. Here $\psi_B^+(.5,\mu)$ is specified exactly so that the scalar flux error is due to the angular quadrature discretization only and as we expect the error is reduced at the interface. As observed in previous benchmark problems the angular quadrature approximation has the most significant effect on the error and the spatial discretization is not as important.

The even parity angular flux error $\|\psi_E^+\|_\infty$ is tabulated in Table 3.2. Eight selected error traverses corresponding to $I = 16$ or $M = 8$ (DFD) and $M = 9$ (FEM) are displayed in Figs. 3.6 and 3.7 at $x = 0$ and $x = .25$ respectively. For the 8 angle discretization in the DFD method and for nearly all angular discretization in the FEM method, the angular location of the maximum error is located at the angular coordinate nearest to zero. As we approach $x = .5$ the angular error decreases due to the exact boundary condition and the location of the maximum error shifts closer to $\mu = 0$.

Table 3.1. Maximum absolute signed scalar flux error $\pm\|\phi_E\|_\infty$ tabulated for twenty space/angle discretization sets of Benchmark #5 for DFD and FEM methods

(a) DFD

BEAPAC 05/76 BP# 5.5 1 CELL MODES ANALYSIS X(0,.5) S=1, X(.5,1.5) S=0, NUO=1.05

MAX. ABS. SCALAR FLUX ERROR AND LOCATION (GLOBAL)

I: NO. OF XMESH INTERVALS J: NO. OF MU POINTS

	I \ J	1	2	4	8
ERROR	1	9.58D-02	-2.73D-02	-5.33D-03	1.26D-02
EXACT		1.113	0.790	0.790	1.113
X LOC		0.0	0.500	0.500	0.0
ERROR	2	1.02D-01	-3.76D-02	-5.33D-03	7.64D-03
EXACT		1.064	1.113	0.790	1.064
X LOC		0.250	0.0	0.500	0.250
ERROR	4	1.01D-01	-4.12D-02	-6.30D-03	4.51D-03
EXACT		1.064	1.113	1.113	0.976
X LOC		0.250	0.0	0.0	0.375
ERROR	8	1.00D-01	-4.24D-02	-8.20D-03	2.80D-03
EXACT		1.064	1.115	1.027	0.907
X LOC		0.250	0.063	0.313	0.438
ERROR	16	1.00D-01	-4.27D-02	-8.93D-03	2.33D-03
EXACT		1.064	1.115	1.004	1.004
X LOC		0.250	0.063	0.344	0.344

(b) FEM

BEAPAC 05/76 BP# 5.6 1 CELL MODES ANALYSIS X(0,.5) S=1, X(.5,1.5) S=0, NUO=1.05

MAX. ABS. SCALAR FLUX ERROR AND LOCATION (GLOBAL)

I: NO. OF XMESH INTERVALS J: NO. OF MU POINTS

	I \ J	2	3	5	9
ERROR	1	6.14D-02	4.18D-02	-4.67D-02	-5.97D-02
EXACT		0.790	0.790	1.113	1.113
X LOC		0.500	0.500	0.0	0.0
ERROR	2	7.21D-02	4.18D-02	1.23D-02	-1.76D-02
EXACT		1.064	0.790	0.790	1.064
X LOC		0.250	0.500	0.500	0.250
ERROR	4	9.03D-02	5.07D-02	1.23D-02	-8.01D-03
EXACT		0.976	0.976	0.790	0.976
X LOC		0.375	0.375	0.500	0.375
ERROR	8	9.19D-02	5.82D-02	1.72D-02	-2.65D-03
EXACT		0.907	0.907	0.907	0.907
X LOC		0.438	0.438	0.438	0.438
ERROR	16	9.28D-02	5.85D-02	2.05D-02	-1.99D-03
EXACT		0.945	0.907	0.860	1.113
X LOC		0.406	0.438	0.469	0.0

(a) DFD

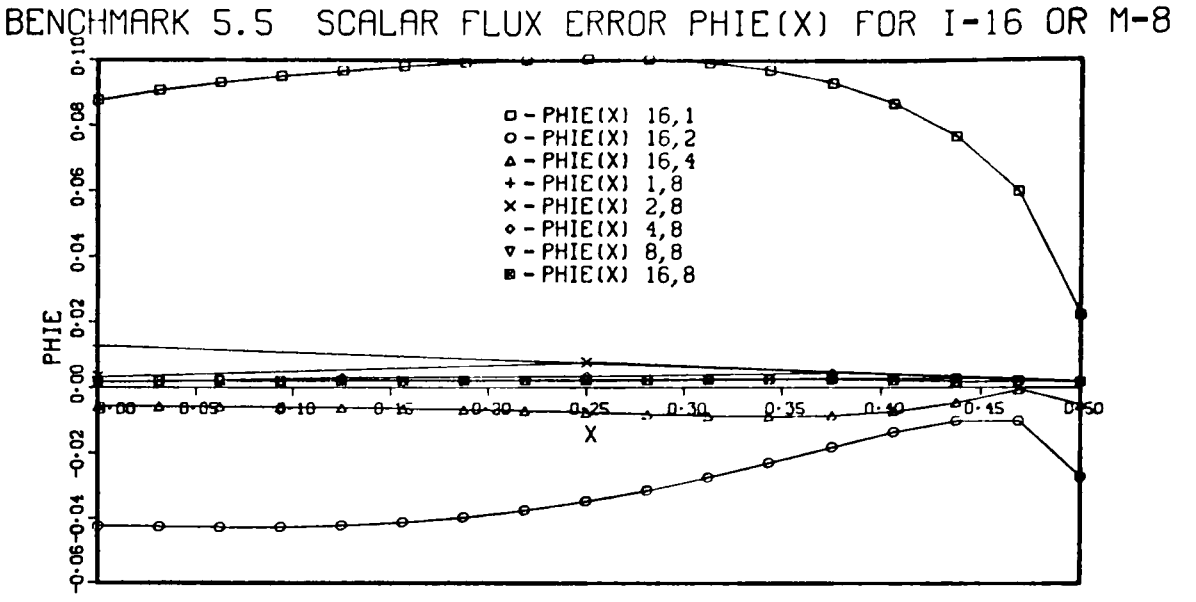

(b) FEM

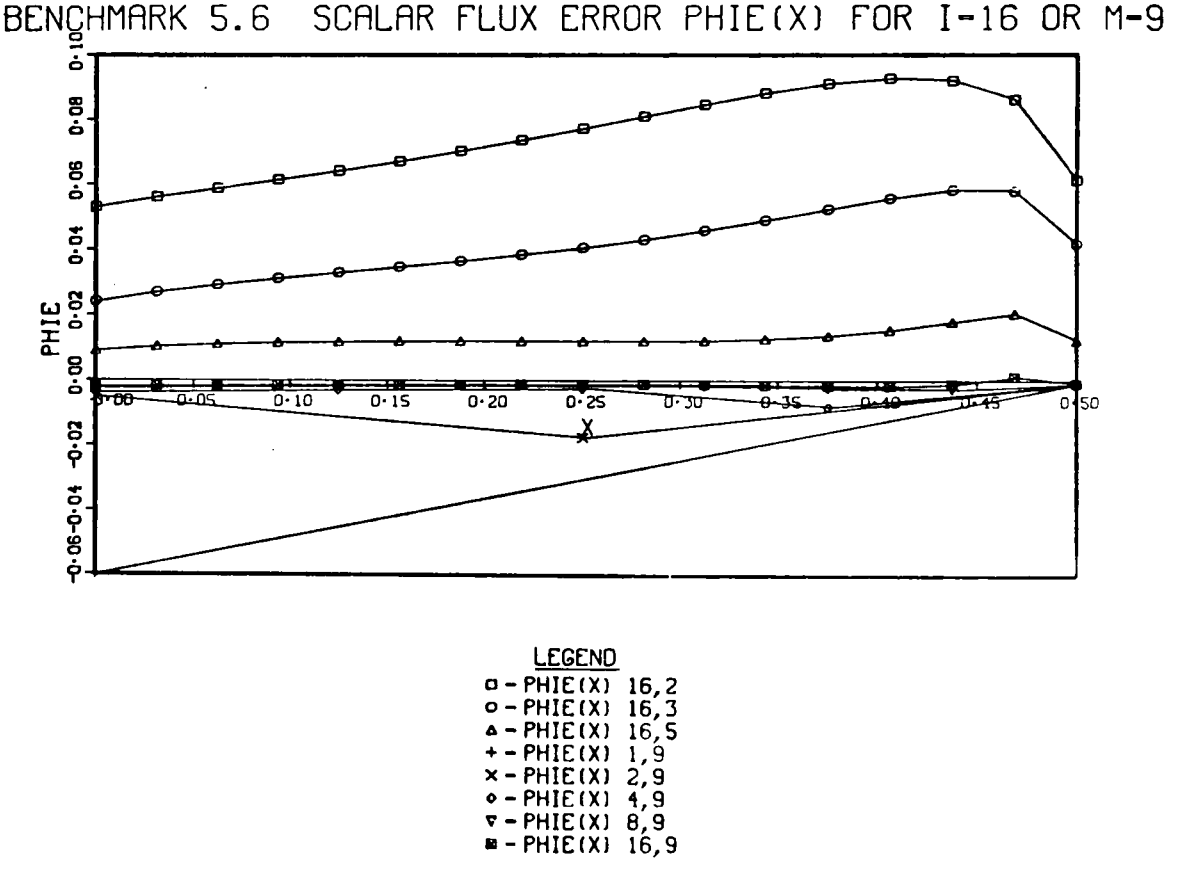

Figure 3.5. Scalar flux error $\phi_E(x)$ for DFD and FEM methods for eight selected discretizations of Benchmark #5

Table 3.2. Maximum absolute signed angular flux error $\pm\|\psi_E\|_\infty$ for twenty space/angle discretization sets of Benchmark #5 for DFD and FEM methods

(a) DFD

BEAPAC 05/76 BP# 5.5 1 CELL MODES ANALYSIS X(0,.5) S=1, X(.5,1.5) S=0, NU0=1.05

MAX. ABS. VECTOR FLUX ERROR AND LOCATION (GLOBAL)

I: NO. OF XMESH INTERVALS J: NO. OF MU POINTS

	I \ J	1	2	4	8
ERROR	1	1.26D-02	9.81D-03	1.15D-02	1.65D-02
EXACT		0.521	0.690	0.612	0.672
X LOC		0.0	0.0	0.0	0.0
MULOC		0.500	0.211	0.330	0.237
ERROR	2	9.63D-03	-3.33D-03	1.06D-02	1.28D-02
EXACT		0.521	0.690	0.761	0.740
X LOC		0.0	0.0	0.250	0.250
MULOC		0.500	0.211	0.069	0.102
ERROR	4	8.84D-03	-6.88D-03	7.51D-03	6.98D-03
EXACT		0.521	0.690	0.701	0.749
X LOC		0.0	0.0	0.375	0.375
MULOC		0.500	0.211	0.069	0.020
ERROR	8	8.64D-03	-7.76D-03	-2.97D-03	1.15D-02
EXACT		0.521	0.690	0.764	0.720
X LOC		0.0	0.0	0.0	0.438
MULOC		0.500	0.211	0.069	0.020
ERROR	16	8.58D-03	-7.99D-03	-1.92D-03	7.74D-03
EXACT		0.521	0.690	0.764	0.665
X LOC		0.0	0.0	0.0	0.469
MULOC		0.500	0.211	0.069	0.020

(b) FEM

BEAPAC 05/76 BP# 5.6 1 CELL MODES ANALYSIS X(0,.5) S=1, X(.5,1.5) S=0, NU0=1.05

MAX. ABS. VECTOR FLUX ERROR AND LOCATION (GLOBAL)

I: NO. OF XMESH INTERVALS J: NO. OF MU POINTS

	I \ J	2	3	5	9
ERROR	1	4.13D-02	-1.49D-01	-1.86D-01	-1.66D-01
EXACT		0.338	0.783	0.783	0.783
X LOC		0.0	0.0	0.0	0.0
MULOC		1.000	0.0	0.0	0.0
ERROR	2	7.69D-02	-6.54D-02	-8.20D-02	-9.48D-02
EXACT		0.773	0.783	0.773	0.773
X LOC		0.250	0.0	0.250	0.250
MULOC		0.0	0.0	0.0	0.0
ERROR	4	1.54D-01	7.43D-02	-4.12D-02	-7.32D-02
EXACT		0.750	0.750	0.773	0.750
X LOC		0.375	0.375	0.250	0.375
MULOC		0.0	0.0	0.0	0.0
ERROR	8	2.04D-01	1.52D-01	7.50D-02	-3.39D-02
EXACT		0.733	0.733	0.733	0.750
X LOC		0.438	0.438	0.438	0.375
MULOC		0.0	0.0	0.0	0.0
ERROR	16	2.31D-01	2.02D-01	1.50D-01	7.42D-02
EXACT		0.721	0.721	0.721	0.721
X LOC		0.469	0.469	0.469	0.469
MULOC		0.0	0.0	0.0	0.0

(a) DFD

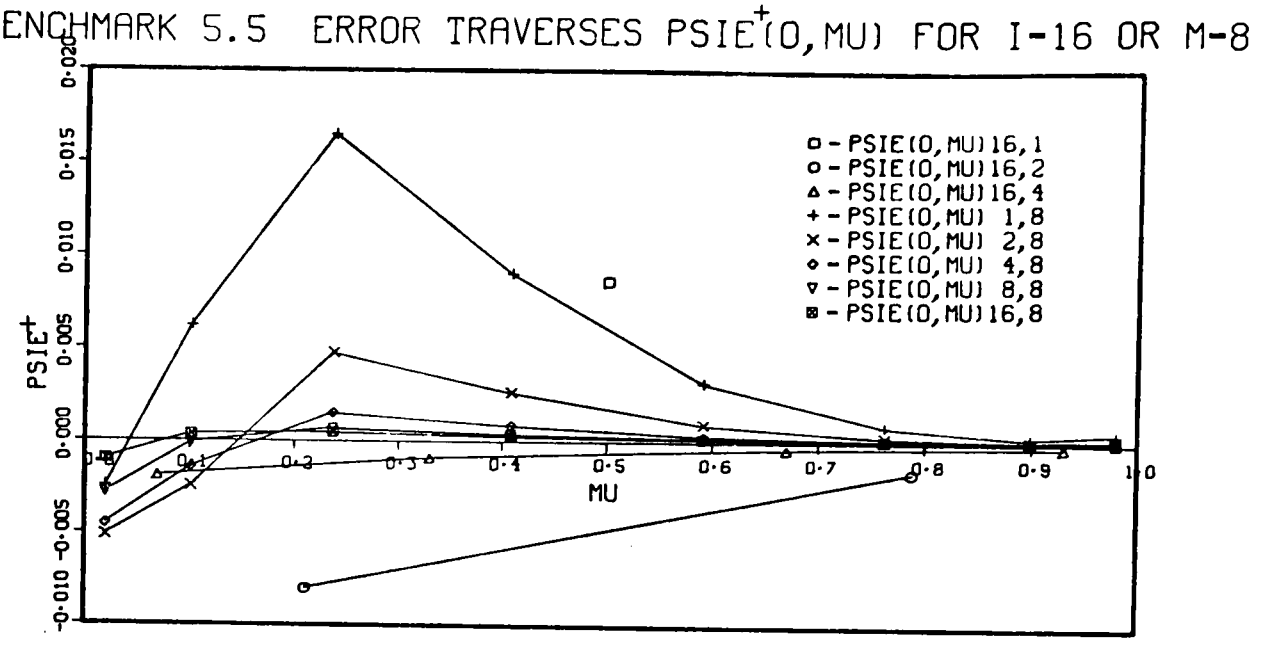

(b) FEM

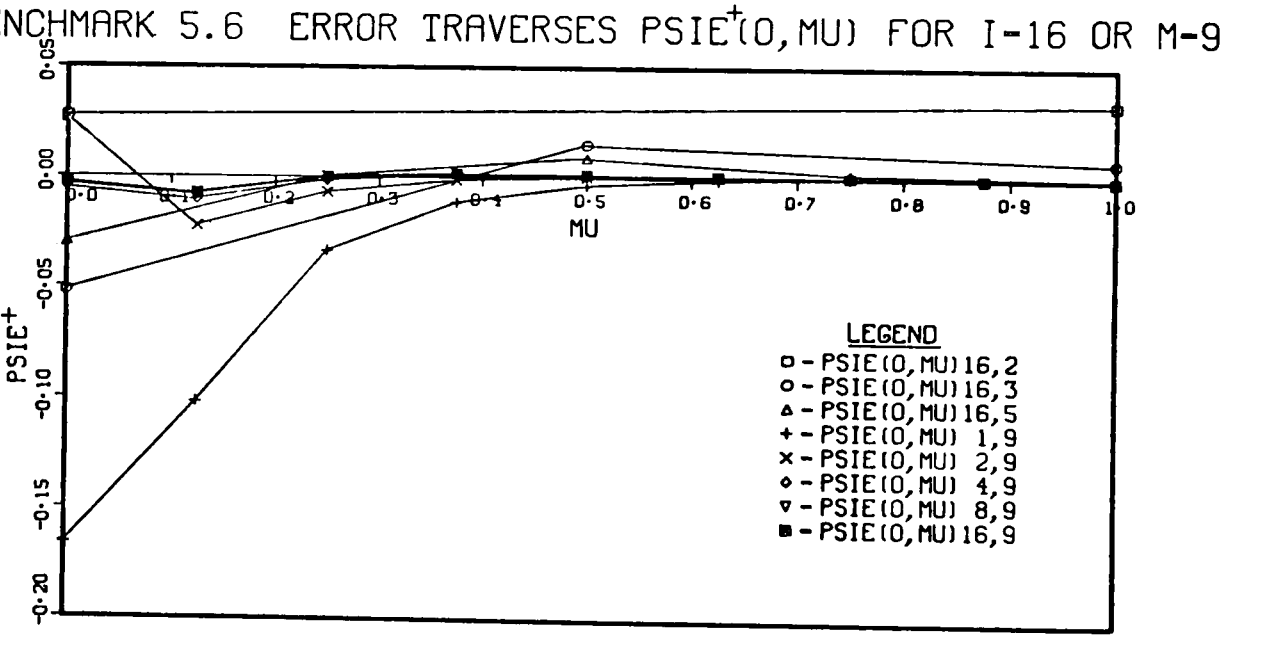

Figure 3.6. Even parity angular flux error traverses $\psi_E^+(0,\mu)$ for DFD and FEM methods for eight selected discretizations of Benchmark #5

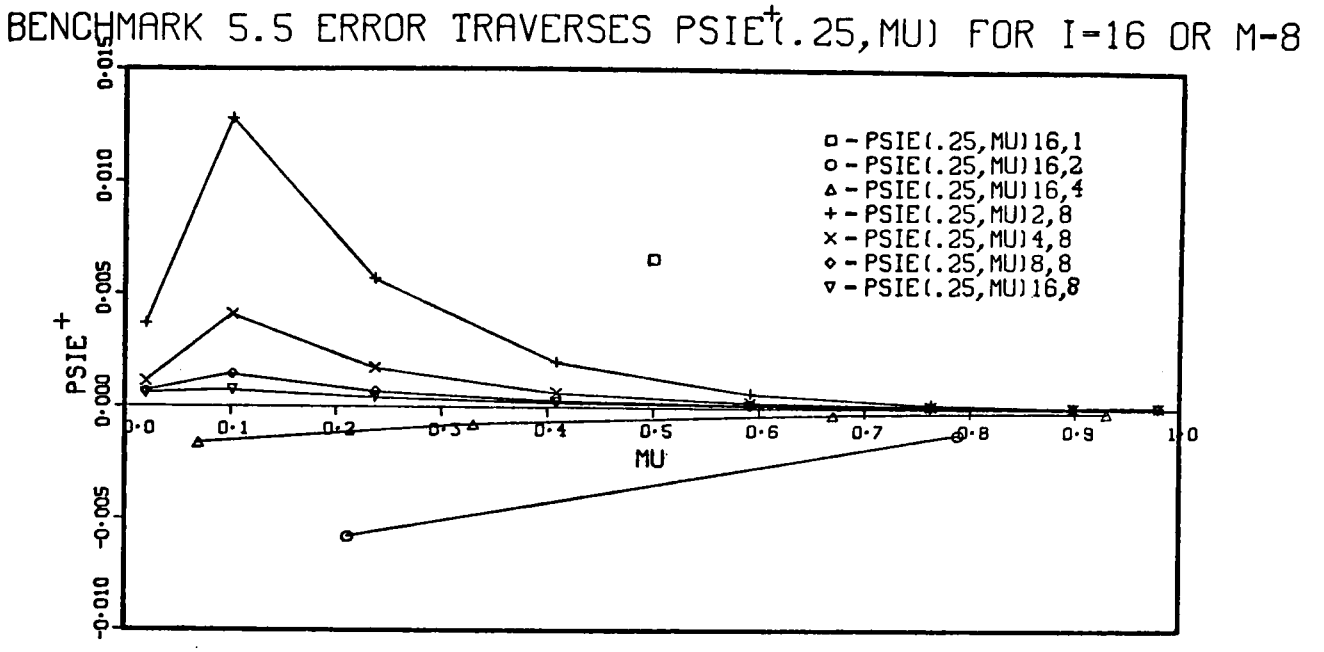

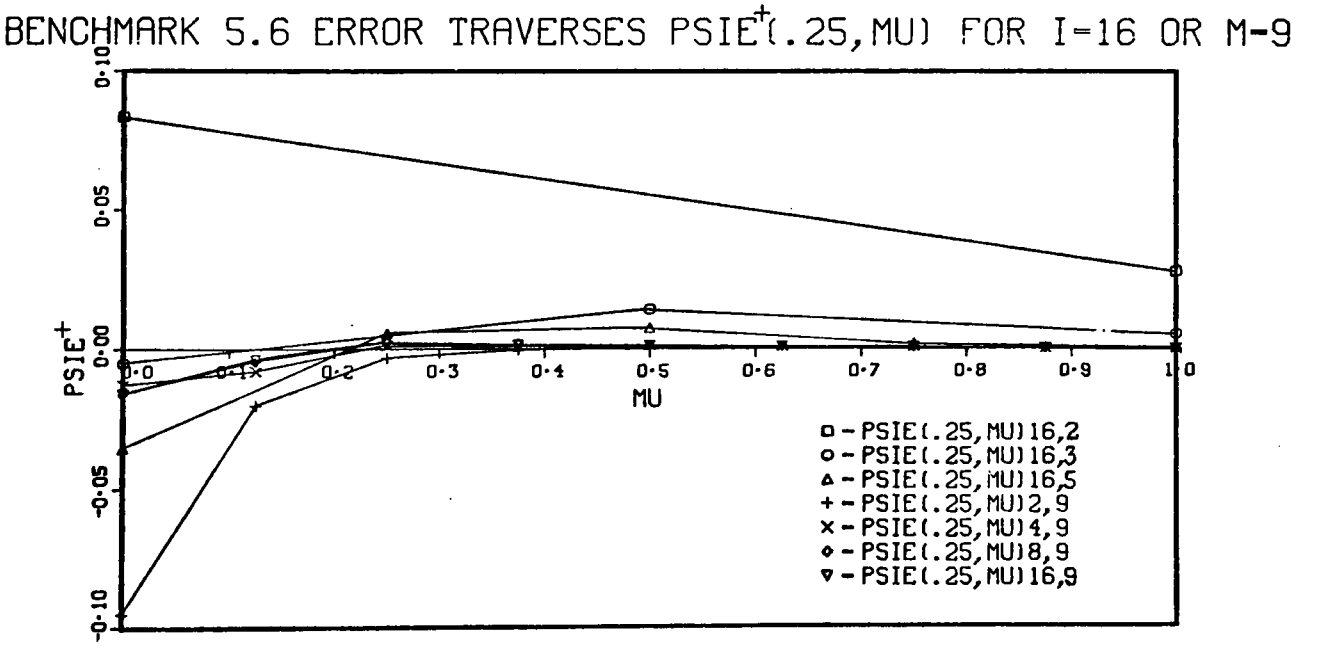

Figure 3.7. Even parity angular flux error traverses $\psi_E^+(.25,\mu)$ for DFD and FEM methods for seven selected discretizations of Benchmark #5

The average absolute scalar flux error and the relative sum error of the scalar flux is tabulated in Table 3.3. The error performance is similar to the angular flux error results previously discussed. For nearly all cases the error reaches a minimum and then increases as the number of spatial mesh intervals are decreased.

Table 3.3. Average absolute scalar flux error and relative sum error of pointwise scalar flux for DFD and FEM methods for twenty discretization sets of Benchmark #5

(a) DFD

BEAPAC 05/76 BP#10.6 1 CELL MODES ANALYSIS X(0,.5) S=1, X(.5,1.5) S=0, NUO=1.05

AVG. ABS. SCALAR FLUX ERROR (GLOBAL)

I: NO. OF XMESH INTERVALS J: NO. OF MU POINTS

I \ J	1	2	4	8
ERROR 1	5.90D-02	2.56D-02	4.46D-03	7.19D-03
ERROR 2	7.13D-02	3.11D-02	3.99D-03	4.26D-03
ERROR 4	8.03D-02	3.19D-02	5.64D-03	2.91D-03
ERROR 8	8.54D-02	3.14D-02	6.30D-03	2.30D-03
ERROR 16	8.80D-02	3.10D-02	6.47D-03	2.05D-03

(b) FEM

BEAPAC 05/76 BP#10.6 1 CELL MODES ANALYSIS X(0,.5) S=1, X(.5,1.5) S=0, NUO=1.05

AVG. ABS. SCALAR FLUX ERROR (GLOBAL)

I: NO. OF XMESH INTERVALS J: NO. OF MU POINTS

I \ J	2	3	5	9
ERROR 1	4.22D-02	3.29D-02	2.95D-02	3.03D-02
ERROR 2	6.01D-02	3.01D-02	6.46D-03	7.89D-03
ERROR 4	6.85D-02	3.70D-02	1.00D-02	3.62D-03
ERROR 8	7.24D-02	3.99D-02	1.21D-02	1.67D-03
ERROR 16	7.41D-02	4.12D-02	1.29D-02	1.40D-03

(c) DFD

BEAPAC 05/76 BP#10.5 1 CELL MODES ANALYSIS X(0,.5) S=1, X(.5,1.5) S=0, NUO=1.05

REL. ABS. SCALAR FLUX ERROR (GLOBAL)

I: NO. OF XMESH INTERVALS J: NO. OF MU POINTS

I \ J	1	2	4	8
ERROR 1	6.20D-02	2.69D-02	4.69D-03	7.56D-03
ERROR 2	7.21D-02	3.14D-02	4.03D-03	4.30D-03
ERROR 4	7.95D-02	3.15D-02	5.59D-03	2.88D-03
ERROR 8	8.36D-02	3.07D-02	6.17D-03	2.25D-03
ERROR 16	8.57D-02	3.02D-02	6.30D-03	2.00D-03

(d) FEM

BEAPAC 05/76 BP#10.6 1 CELL MODES ANALYSIS X(0,.5) S=1, X(.5,1.5) S=0, NUO=1.05

REL. ABS. SCALAR FLUX ERROR (GLOBAL)

I: NO. OF XMESH INTERVALS J: NO. OF MU POINTS

I \ J	2	3	5	9
ERROR 1	4.44D-02	3.46D-02	3.10D-02	3.19D-02
ERROR 2	6.08D-02	3.04D-02	6.53D-03	7.98D-03
ERROR 4	6.78D-02	3.66D-02	9.91D-03	3.59D-03
ERROR 8	7.09D-02	3.91D-02	1.10D-02	1.83D-03
ERROR 16	7.22D-02	4.01D-02	1.25D-02	1.36D-03

IV. SUMMARY AND CONCLUSION

We have shown how exact one- or two-cell benchmark problems can be created for arbitrary cells within a multicell reference problem using eigenmodes of the homogeneous one-dimensioned monoenergetic transport equation with isotropic scattering. The benchmark problems can be created by manually or automatically selecting eigenmodes combining coefficients.

Several benchmark problem examples illustrated most of the fundamental capabilities (summarized below) of the BEAPAC-1T code.

(1) one or two cell standard and even parity (symmetrized) angular flux benchmark problems.

(2) inhomogeneous vacuum and reflecting boundary conditions.

(3) manual or automatic benchmark solution synthesis.

(4) error analysis of built-in or external methods (via interface files).

(5) relative or absolute error tabulation of maximum, average or relative sum errors of angular and scalar flux.

(6) simple specifications to create arbitrary sets of space/angle mesh refinements for any benchmark problem.

(7) residual calculations for checking the accuracy of the eigenmodes.

The advantage of this automated approach to error analysis is that with a few hours of work and negligible computation costs, the analyst can obtain detailed information on the error performance of a particular method for a particular problem configuration. The major task required of the analyst is to supply the necessary interface data sets to BEAPAC-1T.

Item (7) above proved to be useful in debugging the eigenmodes calculation. The fact that the eigenmodes are exact solutions was an invaluable tool for debugging the transport theory methods built into BEAPAC-1T. Using the interface files of BEAPAC-1T, these exact solutions could be used for similar purposes in externally developed codes.

The least squares modes analysis method has a number of unanswered questions related to the optimum number of modes and placement of least squares points. The results so far are rather encouraging. Implementation of a variant of this method is planned for 1-D transport calculation.

Extensions of the benchmark error analysis techniques to two- and three-dimensional methods is under way.

APPENDIX A

Chapeau Function Expansion of $A(\nu)$

A.1 The Expansion for the Angular Flux

A.1.1 The standard basis

In Section 1.1.3 we constructed benchmark solutions $\psi_B(x,\mu)$ in a cell $D(0,a)$ of the general form

$$\psi_B(x,\mu) = \sum_{n=0}^{N} a_{\pm n} q_{\pm n}(x,\mu). \tag{1.9}$$

The transient elementary solutions $q_{\pm n}(x,\mu)$, $(n = 0,1,\ldots,N-1)$ in the standard basis are obtained from the general solution (1.4b) by requiring $A(\nu)$ and $\tilde{A}(-\nu)$ to have the form

$$A(\nu) = \sum_{n=0}^{N-1} a_n \Theta_n(\nu) \qquad 0 \le \nu \le 1 \tag{1.11a}$$

$$\tilde{A}(\nu) = \sum_{n=0}^{N-1} \tilde{a}_{-n} \Theta_n(-\nu) \qquad -1 \le \nu \le 0 \tag{1.11b}$$

The $\Theta_n(\nu)$ are the Chapeau functions defined by

$$\Theta_n(\nu) = \begin{cases} \dfrac{\nu - \nu_{n-1}}{\Delta\nu_{n-1}} & \nu_{n-1} \le \nu \le \nu_n \qquad n = 1,2,\ldots,N-2 \\[2ex] \dfrac{\nu_{n+1} - \nu}{\Delta\nu_n} & \nu_n \le \nu \le \nu_{n+1} \qquad n = 0,1,\ldots,N-2 \\[2ex] 0 & \text{otherwise} \end{cases} \tag{1.12a}$$

where $\Delta\nu_n = \nu_{n+1} - \nu_n$.

$\Theta_{N-1}(\nu)$ is treated in Appendix A.1.2.

The construction of $q_n(x,\mu)$ will now be developed for the first integral in (1.4b) which, upon substitution of (1.11), yields

$$\text{(1.13a)} \qquad q_n(x,\mu) = \int_{\nu_{n-1}}^{\nu_{n+1}} \Theta_n(\nu)\phi_\nu(\mu)e^{-x/\nu}d\nu \qquad (n = 0,1,\ldots,N-1)$$

Substitution of (1.7), (1.8) and (1.12a) into (1.13) yields

$$\text{(A.1)} \qquad q_n(x,\mu) = \frac{c}{2}\left[\int_{\nu_{n-1}}^{\nu_n} \frac{\nu-\nu_{n-1}}{\Delta\nu_{n-1}} \frac{\nu}{\nu-\mu}\, e^{-x/\nu}d\nu + \int_{\nu_n}^{\nu_{n+1}} \frac{\nu_{n+1}-\nu}{\Delta\nu_n} \frac{\nu}{\nu-\mu}\, e^{-x/\nu}d\nu\right].$$

$$+ \Theta_n(\nu)\left(1 - \frac{c}{2}\,\mu\, \ell n\left|\frac{1+\mu}{1-\mu}\right|\right)e^{-x/\mu} \qquad (n=0,1,2,\ldots,N-2)$$

The first term on the right hand side of (A.1) can be manipulated so that

$$\text{(A.2)} \qquad \int_{\nu_{n-1}}^{\nu_n} \frac{\nu - \nu_{n-1}}{\Delta\nu_{n-1}} \frac{\nu}{\nu - \mu}\, e^{-x/\nu}d\nu = \frac{1}{\Delta\nu_{n-1}}\,[\gamma_{n-1}(x) + (\mu-\nu_{n-1})\beta_{n-1}(x,\mu)]$$

where

$$\text{(A.3)} \qquad \gamma_n(x) = E_3^{(\nu_n,\nu_{n+1})}(x) = \int_{\nu_n}^{\nu_{n+1}} \nu e^{-x/\nu}d\nu$$

and

$$\text{(A.4)} \qquad \beta_n(x,\mu) = I_1^{(\nu_n,\nu_{n+1})}(x,\mu) = \int_{\nu_n}^{\nu_{n+1}} \frac{\nu}{\nu - \mu}\, e^{-x/\nu}d\nu.$$

By similar manipulations, the second term on the right hand side of (A.1) is

$$\text{(A.5)} \qquad \int_{\nu_n}^{\nu_{n+1}} \frac{\nu_{n+1} - \nu}{\Delta\nu_n} \frac{\nu}{\nu - \mu}\, e^{-x/\nu}d\nu = -\frac{1}{\Delta\nu_n}\,[\gamma_n(x) + (\mu-\nu_{n+1})\beta_n(x,\mu)].$$

Upon substitution of (A.2) and (A.5) into (A.1), we obtain the equations (A.6a) to (A.6e) summarized in Table A.1 for the various values of μ. Eq. (A.8) is obtained from

$$\hat{\beta}_n(x,\mu) = \beta_{n-1}(x,\mu) + \beta_n(x,\mu).$$

Appendix B gives formulas for the evaluation of $\gamma_n(x)$ and $\beta_n(x,\mu)$.

A.1.2 A special basis element

In Section 1.1.3 Eq. (1.12b), we introduced a basis element $\Theta_{N-1}(\nu)$ which improves the approximation basis for $A(\nu)$. The corresponding elementary angular flux mode of (1.13a) becomes explicitly

$$\text{(A.9)} \qquad q_{N-1}(x,\mu) = \frac{c}{2}\left[\int_{\nu_{N-2}}^{\beta} \Theta_{N-1}(\nu)\,\frac{\nu}{\nu-\mu}\,e^{-x/\nu}d\nu + \int_{\beta}^{1} \Theta_{N-1}(\nu)\,\frac{\nu}{\nu-\mu}\,e^{-x/\nu}d\nu\right] + \Theta_{N-1}(\nu)\lambda(\mu)e^{-x/\mu}$$

where

$$\beta = \begin{cases} \nu_{N-1} & \mu \neq \nu_{N-1} \\ \nu_{N-1} - b & \mu = \nu_{N-1} \end{cases}$$

which supplements (A.1). The parameter b is chosen to insure series convergence in the second integral of Eq. (A.9).

The first integral in (A.9) is evaluated exactly as the corresponding integral in (A.1) illustrated in Table A.1, except for one special case where $\mu = \nu_{N-1}$. Here we define

$$\text{(A.10)} \qquad \int_{\nu_{N-2}}^{\beta} \frac{\nu-\nu_{N-2}}{\Delta\nu_{N-2}}\,\frac{\nu}{\nu-\mu}\,e^{-x/\nu}d\nu = \frac{1}{\Delta\nu_{N-2}}[\tilde{\gamma}_{N-2}(x) + (\mu-\nu_{N-2})\tilde{\beta}_{N-2}(x,\mu)]$$

Table A.1 Computational equations for $q_n(x,\mu)$

(A.6a) $$q_n(x,\mu) = \frac{c}{2}\left\{\frac{1}{\Delta\nu_{n-1}}\left[\gamma_{n-1}(x) + (\mu-\nu_{n-1})\beta_{n-1}(x,\mu)\right] - \frac{1}{\Delta\nu_n}\left[\gamma_n(x) + (\mu-\nu_{n+1})\beta_n(x,\mu)\right]\right\} + G_n(x,\mu)$$

$n = 0,1,\ldots,N-2, \quad \mu \neq \nu_m, \quad m = 0,1,\ldots,N-1$

(A.6b) $$q_n(x,\mu) = \frac{c}{2}\left\{\frac{1}{\Delta\nu_{n-1}}\left[\gamma_{n-1}(x)\right] - \frac{1}{\Delta\nu_n}\left[\gamma_n(x)\right] + \hat{\beta}_n(x,\mu)\right\} + G_n(x,\mu)$$

$n = 1,2,\ldots,N-2, \quad \mu = \nu_n$

(A.6c) $$q_n(x,\mu) = \frac{c}{2}\left\{\frac{1}{\Delta\nu_{n-1}}\left[\gamma_{n-1}(x)\right] - \frac{1}{\Delta\nu_n}\left[\gamma_n(x) + (\mu-\nu_{n+1})\beta_n(x,\mu)\right]\right\} + G_n(x,\mu)$$

$n = 1,2,\ldots,N-2, \quad \mu = \nu_{n-1}$

(A.6d) $$q_n(x,\mu) = \frac{c}{2}\left\{\frac{1}{\Delta\nu_{n-1}}\left[\gamma_{n-1}(x) + (\mu-\nu_{n-1})\beta_{n-1}(x,\mu)\right] - \frac{1}{\Delta\nu_n}\left[\gamma_n(x)\right]\right\} + G_n(x,\mu)$$

$n = 0,1,\ldots,N-2, \quad \mu = \nu_{n+1}$

(A.6e) $$q_n(x,\mu) = \frac{c}{2}\left\{ - \frac{1}{\Delta\nu_n}\left[\gamma_n(x) + (\mu-\nu_{n+1})\beta_n(x,\mu)\right]\right\} + G_n(x,\mu)$$

$n = 0, \quad \mu = \nu_n$

where

(A.7) $$G_n(x,\mu) = \Theta_n(\mu)\lambda(\mu)e^{-x/\mu}$$

(A.8) $$\hat{\beta}_n(x,\mu) = I_1^{(\nu_{n-1},\nu_{n+1})}(x,\nu_n)$$

where

(A.11) $$\tilde{\gamma}_{N-2}(x) = E_3^{(\nu_{N-2},\beta)}(x) = \int_{\nu_{N-2}}^{\beta} \nu e^{-x/\nu} d\nu$$

(A.12) $$\tilde{\beta}_{N-2}(x,\mu) = I_1^{(\nu_{N-2},\beta)}(x,\mu) = \int_{\nu_{N-2}}^{\beta} \frac{\nu}{\nu-\mu} e^{-x/\nu} d\nu.$$

The second integral on the right side of (A.9) is a Cauchy principal value integral with singularity at $\mu = \nu$. It is denoted by $G(x,\mu)$ where

(A.13) $$G(x,\mu) = \left\{ \begin{array}{ll} 0 & \mu \neq \nu_{N-1} \\ \displaystyle\int_{\nu_{N-1}-b}^{\nu_{N-1}} \frac{\nu-\nu_{N-2}}{\Delta\nu_{N-2}} \frac{\nu}{\nu-\mu} e^{-x/\nu} d\nu & \mu = \nu_{N-1} \end{array} \right\}$$

$$+ \int_{\nu_{N-1}}^{1} \left(\frac{1-\nu}{\Delta\nu_{N-1}}\right)^{\alpha} \frac{\nu}{\nu-\mu} e^{-x/\nu} d\nu.$$

Eq. (A.13) is evaluated using power series expansions which will be derived at the end of this section. The domain of integration is denoted by D_p, $(p = 1,2,3,4,5)$ where the index p is determined by the location of μ with respect to ν_{N-1} and 1. To obtain rapidly converging series and to treat the singularity which occurs when $\nu = \mu$, the domains of integration D_p are partitioned into a set of subdomains $\{SD_q | SD_q \in D_p\}_p$, $p = 1,2,3,4,5$. There are five classes of subdomains SD_q, $q = 1,2,3,4,5$ which may be applicable to the integration over D_p. The domains D_p and their partitions $\{SD_q\}_p$ are illustrated in Table A.2.

The integral in D_p belongs to a class of Cauchy principal value integrals of the general form

(A.14) $$\tilde{G}(x,\mu) = P \int_{\beta}^{1} g(\nu,\mu) e^{-x/\nu} d\nu$$

$$= e^{-x}[G_{1p}(1,\mu) - xG_{2p}(1,\mu)] + x^2 G_{3p}(x,\mu)$$

Table A.2 Partitioning of the Integration Domains D_p for $I(\nu,\mu)$

DOMAIN		Subdomains	Convergence*	Recommended γ
D_1: $\mu < \nu_{N-1}$ $b = \nu_{N-1} - \mu$	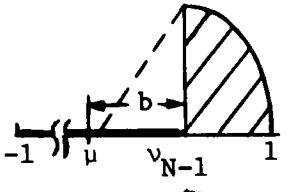	$D_1 = \{SD_1\}$	SD_1: $1-\gamma < 1$	$\gamma > \frac{1}{4}$
D_2: $\mu = \nu_{N-1}$ $b = \min\left(\Delta\nu_{N-2}, \frac{\Delta\nu_{N-1}}{2}\right)$	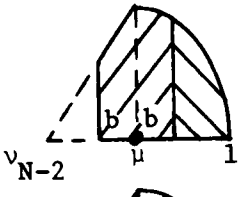	$D_2 = \{SD_2, SD_1\}$	SD_1: $1-\gamma < 1$ SD_2: $\gamma < 1$	$\gamma = \frac{1}{2}$
D_3: $\nu_{N-1} < \mu \leq \nu_{N-1} + \frac{5}{13}\Delta\nu_{N-1}$ $b = \mu - \nu_{N-1}$	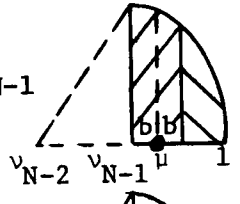	$D_3 = \{SD_3, SD_1\}$	SD_1: $1-\gamma < 1$ SD_3: $\gamma < 1$	$\frac{1}{4} < \gamma < \frac{3}{4}$
D_4: $\nu_{N-1} + \frac{5}{13}\Delta\nu_{N-1} < \mu < 1$ $b = \frac{5}{8}(1-\mu)$	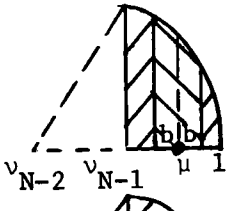	$D_4 = \{SD_4, SD_3, SD_1\}$	SD_1: $1-\gamma < 1$ SD_3: $\gamma < 1$ SD_4: $\frac{1}{1+\gamma} < 1$	$\gamma = \frac{5}{8}$
D_5: $\mu = 1$	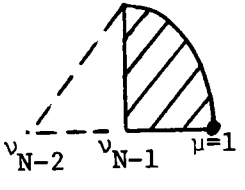	$D_5 = \{SD_5\}$	SD_5: unconditional	

*$b = \gamma(1-\mu)$

where $g(\nu,\mu)$ will have the form (A.18) in this section;

(A.15) $$G_{1p}(\nu,\mu) = P\int_{\beta}^{\nu} g(\nu',\mu)d\nu'$$

(A.16) $$G_{2p}(\nu,\mu) = \int_{\beta}^{\nu} \frac{G_{1p}(\nu',\mu)}{(\nu')^2}\, d\nu'$$

(A.17) $$G_{3p}(\nu,\mu) = \int_{\beta}^{1} \frac{G_{2p}(\nu,\mu)}{\nu^2}\, e^{-x/\nu} d\nu$$

If we define

(A.18) $$g(\nu,\mu) = \Theta_{N-1}(\nu)\,\frac{\nu}{\nu-\mu}$$

then Eq. (A.14) corresponds to Eq. (A.13). Upon substituting (A.18) into (A.15) we can develop computational expressions for (A.15), (A.16) and (A.17). To simplify the resulting expressions we define the following integrals. Let

(A.19) $$\begin{aligned} I(\nu,\mu) &= \int_{\beta}^{\nu} \Theta_{N-1}(\nu')\frac{\nu'}{\nu'-\mu}\, d\nu' \\ &= I_0(\nu,\mu) + \mu \sum_{SD_q \in D_p} I_q(\nu,\mu) \end{aligned}$$

where

(A.20) $$I_0(\nu,\mu) = \int_{\beta}^{\nu} \Theta_{N-1}(\nu)d\nu$$

(A.21) $$I_q(\nu,\mu) = \int_{\underline{\nu}_q}^{\min(\overline{\nu}_q,\nu)} \frac{\Theta_{N-1}(\nu')}{\nu'-\mu}\, d\nu' \ .$$

$\overline{\nu}_q$ and $\underline{\nu}_q$ are the respective upper and lower integration limits for subdomain SD_q. Table A.3 summarizes the computational expressions for (A.20) and the five subdomains for (A.21). Upon substitution of (A.19) into (A.15), the computational expression for (A.15) becomes

Table A.3 Subdomain Integration Formulas

Integration Formulas $0 < \alpha < 1$	Convergence $b = \gamma(1-\mu)$	$\underline{\nu}_q \le \nu \le \overline{\nu}_q$ Subdomain Range	
(A.20a) $I_0(\nu,\mu) = \left\{ \begin{array}{ll} \left.\dfrac{(\nu'-\nu_{N-2})^2}{2\Delta\nu_{N-2}}\right\|_{\nu_{N-1}-b}^{\nu_{N-1}} & \mu = \nu_{N-1} \\ 0 & \mu \neq \nu_{N-1} \end{array} \right\} - \dfrac{1}{\alpha+1}\left.\dfrac{(1-\nu')^{\alpha+1}}{\Delta\nu_{N-1}^{\alpha}}\right\|_{\nu_{N-1}}^{\nu}$			
(A.21a) $I_1(\nu,\mu) = \dfrac{-(1-\mu)^{\alpha}}{\Delta\nu_{N-1}^{\alpha}} \sum_{k=1}^{\infty} \left.\dfrac{t^{\alpha+k}}{\alpha+k}\right\|_{t=\frac{1-\mu-b}{1-\mu}}^{t=\frac{1-\nu}{1-\mu}}$	$1-\gamma < 1$	SD_1: $\mu < 1$ $\overline{\nu}_1 = 1$ $\underline{\nu}_1 = \mu+b$	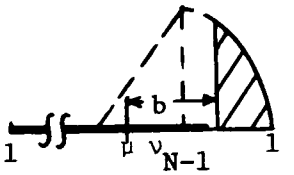
(A.21b) $I_2(\nu_{N-1}+b,\nu_{N-1}) = \dfrac{b}{\Delta\nu_{N-2}} + \sum_{k=1}^{\infty} \binom{\alpha}{k}\left(\dfrac{-t}{k}\right)^k \Bigg\|_{t=0}^{t=\frac{b}{1-\nu_{N-1}}}$	$\gamma < 1$	SD_2: $\mu = \nu_{N-1}$ $\overline{\nu}_2 = \mu+b$ $\underline{\nu}_2 = \mu-b$	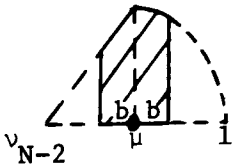
(A.21c) $I_3(\mu+b,\mu) = -2\,\dfrac{(1-\mu)^{\alpha}}{\Delta\nu_{N-1}^{\alpha}} \sum_{k=1}^{\infty} \binom{\alpha}{2k-1} \left.\dfrac{t^{2k-1}}{2k-1}\right\|_{t=0}^{t=\frac{b}{1-\mu}}$	$\gamma < 1$	SD_3: $\nu_{N-1} < \mu < 1$ $\overline{\nu}_3 = \mu+b$ $\underline{\nu}_3 = \mu-b$	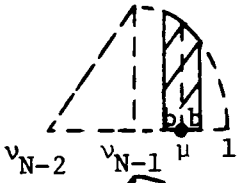
(A.21d)* $I_4(\nu,\mu) = -\dfrac{(1-\mu)^{\alpha}}{\Delta\nu_{N-1}^{\alpha}} \sum_{k=0}^{\infty} \left.\dfrac{t^{k-\alpha}}{k-\alpha}\right\|_{t=\frac{1-\mu}{1-\nu_{N-1}}}^{t=\frac{1-\mu}{1-\nu}}$	$\dfrac{1}{1+\gamma} < 1$	SD_4: $\dfrac{5}{13}(\nu_{N-1}+1) < \mu < 1$ $\overline{\nu}_4 = \mu-b$ $\underline{\nu}_4 = \nu_{N-1}$	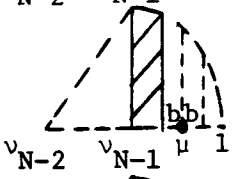
(A.21e) $I_5(\nu,1) = \dfrac{1}{\alpha\Delta\nu_{N-1}^{\alpha}} (1-\nu)^{\alpha} \Bigg\|_{t=\nu_{N-1}}^{t=\nu}$	unconditional	SD_5: $\mu = 1$ $\overline{\nu}_5 = 1$ $\underline{\nu}_5 = \nu_{N-1}$	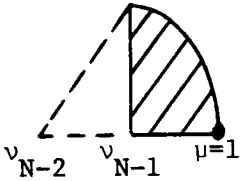

*When $\alpha=1$ the series term for $k=1$ is $\log t$.

(A.22) $$G_{1p}(\nu,\mu) = I_0(\nu,\mu) + \mu \sum_{SD_q \in D_p} I_q(\nu,\mu) \qquad p = 1,2,3,4,5$$

By definition (A.16) can be written

(A.23) $$G_{2p}(\nu,\mu) = \int_\beta^\nu \frac{d\nu'}{(\nu')^2} \int_\beta^{\nu'} \Theta_{N-1}(\nu'') \frac{\nu''}{\nu''-\mu}\, d\nu'' \ .$$

It can be shown that the interchange of integration in (A.23) is valid, so that

(A.24) $$G_{2p}(\nu,\mu) = \int_\beta^\nu \Theta_{N-1}(\nu'') \frac{\nu''}{\nu''-\mu}\, d\nu'' \int_{\nu''}^\nu \frac{d\nu'}{(\nu')^2}$$

which simplifies to

(A.25) $$G_{2p}(\nu,\mu) = \sum_{SD_q \in D_p} I_q(\nu,\mu) - \frac{1}{\nu} G_{1p}(\nu,\mu) \ .$$

Substituting (A.22) into (A.25) we obtain

(A.26) $$G_{2p}(\nu,\mu) = \left(1 - \frac{\mu}{\nu}\right) \sum_{SD_q \in D_p} I_q(\nu,\mu) - \frac{1}{\nu} I_0(\nu,\mu) \ .$$

Eq. (A.17) must be evaluated by numerical integration. The function $G_{2p}(\nu,\mu)$ in the integrand is a well behaved function as required for the interchange of integration to be valid in (A.23), so that the numerical integration is practical. We also note that the integration domain size $\Delta\nu_{N-1}$ is typically on the order of 10^{-3} for the $\Theta_{N-1}(\nu)$ element, hence the truncation order associated with the numerical integration is $O(10^{-3k})$ for quadrature rules of order k. The numerical integration formulas for each domain D_p are summarized in Table A.4. The quadrature points are chosen subject to the condition that any subdomain boundaries must coincide with a quadrature point (illustration in Table A.4).

In the first quadrature interval for each domain D_p, the integrand is approximated by a quadratic polynomial. It is easily shown that the integrand and its first derivative with respect to ν are both zero when

Table A.4 Numerical Integration of $G_{3p}(x,\mu)$

Integration Formula	Integration Parameters $(k=0,1,\ldots,K)$	Quadrature Points
(A.23a) $G_{31}(x,\mu) = \sum_{k=0}^{K} \omega_k \frac{G_{21}(t_k,\mu)}{t_k^2} e^{-x/t_k}$	$t_k = \nu_{N-1} + kh, \quad h = \frac{\Delta\nu_{N-1}}{3}$ $\omega_k = \{1,2,4,1\}\,\frac{h}{3}, \quad K=3$	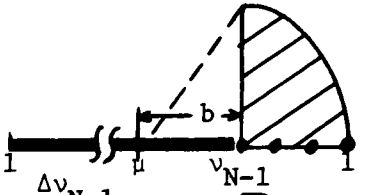
(A.23b) $G_{32}(x,\nu_{N-1}) = \sum_{k=0}^{K} \omega_k \frac{G_{22}(t_k,\nu_{N-1})}{t_k^2} e^{-x/t_k}$	$t_k = \{\nu_{N-1}-b, \nu_{N-1}, \nu_{N-1}+b, 1\}, \quad b=\min\left(\Delta\nu_{N-2}, \frac{\Delta\nu_{N-1}}{2}\right)$ $\omega_k = \{\frac{b}{3}, \frac{5b}{6}, \frac{t_3-t_1}{2}, \frac{t_3-t_2}{2}\}, \quad K=3$	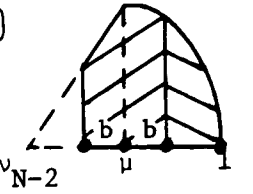
(A.23c) $G_{33}(x,\mu) = \sum_{k=0}^{K} \omega_k \frac{G_{23}(t_k,\mu)}{t_k^2} e^{-x/t_k}$	$t_k = \{\mu_{N-1}, \mu, \mu+b, 1\}, \quad b = \mu-\nu_{N-1}$ $\omega_k = \{\frac{b}{3}, \frac{5b}{6}, \frac{1-\mu}{2}, \frac{1-t_2}{2}\}, \quad K=3$	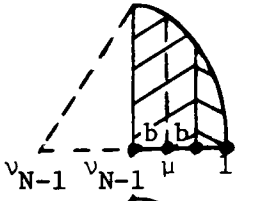
(A.23d) $G_{34}(x,\mu) = \sum_{k=0}^{K} \omega_k \frac{G_{24}(t_k,\mu)}{t_k^2} e^{-x/t_k}$	$t_k = \{\nu_{N-1}, \mu-b, \mu, \mu+b, 1\}, \quad b = \frac{5}{8}(1-\mu), \quad K=4$ $\omega_k = \{\frac{h_0}{3}, \frac{h_0+b}{3}, \frac{4b}{3}, \frac{b}{3}+\frac{h_3}{2}, \frac{h_3}{2}\}, \quad h_k = t_{k+1}-t_k$	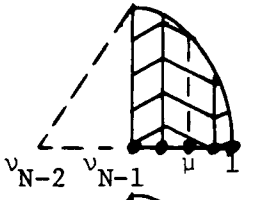
(A.23e) $G_{35}(x,1) = \sum_{k=0}^{K} \omega_k \frac{G_{25}(t_k,1)}{t_k^2} e^{-x/t_k}$	$t_k = \nu_{N-1} + kh, \quad h = \frac{\Delta\nu_{N-1}}{3}$ $\omega_k = \{1,2,4,1\}\,\frac{h}{3}, \quad K=3$	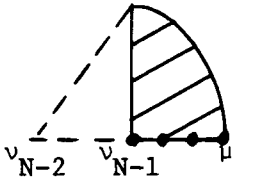

$\nu = \beta$. In the subsequent intervals, Simpson's rule is applied for equal mesh intervals when $p = 1,4,5$ and trapezoidal integration is applied for unequal mesh intervals when $p = 2,3$.

Eq. (A.22) and (A.26) can be substituted into (A.14) to obtain

$$\text{(A.27)} \quad \tilde{G}(x,\mu) = e^{-x}\{(1+x)I_0(1,\mu) + [\mu - x(1-\mu)] \sum_{SD_q \in D_p} I_q(1,\mu)\} + x^2 G_{3p}(x,\mu).$$

Substitution of (A.10) and (A.27) into (A.9) yields the general computational expression

$$\text{(A.28)} \quad q_{N-1}(x,\mu) = \frac{c}{2}[\tilde{\gamma}_{N-2}(x) + (\mu - \nu_{N-2})\tilde{\beta}_{N-2}(x,\mu) + \tilde{G}(x,\mu)] + G_{N-1}(x,\mu).$$

The derivation of the series expressions for Eqs. (A.21a) to (A.21d) is now given. The series are of two types depending on whether or not the subdomain includes the singularity $\nu = \mu$. When $\mu = 1$ (i.e., SD_5) the integral in (A.21) is evaluated directly.

Consider the non-singular case first (i.e., SD_1 and SD_4). The integral of (A.21) is expanded in the following series.

$$\text{(A.29a)} \quad \frac{(1-\nu)^\alpha}{\nu - \mu} = \frac{(1-\nu)^\alpha}{(1-\mu) - (1-\nu)}$$

$$= (1-\mu)^{\alpha-1} \frac{t^\alpha}{1-t} \qquad \text{where } t = \frac{1-\nu}{1-\mu} < 1$$

i.e.,

$$\text{(A.29b)} \quad \frac{(1-\nu)^\alpha}{\nu - \mu} = (1-\mu)^{\alpha-1} t^\alpha \sum_{k=0}^{\infty} t^k$$

so that for SD_1

$$\text{(A.30)} \quad I_1(\nu,\mu) = \frac{1}{\Delta\nu_{N-1}^\alpha} \int_{\nu_{N-1}}^{\nu} \frac{(1-\nu')^\alpha}{\nu' - \mu} d\nu' = \frac{-(1-\mu)^\alpha}{\Delta\nu_{N-1}^\alpha} \int_{\frac{1-\nu_{N-1}}{1-\mu}}^{\frac{1-\nu}{1-\mu}} \sum_{k=0}^{\infty} t^{\alpha+k} dt$$

where $d\nu' = -(1-\mu)dt$

i.e.,

$$\text{(A.31)} \quad I_1(\nu,\mu) = \frac{-(1-\mu)^\alpha}{\Delta\nu_{N-1}^\alpha} \sum_{k=1}^{\infty} \left. \frac{t^{\alpha+k}}{\alpha+k} \right|_{\frac{1-\nu_{N-1}}{1-\mu}}^{\frac{1-\nu}{1-\mu}} \qquad \mu < \nu_{N-1} \leq \nu.$$

For SD_4 the substitution

$$z = \frac{1-\mu}{1-\nu} = \frac{1}{t}, \qquad d\nu = \frac{1-\mu}{z^2}\, dz$$

is made in (A.29a) and (A.30) so that

$$\text{(A.32)} \qquad I_4(\nu,\mu) = -\frac{(1-\mu)^\alpha}{\Delta\nu_{N-1}^\alpha} \sum_{k=0}^{\infty} \frac{z^{k-\alpha}}{k-\alpha}\Bigg|_{\frac{1-\mu}{1-\nu_{N-1}}}^{\frac{1-\mu}{1-\nu}} \qquad \begin{array}{l} \nu_{N-1} < \nu < \mu. \\ \alpha \neq 1 \end{array}$$

Next consider the singular case (i.e., SD_2 and SD_3). The integral in (A.21) is separated into two integrals so that

$$\text{(A.33)} \qquad I_q(\nu,\mu) = \int_{\mu-b}^{\mu+b} \frac{\Theta_{N-1}(\nu)}{\nu-\mu}\, d\nu = \int_{\mu-b}^{\mu} \frac{\Theta_{N-1}(\nu)}{\nu-\mu}\, d\nu + \int_{\mu}^{\mu+b} \frac{\Theta_{N-1}(\nu)}{\nu-\mu}\, d\nu \qquad q = 2,3$$

When q=3 the change of variables $s = \nu-\mu$ in (A.33) yields

$$\text{(A.34)} \qquad I_3(\nu,\mu) = -\frac{(1-\mu)^\alpha}{\Delta\nu_{N-1}^\alpha} \int_0^b \left\{\left(1 + \frac{s}{1-\mu}\right)^\alpha - \left(1 - \frac{s}{1-\mu}\right)^\alpha\right\}\frac{ds}{s}\,.$$

Let

$$\text{(A.35)} \qquad t = \frac{s}{1-\mu}$$

and expand the terms in braces in (A.34) so that

$$\text{(A.36a)} \qquad (1+t)^\alpha = 1 + \binom{\alpha}{1}t + \binom{\alpha}{2}t^2 + \binom{\alpha}{3}t^3 + \ldots$$

$$\text{(A.36b)} \qquad (1-t)^\alpha = 1 - \binom{\alpha}{1}t + \binom{\alpha}{2}t^2 - \binom{\alpha}{3}t^3 + \ldots$$

Subtracting (A.36b) from (A.36a) and substituting the result into (A.34) we obtain

$$\text{(A.37)} \qquad I_3(\nu,\mu) = -\frac{(1-\mu)^\alpha}{\Delta\nu_{N-1}^\alpha}\int_0^{\frac{b}{1-\mu}} \left\{2\left[\binom{\alpha}{1}t + \binom{\alpha}{3}t^3 + \binom{\alpha}{5}t^5 + \ldots\right]\right\}\frac{dt}{t}$$

i.e.,

$$\text{(A.38)} \qquad I_3(\nu,\mu) = -2\,\frac{(1-\mu)^\alpha}{\Delta\nu_{N-1}^\alpha}\sum_{k=1}^{\infty}\binom{\alpha}{2k-1}\frac{t^{2k-1}}{2k-1}\Bigg|_{t=0}^{t=\frac{b}{1-\mu}}$$

When q=2 the change of variables $s = \nu-\mu$ in (A.33) yields

$$\text{(A.39)} \qquad I_2(\nu,\nu_{N-1}) = -\int_0^b \left\{\left(1 - \frac{s}{\Delta\nu_{N-2}}\right) - \left(1 - \frac{s}{\Delta\nu_{N-1}}\right)^\alpha\right\}\frac{ds}{s}\,.$$

Let

$$\text{(A.40)} \qquad t = \frac{s}{\Delta\nu_{N-1}}$$

and expand the terms in braces in Eq. (A.39). Note that in this case the term corresponding to (A.36a) is simply

$$\text{(A.41)} \qquad 1 - t\,\frac{\Delta\nu_{N-1}}{\Delta\nu_{N-2}}$$

and the second term is exactly given by (A.36b). Subtracting (A.36b) from (A.41) and substituting the result into (A.39) we obtain

$$\text{(A.42)} \qquad I_2(\nu,\mu) = -\int_0^{\frac{b}{\Delta\nu_{N-1}}}\left\{t\left[\binom{\alpha}{1} - \frac{\Delta\nu_{N-1}}{\Delta\nu_{N-2}}\right] - t^2\binom{\alpha}{2} + t^3\binom{\alpha}{3} - \ldots\right\}\frac{dt}{t}$$

i.e.,

$$\text{(A.43)} \qquad I_2(\nu,\mu) = \frac{b}{\Delta\nu_{N-2}} + \sum_{k=1}^{\infty}\binom{\alpha}{k}\frac{(-t)^k}{k}\Bigg|_{t=0}^{t=\frac{b}{\Delta\nu_{N-1}}}\,.$$

The series just derived for $I_q(\nu,\mu)$, q = 1,2,3,4,5 are all convergent. The speed of convergence is dependent on the parameters μ, b and γ which are related by the formula $b=\gamma(1-\mu)$. Tables A.2 and A.3 include a summary of the range of γ values which will make the series converge.

Table A.2 includes a column which summarizes recommended values of γ for rapid convergence.

The selection of quadrature points for evaluating Eq. (A.17) in subdomains SD_2 and SD_3 is restricted to the subdomain endpoints due to the symmetric nature of the series evaluation. We can utilize Eq. (A.26) when $\mu=\nu$ so that

$$G_{2p}(\nu,\nu) = \left(1 - \frac{\nu}{\nu}\right) \sum_{SD_q \in D_p} I_q(\nu,\nu) - \frac{1}{\nu} I_0(\nu,\nu) \tag{A.44}$$

i.e.,

$$G_{2p}(\nu,\nu) = -\frac{1}{\nu} I_0(\nu,\nu) \ . \tag{A.45}$$

Therefore, we can include the quadrature point $\nu=\mu$ for domains D_2, D_3 and D_4 which use SD_2 or SD_3 as illustrated in Table A.4.

A.2 The Expansion for the Angular Flux Derivative

A.2.1 The standard basis

In Appendix A.1.1 we developed explicit expressions (A.6a) to (A.6e) to calculate $\{q_n(x,\mu)\}$, the elementary angular flux solutions. These results are extended to calculate

$$\mu\, q_n^{(1)}(x,\mu) = \mu \frac{\partial}{\partial x} q_n(x,\mu) \tag{A.46}$$

where $q_n^{(1)}(x,\mu)$ is the derivative with respect to x of the elementary angular flux. The computational equations are the same as Eqs. (A.6a) to (A.6c) with the following modifications of the $\gamma_n(x)$, $\beta_n(x,\mu)$ and $G_n(x,\mu)$ terms.

The $\gamma_n(x)$ term becomes

$$\mu \frac{\partial \gamma_n(x)}{\partial x} = \mu \frac{\partial}{\partial x} \int_{\nu_n}^{\nu_{n+1}} \nu e^{-x/\nu} d\nu = -\mu \int_{\nu_n}^{\nu_{n+1}} e^{-x/\nu} d\nu = -\mu E_2^{(\nu_n,\nu_{n+1})}(x). \tag{A.47}$$

The $\beta_n(x,\mu)$ term becomes

$$\text{(A.48)} \qquad \mu \frac{\partial \beta_n(x,\mu)}{\partial x} = \mu \frac{\partial}{\partial x} \int_{\nu_n}^{\nu_{n+1}} \frac{\nu}{\nu-\mu} e^{-x/\nu} d\nu = -\mu \int_{\nu_n}^{\nu_{n+1}} \frac{e^{-x/\nu}}{\nu-\mu} d\nu =$$

$$= -\mu \, I_0^{(\nu_n,\nu_{n+1})}(x,\mu).$$

The $G_n(x,\mu)$ term becomes

$$\text{(A.49)} \qquad \mu \frac{\partial G_n(x,\mu)}{\partial x} = \mu \frac{\partial}{\partial x} \Theta_n(\mu)\lambda(\mu)e^{-x/\mu} = -\Theta_n(\mu)\lambda(\mu)e^{-x/\mu}.$$

When $\mu=0$, $n=0$, and $x=0$, a special limit case occurs in (A.48) and (A.49). Eq. (A.48) becomes

$$\text{(A.50)} \qquad \lim_{\mu\to 0} \mu \frac{\partial \beta_0(0,\mu)}{\partial x} = -\lim_{\mu\to 0} \mu \, I_0^{(0,\nu_{n+1})}(0,\mu) = \lim_{\mu\to 0} \mu \log \mu \to 0$$

and Eq. (A.49) becomes

$$\text{(A.51)} \qquad \lim_{\mu\to 0} \mu \frac{\partial G_0(0,\mu)}{\partial x} = \lim_{\mu\to 0} \mu \frac{\partial}{\partial x} \Theta_0(0)\lambda(0)e^{-x/\mu}\Big|_{x=0} = -1.$$

A.2.2 A special basis element

The elementary angular flux derivative $q_{N-1}^{(1)}(x,\mu)$ associated with the special basis element $\Theta_{N-1}(\nu)$ is calculated by differentiating Eq. (A.28) with respect to x. The resulting expression for $\frac{\partial}{\partial x}\tilde{G}(x,\mu)$ will be derived. The remaining terms have already been treated in section A.2.1.

The derivative of $\tilde{G}(x,\mu)$ in Eq. (A.27) becomes

$$\text{(A.53)} \qquad \tilde{G}^{(1)}(x,\mu) = \frac{\partial}{\partial x}\tilde{G}(x,\mu)$$

$$= -e^{-x}\{xI_0(1,\mu) - [x(1-\mu)-1]\sum_{SD_q \epsilon D_p} I_q(1,\mu)\} +$$

$$2xG_{3p}(x,\mu) - x^2 G_{3p}^{(1)}(x,\mu)$$

where

$$\text{(A.54)} \qquad G_{3p}^{(1)}(x,\mu) = -\frac{\partial}{\partial x}G_{3p}(x,\mu) = \int_{\beta}^{1} \frac{G_{2p}(\nu,\mu)}{\nu^3} e^{-x/\nu} .$$

The integration in $G_{3p}^{(1)}(x,\mu)$ is performed numerically using the formulas (A.23a) to (A.23e) that were used to integrate $G_{3p}(x,\mu)$ Eq. (A.17). The only difference between $G_{3p}(x,\mu)$ and $G_{3p}^{(1)}(x,\mu)$ is in the denominator of the integrand. The t_K^2 term is replaced by t_K^3 in formulas (A.23a) to (A.23e) to calculate $G_{3p}^{(1)}(x,\mu)$.

A.3 The Expansion for the Scalar Flux

A.3.1 The standard basis

The elementary scalar flux is defined by

$$\text{(A.55)} \qquad q_n^{(-1)}(x) = \int_{-1}^{1} q_n(x,\mu)d\mu.$$

The normalization condition [Case 1967]

$$\text{(A.56)} \qquad \int_{-1}^{1} \phi_\nu(\mu)d\mu = 1$$

assumed in the derivation of the general solution (1.4a) simplifies the development of $q_n^{(-1)}(x)$.

Substituting (A.1) into (A.55) and reversing the order of integration in variables μ and ν, we find

$$\text{(A.57)} \qquad q_n^{(-1)}(x) = \int_{\nu_{n-1}}^{\nu_n} \frac{\nu-\nu_{n-1}}{\Delta\nu_{n-1}} e^{-x/\nu} d\nu + \int_{\nu_n}^{\nu_{n+1}} \frac{\nu_{n+1}-\nu}{\Delta\nu_n} e^{-x/\nu} d\nu \qquad (n = 0,1,\ldots,N-2)$$

$$= \frac{1}{\Delta\nu_{n-1}} \left[E_3^{(\nu_{n-1},\nu_n)}(x) - \nu_{n-1} E_2^{(\nu_{n-1},\nu_n)}(x) \right]$$

$$- \frac{1}{\Delta\nu_n} \left[E_3^{(\nu_n,\nu_{n+1})}(x) - \nu_n E_2^{(\nu_n,\nu_{n+1})}(x) \right]$$

where (A.56) was applied to the integration over μ. The $E_n^{(\nu_n,\nu_{n+1})}(x)$ functions are described in Appendix B.

The elementary scalar flux $q_{-n}^{(-1)}(x)$ is calculated by

$$\text{(A.58)} \qquad q_{-n}^{(-1)}(x) = q_n^{(-1)}(a-x) \ .$$

A.3.2 A special basis element

The elementary scalar flux $q_{N-1}^{(-1)}(x)$ associated with the special basis element $\Theta_{N-1}(\nu)$ is defined by

$$\text{(A.59)} \qquad q_{N-1}^{(-1)}(x) = \frac{1}{\Delta\nu_{N-2}} \left[E_3^{(\nu_{N-2},\nu_{N-1})}(x) - \nu_{N-2} E_2^{(\nu_{N-2},\nu_{N-1})}(x) \right] + G^{(-1)}(x)$$

where

$$\text{(A.60)} \qquad G^{(-1)}(x) = \int_{\nu_{N-1}}^{1} \left(\frac{1-\nu}{\Delta\nu_{N-1}}\right)^{\alpha} d\nu \ .$$

The $E_n^{(a,b)}(x)$ terms are derived in (A.57).

Similar to Eq. (A.14) we define the general class of integrals

$$\text{(A.61)} \qquad \tilde{G}^{(-1)}(x) = \int_{\nu_{N-1}}^{1} g(\nu) e^{-x/\nu} d\nu$$

$$= e^{-x}\{G_1^{(-1)}(1) - xG_2^{(-1)}(1)\} + x^2 G_{3p}^{(-1)}(x)$$

where $g(\nu)$ has the form (A.65) in this section;

$$G_1^{(-1)}(\nu) = \int_{\nu_{N-1}}^{\nu} g(\nu')d\nu' \tag{A.62}$$

$$G_2^{(-1)}(\nu) = \int_{\nu_{N-1}}^{\nu} \frac{G_1^{(-1)}(\nu')}{(\nu')^2} d\nu' \tag{A.63}$$

$$G_3^{(-1)}(x) = \int_{\nu_{N-1}}^{1} \frac{G_{2p}^{(-1)}(\nu)}{\nu^2} e^{-x/\nu} d\nu. \tag{A.64}$$

If we define

$$g(\nu) = \left(\frac{1-\nu}{\Delta\nu_{N-1}}\right)^{\alpha} \tag{A.65}$$

then Eq. (A.61) corresponds to Eq. (A.60). Upon substituting (A.65) into (A.62), we can develop computational expressions for (A.62), (A.63) and (A.64).

The computational expression for (A.62) becomes

$$G_1^{(-1)}(\nu) = \frac{-1}{\alpha+1} \left(\frac{1-\nu'}{\Delta\nu_{N-1}}\right)^{\alpha+1} \Bigg|_{\nu_{N-1}}^{\nu} . \tag{A.66}$$

By definition (A.63) can be written

$$G_2^{(-1)}(\nu) = \int_{\nu_{N-1}}^{\nu} \frac{d\nu'}{(\nu')^2} \int_{\nu_{N-1}}^{\nu'} \left(\frac{1-\nu''}{\Delta\nu_{N-1}}\right)^{\alpha} d\nu'' . \tag{A.67}$$

Interchanging the integration of ν' and ν'' we find

$$G_2^{(-1)}(\nu) = \int_{\nu_{N-1}}^{\nu} \left(\frac{1-\nu''}{\Delta\nu_{N-1}}\right)^{\alpha} d\nu'' \int_{\nu''}^{\nu} \frac{d\nu'}{(\nu')^2} \tag{A.68}$$

which simplifies to

$$G_2^{(-1)}(\nu) = I^*(\nu) - \frac{1}{\nu} G_1^{(-1)}(\nu) \tag{A.69}$$

where

$$I^*(\nu) = \int_{\nu_{N-1}}^{\nu} \left(\frac{1-\nu''}{\Delta\nu_{N-1}}\right)^{\alpha} \frac{d\nu''}{\nu''} \tag{A.70}$$

Integrating (A.70) by parts we obtain

$$I^*(\nu) = \log \nu'' \left(\frac{1-\nu''}{\Delta\nu_{N-1}}\right)^{\alpha} \Bigg|_{\nu_{N-1}}^{\nu} + I^{(-1)}(\nu) \tag{A.71}$$

where

$$\begin{aligned} I^{(-1)}(\nu) &= \frac{\alpha}{\Delta\nu_{N-1}^{\alpha}} \int_{\nu_{N-1}}^{\nu} \log \nu''(1-\nu'')^{\alpha-1} d\nu'' \\ &= -\frac{\alpha}{\Delta\nu_{N-1}^{\alpha}} \int_{1-\nu_{N-1}}^{1-\nu} \log(1-t)\, t^{\alpha-1}\, dt \\ &= \frac{\alpha}{\Delta\nu_{N-1}^{\alpha}} \int_{1-\nu_{N-1}}^{1-\nu} \sum_{k=1}^{\infty} \frac{t^{\alpha+k-1}}{k}\, dt \end{aligned} \tag{A.72}$$

Evaluating the last integral in (A.72), we obtain

$$I^{(-1)}(\nu) = \frac{\alpha}{\Delta\nu_{N-1}^{\alpha}} \sum_{k=1}^{\infty} \frac{t^{\alpha+k}}{(\alpha+k)k} \Bigg|_{t = \Delta\nu_{N-1}}^{t = 1-\nu} . \tag{A.73}$$

We note that $t = \Delta\nu_{N-1} > 1-\nu$ is typically on the order of 10^{-3} and is always less than .25 so that convergence is rapid in (A.73).

Eq. (A.64) must be evaluated by numerical integration. The function $G_2^{(-1)}(\nu)$ in the integrand is a well behaved function so that numerical integration is practical. Four equally spaced quadrature points t_k are chosen so that

(A.74) $$t_k = kh + \nu_{N-1} \qquad (k = 0,1,2,3), \qquad h = \frac{\Delta\nu_{N-1}}{3} .$$

The integrand is approximated by a quadratic polynomial in the first quadrature interval. It is easily shown that the integrand and its first derivative with respect to ν is zero when $\nu = \nu_{N-1}$. In the subsequent intervals Simpson's rule is applied. The composite integration formula for (A.64) becomes

(A.75) $$G_3^{(-1)}(x) = \sum_{k=0}^{3} \omega_k \frac{G_2(t_k)}{t_k^2} e^{-x/t_k}$$

where

(A.76) $$\{\omega_k | k=0,1,2,3\} = \{1,2,4,1\}\frac{h}{3} .$$

Substitution of (A.69) into (A.61) yields the computational expression

(A.77) $$\tilde{G}^{(-1)}(x) = e^{-x}\{(1+x)G_1^{(-1)}(1) - xI^*(1)\} + x^2 G_{3p}^{(-1)}(x) .$$

APPENDIX B

Exponential Integrals and Related Functions

B.1 The Exponential Integral $E_n(x)$

B.1.1 The general expression

The classical exponential integral is

$$\text{(B.1)} \qquad Ei(x) = -\int_{-x}^{\infty} \frac{e^{-t}}{t}\, dt \qquad (x \neq 0)$$

where the integral is a Cauchy principal value integral when $x > 0$.

The functions $E_n(x)$ are generalization of the function

$$\text{(B.2a)} \qquad E_1(x) = \int_{x}^{\infty} \frac{e^{-t}dt}{t} = -Ei(-x) \qquad (x > 0)$$

and are defined as follows.

$$\text{(B.3)} \qquad E_n(x) = x^{n-1} \int_{x}^{\infty} \frac{e^{-t}}{t^n}\, dt = \int_{0}^{1} \nu^{n-2} e^{-x/\nu} d\nu \qquad (t = x/\nu) \ .$$

Using integration by parts it is easy to show that

$$\text{(B.4a)} \qquad E_n(x) = \frac{1}{n-1}\, [e^{-x} - xE_{n-1}(x)] \qquad (n > 1) \ .$$

Using the FORTRAN routine DEI in the Argonne Applied Mathematics Division program library (Cody 1971) the function Ei(x) is computed on the IBM 370/195 to roughly 50 correct significant bits which is equivalent to a relative error of 10^{-15}. Eqs. (B.2a) and (B.4a) are used to calculate $E_n(x)$ for $n > 0$.

B.1.2 Limit cases

$E_n(0)$ has two limit cases depending on the value of n. If $n = 1$,

(B.2b) $$E_1(0) = \lim_{x\to 0} \int_0^1 \frac{e^{-x/\nu}}{\nu}\, d\nu = \int_0^1 \frac{d\nu}{\nu} = \log \nu \Big|_0^1 \to \infty$$

i.e., the limit does not exist. If $n > 1$, then using (B.4a) we find

$$E_n(0) = \lim_{x\to 0} \frac{1}{n-1} [e^{-x} - xE_{n-1}(x)]$$

$$= \frac{1}{n-1} [1 - \lim_{x\to 0} x\, E_{n-1}(x)] = \ldots$$

$$= \frac{1}{n-1} [1 - 0 + \ldots + 0 + \lim_{x\to 0} x^{n-1} E_1(x)]$$

(B.4b) $$E_n(0) = \frac{1}{n-1} \qquad (n > 1)$$

where

$$\lim_{x\to 0} x^{n-1} E_1(x) = \lim_{x\to 0} x^{n-1} \log \nu \Big|_x^1 = 0 \qquad (n > 1) .$$

B.1.3 The generalized exponential integral $E_n^{(a,b)}(x)$

We define the generalized exponential integral $E_n^{(a,b)}(x)$ by

(B.5) $$E_n^{(a,b)}(x) = \int_a^b \nu^{n-2}\, e^{-x/\nu} d\nu \qquad (x \geq 0,\quad 0 \leq a < b \leq 1,\quad n > 0)$$

$$= x^{n-1} \int_{x/b}^{x/a} \frac{e^{-t}}{t^n}\, dt \qquad (t = x/\nu) .$$

We define $E_1^{(a,b)}(x)$ as follows.

$$E_1^{(a,b)}(x) = \int_{x/b}^{x/a} \frac{e^{-t}}{t}\, dt = \left(\int_{x/b}^{\infty} - \int_{x/a}^{\infty} \right) \frac{e^{-t}}{t}\, dt .$$

Hence by (B.2a) we have

(B.6a) $$E_1^{(a,b)}(x) = E_1(x/b) - E_1(x/a) .$$

Integration by parts of (B.5) gives

$$\text{(B.7a)} \qquad E_n^{(a,b)}(x) = \frac{1}{n-1}\,[(b^{n-1}e^{-x/b} - a^{n-1}e^{-x/a}) - xE_{n-1}^{(a,b)}(x)] \qquad (n > 1)\ .$$

B.1.4 Limit cases for the generalized form

We consider the limit cases of (B.6a) and (B.7a). First, when x=0 and $0<a < b\leq 1$, we find from (B.5) and (B.2b) that (B.6a) becomes

$$\text{(B.6b)} \qquad E_1^{(a,b)}(0) = \int_a^b \frac{d\nu}{\nu} = \log b/a$$

and from (B.4b) and (B.6a) that (B.7a) becomes

$$\text{(B.7b)} \qquad E_n^{(a,b)}(0) = \frac{1}{n-1}\,(b^{n-1} - a^{n-1}) \qquad (n > 1)\ .$$

Secondly, when a=0 and x>0, (B.6a) becomes

$$\text{(B.6c)} \qquad E_1^{(0,b)}(x) = E_1(x/b)$$

and (B.7a) becomes

$$\text{(B.7c)} \qquad E_n^{(0,b)}(x) = \frac{1}{n-1}\,[b^{n-1}e^{-x/b} - xE_{n-1}^{(0,b)}(x/b)] \qquad (n > 1)\ .$$

Finally, consider the case when x=0 and a=0. Then (B.6b) becomes

$$\text{(B.6d)} \qquad E_1^{(0,b)}(0) = \lim_{a\to 0} \log b/a \to \infty$$

and (B.7b) becomes

(B.7d) $$E_n^{(0,b)}(0) = \frac{b^{n-1}}{n-1} \qquad (n > 1) .$$

B.2 The Exponential Integral $I_n(x,\mu)$

B.2.1 The general expression

The integral $I_n(x,\mu)$ is defined (Abu-Shumays, 1973) by

(B.8) $$I_n(x,\mu) \equiv \int_0^1 \frac{\nu^n e^{-x/\nu}}{\nu-\mu}\, d\nu \qquad (n\geq 0,\ x\geq 0,\ |\mu|<1) .$$

It is easily shown that the following recursion relation holds.

(B.9) $$I_{n+1}(x,\mu) - \mu I_n(x,\mu) = \int_0^1 \nu^n e^{-x/\mu} \equiv E_{n+2}(x) \qquad (n \geq 0) .$$

We obtain $I_0(x,\mu)$ from (B.8) as follows.

(B.10) $$I_0(x,\mu) = \int_0^1 \frac{e^{-x/\nu}}{\nu-\mu}\, d\nu = \int_x^\infty \frac{e^{-t}}{t(1-\frac{\mu}{x}t)}\, dt \qquad (t = \frac{x}{\nu})$$
$$= \int_x^\infty \frac{e^{-t}}{t}\, dt - e^{-x/\mu} \int_{-(x/\mu - x)}^\infty \frac{e^{-\tau}}{\tau}\, d\tau \quad (\tau = t - \frac{x}{\mu}) .$$

Hence, using (B.1) and (B.2a) in (B.10)

(B.11a) $$I_0(x,\mu) = E_1(x) + e^{-x/\mu}\, Ei(x/\mu - x) .$$

Rearrangement of (B.9) yields the following recursion relation for n>0.

(B.12a) $$I_n(x,\mu) = E_{n+1}(x) + \mu I_{n-1}(x,\mu) \qquad (n > 0) .$$

B.2.2 Limit cases

We consider the limit cases of (B.11a) and (B.12a). When x=0 and $\mu \neq 0$, $\mu \neq 1$, then for n=0 (B.8) yields

$$I_0(0,\mu) = \lim_{x\to 0} \int_0^1 \frac{e^{-x/\nu}}{\nu-\mu}\, d\nu = \int_0^1 \frac{d\nu}{\nu-\mu}$$

(B.11b) $$I_0(0,\mu) = \log \frac{1-\mu}{|\mu|} .$$

Next, recalling (B.4b), equation (B.12a) becomes

(B.12b) $$I_n(0,\mu) = 1/n + \mu I_{n-1}(0,\mu) \qquad (n > 0) .$$

When $\mu=0$, then if n=0 and (B.3) is used in (B.8)

(B.11c) $$I_0(x,0) = \int_0^1 \frac{e^{-x/\nu}}{\nu}\, d\nu = E_1(x), \qquad (x > 0)$$

and using (B.11c) in (B.12a) yields

(B.12c) $$I_n(x,0) = E_{n+1}(x) \qquad (n \geq 0) .$$

The case when x=0 and $\mu=0$ is directly obtained from (B.2b) and (B.4a) in (B.12c) and yields

(B.12c) $$I_n(0,0) = \begin{cases} \infty & n = 0 \\ 1/n & n > 0 \end{cases} .$$

Finally, when $\mu=1$, (B.11a) does not exist, i.e.,

(B.12e) $$I_n(x,1) \to \infty \qquad (n = 0,1,2,\ldots) .$$

B.2.3 The generalized exponential integral $I_n^{(a,b)}(x,\mu)$

Similar to $E_n^{(a,b)}(x)$ Sect. B.1.3, we define the generalized integral

$$\text{(B.13)} \qquad I_n^{(a,b)}(x,\mu) \equiv \int_a^b \frac{\nu^n e^{-x/\nu}}{\nu-\mu}\, d\nu \quad (x\geq 0,\ |\mu|\leq 1,\ n\geq 0,\ 0\leq a<b\leq 1)\ .$$

Using (B.13) and (B.5), the recursion formula (B.9) is generalized to

$$\text{(B.14)} \qquad I_{n+1}^{(a,b)}(x,\mu) - \mu I_n^{(a,b)}(x,\mu) = \int_a^b \nu^n e^{-x/\mu} d\mu \equiv E_{n+2}^{(a,b)}(x) \quad (n \geq 0)\ .$$

$I_0^{(a,b)}(x,\mu)$ is derived as follows:

$$I_0^{(a,b)}(x,\mu) = \int_a^b \frac{e^{-x/\nu}}{\nu-\mu}\, d\nu$$

$$= \left(\int_0^b - \int_0^a\right) \frac{e^{-x/\nu}}{\nu-\mu}\, d\nu$$

$$\text{(B.15)} \qquad I_0^{(a,b)}(x,\mu) = I_0^b(x,\mu) - I_0^a(x,\mu)$$

where from (B.10) with the integration limit 1 replaced by b we find

$$\text{(B.16)} \qquad I_0^b(x,\mu) \equiv \int_0^b \frac{e^{-x/\nu}}{\nu-\mu}\, d\nu = E_1(x/b) + e^{-x/\mu} Ei(x/\mu - x/b)\ .$$

The definition

$$\text{(B.17)} \qquad Ei^{(a,b)}(x/\mu - x) \equiv Ei(x/\mu - x/b) - Ei(x/\mu - x/a)$$

combined with (B.16) in (B.15) yields

$$\text{(B.18a)} \qquad I_0^{(a,b)}(x,\mu) = E_1^{(a,b)}(x) + e^{-x/\mu} Ei^{(a,b)}(x/\mu - x)\ .$$

Rearrangement of (B.14) yields the recursion relation

(B.19a) $$I_n^{(a,b)}(x,\mu) = E_{n+1}^{(a,b)}(x) + \mu I_{n-1}^{(a,b)}(x,\mu) \qquad (n > 0) .$$

B.2.4 Limit cases for the generalized form

We consider the limit cases of (B.18a) and (B.19a). When x=0 and $\mu\neq 0$, $\mu\neq a$, $\mu\neq b$ in (B.13), we find

$$I_0^{(a,b)}(0,\mu) = \int_a^b \frac{d\nu}{\nu-\mu}\, d\nu$$

i.e.,

(B.18b) $$I_0^{(a,b)}(0,\mu) = \log \left|\frac{b-\mu}{\mu-a}\right|$$

and

(B.19b) $$I_n^{(a,b)}(0,\mu) = E_{n+1}^{(a,b)}(0) + \mu I_{n-1}^{(a,b)}(0,\mu) \qquad (n > 0) .$$

When $\mu=0\neq a$ and $x>0$, we find from (B.13) and (B.14) that

(B.18c) $$I_0^{(a,b)}(x,0) = E_1^{(a,b)}(x)$$

and

(B.19c) $$I_n^{(a,b)}(x,0) = E_{n+1}^{(a,b)}(x) \qquad (n > 0) .$$

When x=0 and $\mu=0\neq a$, (B.13) yields

(B.18d) $$I_0^{(a,b)}(0,0) = \log b/a$$

and

(B.19d) $$I_n^{(a,b)}(0,0) = E_{n+1}^{(a,b)}(0) \qquad (n > 0) .$$

When $\mu=a\neq 0$ we find

(B.18e) $$I_0^{(a,b)}(x,a) = \{E_1^{(a,b)}(x) + e^{-x/a}[Ei(x/a - x/b) - \lim_{\mu\to a} Ei(x/\mu - x/a)]\}$$

$$\to -\infty$$

since

$$\lim_{\varepsilon\to 0} Ei(\varepsilon) \to \infty .$$

When $n>0$ we have

$$I_n^{(a,b)}(x,a) = E_{n+1}^{(a,b)}(x) + aI_{n-1}^{(a,b)}(x,a)$$

$$= \ldots$$

(B.19e) $$I_n^{(a,b)}(x,a) = E_{n+1}^{(a,b)}(x) + a^n I_0^{(a,b)}(x,a) \to \infty .$$

Analogous formulas can be developed for the case $\mu=b$ and $a\neq 0$ with precisely the same results for the limits. When $\mu=a=0$ we find from (B.6a), (B.18c) and (B.19c) that

(B.19f) $$I_n^{(0,b)}(x,0) = \begin{cases} \infty & x=0 \\ E_{n+1}(x/b) & x\neq 0 \end{cases} \qquad n \geq 0 .$$

When $\mu=b$ and $a=0$ we find from (B.18e) that

(B.18g) $$I_0^{(0,b)}(x,b) = E_1(x/b) + e^{-x/b}\left(\lim_{\mu\to b} Ei(x/\mu - x/b)\right) \to \infty$$

and

(B.19g) $$I_n^{(0,b)}(x,b) = E_{n+1}(x/b) + bI_{n-1}^{(0,b)}(x,b) \to \infty .$$

REFERENCES

I. K. Abu-Shumays, E. H. Bareiss, *On the Structure of Isotropic Transport Operators in Space*, (Chapter in Transport Theory, Vol. I, SIAM-ANS Proceedings, Providence, R.I. (1969).

ARGONNE CODE CENTER: "Benchmark Problem Book. Numerical Determination of the Space, Time, Angle, or Energy Distribution of Particles in an Assembly," Argonne National Laboratory ANL-7416 (1968) (revised 1971).

E. H. Bareiss, "Flexible Transport Theory Routines for Nuclear Reactor Design," DTMB Report 1030, July (1956).

E. H. Bareiss, "A Spectral Theory of the Stationary Transport Operator in Slab Geometry," *J. of Math. Anal. and Appl.*, 13 (200-222) (1966).

E. H. Bareiss, "Numerical Solution of the Neutron Transport Equation," Lecture, Symposium on Numerical Solution of Integral Equations and Physical Applications, SIAM Fall Meeting, Madison, Wisconsin, Oct. 11-13 (1971).

E. H. Bareiss, K. L. Derstine, "A User's Manual for BEAPAC-1T," report to be published (1977).

B. G. Carlson, K. D. Lathrop, "Transport Theory. The Method of Discrete Ordinates," in *Computing Methods in Reactor Physics*, H. Greenspan, et al., Eds., Gordon and Breach, New York (1968).

K. M. Case, P. F. Zweifel, "Solutions of the Homogeneous, One Speed Equation," in *Linear Transport Theory*, Addison Wesley, Reading, 58-93 (1967).

W. Cody, K. Paciorek, Subroutine DEI, Argonne National Laboratory, Applied Mathematics Division Subroutine Library, ANL-C375S-1 DEI (1968) revised (1971).

B. Davison, *Neutron Transport Theory*, Oxford (1957).

R. J. Hangelbroek, "A Functional Analytic Approach to the Linear Transport Equation," Rijksuniversiteit te Groningen, Ph.D. thesis (1973).

E. Inonu, Lecture, Fourth National Conference on Transport Theory, VPI&SU, Blacksburg, Virginia, March 10-15 (1975).

E. Isaacson, H. B. Keller, *Analysis of Numerical Methods*, Wiley, New York (1966).

E. W. Larsen, "Solution of Neutron Transport Problems in L_1^*," *Comm. Pure and Appl. Math.*, Vol. 28, 729-746 (1975).

W. F. Miller, "Application of Finite Elements to One- and Two-Dimensional Neutron Transport," Ph.D. thesis, Northwestern University (1973).

I. Stakgold, *Boundary Value Problems of Mathematical Physics*, Volume I, Macmillan, Toronto (1969).

W. G. Strang, G. J. Fix, *An Analysis of the Finite Element Method*, Englewood Cliffs, N.J., Prentice-Hall (1973).

V. S. Vladirimov, "Mathematical Problems in the One Velocity Theory of Particle Transport," Atomic Energy of Canada, Ltd., Ontario (1963), translated from Trans. V. A. Steklov Mathematical Institute, 61 (1961).

P. F. Zweifel, W. Greenberg, Proceedings, Fourth National Conference on Transport Theory, VPI&SU, Blacksburg, Virginia, March 10-15, 1975, to appear (1976).

ACKNOWLEDGEMENTS

The authors wish to thank Drs. Cyrus H. Adams, Donald R. Ferguson, Ely M. Gelbard, Albert A. Grau, Herbert H. Henryson II, Elmer E. Lewis, Hal Sudborough, and Bert J. Toppel for valuable discussions and suggestions. Special thanks are due to Judy Beumer who patiently and cheerfully typed the report.

NOMENCLATURE

Symbol	Description
a	Width of computational cell.
a_n	Combining coefficients for elementary solutions $q_n(x,\mu)$.
$\tilde{a}_{-n}$	Combining coefficients for elementary solutions $q_{-n}(x,\mu)$. After defining $\tilde{a}_{-n}$, subsequent references to a_{-n} denote $\tilde{a}_{-n}$.
α	Exponent of Chapeau function $\theta_{N-1}(\nu)$ in $q_{N-1}(x,\mu)$ mode for $\nu_{N-1} \leq \nu \leq 1$ $(0 < \alpha \leq 1)$.
$c(x)$	Macroscopic mean number of secondaries per collision.
$D(0,a)$	Denotes the domain $0 \leq x \leq a$ and $\lvert\mu\rvert \leq 1$.
$f_1(0,\mu), f_2(a,\mu)$	Inhomogeneous boundary term for incident flux boundary condition.
μ	Angular direction cosine.
$\psi(x,\mu), \phi(x)$	Neutron angular (scalar) flux distribution at location x with direction cosine μ.
$\psi^+(x,\mu)$	Even parity neutron angular flux distribution for the symmetrized transport equation.
$\underline{\psi}_A, \underline{\phi}_A$	Neutron angular (scalar) flux distribution located on the mesh nodes for the benchmark cell modes analysis.
$\psi_B(x,\mu), \phi_B(x)$	Neutron angular (scalar) flux distribution for exact benchmark problem.
$\underline{\psi}_C, \underline{\phi}_C$	Neutron angular (scalar) flux distribution obtained by approximate numerical methods.
$\underline{\psi}_E, \underline{\phi}_E$	Neutron angular (scalar) flux distribution error.
$\underline{\psi}_R, \underline{\phi}_R$	Neutron angular (scalar) flux distribution for multicell reference problem.
$q_0^{\pm}(x,\mu)$	Elementary asymptotic neutron angular flux solution.
$q_{\pm n}(x,\mu)$	Elementary asymptotic and transient neutron angular flux solution.

Symbol	Description
$S(x,\mu)$	Distributed neutron source at location x with direction cosine μ.
$\sigma(x)$	Macroscopic total cross section.
$\theta_n(\nu)$	Chapeau function base functions for expansion of $A(\nu)$.
ν	Transient eigenvalue spectrum of the homogeneous transport equation.
$\nu_{0^\pm}$	Asymptotic eigenvalues of the homogeneous transport equation.
x	Spatial position coordinate.

Subscripts	Description
i	Index of spatial variable x, i=1,2,...,I.
m	Index of angular direction cosine μ, m=1,2,...,M.
n	Index of elementary solutions (modes), n=0,1,...,N and transient eigenvalue spectrum variable ν.
$0^\pm$	Index of asymptotic elementary solutions.

Distribution for ANL-76-59

Internal:

M. V. Nevitt
R. J. Royston
R. Avery
C. E. Till
D. C. Price
G. T. Garvey
K. L. Derstine
E. H. Bareiss (70)
P. Witkowski (10)
A. B. Krisciunas
ANL Contract Copy
ANL Libraries (5)
TIS Files (6)

External:

ERDA-TIC, for distribution per UC-32 (201)
Manager, Chicago Operations Office
Chief, Chicago Patent Group
President, Argonne Universities Association
Applied Mathematics Division Review Committee:
  P. J. Eberlein, SUNY at Buffalo
  G. Estrin, U. California, Los Angeles
  W. M. Gentleman, U. Waterloo
  E. N. Pinson, Bell Telephone Labs.
  Saul Rosen, Purdue U.
  J. M. Ortega, NASA Langley Research Center
Applied Physics Division Review Committee:
  R. M. Brugger, U. Missouri, Columbia
  P. Greebler, General Electric Co., Sunnyvale
  R. L. Hellens, Combustion Engineering
  J. M. Hendrie, Brookhaven National Lab.
  J. S. King, U. Michigan
  W. B. Loewenstein, Electric Power Research Institute

ARGONNE NATIONAL LAB WEST
3 4444 00023945 9